Amyloid-β aggregation and maturation dynamics and microglial response in evolving amyloid plaque pathology

Katie Stringer

UCL

Thesis submitted for the degree of
Doctor of Philosophy

June 2022

DECLARATION

I, Katie Stringer, confirm that the work presented in this thesis is my own. Where information has been derived from other sources, I confirm that this has been indicated in the thesis.

Acknowledgements

Firstly, I would like to express my deepest thanks to my supervisor, Dr Jörg Hanrieder, for his excellent guidance, support and friendship throughout my PhD. It's rare to find someone who has a real balance of knowledge, good humour and kindness, and it truly has been a pleasure to work with you.

I would also like to thank Prof Frances Edwards for her supervision over the years, for always pushing for excellence, and for her very useful input into my thesis. I especially would like to thank Dr Damian Cummings for everything he has done not just for myself but also for the entire lab over the years, and particularly for his dedicated teaching and training, patience and kindness.

I would also like to thank my lovely Edwards lab members. I consider myself very lucky to have met some friends for life, and truly you have all made this an incomparable experience for me. Particularly, I would like to thank my PhD sisters Kari and Diana – we were on this PhD journey together from the start, and you both made me look forward to coming into the lab every day. I would also like to thank Sneha and Jack for always being so helpful with my project, but also for their friendship. I extend my gratitude to the other lab members that I met along the way, especially Dervis for his incredible mentoring and training when I first joined the lab, but also Tashu for her kindness and life guidance, and also Eugenia, Jon, Mila and George.

I would also like to thank my teammates in the Analytical Neurochemistry group over at Gothenburg University: Wojciech, Ambra, Patrick, Srinivas, Junyue, Karolina and Ajay. Moving to Gothenburg during a pandemic wasn't easy, but you all made me feel so welcome. I've enjoyed some memorable moments at conferences and in Gothenburg with you all, and thank you all for your scientific expertise and friendship.

I'd like to thank Fiona for being there for me, as always, during the (many many!) ups and downs of my entire PhD, and also Charles for being a ray of sunshine and pillar of support during my thesis writing. You both made life so much easier for me just by being around, and I'm very lucky to have you.

And lastly, to the rest of my friends and family that I haven't named (you know who you are) – thank you as always, for being so patient and supportive over the last four years.

Abbreviations

AD	Alzheimer’s disease
APOE	Apolipoprotein E
APP	Amyloid precursor protein
Aβ	Amyloid-beta
BACE	Beta-secretase
CD33	Siglec-3
CD47	Cluster of differentiation-47
CLU	Clusterin
CNS	Central nervous system
CR	Congo red
CR1	Complement receptor 1
CSF	Cerebrospinal fluid
CSF1R	Colony-stimulating factor 1 receptor
DAM	Disease-associated microglia
DAP12	DNAX-activating protein of 12 kDa
fAD	Familial Alzheimer’s disease
GWAS	Genome-wide association studies
Iba1	Ionized calcium-binding adaptor molecule 1
IMS	Imaging mass spectrometry
iSILK	Imaging mass spectrometry combined with stable isotope labelling kinetics
LCOs	Luminescent conjugated oligothiophenes
LDL	Low-density lipoprotein
LTP	Long-term potentiation
MALDI	Matrix-assisted laser desorption/ionisation
MCI	Mild cognitive impairment
MRI	Magnetic resonance imaging
MS	Mass spectrometry
NfL	Neurofilament light chain
NFTs	Neurofibrillary tangles
OHSC	Organotypic hippocampal slice culture

PET	Positron emission tomography
PSD95	Postsynaptic density-95
PS1	Presinilin-1
PS2	Presinilin-2
sAD	Sporadic AD
SIL	Stable isotope labelling
SILAC	Stable isotope labelling in cell culture
SILAM	Stable isotope labelling in mammals
SILK	Stable isotope labelling kinetics
Th	Thioflavin-S
TREM2	Triggering receptor expressed on myeloid receptors 2
WAM	White matter-associated microglia

ABSTRACT

Amyloid-beta (Aβ) plaque deposition is one of the major pathological features of Alzheimer's disease; however, the mechanism by which this occurs remains unclear. Microglia, the immune cells of the brain, have been shown to interact with plaques, but their significance to Aβ deposition is unknown.

This project aims to assess Aβ deposition both *in vivo* and in cultures obtained from amyloid precursor protein (*App*) knock-in mice (App^{NL-F} and App^{NL-G-F}), and also assess the interaction with microglia. Using a novel chemical imaging paradigm termed 'iSILK', involving stable isotope labelling and *in situ* mass spectrometry methods, here we analysed specific aggregation dynamics of individual Aβ species on a nanometer level. Additionally, we employed amyloid-specific dyes with high binding specificity in conjunction with hyperspectral and confocal imaging to quantitatively delineate plaque conformation and microgliosis in these mice.

In these mice, iSILK revealed that plaques first form an aggregated core of entirely Aβ1-42, followed by further Aβ1-42 deposition, aggregation and later secretion and deposition of Aβ1-38. In addition, cortical plaques form prior to hippocampal plaques, which was further confirmed by hyperspectral imaging of the same plaques. Comparison between genotypes showed that App^{NL-G-F} mice have the most structurally mature plaques and increased plaque-associated microgliosis compared to age-matched App^{NL-G-F} mice. Furthermore, perturbation of microglia in App^{NL-F}/$Trem2^{R47H}$ mice resulted in a significant reduction of plaque coredness, alongside alterations in plaque-associated microgliosis. Organotypic hippocampal slice cultures experiments demonstrated that even with external manipulation, cultures from *App* knock-in mice do not develop amyloid plaques. Overall, the results of this study highlight important differences in amyloid plaque composition and microglial response depending on *App* genetic mutation, and also implicate the role of triggering receptor expressed on myeloid receptors 2 in facilitating plaque maturation. This work provides a basis for further development of therapeutic targets for individuals with these variants.

IMPACT STATEMENT

Alzheimer's disease (AD) is the most common cause of dementia, accounting for over 50% of all dementia cases. With 10 million new cases each year, the impact on society and the economy is huge, in addition to the psychological effects on sufferers and their carers. A major hallmark pathology of AD is amyloid-beta (Aβ) plaque deposition; however, the process is complex and there is heterogeneity between individuals, and there remains a lot to be understood. Additionally, recent advances in AD research have highlighted microglia, the immune cells of the brain, as being significant contributors to AD pathology. Understanding the specific dynamics of plaque deposition, and the interaction with microglia, will be a crucial step toward finding a cure.

To investigate this, I made use of a new chemical imaging paradigm involving stable isotope labelling combined with imaging mass spectrometry to assess the timeline of plaque deposition. This was examined in amyloid precursor protein (*App*) knock-in mouse models, which are more representative of human AD pathophysiology compared with traditional transgenic AD models. I additionally used a new *App* KI model with a perturbed microglial response to directly assess the impact of the microglial receptor triggering receptor expressed on myeloid receptors 2 on plaque conformation. The work presented here utilises novel and quantitative methods to directly contribute to the understanding of the pattern of plaque deposition, what plaques are composed of, and microglial/plaque interactions. To the best of our knowledge, these techniques have never been employed in these mouse models before. Here, I have shown temporal and regional alterations in Aβ plaque deposition, and significant changes in plaque composition when microglia are impaired. Overall, these results provide one of the first insights into the nature of Aβ and glial pathology in mouse models which are more representative of human disease. This will help contribute to further clinical research into potential therapeutics for AD.

The iSILK results have already been published in the Journal of Biological Chemistry (Michno et al., 2021), and the plaque conformation and microglia results will be written for publication later this year. These publications will provide mechanistic insight into amyloid pathology in AD, and provide a basis for future research. Although the Covid-19 pandemic meant that I wasn't able to attend a number of conferences and workshops, I was able to present poster material at three conferences, both in person (ADPD – Lisbon, 2019; Mass Spectrometry & Advances in the Clinical Lab – Salzburg, 2019) and virtually (FENS – 2020; Society for Neuroscience – 2021). For Mass Spectrometry & Advances in the Clinical Lab 2019, I was awarded a Young Investigator grant, enabling me to present there and network with like-minded scientists. Additionally, I helped communicate current AD research with the public by demonstrating microscopy skills at UCL ARUK outreach events in 2018 and 2019, and I was involved in hosting In2Science students in the lab. Furthermore, I was awarded runner-up in UCL's 'Three-Minute Thesis' competition in 2019, where I summarised my PhD work in lay terms in three minutes.

CONTENTS

Chapter 1: Literature Review

Chapter 2: Methods

Chapter 5: Imaging plaque formation dynamics using iSILK

Chapter 6: The association between plaque conformation and microgliosis in *App* KI mice

Chapter 7: Discussion

List of figures

Chapter 1:

Chapter 2

Chapter 3

Chapter 4

Chapter 5

Chapter 6

List of tables

Chapter 1

Chapter 2

Chapter 1: Literature Review

1.1 Alzheimer's disease

It is estimated that there are currently over 50 million people in the world living with dementia, with the Global Burden of Disease Study 2019 estimating the number expected to triple to 152 million by 2050, particularly in low- and middle-income countries (Livingston et al., 2017). Alzheimer's disease (AD) is the most common cause of dementia, accounting for over 50% of all dementia cases. With 10 million new cases each year, the impact on society and the economy is huge, in addition to the psychological effects on sufferers and their carers. However, there is still no effective treatment. Therefore, understanding the pathology of this disorder represents a crucial step towards finding a cure.

1.1.1 Pathology

AD was first identified in 1907 by Dr Alois Alzheimer, who observed the presence of abnormal aggregated protein in the *post-mortem* brains of patients (Alzheimer, 1907). The hallmark pathologies of AD are amyloid-beta (Aβ) plaques and neurofibrillary tangles (NFTs), leading to neurodegeneration (Serrano-Pozo et al., 2011). Aβ plaques are extracellular deposits of Aβ protein in the brain parenchyma, and also occur in cerebral blood vessels (called cerebral amyloid angiopathy). NFTs are composed of intracellular aggregated hyperphosphorylated tau protein, and are thought to arise from mis-localisation of tau and subsequent deregulation of microtubule dynamics (Alonso et al., 2008). Aβ plaques accumulate first and result from cleavage of APP by beta secretase and gamma secretase into many different isoforms of Aβ, including Aβ1-40 and Aβ1-42, which readily aggregate to form structures such as oligomers and amyloid fibrils. Over a period of up to decades, insoluble aggregated forms of Aβ recruit surrounding soluble Aβ to aggregate and deposit around neurons, contributing to synaptic dysfunction and neuronal cell death (Lambert et al., 1998;

Townsend et al., 2006). Subsequent to changes in Aβ, the microtubule associated protein tau becomes hyperphosphorylated and aggregates to form NFTs, leading to neuronal damage and neurodegeneration (Hardy and Selkoe, 2002).

The interaction between Aβ and tau is unclear, but one proposed idea is the 'amyloid cascade hypothesis', which outlines how early Aβ accumulation is an initiating factor for later pathology (Hardy and Higgins, 1992). Indeed, Aβ-induced toxicity has been shown to depend on the levels of tau (Beach et al., 1989; Itagaki et al., 1989; Rogers et al., 1988), emphasizing their link. Further support for the amyloid cascade hypothesis comes from a number of sources. Human biomarker studies using amyloid-positron emission tomography (PET) or cerebrospinal fluid (CSF) analysis have demonstrated how changes in tau occur many years after Aβ (Bateman et al., 2012). Additionally, over 50% of individuals with Down's syndrome (who harbour three copies of the *APP* gene due to trisomy 21) will develop AD before the age of 50 (Ballard et al., 2016); and mutations within and immediately next to the Aβ region of *APP* causes aggressive forms of fAD, highlighting the role of APP in contribution to disease.

In line with Aβ and tau pathology, glial activation occurs in microglia (the resident immune cells of the brain) and astrocytes. It is now well established that in AD, both cell types respond to tissue inflammation signals and migrate to sites of Aβ plaques and NFTs (Ittner et al., 2010; Leroy et al., 2012; Rapoport et al., 2002). This is now understood to not only be a response mechanism but an equal contributor to disease progression, through complex pro- and anti-inflammatory signalling interactions (Heneka et al., 2015).

1.1.2 Risk factors for AD

AD can be divided into two sub-types: sporadic AD (sAD), which occurs after about the age of 65; or familial AD (fAD), occurring primarily between the ages of 45-60 (Campion et al., 1999). The rarer fAD exhibits autosomal-dominant inheritance, and is linked to mutations in three genes: amyloid precursor protein (*APP*), presenilin-1 (*PS1*) and presenilin-2 (*PS2*) (Berezovska et al., 2005; Scheuner et al., 1996). It was the discovery of disease mutations in these three

genes that were key to the development of the amyloid cascade hypothesis (Hardy and Selkoe, 2002). sAD is termed sporadic, as cases are not genetically predetermined (although there are attributed genetic risk factors), and accounts for over 95% of AD cases. This is thought to arise from a complex interplay between genetic and environmental factors. Although ageing is the single biggest risk factor for AD (Guerreiro and Bras, 2015), up to a third of AD cases could be attributed to seven potentially modifiable external risk factors: obesity, smoking, diabetes, hypertension, depression, lack of cognitive activity, and low level of education (Barnes and Yaffe, 2011; Killin et al., 2016). These are important to consider as they are preventable, through education schemes and governmental changes.

Genome-wide association studies (GWAS) have highlighted the impact of genes in AD aetiology (Karch and Goate, 2015). The strongest genetic risk factor for sAD known to date is the ε4 allele of the apolipoprotein E (*APOE*) gene (Corder et al., 1993; Sanan et al., 1994), which encodes for the protein APOE, a lipoprotein expressed primarily in the liver and then in the brain (Mahley and Rall, 2000).

The human *APOE* gene exists as three different alleles: ε2, ε3 and ε4. Of all the alleles, *APOE4* appears to have the biggest effect: one or two copies of the allele has been found to increase the risk of developing AD by 3- and 12-fold, respectively (Verghese et al., 2011). Conversely, *APOE2* carriers may be protected against AD to some degree, whereas *APOE3* does not appear to alter disease risk (Corder et al., 1993). It is unclear what mechanism underlies this isoform-specific effect, but there may be an interaction between APOE and Aβ. *APOE4* may change the normal function of microglia by binding to Aβ and preventing its clearance. Indeed, *APOE3* carriers have been shown to have fewer Aβ plaques and oligomers than *APOE4* carriers in both humans (Hashimoto et al., 2012; Koffie et al., 2012; Schmechel et al., 1993) and mice (Fagan et al., 2002; Hudry et al., 2013).

The significance of the microglial response in AD is supported by evidence that disease risk is associated with genes for immune receptors. GWAS studies have highlighted a number of microglial or microglia-associated genes that are

implicated in AD, such as clusterin (*CLU*), Siglec-3 (*CD33*), 1-phosphatidylinositol 4,5-bisphosphate phosphodiesterase gamma-2 and complement receptor 1 (*CR1*) (Jansen et al., 2019). The most prominent microglial risk gene is triggering receptor expressed on myeloid cells 2 (*TREM2*), of which the R47H missense mutation increases susceptibility to AD by 2 to 4.5-fold (Guerreiro et al., 2013a; Jonsson et al., 2013). APOE has also been shown to interact with microglia and trigger a cascade of events resulting in enhanced transcription of APP, thereby increasing levels of Aβ (Huang et al., 2017). Additionally, research has shown that the *APOE4* allele results in increased microgliosis compared with *APOE3,* in both humans (Minett et al., 2016) and in mouse models expressing human isoforms of *APOE* (Rodriguez et al., 2014). APOE is also upregulated in disease-associated microglia (DAM), further suggesting an interaction between APOE, Aβ and microglia. Overall this further highlights the role that genes and immune cells have in AD risk; however, sAD is generally thought to arise from a complex interplay between genetic and environmental factors (Barnard et al., 2014).

1.2 Clinical symptoms and diagnosis

Clinical symptoms of AD include initial problems with episodic memory and difficulties multi-tasking, followed by more profound cognitive impairment as the disease progresses, including behavioural and mood changes, and eventual decline into full dementia (Jost and Grossberg, 1995). Confusingly, plaque pathology does not correlate with disease stage (Nelson et al., 2012); rather, region-specific synapse loss has been shown to correlate best with cognitive deficit (DeKosky and Scheff, 1990; Spires-Jones and Hyman, 2014; Terry et al., 1991), potentially because synaptic function underlies cognitive performance. Synapse loss has been proposed to be a downstream effect of amyloidosis, tauopathy and inflammation.

1.2.1 Diagnosing AD

There is no single test to diagnose AD or other forms of dementia. Traditionally, dementia is diagnosed based on a combination of patient health history, the pattern of cognitive deficits, and a panel of clinical investigations including

structural brain imaging and blood tests (Blennow et al., 2006; Porsteinsson et al., 2021). However, there is great heterogeneity in the pathology and clinical presentation of AD, which makes diagnosis difficult (Blennow and Wallin, 1992). AD cannot be definitively diagnosed until *post-mortem* neuropathologic evaluation, upon identification of both Aβ plaque deposition and NFTs (Braak et al., 2006; Braak and Braak, 1991).

As clinical features of AD are thought to emerge many decades after amyloid pathology has started (Bateman et al., 2012), it is incredibly important to develop effective methods to identify the disease in its early stages. As AD shares the feature of abnormal protein aggregates with other dementias, such as dementia with Lewy bodies (DLB) or frontotemporal dementia (FTD) (Matej et al., 2019), it is crucial to keep developing new diagnostic tools to be able to accurately distinguish between these disorders. Amyloid and tau can now be imaged in live patients (Scholl et al., 2016; Suppiah et al., 2019), and functional imaging approaches such as PET, magnetic resonance imaging (MRI) to measure brain atrophy, and quantitative electroencephalogram are all being used to aid the diagnosis of AD (Jack et al., 2013).

1.2.2 Treatments for AD

Despite robust studies detailing the involvement of Aβ and tau in AD, treatments targeting aggregated peptide removal have repeatedly failed in clinical trials. There were high hopes for several anti-Aβ antibodies (aducanumab and BAN2401, which target fibrillar Aβ; and solanezumab for monomeric Aβ), and indeed there was a modest reduction in the rate of cognitive decline in subsets of AD patients. However, the side effects such as cerebral microhaemorrhages and vasogenic edema have limited their clinical efficacy (Honig et al., 2018; Salloway et al., 2014).

Recent work has suggested that it is in fact Aβ oligomers, rather than the plaques themselves, that are more responsible for neurotoxicity (Viola and Klein, 2015). Therefore, new therapeutics that target oligomeric Aβ, rather than other forms, may be more effective. Another explanation is that treatment is occurring far too late in disease course – anti-Aβ or -tau compounds may only be effective in the

very early stages. Therefore, it is critical to identify fluid biomarkers, such as in blood or urine, that can be screened to identify AD onset before cognitive symptoms have started.

Very recently, the top-line Phase 3 clinical trial results were released for the anti-amyloid antibody lecanemab, where Biogen/Eisai reported that all primary and secondary endpoints were met. Significantly, these data provide the first example of a therapeutic antibody that changes the course of AD pathology, and certainly strengthen the amyloid cascade hypothesis (Biogen, 2022).

1.2.3 Biomarkers for AD

Currently, AD is only definitely diagnosed *post-mortem* (Braak et al., 2006; Braak and Braak, 1991). The identification of AD-related biomarkers in blood, plasma and CSF would allow for a less invasive and more accurate diagnosis of the disease during the patient's life, and would also allow for therapeutic intervention before too much pathological damage. Biomarkers which are perturbed in AD and are detectable in fluid include Aβ, neurofilament light chain (NfL), tau and synaptic proteins, and are the centre of fluid biomarker research today.

Changes in CSF Aβ are believed to be one of the first signs of AD. In particular, low CSF Aβ1-42 correlates with amyloid burden because in the brain, this sticky peptide has already aggregated into plaques, leaving less to be secreted into the extracellular space (Strozyk et al., 2003). The development of PET ligands targeting fibrillar Aβ led to multiple studies confirming around 90% concordance between low CSF Aβ1-42 levels and positive amyloid PET scans (Blennow et al., 2015). However, Aβ aggregation starts many years before clinical symptoms emerge. A recent study correlated higher CSF Aβ1-42 levels with better cognitive health and hippocampal volume, regardless of plaque burden, suggesting that it is in fact the soluble forms of Aβ that are influencing dementia symptoms (Sturchio et al., 2021). This also could be why anti-amyloid drugs have low efficacy, as they target plaques rather than soluble Aβ. Therefore, it would be useful to examine nonfibrillar forms of Aβ such as oligomers and protofibrils, which are more representative of the dynamic profile of Aβ during early disease.

It is important to also consider other isoforms of Aβ, of which Aβ1-40 is the most abundant in CSF (Portelius et al., 2007). A 1998 study found that combined Aβ1-40 and Aβ1-42 analysis improved the diagnostic accuracy for AD (Shoji et al., 1998), with a subsequent study showing that the CSF Aβ1-42/Aβ1-40 ratio was better than Aβ1-42 alone in correlating with p-tau levels (Wiltfang et al., 2007). Higher CSF Aβ1-38 has been shown to potentially be protective in individuals positive for AD biomarkers (as determined by CSF p-tau/Aβ1-42 ratio), by slowing decline in Mini-Mental State Examination scores (Cullen et al., 2021). This highlights the potential pathogenic significance of secretion and deposition of Aβ1-38, a peptide not as thoroughly researched as Aβ1-42 and Aβ1-40. An intriguing recent study found that plasma Aβ1-42/40 ratio drops in blood potentially years before CSF, opening up a potential screening window. In this study, both CSF Aβ1-42 and Aβ1-40 levels increased with age, so the ratio stayed the same; however, in plasma, Aβ1-40 levels increased over time more than Aβ1-42, suggesting that clearance of Aβ1-42 starts to falter (Li et al., 2022). CSF Aβ1-42/Aβ1-40 ratios have also been used to distinguish AD from other neurodegenerative diseases, such as DLB or FTD, which share common pathological features (Paterson et al., 2018). Considering these diseases often have an overlap of cognitive symptoms (Matej et al., 2019), being able to differentiate them at the molecular level is highly useful in order to tailor the correct treatment plan for the patient. Overall, these studies implicate Aβ metabolism and clearance as early factors contributing to AD development, rather than amyloid plaque burden.

1.3 Amyloid pathology

In line with the amyloid cascade hypothesis, Aβ has been shown to be critical for the initiation and progression of AD pathology. Downstream, this further leads to tau pathology, synaptic alterations and neurodegeneration.

1.3.1 APP processing and Aβ aggregation

APP is an endogenous transmembrane protein of varying amino acid length, that comprises a large extracellular N-terminal domain and a smaller intracellular C-terminal domain. APP is believed to have a role in modulating neuronal

differentiation, growth, branching and synaptogenesis (Roch et al., 1994). However, its precise role remains unclear, particularly as deletion of *App* in mice appears to have no significant effect (Herms et al., 2004; Wang et al., 2005). APP is produced in large amounts by neurons (Lee et al., 2008) and is sequentially cleaved by several proteases along two pathways: the amyloidogenic and the non-amyloidogenic. Along the non-amyloidogenic pathway, APP is cleaved by the α- and β-secretases to form sAPPα and C83. If APP is instead processed along the amyloidogenic pathway, β-secretase cleaves APP into a shorter 99 amino acid long C-terminal fragment (known as CTFβ and C99), which is subsequently processed by γ-secretase into an Aβ peptide and a longer soluble N-terminal fragment (sAPPβ), which been implicated to function as a death receptor 6 ligand and modulate axonal pruning and neuronal cell death (Nikolaev et al., 2009). Figure 1 shows the amyloidogenic pathway of APP processing.

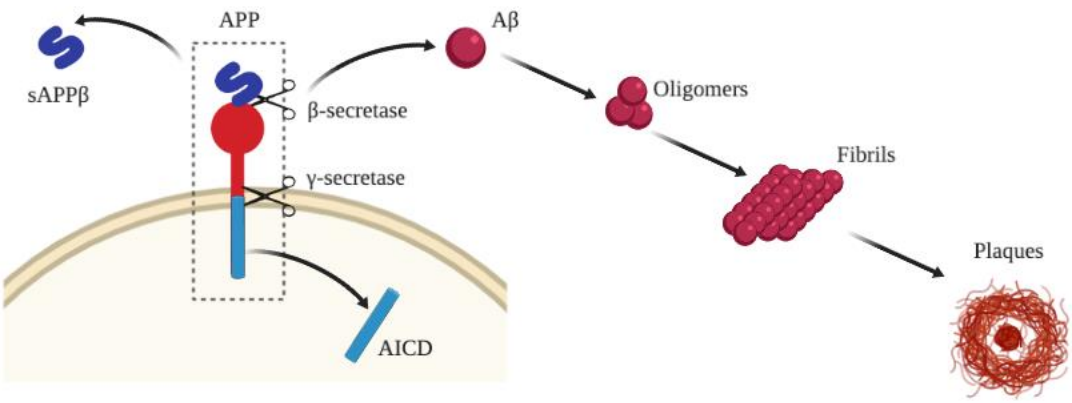

Figure 1. The amyloidogenic pathway of APP processing. Cleavage of transmembrane APP by β-secretase generates sAPPβ. C99 is cleaved by γ-secretase, generating AICD and Aβ. Once oligomerised, Aβ subsequently protofibrils, which come together to form insoluble long, mature fibrils, with then further aggregate to form plaques.
Abbreviations: s, soluble; APP, amyloid precursor protein; Aβ, amyloid-beta.

In terms of the amyloidogenic pathway, beta-secretase 1 (BACE1) was identified as a major β-secretase. Therefore, BACE1 may be a therapeutic target for AD, to prevent overactivation of the amyloidogenic pathway (and therefore overproduction of Aβ). BACE1 inhibition in AD mouse models has been shown to ameliorate neuronal loss and memory deficits alongside a marked reduction in Aβ1-40/42 levels (Ohno et al., 2007; Ohno et al., 2004). Additionally, AD brains

have shown increased BACE1 activity (Johnston et al., 2005; Yang et al., 2003), implicating abnormal activation of BACE1 as a pathological mechanism. However, inhibition of BACE1 carries potentially toxic effects; for example, BACE1 knock-out mice had a high mortality rate in the first weeks after birth and were smaller and more hyperactive than their wild-type (WT) counterparts (Dominguez et al., 2005). As BACE1 has multiple other substrates, including voltage-gated sodium channel (Nav1) β2 subunit, Golgi-localized membrane-bound α2,6-sialyltransferase and P-selectin glycoprotein ligand-1 (Vassar et al., 2009), it is likely that drugs targeting BACE1 will have unwanted effects on other physiological pathways.

γ-secretase cleavage of APP via the tripeptide cleavage process can generate both Aβ1-40 and Aβ1-42. This occurs via a pathway that generates Aβ1-40 and APP intracellular domains (AICD) 50-99 or Aβ1-48 and AICD 49-99 (Kakuda et al., 2006)**.** Following this, Aβ1-49 and Aβ1-48 are cleaved sequentially in three amino acid increments to produce mainly Aβ1-40 and Aβ1-42, respectively (Takami et al., 2009).

In total, Aβ has over 15 different isoforms and truncations, with Aβ1-40 being the most abundant. The longer isoforms, especially Aβ1-42, are more fibrillogenic and hydrophobic, and therefore more predisposed to aggregate (De Felice et al., 2008; Esch et al., 1990; Jarrett et al., 1993). Traditionally, Aβ1-42 has been viewed as the most pathogenic peptide in regard to plaque deposition; however, a growing body of evidence has implicated the involvement of both Aβ1-38 and Aβ1-40 (Lehmann et al., 2020; Michno et al., 2021; Michno et al., 2019c). Additionally, these peptides have been proposed to have several physiological roles, including neurogenesis, calcium homeostasis, and modulation of synaptic activity and plasticity (and therefore learning and memory) (Garcia-Osta and Alberini, 2009; Muller et al., 2017). In the healthy brain, a fine balance between Aβ production and clearance exists. There are several factors that influence the dynamic equilibrium of Aβ, including its location, source and the specific enzyme that is degrading it (Saido and Leissring, 2012). However, the precise physiological role of Aβ remains unclear.

One hypothesis is that, in AD, a disruption of clearance mechanisms, combined with a natural elevation of Aβ levels with age, results in either overproduction or reduced clearance of Aβ. The former is supported by individuals with fAD who have an increase in Aβ production due to missense mutations; the latter is supported by sAD cases who may have underlying genetic risk factors combined with lifestyle triggers that contribute to disrupted clearance mechanisms of Aβ, as supported by CSF studies (Mawuenyega et al., 2010; Rodrigue et al., 2009). Different proteases are responsible for degradation of Aβ substrates; for example, neprilysin, insulin-degrading enzyme and angiotensin-converting enzyme degrade non-aggregated forms of Aβ; whereas matrix metalloproteinase-2 and -9, and cathepsin B and D degrade aggregated Aβ. A disruption of this dynamic equilibrium affects the overall concentration of Aβ peptide (including its proteoforms: Aβ1-38, -40 and -42), as well as Aβ aggregates such as oligomers (Saido and Leissring, 2012).

Ultimately, both reduced clearance and overproduction leads to excess forms of Aβ in the brain with a propensity to oligomerise. Once oligomerised, Aβ forms protofibrils, which come together to form insoluble long, mature fibrils (Bitan et al., 2003; Carulla et al., 2009), which are the primary component of Aβ plaques. Certain misfolded oligomers called ‘seeds’ can induce other Aβ molecules to take the misfolded form, leading to a cascade of misfolded proteins similar to a prion infection (Harper and Lansbury, 1997; Jarrett et al., 1993). All forms of Aβ prior to fibrils are considered ‘soluble’.

Converging evidence suggests that, rather than oligomers serving as an intermediate step to development of Aβ plaques, they are in fact initiators of the pathological process. In the preclinical phase of AD, soluble oligomeric Aβ accumulates to a threshold that eventually leads to symptomatic AD. Indeed, previous work in our lab showed that hippocampal CA3 pyramidal cells in transgenic TASTPM mice (harbouring the Swedish mutation in *APP* and the M148V mutation in *PS1*) exhibit increased release probability (the probability of a synaptic vesicle to release its transmitter content in response to an action potential – a major determinant of synaptic strength) even before plaque formation (Cummings et al., 2015). We also demonstrated increased release probability in *App* knock-in (KI) mice during pre-plaque stages or early plaque

deposition (Benitez et al., 2021; Saito et al., 2014). This suggests that soluble forms of Aβ are affecting the network prior to insoluble Aβ aggregation and deposition. Aβ oligomers have been demonstrated to trigger damage to the surrounding environment via gliosis, oxidative damage, tau hyperphosphorylation, and synaptic and mitochondrial toxicity (Kurz and Perneczky, 2011), thereby driving the brain to the tipping point where neurodegeneration occurs. In both AD animal models (Cleary et al., 2005; Shankar et al., 2008) and in humans (Lesne et al., 2013; Perez-Nievas et al., 2013), oligomers can drive cognitive impairment; and *in vitro*, exposure to oligomers rapidly reduces the expression of synaptic proteins involved in neurotransmission and learning and memory (Lacor et al., 2007) and over time, loss of synapses and spines (Wang et al., 2017). There may also a link between oligomeric Aβ and tau, as tau contributes to oligomeric Aβ-related synapse loss (Ittner and Ittner, 2018; Ittner et al., 2010); and reduction of tau levels rescues some of these synaptotoxic effects (Roberson et al., 2007) however, the underlying mechanisms are unclear.

Limited understanding of specific Aβ dynamics may be one of the reasons why drugs targeting Aβ have had no success (Mehta et al., 2017). Therefore, understanding at a subcellular level which Aβ species are the most harmful, and how this impacts the surrounding cellular network over time, represents a critical step towards identifying and targeting biological pathways to effectively halt further deficit.

1.3.2 Plaque conformational polymorphism

In AD, individuals display differences in both plaque morphology and composition (Dickson and Vickers, 2001; Rasmussen et al., 2017; Tycko, 2015). However, it is unclear whether this represents different plaque type, or just different stages of growth for the individual plaque. Chemical dyes specific for β-pleated sheets, such as Congo red (CR) or Thioflavin-S (Th) in conjunction with immunohistochemistry (IHC) are commonly used to classify plaque types into mature/dense-cored (CR/Th positive) and immature/diffuse (IHC positive; CR/Th negative) plaques. In sAD, Th-positive plaques are associated with dystrophic neurites, synaptic and neuronal loss and increased glial activation (Serrano-Pozo et al., 2011). Dense-core plaques are consequently regarded as more neurotoxic

(Howie and Brewer, 2009). However, confusion lies in the fact that diffuse plaques occur even in cognitively normal elderly individuals, and therefore are not included in the pathological diagnosis of AD (Edwards, 2019). Therefore, are diffuse plaques a precursor to cored plaques, or are they formed through distinctly separate mechanisms? Recently developed electro-optically active oligomeric probes, luminescent conjugated oligothiophenes (LCOs), can distinguish between plaques with different conformations (Nystrom et al., 2017; Rasmussen et al., 2017).

Using these tools, studies of Aβ aggregates have shown a high degree of conformational variation among oligomers, protofibrils, fibrils and plaques (Hammarstrom et al., 2010; Rasmussen et al., 2017). Aβ can aggregate into unique structural variants depending on disease type; for example, different plaque conformations have been found in fAD vs. sAD cases (Dickson and Vickers, 2001); and the arrangement of Aβ varies within and among plaques, even in the same individual (Liu et al., 2016; Rasmussen et al., 2017). Cryo-electron microscopy and solid-state nuclear magnetic resonance spectroscopy studies have also shown that polymorphism exists within peptides; for example, Aβ1-42 can fold in different ways that yield multiple structural models of fibrils (Gremer et al., 2017; Lu et al., 2013; Qiang et al., 2017; Saido and Leissring, 2012). These conformational polymorphisms thus pose a huge challenge to the detection of plaques for diagnostics (Hammarstrom et al., 2010), and for the development of therapeutics targeting Aβ aggregates.

Diffuse plaques could be regarded as an earlier and possibly neuroprotective form, by recruiting toxic soluble Aβ to localise the damage (Edwards, 2019). Cored plaques may be formed at later stages of disease and trigger early cognitive deficits via hyperphosphorylated tau (Dickson and Vickers, 2001); however, amyloid burden alone does not correlate with dementia severity (Ingelsson et al., 2004). Therefore, understanding the function and neurotoxicity of plaques remains critical for the development of AD treatments. However, the disconnect between plaque burden and cognitive deficit suggest that there are other mechanisms at play, such as overreactive glia or NFTs.

1.3.3 Plaque growth and spread

Plaque growth is a complex event and may involve selective processing of APP into its metabolites, followed by recruitment of different peptides over time. In both humans and *APP* transgenic mice, premature diffuse plaques are associated with higher levels of Aβ1-42, whereas neurotoxic cored plaques contain more Aβ1-40, implicating Aβ1-40 deposition as a secondary event. The ratio of Aβ1-40/Aβ1-42 increases over time in these mice, involving hydrophobic priming of Aβ1-42 through pyroglutamation followed by Aβ1-40 deposition and core formation. This indicates that Aβ1-42-rich premature plaques serve as a precursor for senile plaques (Michno et al., 2019a). Additionally, Aβ1-38 secretion and deposition occurs after Aβ1-42 deposition in *App* KI mice, as evidenced by an Aβ1-42-rich core and more Aβ1-38 in the periphery of plaques (Enzlein et al., 2020; Michno et al., 2021), suggesting that individual plaques evolve over time. Therefore, pre-formed plaques may serve as a platform for Aβ1-38 to attach to and misfold. A pre-cored plaque stage may be a key point of therapeutic intervention; therefore, it is critical to understand which mechanism draws in Aβ1-40 and encourages plaque maturation.

Further studies have highlighted the theory that individual plaques may evolve over time. In Down's syndrome patients, diffuse Aβ1-42-rich plaques were found to precede cored plaques containing Aβ1-40 (Iwatsubo et al., 1995). *Post-mortem* studies have shown that plaque type varies with age: diffuse extracellular plaques were found in 12 year-old children, whereas compact plaques were not seen until the age of 30 (Lemere et al., 1996), suggesting that diffuse plaques may morph into compact plaques over a lifetime. However, this is challenged by a particular study in mice, where diffuse Aβ accumulation was found to occur independently of compact plaque formation, suggesting that diffuse and compact plaques develop via separate pathways (Lord et al., 2011).

In terms of how plaques spread, different brain regions show selective vulnerability to amyloid pathology. In humans, amyloid spread is much less predictable than NFTs, but two staging systems have been proposed based on the patterns noticed in *post-mortem* evaluation of individuals with AD. The first is by Braak and Braak (Braak and Braak, 1997), and the second by Thal and colleagues (Thal et al., 2002).

Both of these staging systems identify that cortical and hippocampal areas are affected in early- and mid-stage AD, and this is supported by multiple other studies. An early *post-mortem* study in Down's syndrome patients revealed that the amygdala, entorhinal cortex are first and worst affected, followed by spread to other cortical and subcortical areas, and the olfactory bulb (Mann et al., 1986). In humans, the neocortex and dentate gyrus show a disease-related decline in numerical synaptic density, which correlates with cognitive decline (Scheff and Price, 2006). An MRI study demonstrated that AD patients have accelerated loss in hippocampal volume compared with controls (Schuff et al., 2009). Vulnerability of the hippocampus in AD may be mediated by dysfunctional adult hippocampal neurogenesis (Mu and Gage, 2011), which may contribute to deficits in learning and memory observed in individuals with AD. This hippocampal susceptibility to pathology is reflected when examining plaque distribution in AD mouse models; for example, *App*$^{NL-G-F}$ mice have a heavier plaque load in specific areas such as the CA1, as demonstrated by the de Strooper lab (Rice et al., 2020) and our lab (Vitanova, 2021). Additionally, neuronal and synaptic activity may underlie regional vulnerability; for example, *App*$^{NL-G-F}$ mice display deficits in long-term potentiation (LTP) in the cortex prior to the hippocampus (Latif-Hernandez et al., 2020); transgenic mice show impairment in hippocampal LTP after exposure to soluble Aβ (Rowan et al., 2003); and early plaque pathology is associated with loss of spontaneous action potential-mediated activity in the CA1 and dentate gyrus of the hippocampus (Cummings et al., 2015). Overall, this highlights the importance of considering potential differences in AD pathology between brain regions.

1.4 Microglia

1.4.1 Microglia in the healthy brain

Microglia are derived from myeloid progenitor cell lineage and serve as the 'immune cells' of the brain. During embryonic development, they migrate from the embryonic yolk sac to the brain and grow into immature microglia, where they constitute 5-10% of all brain cells (Ginhoux et al., 2010; Li and Barres, 2018).

Local cell signalling causes microglia to adopt tissue-specific signatures, creating a distinct and heterogeneous populations across the brain (Gautier et al., 2012; Hickman et al., 2013; Li et al., 2019). Microglia contribute to the homeostasis of the brain by display a ramified or 'branch-like' morphology, in which their processes are continuously sampling the environment by extending and contracting (Kettenmann et al., 2011). Microglia also respond to tissue injury by migrating to the site and assuming an 'activated' state, allowing them to phagocytose toxic material and release pro- or anti-inflammatory factors such as cytokines, chemokines and reactive oxygen species (Kettenmann et al., 2011).

Initially, microglia were believed to have only two forms: pro-inflammatory (in response to disease) and homeostatic (sampling the environment). The development of new techniques, such as single-cell genomics, bioinformatics, proteomics and epigenetics has allowed for characterisation of immune cell types and states; in fact, a wide range of current research has revealed that there are multiple subpopulations of microglia within the brain, all carrying out different roles (Butovsky et al., 2014; Hickman et al., 2013; Holtman et al., 2015). They are highly mobile and reactive, both responding to cell signalling molecules and releasing their own to modulate the integrity of neuronal networks and synaptic functioning. They also play a role during human nervous system development, when excess neuronal connections are formed that require pruning (Katz and Shatz, 1996). In the dentate gyrus, ramified microglia engulf apoptotic neuroblasts (Sierra et al., 2010) and are involved in the pruning and remodelling of synapses, thus carving out appropriate neural circuits in the brain (Paolicelli et al., 2011). Microglia also aid synaptic pruning by interacting with the complement system, which is a cascade formed of protein complexes that aids the immune system in eliminating invading pathogens (Dunkelberger and Song, 2010). In mice, C1q, the initiator of the complement cascade, is activated by astrocytes and then further activates C3b, which attaches to neurites and tags them for elimination. Deposited C3 then activates C3 receptors on microglia, initiating microglia-mediated phagocytosis of inappropriate synapses (Bialas and Stevens, 2013; Stevens et al., 2007). In addition, microglia play a role in adult hippocampal neurogenesis by phagocytosing apoptotic new-born cells (Sierra et al., 2010). It appears that microglia have important functions surrounding reorganisation of hippocampal synapses, both throughout development and adult life. Altogether,

research up until now has shown how microglia play an active role in the functioning of the central nervous system.

1.4.2 Microglia in AD

Over the past decade, GWAS studies have highlighted several microglia-specific genes that are strongly associated with AD risk, including mutations in the gene encoding for TREM2 (Guerreiro et al., 2013a; Jonsson et al., 2013) and CD33 (Stewart et al., 2010). This has shifted the attention in the field towards the interaction between microglia and AD-related pathology, in line with consistent evidence that glial activation is a component of AD (Itagaki et al., 1989).

The precise function of microglia in relation to AD pathology remains unclear. Microglia have repeatedly been demonstrated to cluster around plaques and undergo morphological and gene expression changes (Medawar et al., 2019). However, it is unclear whether microglia facilitate plaque deposition, or aid removal of toxic Aβ. Initially, microglia are thought to be neuroprotective by removing of synaptic damage in and around plaques (Edwards, 2019). Murine microglia have been shown to cluster round plaques and promote them to become denser and more compact, by compartmentalising them to restrict the formation of protofibrillar Aβ, thereby reducing neuritic dystrophy (Bolmont et al., 2008; Meyer-Luehmann et al., 2008). Cell-surface receptors on microglia are able to bind to soluble Aβ oligomers and Aβ fibrils (Salih et al., 2019), after which the cell becomes activated to produce proinflammatory cytokines and chemokines (Stewart et al., 2010). However, microglia have also been shown to secrete factors that mediate Aβ fibrillisation (Venegas et al., 2017) or physically ingest and modify extracellular Aβ which is then released to seed further plaques. Therefore, different subpopulations of microglia may have different roles, or the individual microglia may switch function over the course of the disease.

Studies involving colony-stimulating factor 1 receptor (CSF1R), of which signalling is critical for microglia survival, also highlight the role of microglia in plaque maturation. When CSF1R is depleted using an inhibitory drug called PLX5622, 5xFAD mice demonstrate reduced plaque formation, apart from in

areas where microglia survive (Condello et al., 2015). In our lab's previous work, microglial ablation resulted in a reduction of small plaques in *App*$^{NL-G-F}$ mice (Benitez et al., 2021). This suggests that microglia contribute to plaque maturation in some way, potentially by compacting soluble Aβ into plaques and thus reducing the spread of Aβ toxicity. Interestingly, even prior to plaque deposition, microglia numbers are significantly higher in transgenic AD mouse models compared with WT mice (Medawar et al., 2019), suggesting an increase in proliferation in response to early accumulation of soluble Aβ, or small plaques below the detection threshold. Over time, chronic activation in response to excess Aβ release may push a switch from a neuroprotective to a neurotoxic phenotype via proinflammatory signalling cascades (Sawada et al., 2008), although how this occurs is unclear.

Emerging evidence is showing that rather than all microglia experiencing this switch, there are many different subtypes of microglia, each with distinct functions. A pivotal transcriptional study in WT and AD-transgenic mice identified a neurodegeneration-specific subset of the cells, termed 'DAM' (Keren-Shaul et al., 2017). DAM are suggested to play a protective role (via the TREM2 signalling pathway) by displaying a specific sensory mechanism to detect damage within the central nervous system (CNS) (Huang et al., 2017). Their existence was also confirmed in other AD models (Ajami et al., 2018; Friedman et al., 2018), implicating that under Aβ pathological conditions, a certain population of microglia are assigned to prevent further damage. A new subset of microglia, termed white-matter-associated microglia (WAM), were recently shown to exist across many different mouse models, including 5xFAD, App/PS1 and *App*$^{NL-G-F}$. WAM were shown to engulf old and fraying myelin debris, and interestingly, they displayed a similar gene expression profile to DAM, but appeared to allow plaques to grow (Safaiyan et al., 2021). Overall, this highlights how in mice, microglia are heterogenous cells that elicit specialised responses to different pathologies.

While certain groups of microglia may be protective, there are microglia-associated mechanisms that lead to synaptotoxicity. The classical complement cascade, which is typically activated during neurodevelopment, has been shown in mice to be inappropriately activated and mediate synaptic loss in the early stages of pathology (Hong et al., 2016). If left unchecked, the mechanisms

involved in microglia-mediated synaptic development can turn pathological, severely affecting synapses. Indeed, early AD research showed that many of the complement proteins were localised to neuritic plaques (Eikelenboom and Stam, 1982), and AD patients display elevated CSF concentrations of C3 and CR1, two of the complement proteins, indicating perturbations in the pathway (Daborg et al., 2012).

It is important to note that microglial signatures in humans can vary considerably from mice. Human transcriptomic studies have reported a wide array of findings, such as no DAM signature at all (Mathys et al., 2019), or an incomplete DAM pattern, involving upregulation of key DAM genes such as *TREM2, APOE* and *CD68*, but no detection of other markers such as *CST7* and LPL (Sayed et al., 2020). Proteomic studies have further highlighted the limited overlap between human and mouse AD microglial signatures, where upregulated human astrocyte-microglial metabolism-associated genes were only partially mirrored in mice (Johnson et al., 2020). However, a recent study demonstrated that the microglial sensome, i.e. the set of genes associated with microglia continuously sensing the environment and responding to those changes, had 57 genes conserved between mice and humans (Abels et al., 2021). It is clear that microglial genes have vast applicability in physiology and pathology; therefore, further proteomic and transcriptomic studies are required to better understand how accurately we can model human diseases such as AD in mice.

An individual's genetic variability in the microglial response to Aβ deposition has also been identified as a major determinant for AD risk (Salih et al., 2019). For example, tolerance to plaque load may be determined by the ability of the microglia to remove damaged synapses (Edwards, 2019). This suggests transcriptional changes in microglia in response to Aβ pathology, highlighting the importance of investigating their interaction.

1.4.3 TREM2

TREM2 is a cell-surface transmembrane glycoprotein receptor, which in the brain is expressed exclusively on the surface of glial cells. It is not clear whether TREM2 is expressed in all microglia or only a subset, and interestingly, its

expression is modulated by inflammation in the surrounding environment. TREM2-positive cells in the AD mouse brain have been shown to be resident microglia, rather than infiltrating monocytes (Wang et al., 2016).

TREM2 has been shown to be involved in numerous processes, including phagocytosis, inflammatory signalling, and myeloid proliferation, migration and survival. TREM2 mediates two pathways to regulate the microglial phenotype; one is phagocytic (Frank et al., 2008; Takahashi et al., 2007), and the other suppresses inflammatory signalling (Piccio et al., 2007). TREM2 acts primarily through interaction with DNAX-activating protein of 12 kDa (DAP12), forming a DAP12-TREM2 complex that mediates microglial activation, cell survival, phagocytosis and cytokine production (Ma et al., 2015). Once TREM2 associates with DAP12, tyrosine phosphorylation of DAP12 occurs within its immunoreceptor tyrosine-based activation motives by Src family kinases, resulting in a cell signalling cascade and immune response (Lanier et al., 1998). Other TREM2 ligands include lipids (Cannon et al., 2012) and apolipoproteins such as APOA1, APOA2, APOB, CLU and APOE (Atagi et al., 2015; Song et al., 2017; Yeh et al., 2016).

1.4.4 TREM2 in AD

TREM2 was first implicated in having a role in disease when TREM2/DAP12 mutations were shown to cause Nasu-Hakola disease, which is characterised by extensive white matter loss and frontotemporal-like dementia (Paloneva et al., 2002). The link between TREM2 and AD was then demonstrated in 2013, when two independent GWAS studies highlighted a rare variant in exon 2 of the *TREM2* gene, causing an arginine-to-histidine substitution at amino acid position 47 (R47H), which increases the risk of developing AD by 2- to 4-fold (Guerreiro et al., 2013a; Jonsson et al., 2013), similar to the risk when carrying one copy of the APOE4 allele. This was further confirmed by numerous other studies (Benitez et al., 2013; Finelli et al., 2015; Ruiz et al., 2014), highlighting the pathophysiological role of TREM2. Indeed, TREM2 is upregulated in AD patients (Frank et al., 2008; Takahashi et al., 2007), and CSF TREM2 is a potential biomarker of AD-related neurodegeneration (Suarez-Calvet et al., 2016). Several other variants of TREM2 were then identified as risk factors for AD, including R62H, d87N, H157Y, T96K

and R136Q (Guerreiro et al., 2013c; Jin et al., 2014; Sims et al., 2017; Song et al., 2017). However, it is unclear what the precise role of TREM2 is in this context, although the *R47H* mutation has been shown to change the conformation of the ligand-binding region of TREM2 and therefore reduces binding of its ligands, including CLU, low-density lipoprotein (LDL) and APOE (Atagi et al., 2015), and CLU-LDL lipoprotein-associated Aβ1-42 aggregates (Yeh et al., 2016).

Trem2 mouse models have helped with understanding of the involvement of TREM2 protein in sAD. There is now a strong line of evidence showing the strong association of Trem2 with Aβ. We previously reported that *Trem2* is upregulated in both the cortex and hippocampus of TASTPM mice, and is strongly connected with other genes associated with Aβ pathology (Matarin et al., 2015). Additionally, Trem2 facilitates Aβ1-42 uptake alongside downregulation of the microglial pro-inflammatory cytokine response (Jiang et al., 2014). Interestingly, recent work has shown that *in vitro,* oligomeric Aβ binds directly to Trem2 and activates signalling with DAP12. Numerous studies have reported that Trem2-deficient mouse models show decreased microglial activation, resulting in a reduction of plaque-associated microglia and altered plaque morphology (Jay et al., 2015; Wang et al., 2015; Yuan et al., 2016).

The recent development of *Trem2* mouse models with the R47H mutation has yielded further valuable information about the role of this variant. 5xFAD mice expressing human $Trem2^{R47H}$ were first developed in 2018, and show impairment in microglial clustering around plaques, and reduced microgliosis and microglia density in both the cortex and hippocampus (Song et al., 2018). Additionally, soluble Trem2 was found to colocalise with neurons and plaques in mice carrying the common variant of human *TREM2*, indicating that in mice, Trem2 has a role in recognising damaged neurons (Song et al., 2018). Intriguingly, this is impaired in $Trem2^{R47H}$ mice, highlighting an interaction between Aβ and soluble Trem2 (Zhong et al., 2018). Cheng-Hathaway and colleagues subsequently crossed these mice with App/PS1 mice to examine the effects of the *R47H* mutation in relation to Aβ (Cheng-Hathaway et al., 2018). These mice display reduced quantities of dense-cored plaques (Cheng-Hathaway et al., 2018), suggesting an impairment in the ability of microglia to compact plaques. Mice harbouring the R47H point mutation were also demonstrated to have reduced microglial density

and downregulated *Trem2* expression (Xiang et al., 2018). Overall, this suggests that the R47H mutation causes loss-of-function of TREM2. Additionally, TREM2 may have a progression-dependent effect on amyloid burden. A particular study demonstrated that Trem2 deletion has no effect on plaque burden until advanced stages of pathology in 5xFADxTrem2$^{-/-}$ mice (Wang et al., 2016). In 2 month-old APP/PS1-21 mice, Trem2 depletion resulted in reduced plaque size and area, whereas the opposite effect was found in 8 month-old mice (Jay et al., 2017). Therefore, TREM2 may have a greater contribution to Aβ deposition early in pathology, with this effect waning as the disease progresses.

Recently, our lab reported that *App*$^{NL-F}$ mice display upregulated plaque-induced gene expression exclusively in microglia touching plaques, with the *Trem2*^{R47H} mutation ameliorating this effect, suggesting that microglia must touch plaques before *Trem2* gene expression is increased (Wood et al., 2022). This same study showed that *App*$^{NL-F}$/*Trem2*^{R47H} mice exhibit a higher density of plaques in the hippocampus than *App*$^{NL-F}$ mice, driven by a larger number of smaller sized plaques (Wood et al., 2022). Overall, this suggests that a perturbed microglial response in *App*$^{NL-F}$/*Trem2*^{R47H} mice may be affecting plaque clearance. Therefore, microglia may have an essential role for the clearance of smaller plaques, whilst not having much of an effect on larger plaques. Alternatively, the barrier formation function of microglia (Condello et al., 2015) may be lost in these mice, resulting in increased breaking off of smaller plaques from bigger plaques. Therefore, it would be useful in this context to further explore the effects that the *Trem2*^{R47H} mutation has on microglial activation and plaque morphology.

1.5 Models of AD

A fully representative mouse model of AD, which develops plaques that naturally leads to tangles, still does not exist. However, there are hundreds of well-established AD mouse models, many of which that have been developed on the basis of the amyloid hypothesis (McGowan et al., 2006).

1.5.1 Transgenic mouse models

Over the past few decades, transgenic mouse models engineered with the overexpression of AD-related proteins, such as App, PS1 and PS2, Trem2 and ApoE (Hall and Roberson, 2012) have been widely used in AD research. Transgenic mice are generated by random insertion of the transgene into the genome, thereby increasing the copy number of the gene (Chartier-Harlin et al., 1991; Goate et al., 1991). Three isoforms of human *APP* (695, 751 and 770 hAPP) have been used for the generation of transgenic lines. *APP* gene mutations are named after the place of discovery, such as the Indiana (V717F) (Murrell et al., 1991), Swedish (K670N and M671L) (Mullan et al., 1992), London (V717I) (Goate et al., 1991) and Arctic (E693G) (Nilsberth et al., 2001). Table 1 summarises some of the most used transgenic mouse models for the study of AD.

Tg line	**Transgene**	**Promoter**	**Features**	**Reference**
APP23	huAPP$_{751}$ (Swe)	Mouse *Thy-1*	Aβ plaques at 6 mo; gliosis; hippocampal neuronal loss; dystrophic neurites containing hyperphosphorylated tau; spatial memory deficits	(Sturchler-Pierrat et al., 1997)
TgJ20	hAPP$_{770}$ (Swe/Ind)	PDGF	Aβ plaques at 8 mo; gliosis	(Mucke et al., 2000)
TgTASTPM	*PS1:* M146V	*Thy-1*	Aβ plaques at 3-6 months old; gliosis; localised neuron loss	(Howlett et al., 2004)
APP/PS1 Line 85	mo/huAPP$_{695}$ (Swe); Tg huPSEN1 (ΔE9)	Mouse *Prnp*	Aβ plaques at 6 mo; gliosis; impaired memory and learning	(Jankowsky et al., 2004)

APPPS1	huAPP$_{695}$ (Swe); huPSEN1 (L166P)	Mouse *Thy-1*	Aβ plaque deposition from 6 weeks old in the cortex and 3-4 mo in the hippocampus; significant decrease in CSF Aβ1-42 concentrations with age; impaired LTP	(Radde et al., 2006)
5xFAD Tg6799	huAPP$_{695}$ (Swe/Flo/Lon); huPSEN1 (M146 L/L286 V)	Mouse *Thy-1.2*	Aβ plaque deposition from 2 mo; gliosis, downregulation of synaptic markers; impaired LTP and spatial working memory	(Oakley et al., 2006)
hTau.P301S	huMAPT$_{4R0N}$ (P301S)	Mouse *Thy-1.2*	NFTs from 3 mo; gliosis from 5-6 mo; memory deficits from 2.5 mo	(Allen et al., 2002)
3xTg-AD	huAPP$_{695}$ (Swe); MAPT$_{4R0N}$ (P301L); *PSEN1* ^{M146V} knock-in	Mouse *Thy-1*	Aβ plaque deposition from 3-4 mo; gliosis; tau immunoreactivity in hippocampal CA1 neurons but no tau pathology; cognitive impairment from 4 mo	(Oddo et al., 2003b)

Table 1. Summary of the most commonly used transgenic AD mouse models.
Abbreviations: mo, months old; NFTs, neurofibrillarary tangles; LTP, long-term potentiation; Swe, Swedish; Flor, Florida; Lon, London; Ind, Indiana; APP, amyloid precursor protein; PS1, presinilin-1; MAPT, microtubule associated protein tau; AD, Alzheimer's disease.

Throughout the last few decades since their development, these mice have proved highly useful and have been the basis for hundreds of AD-related studies. The 5xFAD model has been particularly popular; these mice carry five mutations in the *App* and *Ps1* transgenes, and develop widespread plaque pathology, gliosis, synaptic degeneration, neuronal loss and cognitive deficits (Oakley et al., 2006).

Whilst no doubt useful, it is important to note that due to random insertion of the transgene, the number of gene copies of *App* is significantly increased, thus App is overexpressed which in turn leads to leads to overproduction of other App fragments in addition to Aβ. This may result in multiple other phenotypes that may not accurately reflect the human disease. Additionally, there are potential extra artefacts related to the random insertion into the genome which may interfere with expression of other unrelated genes, as well as the use of a range of different promoters that result in *App* being expressed at different times and places than would be the case with the *App* promoter. Another key limitation of *App* transgenic models is that there is no model where Aβ plaques naturally lead to tau tangles, making them not fully representative of human AD. This problem was addressed in part by the development of models which also included a *MAPT* tau mutation, such as the 3xTg (Table 1) which overexpresses *App*, *Ps1* and *MAPT* (Oddo et al., 2003b). However, a concern with this is that in humans, the development of tau tangles arises from accumulating Aβ rather than from tau mutations, therefore again these mice are not as comparable with human AD. Overall, transgenic models provide good mechanistic insight into early AD-related pathological mechanisms, but their conclusions should not be over-extrapolated due to the potential confounding effects from *App* overexpression.

1.5.2 App knock-in models

App KI mouse models were first developed in 2014 to overcome the issues associated with transgenic models. These models have an advantage in that

promoter-driven gene expression is used to increase pathogenic levels of Aβ without overexpressing App. Saito and colleagues (Saito et al., 2014) humanised the murine Aβ sequence by replacing three amino acids, and one to three fAD mutations were inserted into the App sequence. These mutations are: the Swedish (KM670/671NL), which increases beta site cleavage of App leading to an increase in Aβ1-40 and -42 levels, the Beyreuther/Iberian (I716F), which alters gamma-cleavage at the C-terminal position, leading to a rise in the ratio of Aβ1-42 to -40, and the Arctic (E693G), which predisposes the oligomerisation of Aβ fibrils (Saito et al., 2014).

Three strains of mice have been generated using this model; *App*^{NL} (harbouring the Swedish mutation), *App*$^{NL-F}$(harbouring the Swedish and Beyreuther/Iberian mutations), and *App*$^{NL-G-F}$(with an additional Arctic mutation) (Fig. 2). Both *App*$^{NL-F}$and *App*$^{NL-G-F}$ models exhibit a progressive rise in amyloidosis, with *App*$^{NL-F}$ mice starting to develop plaques at around 9 months, and *App*$^{NL-G-F}$ at 2 months. Hence, the former is an excellent model for studying early pathological changes, whereas the latter is good for examining advanced, post-plaque alterations in the brain. Microgliosis and astrogliosis have also been observed around plaques, with *App*$^{NL-G-F}$ mice showing increased microglia density in the cortex from 6 months old and the hippocampus from 9 months old, and *App*$^{NL-F}$ displaying microglial alterations from 24 months of age (Benitez et al., 2021). However, there is no evidence of NFTs or neurodegeneration (Saito et al., 2014).

In terms of behaviour, *App*$^{NL-G-F}$ mice display cognitive deficits from around 6 months old (Masuda et al., 2016; Mehla et al., 2019; Sakakibara et al., 2018), as well as exploratory behaviour and memory impairments (Pauls et al., 2021; Whyte et al., 2018). *App*$^{NL-F}$ mice, which represent a slower model of amyloid deposition, show early pre-plaque alterations in paired-pulse ratios (Benitez et al., 2021), synaptic protein levels (Schedin-Weiss et al., 2020) and Morris water maze performance (Shah et al., 2018), but overall exhibit a more modest phenotype compared to *App*$^{NL-G-F}$. Previous work by our lab showed that both models display changes in the frequency of spontaneous excitatory postsynaptic currents during mid- to late-pathology (9 months for *App*$^{NL-G-F}$ and 20 months for *App*$^{NL-F}$). Overall this suggests that early soluble Aβ may initiate certain behavioural and synaptic deficits, perhaps due to its interference with presynaptic

activity. This is supported by a particular study demonstrating that both models have impaired presynaptic protein turnover at 6 months old but not at 12 months old, highlighting the early vulnerability in synapse dynamics (Hark et al., 2021).

Recently, a new *App* KI mouse model with three humanised *APP* mutations (Swedish KM670/671NL, Arctic E693G and Austrian T712I) was developed (APP^{SAA}) (Xia et al., 2021). By 2 months old, these mice have an increased Aβ1-42/40 ratio in the brain, plasma and CSF compared to WTs. Amyloid plaques develop at 4 months old, and follow a pattern of spread consistent with humans (Thal et al., 2002): cortex/hippocampus first, followed by the entorhinal region, amygdala, thalamus and striatum. In particular, these mice demonstrate altered glial responses and increased neurodegeneration markers such as CSF tau and Nfl (Xia et al., 2021).

App KI models have a particular advantage over transgenic models in that they avoid overexpression of *App.* However, these models do have their limitations, in that they do not develop tau tangles, and are therefore only useful to explore early amyloid-related pathology and the effects on the surrounding cellular network. In humans, tau pathology may not emerge for up to two decades (Bateman et al., 2012); therefore, the age to which mice live could be a constraint for observing this effect. It is also important to highlight that App^{NL-G-F} mice are an aggressive model of amyloid pathology, with very early-onset plaque development (from 2 months old) due to the additional Arctic mutation which increases the propensity of Aβ to aggregate (Saito et al., 2014). This is faster than would occur in humans, and additionally unrepresentative of human AD, as this combination of fAD mutations has not been identified. However, these mice are very useful for quickly and cheaply observing the initial effects of Aβ, and they also display altered glial responses, and are therefore a good model for the present work. App^{NL-F} mice are arguably more representative of human AD due to a slower rate of amyloid deposition, but present time and cost constraints in that they do not develop plaques until 9 months old, and do not show significant glial alterations until later on in pathology (Benitez et al., 2021; Saito et al., 2014). However, these models remain useful for identifying Aβ pathogenesis and early biomarkers.

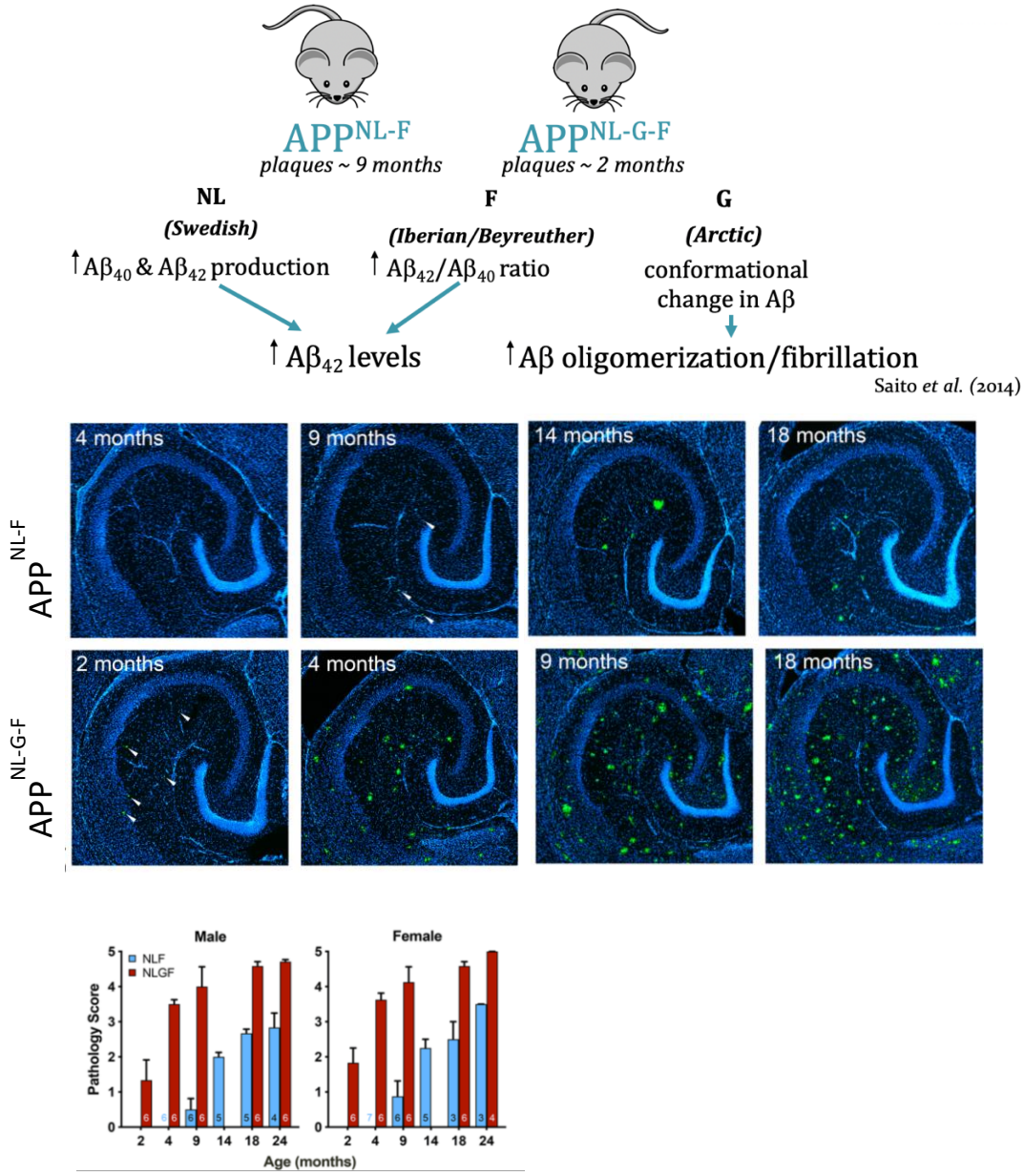

Figure 2. **Plaque pathology over time in *App*$^{NL-F}$ and *App*$^{NL-G-F}$ mice.** The predisposition towards early plaque deposition results in a different insoluble/soluble Aβ equilibrium compared with *App*$^{NL-F}$ mice. Both mouse models develop amyloid plaques but no evidence of tau pathology, with *App*$^{NL-G-F}$ mice developing plaques at 2 months, and *App*$^{NL-F}$ developing plaques at around 9 months (Saito et al., 2014). Plaques were detected using LCOs (green) in the hippocampus of (A) *App*$^{NL-F}$ and (B) *App*$^{NL-G-F}$ mice. DAPI (blue) was used as a nuclear counterstain. (C) Plaque pathology scores in male and female *App*$^{NL-F}$ and *App*$^{NL-G-F}$ mice. Figure adapted from Benitez et al. (2021).

1.5.3 Cellular models

1.5.3.1 Induced pluripotent stem cells

Induced pluripotent stem cells (iPSCs) are pluripotent stem cells derived from adult somatic cells. Cells can be generated from a patient with a specific genotype or phenotype of interest, and then differentiated into a target cell type, such as neurons or glia. In this way, *in vitro* models with the patient's specific genome can be used for study into the precise disease mechanism of interest. For example, iPSCs have been widely used to assess cellular mechanisms in AD, including in neurons (Israel et al., 2012), astrocytes (Oksanen et al., 2017) and microglia (Reich et al., 2020). iPSCs derived from AD-linked mutations in *PS1* and *PS2* have shown that much like neurons derived from sAD patients, they have greater vulnerability to Aβ-induced toxicity and oxidative stress compared to cells from healthy controls (Ochalek et al., 2017). Additionally, glutamatergic neurons expressing mutated APP^{V717I} showed altered subcellular distribution of APP and cleavage of β- and γ-secretases, demonstrating the mechanism underlying the perturbed Aβ production in these cells (Muratore et al., 2014).

iPSCs can also be differentiated into microglia-like cells, allowing for the study of microglia in health and disease. For example, iPSC-derived microglia-like cells from patients with *TREM2* mutations demonstrated reduced *TREM2* expression and secretion, and impairments in phagocytosis and cytokine release and migration (Garcia-Reitboeck et al., 2018)**.** A further study showed that mutant *TREM2* in these cells experienced abnormal accumulation, proteolysis and trafficking (Brownjohn et al., 2018). Such studies no doubt provide valuable insight into disease mechanisms in human-specific cells.

This technique has been revolutionary in recent years, by allowing for an endless supply of human cells expressing disease-causing genes. iPSCs also have a significant advantage over animal models in that they don't have exogenous gene expression, and therefore are more genetically representative of humans. However, some concerns lie in that iPSCs are 'rejuvenated' and don't reflect the age of the donor (Lee et al., 2020). An additional key limitation of studying just one cell type is that interactions across multiple cell types can't be examined; therefore, a new '3D culture' system was recently developed, whereby iPSC-

derived neurons, astrocytes and immortalised human microglia were co-cultured. The authors found that this system successfully recapitulates AD phenotypes, including Aβ aggregation, phosphorylated tau and neuroinflammation (Park et al., 2018).

1.5.3.2 Organotypic hippocampal slice culture

The hippocampus is one of the earliest and most-affected areas in AD and is therefore a critical area to investigate (Davies et al., 1988). Primary cell culture systems allow for easy manipulation and examination of hippocampal cells, but are not fully representative of the internal environment of an animal due to the lack of other cell types. Organotypic hippocampal slice culture (OHSC), where whole hippocampal brain sections are cultured, represents a three-dimensional cell culture technique that maintains the structural integrity of hippocampal networks, including glial cells, providing a more *in vivo*-like environment compared with primary cell culture (Stoppini et al., 1991). An additional advantage is that many brain slices can be obtained from one animal, with each subjected to separate testing conditions, thereby reducing the numbers of animals required. Brain slices are typically obtained from young postnatal animals (<P7) because of improved morphology and survival of up to several months. Once cut, slices are cultured for 10-14 days before treatment, to allow them to 'recover' from the slicing process, which typically results in activated microglia, astrogliosis, and an excess release of glutamate and inflammatory factors due to tissue injury.

OHSCs have been applied to the study of Aβ. Acute slices from AD transgenic mice are widely used for electrophysiology, and have demonstrated Aβ-associated synaptic alterations (Cummings et al., 2015). In terms of cell culture, many groups have attempted to model Aβ plaque deposition using slices from transgenic AD mouse models, however with limited success. Slices simply cultured without external manipulation do not develop amyloid plaques; for example, OHSCs from TgCRND8 mice did not develop plaques even after 4 months in culture (longer than it would take in the living mouse) (Harwell and Coleman, 2016), and cultures from 3xTg-AD pups demonstrated increased Aβ1-42 levels after only 4 weeks in culture, however also in the absence of Aβ

deposition (Croft et al., 2017). However, one study in 2016 demonstrated that application of exogenous Aβ, obtained from *App23* or *App/PS1* brain homogenate plus synthetic Aβ1-40, resulted in OHSCs developing plaques after 10 weeks in culture (Novotny et al., 2016). If replicable, the potential application of this model is vast, as amyloid aggregation dynamics could be visualised with ease. Numerous studies have also tried applying OHSC to sections from adult AD mice, who already bear plaques, but there is limited neuronal survival (Humpel, 2015b), with only 5-10% of cultures surviving a month in culture (Staal et al., 2011; Su et al., 2011). This may be due to greater vulnerability to the culture environment or reduced plasticity compared with slices from younger mice.

Although it is difficult to assess plaque growth in OHSCs, they may prove useful to assess other features of AD, such as tau pathology, neuroinflammation, synapse loss and gliosis. The study of tau has been particularly successful, as multiple AD models have shown that tau pathology occurs faster *in vitro* compared to *in vivo*. OHSCs from JNPL3 and hTau mice develop phosphorylated tau at just 2 weeks in culture (Duff et al., 2002) compared to *in vivo* at 5 or 6 months, respectively (Andorfer et al., 2003). Additionally, OHSCs from 3xTg-AD mice show tau phosphorylation at 4 weeks in culture compared to 12-15 months old *in vivo* (Oddo et al., 2003a; Oddo et al., 2003b). Recently, using rAAVs to express mutant *MAPT* in OHSCs resulted the formation of tau inclusions followed by cell loss (Croft et al., 2019). In this context, OHSCs provide an efficient and simple way of assessing tau dynamics. Additionally, OHSCs may be useful to study neuroinflammation and glial responses because they retain all the cell types of the CNS. Aβ-treated OHSCs have been used to examine the effects of anti-inflammatory compounds against loss of serotonergic, cholinergic and dopaminergic neurons (Hochstrasser et al., 2013). In terms of glia, studies have used cultured brain slices to assess astrocyte response to Aβ (Xu et al., 1999), the role of microglia in plaque clearance (Hellwig et al., 2015b), Trem2 (Mazaheri et al., 2017) and ApoE (Marksteiner and Humpel, 2008). These studies highlight how OHSCs offer the ease of *in vitro* approaches whilst maintaining the cellular network of the intact brain, and can provide insight into the molecular mechanisms underlying neurodegenerative pathologies.

1.6 Neurochemical tools to probe AD pathology

1.6.1 Fluorescent amyloid imaging

Plaques are commonly visualised by chemical staining involving Th or IHC. Fluorescent microscopy strategies allow for multiplexed imaging of plaques. Moreover, new amyloid-specific probes (LCOs) allow delineation of structural aspects of polymorphic plaque pathology. LCOs bind to the beta-pleated sheet of amyloid fibrils (and other aggregated structures) and display spectral differences based on the twisting of the flexible LCO backbone (Aslund et al., 2009; Klingstedt et al., 2011). Upon binding, LCOs adopt a more planar arrangement and undergo a change in effective conjugation, and subsequently emit a shift in excitation/emission, which can be detected by hyperspectral imaging (a combination of light microscopy and spectroscopy), whereby a spectral detector collects spectrally separated emission light for every pixel within an image. This technique is particularly useful for analysis of overlapping fluorophores leading to signal bleed-through, and also allows for high-speed acquisition of multiple spectral profiles at the same time. LCOs have been shown to bind more accurately to pathological protein aggregates compared to standard amyloid dyes, and can also be used to determine aggregate morphology (Magnusson et al., 2014). Indeed, a particular study in APP/PS1 and APP23 mice demonstrated that LCOs can distinguish differences in Aβ plaque structure between genotypes (Heilbronner et al., 2013), highlighting the value of LCOs in elucidating plaque morphology.

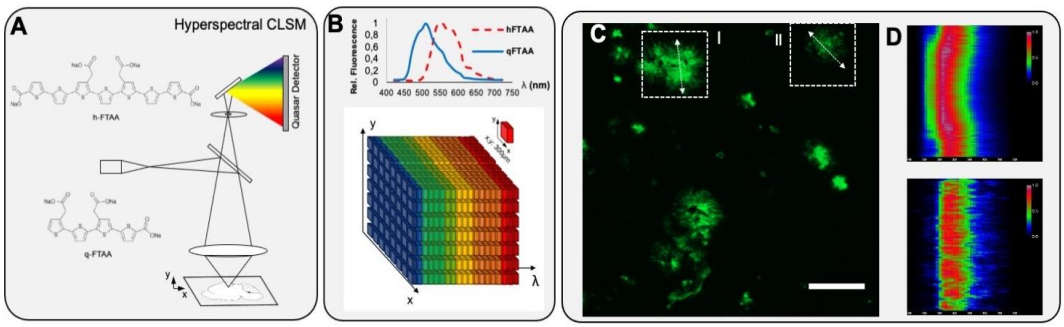

Figure 3. Principles of LCO imaging.

(A) Staining for LCOs (qFTAA and hFTAA). qFTAA binds preferentially to more mature fibrils, whereas hFTAA recognises both mature and immature, prefibrillar Aβ. (B) The LCO probes have different emission properties that are delineated by CLSM using a spectral detector providing a continuous emission spectrum (32+2 channels) with each pixel generating a lambda stack. (C,D) The shift in emission spectra is illustrated in normalised intensity map of line scans across the plan ROI, showing a characteristic blue-shift across the core.

Abbreviations: qFTAA, quadro-formyl thiophene acetic acid; hFTAA, heptameric formyl thiophene acetic acid; LCOs, luminescent conjugated oligothiophenes; CLSM, confocal laser scanning microscopy. *Figure adapted from (Michno et al., 2021).*

1.6.2 Mass spectrometry in AD

The best therapeutic window for anti-AD drugs would be right at the start of the disease, before too many Aβ plaques have had a chance to grow and create damage to the surrounding neuronal network; however, this is almost impossible due to cognitive symptoms only appearing years after disease onset (Bateman et al., 2012). AD mouse models are a good way of observing these early mechanisms; however, until recently, there has been a lack of imaging techniques with the appropriate spatial resolution, specificity and sensitivity to measure early Aβ processes on a subcellular level.

Mass spectrometry (MS) has recently been increasingly used in bioanalytical science, particularly in proteomics (Aebersold and Mann, 2003). The introduction of soft ionisation techniques such as matrix-assisted laser desorption ionisation (MALDI) (Karas and Hillenkamp, 1988) and electrospray ionisation (ESI) (Fenn et al., 1989) MS enabled fast, sensitive and chemically specific detection of intact large biomolecules. Today, MS is the key technique for protein and peptide identification, characterisation and quantification, and is highly used for clinical screening of metabolites and proteins in blood, CSF and tissue.

Studies using MS have been instrumental for the identification of novel AD biomarkers and key pathogenic species involved in AD, such as Aβ and tau proteoforms (Goedert et al., 1989; Portelius et al., 2006). MS studies in whole-brain extracts of AD patients have revealed that sAD, fAD and cognitively unaffected but amyloid-positive (CU-AP) patients have similar overall Aβ proteoform profiles, but may have differences in Aβ proteoform quantities. For

example, even though both AD and CU-AP patients have Aβ1-40 and -42 peptides, MALDI-MS revealed that the former have a higher portion of Aβ1-40 and lower portion of Aβ1-42, compared with the latter (Gkanatsiou et al., 2019). A study in whole-brain extracts from cerebellum, cortex and hippocampus of sAD and fAD (with Swedish and *PS1* mutations) cases revealed multiple C- and N-terminally truncated Aβ proteoforms, but overall no significant differences in Aβ proteoform coverage patterns between the two groups (Portelius et al., 2010), highlighting the overlapping amyloid profiles of these two diseases.

However, much of MS-based proteomic work has been conducted on whole plaques extracted and purified from brain samples, therefore individual plaque composition cannot be determined. Additionally, a major limitation in proteomics is that there is a lack of spatial information in regard to analyte localisation. Given the intricacies of the CNS, it remains critical to understand precise protein and peptide distribution in AD, to understand region-specific roles and vulnerabilities. Furthermore, analysis into peptide composition at the single-plaque level may provide additional insight into how Aβ aggregates and deposits.

1.6.3 Mass spectrometry-based imaging

Recent advances in imaging technologies such as imaging mass spectrometry (IMS) greatly increase the resolution of such events. IMS is a powerful chemical imaging technique that can be used to measure Aβ patterns at single plaque resolution (Carlred et al., 2016; Kakuda et al., 2017; Kaya et al., 2018; Michno et al., 2018; Michno et al., 2019a). This involves collecting mass spectra at defined pixel-by-pixel points across a sample, and the resulting spectral peak for the molecule of interest is then used to map its distribution across the sample. The image integrity is assessed by overlaying it with a consecutive brain section that has been subjected to immunohistochemistry or staining, allowing for comparison of molecule distribution (Miura et al., 2010). In this way, the lipid, protein and peptide species and localisation can be identified *in situ* with high chemical specificity (Hanrieder et al., 2015; Hanrieder et al., 2013).

IMS allows for visualisation and analysis of hundreds of molecules at the same time, whilst providing spatial information that traditional MS methods do not. A

particular advantage of IMS is that prior visualisation of the target protein (e.g. using antibodies) isn't required, and therefore binding/specificity issues are avoided. Furthermore, the samples require minimal preparation and treatment. However, despite advantages in high spatial resolution and molecular specificity, IMS has its limitations. Whilst there certainly is a possibility to simultaneously detect many classes of metabolites, ion suppression may occur, whereby each metabolite impairs the desorption and ionisation efficiency of every other molecule (Chughtai and Heeren, 2010). As a result, more abundant metabolites are selectively ionised, leading to increased signal from high-abundance metabolites. Another disadvantage comes from the sample preparation itself, whereby thawing the tissue can lead to degradation of analytes that are not stable at room temperature, thus skewing the results (Chughtai and Heeren, 2010).

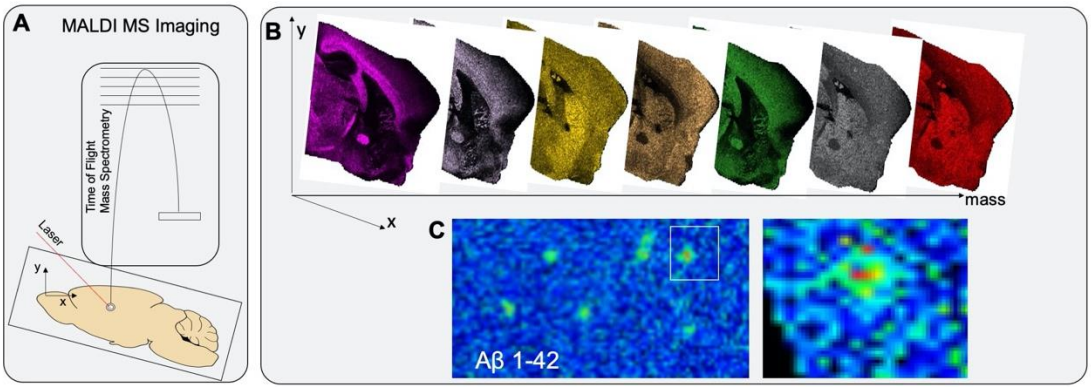

Figure 4. Workflow of MALDI-IMS. (A) The tissue of interest is sectioned and mounted onto a special glass slide, followed by precoating with a matrix before subject to scanning with a laser probe. Ionisation generates larger intact molecular species, including peptides and proteins. (B) MALDI single ion images outline different Aβ isotopologues across the brain at the single plaque level. (C) Here, total ^{15}N-Aβ1-42 [Σ mass/charge ratio (*m*/*z*) 4450 to 4465] localizes predominantly to the plaque core.

Abbreviations: MALDI-IMS, matrix-assisted laser desorption/ionisation imaging mass spectrometry.

In AD research, IMS is becoming a popular method to elucidate plaque-associated protein, lipid and metabolite profiles. Two main IMS systems have been applied: Time-of-Flight Secondary Ion Mass Spectrometry (TOF-SIMS) and Matrix-Assisted Laser Desorption/Ionisation (MALDI)-IMS. For MALDI-IMS, a

special matrix is applied to the sample, followed by desorption/ionisation of the sample with a laser beam (Buchberger et al., 2018), whereby accelerated ions fly towards the detector and the flying time (and *m/z*) is calculated, on the principle that ions with a lower mass have a shorter time of flight compared to heavier ones. For a typical MALDI-IMS workflow, see Fig. 4.

Such studies have yielded useful information about the composition of plaques in AD. The very first application of IMS for analysis of individual plaques showed that Aβ proteoforms were both N- and C-terminally truncated in senile plaques and leptomeningeal CAA (Kakuda et al., 2017). A recent study revealed that Aβ4-42 and Aβ1-42, are the primary species in both cored and diffuse sAD and CU-AP plaques, and that Aβ1-40 was present in highly cored plaques (Michno et al., 2019a). Additionally, diffuse plaques in sAD contained 3pE-42 as compared to diffuse plaques CU-AP patients. This suggests a hydrophobic functionalization of Aβ1-42 specific to AD plaque pathology that enables deposition of less aggregation prone Ab species incl 1-40 upon plaque maturation into cored plaques (Michno et al., 2019a).

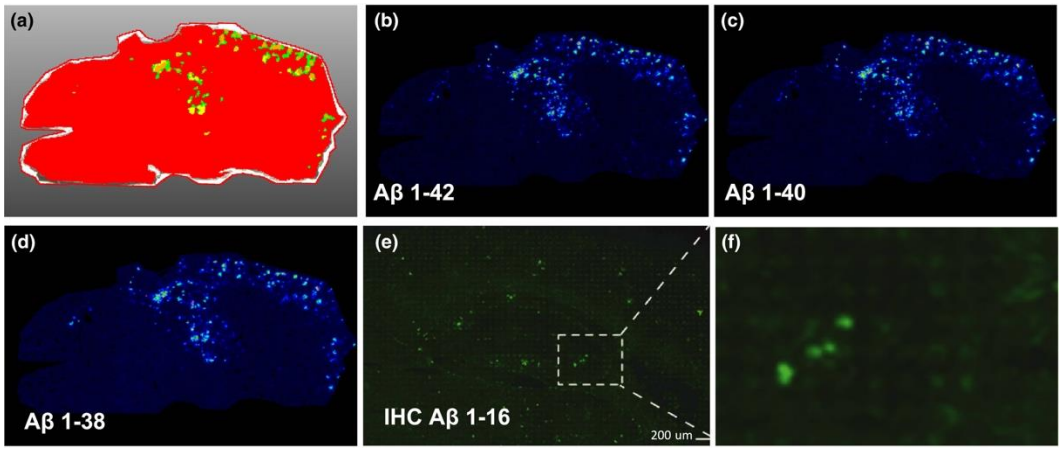

Figure 5. MALDI-IMS of multiple amyloid species in 18 month-old tgAPPArcSwe transgenic AD mice. (a) Hierarchical cluster analysis shows histological features resembling plaque pathology (yellow, green). (b-d) Examination of variables in the clusters reveals various Aβ species within brain sections. (e, f) Aβ-antibody staining on the same section confirms the localisation of Aβ plaques. *Figure adapted from (Carlred et al., 2016).*

Abbreviations: MALDI-IMS, matrix-assisted laser desorption/ionisation imaging mass spectrometry; Aβ, amyloid-beta; IHC, immunohistochemistry.

Other methods of mass spectrometry are also continuously being developed, and providing further high-resolution insight into AD. The newly developed synaptometry by time-of-flight (SynTOF) (Gajera et al., 2021; Gajera et al., 2019) utilises single-synapse analysis combined with mass cytometry to characterise up to millions of individual synapses. Interestingly, human AD synapses contain little Aβ, in contrast to *App* transgenic mouse models (Phongpreecha et al., 2021), emphasising that despite the significant advances that have been made in developing more representative AD mouse models, there remains some key differences with humans.

1.6.4 Spatial and temporal assessment of protein dynamics using metabolic labelling

The current neurochemical tools, including MS, used to understand AD pathology are commonly limited to static analysis and do not provide insights on protein dynamics. This is critical, as AD pathology and amyloid plaque formation specifically, are highly dynamic processes that are difficult to capture with time course experiments based on repetitive sampling of either clinical samples or collecting mice at different timepoints. These limitations can be overcome by *in vivo* labelling (metabolic labelling) with stable isotopes in combination with MS techniques (Oda et al., 1999).

Stable isotopes (such as ^{15}N) have the same number of protons but a different number of neutrons as common elements (such as ^{14}N), which results in the same physical properties but a difference in mass and can hence be distinguished in mass spectrometry. Here, stable isotopes (e.g. ^{15}N, ^{13}C, ^{18}O or ^{2}D) are provided systemically by infusion or diet and incorporated into newly synthesized proteins (i.e. metabolic labelling).

MS and metabolic stable isotope labelling (SIL) was introduced 20 years ago (Oda et al., 1999) and most prominently used for cell culture, termed ‘stable isotope labelling by amino acids in cell culture’ (SILAC) (Ong et al., 2002). Similarly, this approach has been introduced to mammalian organisms termed ‘stable isotope labelling in mammals’, or ‘SILAM’), whereby fractionally heavier, non-radioactive isotopes of natural elements (e.g. ^{15}N, ^{13}C, ^{2}H) are introduced

into the amino acid structure that is supplemented into the mouse feed, which then uniformly labels the proteome of all newly synthesised proteins. By having a feeding (‘pulse’) period followed by a rest (‘chase’) period, later ‘heavy’ form of the proteins can be differentiated from the earlier endogenous unlabelled ‘light’ proteins by MS (McClatchy et al., 2007; McClatchy and Yates, 2008, 2014).

A very elegant SIL strategy has been developed for following protein kinetics *ex vivo* in AD pathology, termed ‘stable isotope labelling kinetics’ (SILK). Importantly, SILK was successfully introduced for probing Aβ and tau turnover in CSF from AD patients, revealing significant insights on protein clearance impairment associated with AD pathology (Bateman et al., 2006a). In detail, SILK was used to measure the turnover of proteins such as Aβ, tau and APOE. In these pioneering studies, labelled amino acids (such as $^{13}C_6$) can be safely administered to AD patients and then serially measured from blood or CSF (Bateman et al., 2006b; Paterson et al., 2019; Wildsmith et al., 2012). This provides dynamic measures of protein production and clearance, giving a more detailed overview of the mechanisms underlying alterations of biomarker levels in AD (Patterson et al., 2015; Potter et al., 2013). A SILK assessment into Aβ1-38, -40 and -42 kinetics demonstrated a general decline in Aβ turnover rate with age (Patterson et al., 2015). Additionally, Aβ1-38 and -40 had similar kinetics regardless of amyloid-PET Aβ status in the individual, whereas soluble Aβ1-42 was increased in Aβ-positive patients. Other variables such as how pharmacotherapies or sleep affects Aβ clearance rates have also been assessed. A SILK study assessing daily Aβ1-40 and -42 fluctuations demonstrated an early age-associated loss of Aβ1-42 day/night levels, and a decline in Aβ1-42 over time in amyloid-negative individuals; however, this effect was lost in those with amyloidosis (Lucey et al., 2018). This indicates that amyloid deposition affects the dynamic equilibrium of Aβ1-42, which subsequently affects the sleep-wake cycle. Overall this highlights how SILK allows for the assessment of peptide activity over time, providing valuable insight into the nature of how Aβ behaves in health and disease.

SILK has also been applied to cell culture, termed ‘stable isotope labelling with amino acids in cell culture’ (SILAC). In such experiments, typically $^{13}C_6$-leucine is incorporated into newly synthesised proteins to understand protein kinetics. In

iPSC neurons, disease-associated tau species showed increased turnover (Sato et al., 2018), suggesting that proteostasis differs according to peptide species. In terms of Aβ, SILAC has been used to compare Aβ-treated cells with control cells to then assess alterations in protein levels (Andrew et al., 2019; Correani et al., 2017). A particular advantage of SILAC is that the role of a specific cell type can be directly examined, as opposed to *in vivo* where many other cell types may have an influencing factor. However, this is also a limitation, as the lack of other cell types means that the complex brain environment is not recapitulated.

Very importantly, SIL has already been applied to AD mouse models, with promising results. At shorter labelling periods, chimeric proteins consisting of both ^{15}N and ^{14}N atoms dominate the brain proteome (Savas et al., 2016), impairing the ability to assess global protein lifetimes. This is because chimeric proteins are difficult to identify by MS due to their broadened isotopic envelope, due to the fact that the cut-off for protein detection in MALDI is typically 20kDa in linear TOF mode, and 6kDa in reflector TOF mode. Small proteins above 6kDa can only be detected in linear mode. However, at this m/z the mass resolution is too poor to quantify label incorporation due to peak broadening. Therefore, extended pulse/chase periods are recommended. Indeed, a previous ^{15}N study in WT mice demonstrated a three-fold reduction in the number of measured proteins after a 1- or 2-month chase, compared to very long or short chase periods (Savas et al., 2016). In *App* KI mice, SILK demonstrated that 6 month-old *App*$^{NL-F}$ and *App*$^{NL-G-F}$ had significantly increased synaptic protein levels compared to *App*^{NL} controls, whereas by 12 months, those elevated protein levels were decreased relative to *App*^{NL}. (Hark et al., 2021). This suggests that *App* KI mice display early vulnerability to synaptic pathology, but as synapses degenerate, alterations in protein expression levels occur again. Overall, this highlights how SILK can be used to effectively measure protein dynamics over time.

While these studies no doubt provide significant insight into protein turnover dynamics, there is a lack of information about spatial isotope incorporation; however, chemical imaging technologies such as IMS can increase the resolution of these events. The localisation of plaque-associated peptides and lipids can also be assessed in this way (Kaya et al., 2017a; Michno et al., 2018; Michno et

al., 2019e). These results can be validated by parallel experiments involving amyloid staining of the brain section, followed by laser microdissection of the plaques and immunoprecipitation to purify Aβ. Samples are then analysed by MALDI-MS for assessment of the molecular composition of the plaque and further verification of IMS findings.

SILK combined with MALDI-IMS allows for visualisation of old versus new protein based on the spectral peaks for heavier vs. light proteins, e.g. ^{14}N versus ^{15}N, and therefore the pattern of Aβ deposition over time can be determined. Here in our lab, we applied metabolic isotope labelling to *App*$^{NL-G-F}$ mice to determine spatial plaque growth dynamics. Using MALDI-IMS to assess amyloid aggregation at the single plaque level, we found that Aβ1-42 deposits first, forming an initial core followed by later secretion and deposition of Aβ1-38. Additionally, usage of pulse/chase feeding regimes allowed us to determine that plaques formed in the cortex prior to the hippocampus, providing useful temporal and spatial information about plaque growth (Michno et al., 2021).

Taken together, Aβ pathogenesis is a highly complex event, involving morphologically heterogeneous plaques, structural polymorphism of Aβ fibrils, and intricate effects on the surrounding cellular network. Therefore, it is important to utilise new technologies to explore this at a high resolution. Being able to run animal and human SILK studies in parallel will no doubt provide invaluable information not only about the efficacy of the technique itself, but also about how newly formed Aβ behaves.

1.7 Summary and the present study

In AD, the precise dynamics of how amyloid plaques form, which Aβ species they are composed of, and what their effect is on the surrounding environment remain unclear. This may be why drugs targeting amyloid have consistently failed clinical trials. However, significant previous evidence has implicated soluble and insoluble Aβ and gliosis as key players in AD. The chemical imaging techniques in this project remain novel; therefore, being able to use the latest techniques to elucidate single plaques at an ultrastructural and nanometre level represents a

critical step towards our understanding of disease pathogenesis. Additionally, the development of isotope labelling of proteins followed by high-resolution imaging of such isotopes opens up the possibilities for measuring spatial protein turnover kinetics in tissue. This will also provide information for future human studies using the same techniques, and serve as a trial for methods of tissue analysis that are currently being applied to human samples.

Compared with transgenic mice, *App* KI mice are arguably more representative of human AD due to the knock-in of humanised fAD mutations. In *App*$^{NL\text{-}G\text{-}F}$ mice, the predisposition towards Aβ fibrillation and early plaque deposition results in a different insoluble/soluble Aβ equilibrium compared with *App*$^{NL\text{-}F}$ mice, but also alterations in microglial and synaptic changes (Benitez et al., 2021). Therefore, this project will not only characterise plaque polymorphism and how it relates to the timeline of pathology, but also compare gliosis between the two lines to understand why cellular responses are affected by the balance of insoluble and soluble Aβ.

Therefore, the primary aim of this study was to characterise plaque deposition at the single plaque level and assess potential changes in microglia number and activation. These changes were compared in a model of slow deposition in old age (*AppP*$^{NL\text{-}F}$) with a model where Aβ is structurally changed to more rapidly deposit (*App*$^{NL\text{-}G\text{-}F}$), at both early and late stages of pathology (4 and 18 months for *App*$^{NL\text{-}G\text{-}F}$; 9 and 18 months for APP$^{NL\text{-}F}$). Additionally, as the R47H mutation of the *TREM2* gene has recently been identified as a risk factor for AD and a key player in plaque deposition, microgliosis was assessed in *App*$^{NL\text{-}F}$ mice harbouring the *Trem2*^{R47H} mutation. A secondary aim was to develop an OHSC model in parallel from *App* KI neonatal mice that develops Aβ plaque-like pathology, to determine the pattern of Aβ deposition in an *in vitro* model.

Chapter 2: Materials and Methods

2.1 Animals

All animal experiments were performed in accordance with animal protocols authorised by the UK Home Office Animals (Scientific Procedures) Act 1986 regulations and with local ethical approval. Mice were housed in cages of up to five in individually ventilated cages at the Biological Services Central and Cruciform Units of University College London. Mice were housed under a 12/12 h light/dark cycle with controlled temperature and humidity, and given food and water *ad libitum*.

For OHSCs, P5-7 *App*$^{NL-G-F}$, *App*$^{NL-F}$ and WT C57Bl/6J control pups of either gender were used. For iSILK experiments, male homozygous *App*$^{NL-G-F}$ (ranging from 6-17 weeks old) and *App*$^{NL-F}$ (from 6-18 months old) were used. For imaging experiments, male homozygous *App* KI mice (*App*$^{NL-G-F}$ and *App*$^{NL-F}$), mice homozygous for both APP^{NL-F} and the TREM2^{R47H} mutation (*App*$^{NL-F}$/*Trem2*^{R47H}), or age-matched WT C57Bl/6J control mice were used. *Trem2*^{R47H} mice were obtained from the Jackson Laboratory which were subsequently crossed in-house with *App*$^{NL-F}$ mice. *App* KI mice were a gift from the Saido group, who originally developed the model (Saito et al., 2014). For imaging experiments, mice aged 4, 9 and 18 months old were used.

2.2 Metabolic labelling

For iSILK experiments, male homozygous *App*$^{NL-G-F}$ mice (n=3/condition) were fed a ^{15}N-labelled diet comprised of ^{15}N-labelled algae protein (spirulina) that upon digestion serves as amino acid precursor for protein synthesis(cat. no. MLK-SPIRULINA-N, Cambridge Isotopes Ltd., Leicestershire, UK). This was mixed 1:3 with standard chow, with the following labelling schemes:

Scheme 1: 10-week PULSE (weeks 7 – 17), no CHASE
Scheme 2: 4-week PULSE (weeks 6 – 10), 7-week CHASE

Scheme 2b: 4-week PULSE (weeks 6 – 10), 4-week CHASE
Scheme 2c: 4-week PULSE (weeks 6 – 10), 10-week CHASE
Scheme 3: 4-week PULSE (weeks 10 – 14), 4-week CHASE

This time period was chosen as it is a sufficient window to label the first seeds of Aβ until small plaques have formed.

For *App*$^{NL-F}$ mice, males were fed the same ^{15}N-labelled diet as above but from 6-10 months of age (n=3) or from 6-10 months followed by a 6-month chase period (n=4). A brief overview of factors to consider during metabolic labelling is provided below (Fig. 6).

Age-matched WT control animals (n=3) for each scheme received control ^{14}N spirulina diet also mixed 1:3 with standard chow.

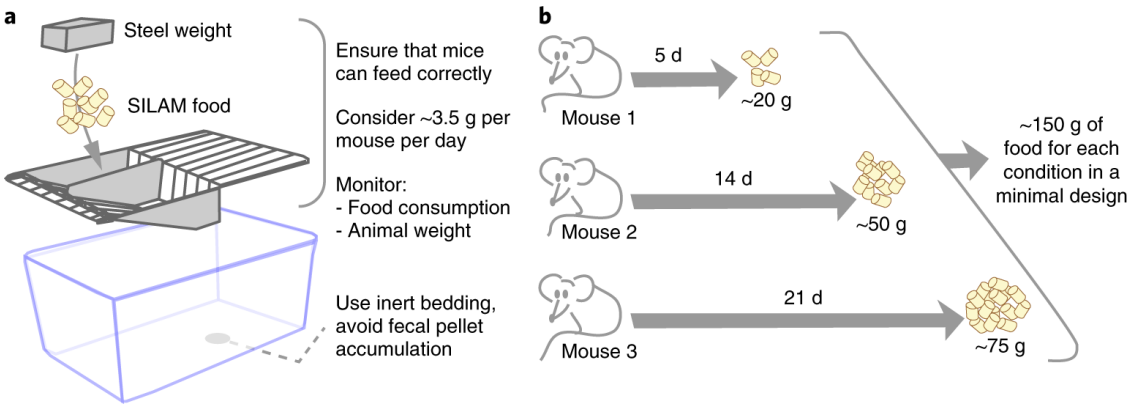

Figure 6. Schematic of metabolic labelling and factors to consider.
(a) Mice should have easy access to pellets; this can be achieved either through a steel weight on top of the food, or by placing food directly in the cage in bowls suspended from the steel bars above. Food consumption and animal weight should be recorded throughout the experiment, to ensure adequate food intake. Bedding should be changed regularly to avoid mouse consumption of fecal pellets, which can interfere with labelling. Calculate approx. 3.5 g food/mouse/day. (b) Estimated food consumption for a short experimental design. *Figure taken from (Alevra et al., 2019).*

2.3 Preparation of mouse tissue

For imaging experiments, mice were killed by decapitation and the brain was rapidly extracted on ice. One hemisphere was snap-frozen on dry ice and stored at -80°C for future use; the other was drop-fixed in 4% paraformaldehyde solution and stored at 4°C overnight, followed by washing three times with 0.01 M PBS and then storage in PBS with 30% sucrose and 0.03% sodium azide at 4°C until ready for IHC and imaging.

^{15}N-fed and control mice were decapitated, and the brain was rapidly removed on ice and hemisected. One hemisphere was snap-frozen immediately in liquid nitrogen-cooled isopentane, and stored at -80 °C until use. The other hemisphere was dissected into anatomical regions and drop-fixed in 4% paraformaldehyde at 4°C, after which the tissue was subjected to further processing at the University of Gothenburg for electron microscopy or nanoSIMS as described in (Michno et al., 2019b).

2.4 Preparation of OHSCs

OHSCs were prepared from pups according to the interface method (Stoppini et al., 1991), with slight modifications (Fig. 7). All procedures were performed under sterile conditions. Briefly, pups were killed by decapitation, following which the brain was rapidly removed on ice, hemisected and cut transverse to the long axis of the hippocampus. Brains were glued down (Loctite) on the cut side onto a vibratome stage and flooded with ice-cold slicing buffer consisting of Earle's Balanced Salt Solution (EBSS; Gibco-Invitrogen) and 1M Hepes (Sigma-Aldrich). Slices (300 µm thick; average six per pup) were obtained using a vibratome (Campden Instruments), using sterile syringe needles to dissect out the hippocampus. Using a sterile glass dropper, each hippocampal slice was placed onto a section of 0.45 µm semipermeable membrane termed 'confetti' (Millipore), of which up to three were then placed on a 0.4 µm culture plate insert (Millipore) in six-well plates. Each well contained 1 ml pre-warmed culture mediµ (pH 7.25, 315 mOsm/l), comprising 50% Minimum Essential Medium plus Glutamax-1, 25% horse serum, 18% EBSS, 5% EBSS plus 0.72 M D-glucose, 50 units/ml penicillin/streptomycin (all from Gibco-Invitrogen), and 6.25 units/ml nystatin (Sigma-Aldrich). The medium was completely changed 1 h after slicing to remove any excess glutamate produced after slice injury. For untreated slices, 50%

medium was replaced once a week to allow for both Aβ accumulation and adequate delivery of nutrients (Harwell and Coleman, 2016). For seeding experiments, media was replenished three times a week. Slices were cultured for up to 16 weeks at 37°C in 5% CO_2.

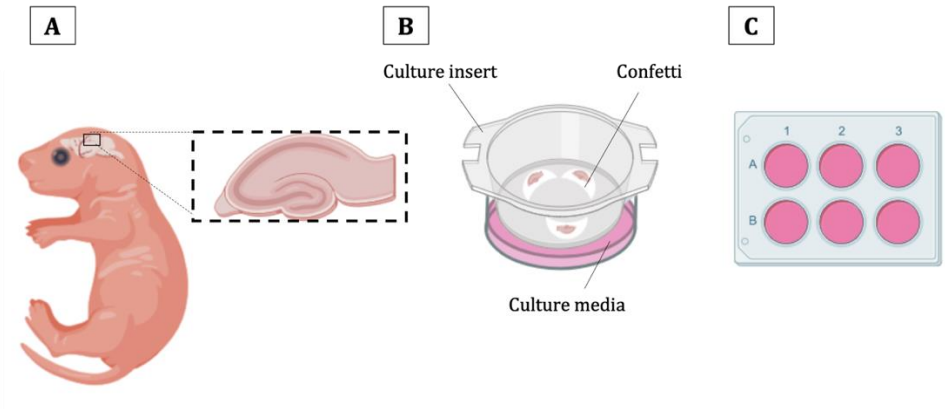

Figure 7. Preparation of organotypic hippocampal slice cultures.
(A) Hippocampal slices (300-µm thick) are sectioned from P5-7 mouse pups using a vibratome. (B) Each culture insert rests on 1 ml culture medium in a six-well plate. (C) Slices are cultured for the desired length of time at 37°C in 5% CO_2.

2.5 Seeding experiments

Aβ seeding experiments were performed on OHSCs prepared from P5-7 *App*$^{NL-G-F}$, APP^{NL-F} and WT pups. A previous protocol was used, with slight modifications (Novotny et al., 2016). Slices were maintained in culture for 10 days before manipulation, to allow time for them to recover from the slicing process (Fig. 5). OHSCs were treated with brain homogenate from older animals bearing plaques, or synthetic Aβ1-40 or Aβ1-42 peptide, or a combination of all three (Table 2).

OHSC genotype	Brain homogenate	Peptide added
***App*$^{NL-G-F}$**	From aged *App*$^{NL-G-F}$	None
	None	Aβ1-42
	From aged *App*$^{NL-G-F}$	Aβ1-42
	TASTPM	Aβ1-40
		Aβ1-42
WT	From aged *App*$^{NL-G-F}$	None
	None	Aβ1-42
	From aged *App*$^{NL-G-F}$	Aβ1-40
	From aged *App*$^{NL-G-F}$	Aβ1-42
	None	Aβ1-40 and Aβ1-42
	TASTPM	Aβ1-40
		Aβ1-42

Table 2. Aβ seeding schemes for organotypic hippocampal slice cultures.
Combinations of treatment of OHSCs, using brain homogenate from older plaque-bearing mice and synthetic peptide (1.5 µm).
Abbreviations: OHSC, organotypic hippocampal slice culture; WT, wild-type.

2.5.1 Adding brain homogenate from older animals

Brain homogenate was obtained from either homozygous *App*$^{NL-G-F}$ animals aged 12 months and above, or heterozygous TASTPM animals aged 9 months and above. Heterozygous TASTPM mice express human *APP* with the Swedish mutation and *PS1* with the M146V mutation, and develop mature plaques at 8 months old (Matarin et al., 2015). Brains were collected into autoclaved Costar 'non-sticky' Eppendorf tubes, snap-frozen and stored at -80 °C until ready for homogenisation. Tissue was homogenised at 10% (w/v) in sterile phosphate-buffered saline (PBS) using a glass tissue dounce, which was fully turned ten times per hemisphere. The tissue was subsequently vortexed for 15 s, followed by sonication for 15 s. The tissue was then centrifuged at 3000 x g for 5 min at 4 °C. The supernatant (soluble fraction) and pellet (insoluble fraction) were separated and both stored at -80 °C until use. On the day of use, the supernatant was briefly thawed under UV light for sterility. At 10 days *in vitro* (DIV), 2 µl brain extract was pipetted once onto the surface of each slice.

2.5.2 Adding synthetic Aβ peptide

A stock solution of 100 mM synthetic Aβ1-40 (A-1153-2, rPeptide, Watkinsville, Georgia, USA) or Aβ1-42 (A-1163-2, rPeptide) peptide was made up in sterile PBS. This was vortexed for 15 s on wet ice, aliquoted and kept at -80 °C until ready for use. On the day of use, aliquots were added to the feeding medium to make up a final concentration of 1.5 µm. OHSCs were supplemented with this three times a week for 9 weeks.

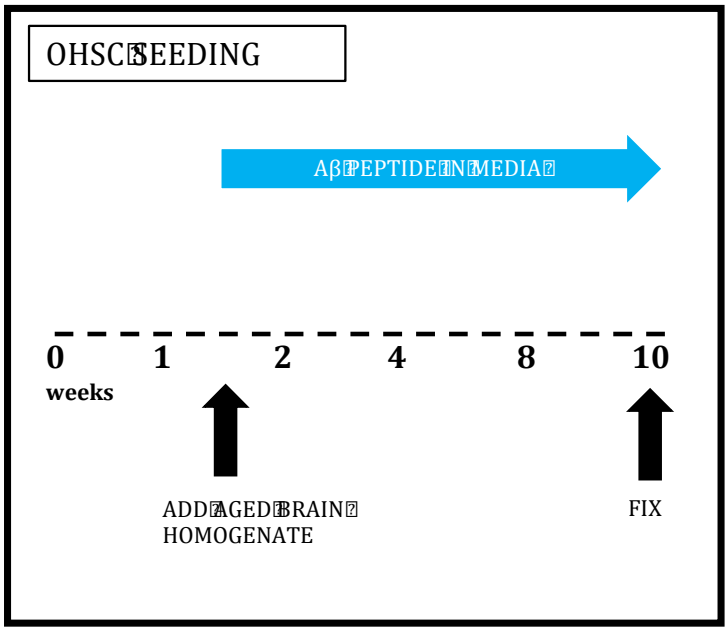

Figure 8. Seeding scheme for organotypic hippocampal slice cultures.
Cultures are obtained from *App*$^{NL-G-F}$, *App*$^{NL-F}$ and WT pups (P5-7) mice. At 10 DIV, slices are seeded once with brain homogenate from older plaque-bearing animals, and also continuously supplied with synthetic Aβ1-42 or Aβ1-40 in the culture media until week 10. After 10 weeks, sections are fixed in paraformaldehyde and subsequently processed for immunohistochemistry. Abbreviations: OHSC, organotypic hippocampal slice culture; DIV, days *in vitro*.

Two LCO fluorophores, quadro-formyl thiophene acetic acid (qFTAA) and heptameric formyl thiophene acetic acid (hFTAA), were used for the staining of both fresh-frozen and formalin-fixed tissue (Nystrom et al., 2013; Rasmussen et

al., 2017). Fresh-frozen mouse brain tissue sections (12-µm thick) were cut using a cryostat microtome at -18°C, and consecutive sections were collected on 0.17 PEN membrane slides (Zeiss/P.A.L.M., Microlaser Technologies, Bernsried, Germany), or on indium tin oxide slides for MALDI, and stored at −80°C. Before staining, sections were thawed in a desiccator and fixed at -20°C for 10 min in 95% ethanol, followed by double-staining for 30 min in the dark with 2.4 µm qFTAA and 0.77 µm hFTAA in PBS, as previously described (Nystrom et al., 2013; Rasmussen et al., 2017). Sections were subsequently washed with ddH_20 water and dried in a desiccator.

For staining of OHSCs, slices were washed in PBS for 10 min three times followed by double staining with 2.4 µm qFTAA and 0.77 µm hFTAA for 30 min in the dark. Slices were then rinsed once with PBS for 10 min, stained with 4′,6-diamidino-2-phenylindole (DAPI; 1:10,000 in PBS) for 5 min, washed once more with PBS for 10 min, and then mounted onto Superfrost Plus glass slides (Thermo Fisher Scientific, Waltham, MA, USA) using Fluoromount-G medium (SouthernBiotech, Birmingham, AL, USA), and left to dry before imaging.

2.6 Immunohistochemistry

The PFA-fixed hemisphere of *App* KI mice was sectioned transverse to the long axis of the hippocampus at 30 µm thickness using a frozen sledge microtome (SM 2000-R, Leica). Serial sections were collected until the hippocampus was no longer visible, and stored free-floating at 4°C in 24-well plates containing PBS with 0.03% sodium azide. For IHC, sections were washed once in PBS and then for 10 min three times in 0.3% Triton X-100 in PBS (PBST). Subsequently, sections were incubated for 1 h in a blocking solution of 3% goat serum (Novex, cat no. PCN5000) in 0.3% PBST. Sections were then incubated overnight with primary antibodies (Table 3) in blocking solution at 4°C. The next day, sections were washed for 10 min three times in 0.3% PBST followed by incubation with secondary antibodies in blocking solution (Table 3) for 2 h in the dark at room temperature. Following this, sections were washed in once in PBS for 10 min, stained with LCOs (qFTAA and hFTAA; Table 3) for 30 min in the dark, washed in PBS for 10 min, then incubated for 5 min in DAPI (Table 3). Finally, slices were floated in PBS and mounted onto Superfrost Plus glass slides (Fisher). Sections

were air-dried in the dark for 1 h, followed by application of Fluoromount-G medium (SouthernBiotech, Alabama, USA) and coverslips.

Antibody	**Dilution**	**Catalogue number**
Rabbit anti-Iba1	1:1000	Wako, 019-19741
Rat anti-CD68	1:500	BioRad, MCA 1957.
Goat anti-rabbit Alexa Fluor 594	1:1000	Invitrogen, a-11032
Goat anti-rabbit Alexa Fluor 647	1:1000	Invitrogen, a-21244
LCOs (qFTAA and hFTAA)	qFTAA: 1:5000; hFTAA: 1:10,000	Donated by Jörg Hanrieder
DAPI	1:10,000	Abcam, ab228549

Table 3. Antibodies and dyes used in the present work.
Abbreviations: Iba1, ionised calcium-binding adapter protein-1; CD68, cluster of differentiation 68; DAPI, 4′,6-diamidino-2-phenylindole; LCOs, lumoinescent conjugated oligothiphenes; qFTAA, quadro-formyl thiophene acetic acid; hFTAA, hepta-formyl thiophene acetic acid.

2.7 Mass spectrometry

2.7.1 MALDI-IMS

For MALDI-IMS, frozen tissue sections (12-µm thick), consecutive to those collected on polyethylene naphthalate (PEN) slides for LCO staining, were thaw-mounted on special-coated, conducting glass slides (indium tin oxide; Bruker Daltonics, Bremen, Germany) and stored at −80 °C. Sections were washed sequentially as follows: 100% EtOH for 60 s, 70% EtOH for 30 s, Carnoy's fluid (6:3:1 EtOH/chloroform/acetic acid) for 110 s, 100% EtOH for 15 s, in ethanol H_2O with 0.2% TFA for 60 s, and 100% EtOH for 15 s. Formic acid vapour was

applied to tissue for 20 min. The matrix compound (2,5-dihydroxyacetophenone) was applied using a TM Sprayer (HTX Technologies, Chapel Hill, NC). A matrix solution (15 mg/ml 2,5-dihydroxyacetophenone in 70% acetonitrile, 2% acetic acid, 2% TFA) was sprayed onto tissue sections as described: nitrogen flow (10 p.s.i.), spray temperature (75 °C), nozzle height (40 mm), eight passes with offsets and rotations, spray velocity (1000 mm/min), and isocratic flow of 100 µl/min using 70% acetonitrile as pushing solvent. Following the matrix deposition, the preparations were recrystallized with 5% methanol at 85 °C for 3 min as described previously (Kaya et al., 2017a; Yang and Caprioli, 2011).

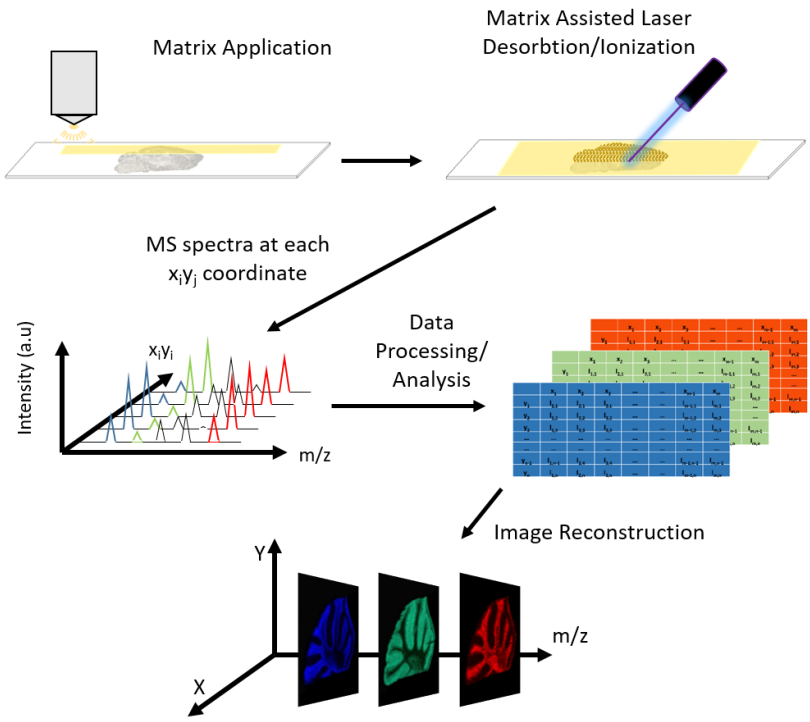

Figure 9. Schematic of workflow for MALDI-IMS. The tissue of interest is sectioned and mounted onto a special glass slide, followed by precoating with a matrix before subject to scanning with a laser probe. The MS spectra at each point on the section is mapped and constructed into single ion images.

2.7.2 Data acquisition

A high-speed MALDI-TOF instrument (rapifleX TissueTyper ToF/ToF, Bruker Daltonics) was used for MALDI-IMS experiments. A scanning Smartbeam 3D laser with a beam diameter of 10 µM is used at a frequency of 1000 Hz, a laser power of 90%, and 200 shots per pixel. A mass range of 2000-20,000 *m/z* (tuned for mass range of Aβ peptides at around 4000 *m/z*) was used in a linear positive mode. The system was calibrated pre-acquisition with peptide calibration standard I and synthetic Aβ peptides (Aβ1-38, -39, -40, -42, -43, -44, -45, -46, -47 and -48) to ensure calibration over the entire range of Aβ isoforms. Spectra were acquired using custom laser settings with a field size of 10 µm. FlexImaging 5.0 software (Bruker Daltonics) was used for data acquisition and processing. The average spectra of the annotated ROIs were normalised to total ion current, and the file exported as csv. in FlexImaging. Subsequent binning analysis involved importing all ROI data into Origin (v.8.1; OriginLab, Northampton, MA, USA), where peaks and peak widths were detected on average spectra of each region of interest using the implemented peak analyser function. Bin borders for peak integration were exported as tab delimited text file, following which bin borders were used for area under curve peak integration within each bin (pea-bin) of average spectra of all individual regions of interest. An R script developed in-house was used and data was log transformed. Univariate comparisons between groups were performed using a paired two-tailed t-test and data are presented as the mean ± standard deviation ($P<0.05$).

2.7.3 MALDI-IMS data analysis

Plaque ROIs (whole plaque, core, and periphery) were annotated on the basis of the coaligned LCO fluorescent images acquired on consecutive sections. Total ion current normalized average spectra of the annotated ROIs were exported as *.csv file.

Isotope pattern analysis was performed in GraphPad Prism (version 7). Here, MALDI-IMS ROI spectral data were loaded into Prism, and average distribution curves were fitted to the individual peptide isotope signal pattern. The centroid was used as a measure for average isotope incorporation, allowing either signal comparisons of the corresponding isotopologue (*m*/*z* value) and for comparative

analysis in between distinct ROI (plaque cortex versus plaque hippocampus) and peptides (Aβ1-42 and Aβ1-38). Univariate comparisons between the groups were performed using unpaired, two-tailed *t* test (P<0.05).

For individual peak statistics, ROI spectra data files were imported into Origin (version 8.1, OriginLab, Northampton, MA, USA) for peak detection and peak width determination using the implemented peak analyser function. The determined peak widths that serve as bin borders for peak integration were exported as tab delimited text file. The bin borders were used for area under curve peak integration within each bin (peak-bin) of all individual ROI average spectra using an in-house developed R script. Data were log-transformed. Univariate comparisons of distinct isotopologue signals (*m*/*z*) between the intraplaque regions (core versus periphery) were performed using unpaired, two-tailed *t* test (P<0.05). IMS/LCO Pearson r correlations were two-tailed and performed using GraphPad Prism (version 7) where P<0.05.

2.8 Imaging

2.8.1 Fluorescence microscopy

Photomicrographs of OHSCs were taken using an epifluorescent EVOS FL Auto Cell Imaging System microscope (Life Technologies) under a 20X objective by area-defined serial scanning using constant light, gain and exposure settings. LCO was detected at a wavelength of 488 nm and DAPI at a wavelength of 356 nm. Images from each channel were saved separately.

2.8.2 Confocal and hyperspectral microscopy

A Zeiss LSM 780 confocal microscope with a spectral detector was used to acquire spectra of plaques. Amyloid plaques stained with LCOs (qFTAA and hFTAA) were randomly chosen from the cortex and the hippocampus of brains sections. Z-stacks of plaques (20 stacks per plaque, 1-µm apart) were acquired using a 20X air objective, and continuous emission spectra were acquired from 470 to 695 nm. The plane with the most ‘core’ (the biggest spectral shift to the

left) was chosen for analysis. From this plane, spectra readings were taken from a small circle drawn in the very centre of each plaque (a few pixels in diameter) in order to take a reading from the true 'core' of the plaque. A total of 8-15 plaques per brain region (cortex and hippocampus) per mouse were analysed, and a total of 4-6 mice per group were analysed. The ratio of the intensity of emitted light at 500 nm and 580 nm was used to differentiate plaque characteristics: the higher the ratio, the more mature the structure.

For microglia, images were acquired using a regular confocal setup on a Zeiss LSM 780. Z-stacks were acquired of the same tissue area and plane as plaques (20 stacks per image, 1-µm apart). DAPI was detected at a wavelength of 356 nm, CD68 at 594 nm, and Iba1 at 647 nm. Constant light intensity, gain and exposure were used for image acquisition. A minimum of 4 sections were imaged and used as a mean for each animal, and a total of 4-6 mice per group were analysed.

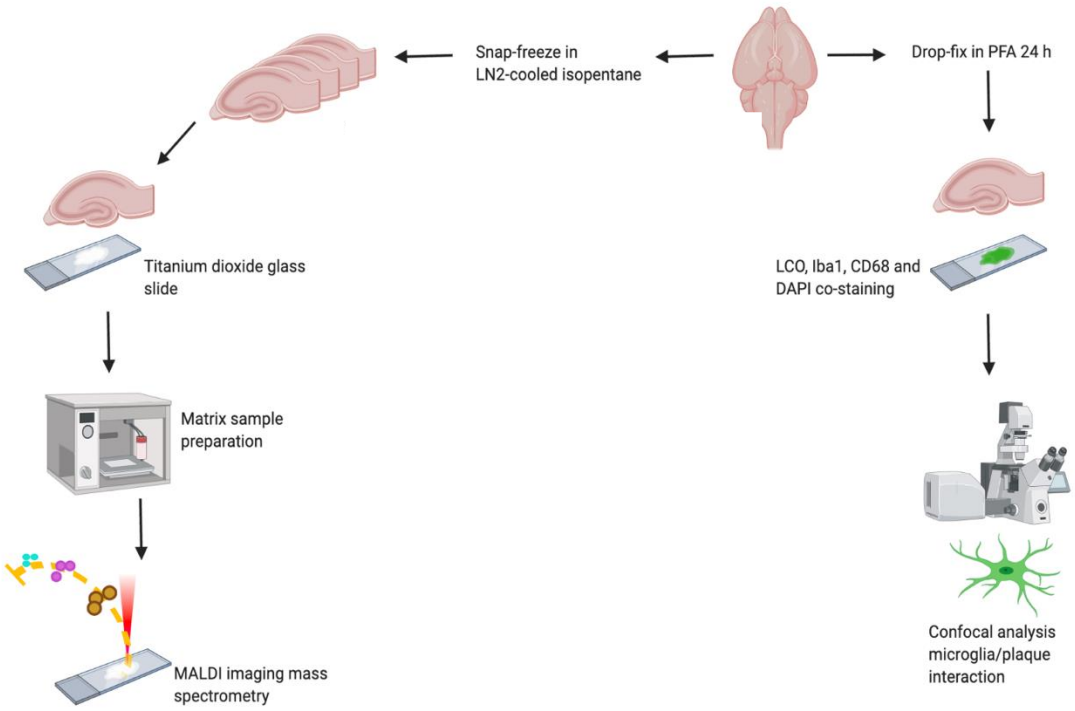

Figure 10. Schematic of MALDI-IMS/hyperspectral imaging workflow on sections obtained from one animal brain. Once removed from the skull, one hemisphere of the brain is (1) drop-fixed in PFA for 24 h, whilst the other hemisphere is (2) snap-frozen in liquid nitrogen-cooled isopentane. For (1), the hemisphere is sectioned at 30 µm and subsequently processed for

immunohistochemistry, involving staining for amyloid plaques (LCOs), microglia morphology (Iba1), microglial activation (CD68) and nuclei (DAPI). Sections are then imaged using a confocal laser scanning microscopy with a spectral detector. For (2), the hemisphere is sectioned at 12 µm, with sections being mounted on MALDI slides. MALDI slides undergo matrix sample preparation, followed by MALDI-IMS.

Abbreviations: qFTAA, quadro-formyl thiophene acetic acid; hFTAA, heptameric formyl thiophene acetic acid; LCOs, luminescent conjugated oligothiophenes; MALDI, matrix-assisted laser desorption/ionisation; IMS, imaging mass spectrometry; LMD, laser microdissection; IP, immunoprecipitation; Iba1, ionised calcium-binding adapter protein-1; CD68, cluster of differentiation 68; DAPI, 4′,6-diamidino-2-phenylindole; PFA, paraformaldehyde; PEN, polyethylene naphthalate.

2.9 Image analysis

Custom-written semi-automated macros within Fiji ImageJ were used for analysis. The macros are available at: https://zenodo.org/record/5847431

2.9.1 Plaque thresholding macro

Images of the hippocampus and cortex for each mouse were converted into an 8-bit colour and thresholded with the 'Otsu' threshold to remove background. Particles <10 µm^2 were counted as noise and excluded from the analysis.

2.9.2 Plaque concentric circles macro

For each plaque within the selected hippocampal or cortical region, concentric circles were drawn outwards with increasing 10 µm radii from the plaque, reaching a final circle with a radius of the average plaque radius plus 100 µm. Where two plaques are distanced <200 µm apart, concentric circles terminated at the nearest 10 µm to the halfway point to avoid overlapping data. As most plaques were not more than 100 µm apart, data here are shown up to 50 µm from the plaque edge. For images from WT mice, ten randomly placed circles each with a 10 µm radius were positioned within the image to imitate the measurement in relation to plaques above. Circles were drawn outwards with incrementing 10 µm radii reaching distance of 100 µm from the inner circle. Again, data here are shown up to 50 µm from the central circle.

2.9.3 Iba1/CD68 intensity macro

For measurement of Iba1 expression, fluorescence intensity of Iba1 staining (AU/pixels) was calculated for plaque regions and radiating concentric rings. For CD68 expression, pixels colocalising with Iba1 pixels were calculated in the same way.

2.9.4 Microglial density

Following running of macros, microglial number (cells positive for both Iba1 and DAPI) within every two circles (classed as ‘on plaque’, 0 – 10 µm; ‘peri-plaque’, 10 – 30 µm; ‘away from plaque’, 30 – 50 µm) were counted using Fiji ImageJ software. Density was calculated by dividing by ring area in mm^2. Where a microglial cell was overlapping two circles, it was always counted as part of the innermost circle.

2.10 Statistical analysis

All data analyses were performed blinded to condition or genotype. Statistical analyses were performed using GraphPad Prism 9 (La Jolla, California, USA). Where multiple slices/images were obtained from one animal, data were averaged to obtain a mean for that animal, which was subsequently used for analysis. Data were analysed using t-tests, one-way or two-way ANOVAS as appropriate, with the appropriate post-hoc test. Graphs show mean ± standard error of the mean. All diagrams in this work were created with GraphPad Prism 9, Microsoft PowerPoint or Biorender.com.

Chapter 3: Modelling amyloid deposition in organotypic hippocampal slice culture

3.1 Introduction

The hippocampus is one of the earliest and most-affected areas in AD and is therefore a critical area to investigate (Davies et al., 1988). Primary cell culture systems allow for easy manipulation and examination of hippocampal cells but are not fully representative of the internal environment of an animal due to the lack of other cell types. OHSC, where whole hippocampal brain sections are cultured, represents a three-dimensional cell culture technique that maintains the structural integrity of hippocampal networks, including glial cells, providing a more *in vivo*-like environment compared with primary cell culture (Stoppini et al., 1991).

The applications of OHSCs are vast. OHSCs can be used for electrophysiology, live imaging and molecular biology techniques, and the study of neurodegeneration, oxidative stress, ischaemia and spine/synaptic mechanisms, to name a few (Humpel, 2015a). Aβ plaque deposition in OHSCs has been attempted many times before by multiple research groups, with limited success. OHSCs from AD model pups, including the TgCRND8 (Harwell and Coleman, 2016) and 3xTg-AD, do not develop amyloid plaques without external manipulation (Croft et al., 2017). OHSCs cultured from adult mice, who already bear plaques, have limited neuronal survivability beyond a few days in culture, potentially due to reduced plasticity and increased sensitivity to the culture environment (Humpel, 2015b). However, one study in 2016 demonstrated that application of exogenous Aβ, obtained from APP23 or APP/PS1 brain homogenate, plus supplementation of synthetic Aβ1-40, resulted in OHSCs developing plaques after 10 weeks in culture (Novotny et al., 2016). If replicable, the potential application of this model is vast, as amyloid aggregation dynamics could be visualised with ease.

Given how OHSCs offer the ease of *in vitro* approaches whilst maintaining the cellular network of the intact brain, the aim in this chapter was to develop a model of Aβ deposition in OHSCs obtained from neonatal *App* KI pups. This would therefore provide key insight into the molecular mechanisms underlying not only

plaque formation, but the effects of toxic Aβ species on surrounding neurons and glial cells. If successful, further down the line this model could provide a simple and effective way of screening the potential therapeutic benefit or toxicity of novel anti-amyloid drugs.

3.2 Finding 1 - OHSCs from *App*$^{NL-G-F}$ pups do not develop amyloid deposits, even after 16 weeks in culture

It has been notoriously difficult to establish a slice culture model that naturally develops Aβ deposits, even with slices taken from mice overexpressing *App* (Harwell and Coleman, 2016). It was hoped that the new *App* KI models may be more successful, particularly the *App*$^{NL-G-F}$, where presence of the Arctic mutation causes increased oligomerisation of Aβ (Saito et al., 2014), and therefore increases the likelihood of amyloid deposition. Preliminary experiments involving culturing slices with a standard feeding protocol (media change three times a week) failed to yield any form of Aβ deposition even after a 16-week culture (these mice develop plaques at around 8 weeks *in vivo*). Therefore, the feeding frequency was reduced to a 50% media change once a week, to avoid washing away excess Aβ secreted into the media (Harwell and Coleman, 2016). This new feeding protocol also did not result in any form of Aβ deposition in OHSCs after the same duration of culturing (data not shown).

Long-term culture of slices from adult mice with existing plaque pathology (*App*$^{NL-G-F}$ aged 5 months and above) was attempted using an adjusted slicing and feeding protocol (Jang et al., 2018), however, widespread cell death occurred after 3 weeks in culture and this approach was abandoned.

3.3 Finding 2 - Seeded Aβ deposit morphology and density depends on the type and combination of synthetic Aβ peptide and brain homogenate added

As the initial approaches were unsuccessful, the addition of exogenous Aβ peptides was attempted based on a previously published protocol (Novotny et al., 2016), with slight modifications.

Initially, seeding experiments were performed on OHSCs from *App*$^{NL-G-F}$ pups, due to this being a more aggressive model of amyloid deposition compared to *App*$^{NL-F}$. Novotny et al. reported that Aβ deposition can be induced even in WT cultures after application of exogenous Aβ; therefore, here, WT OHSCs were treated in parallel for comparison (Table 2; Methods). Brain homogenate from aged *App*$^{NL-G-F}$ mice was added once at 10 DIV to encourage seeding of Aβ, after which 1.5 µm synthetic Aβ1-42 peptide was continuously supplemented in the media until week 10. Once the treatment schedule was complete, OHSCs were fixed in 4% PFA, double-stained with LCOs (qFTAA and hFTAA) and imaged with an epifluorescent microscope.

The results demonstrated that after 10 weeks in culture, untreated OHSCs from both *App*$^{NL-G-F}$ (Fig. 11A) and WT (Fig. 11D) pups did not develop any form of plaque pathology. OHSCs treated with just synthetic Aβ1-42 peptide had widespread small deposits of Aβ within the slice, for both *App*$^{NL-G-F}$ (Fig. 11B and C) and WT (Fig. 11E and F). In WT slices, the addition of synthetic Aβ1-40 peptide alongside Aβ1-42 resulted in deposits with slightly different morphology (Fig. 11G and H), compared with those treated with just Aβ1-42. However, these results were highly variable between cultures; therefore, it is difficult to draw definite conclusions about Aβ deposit morphology due to the addition of synthetic Aβ.

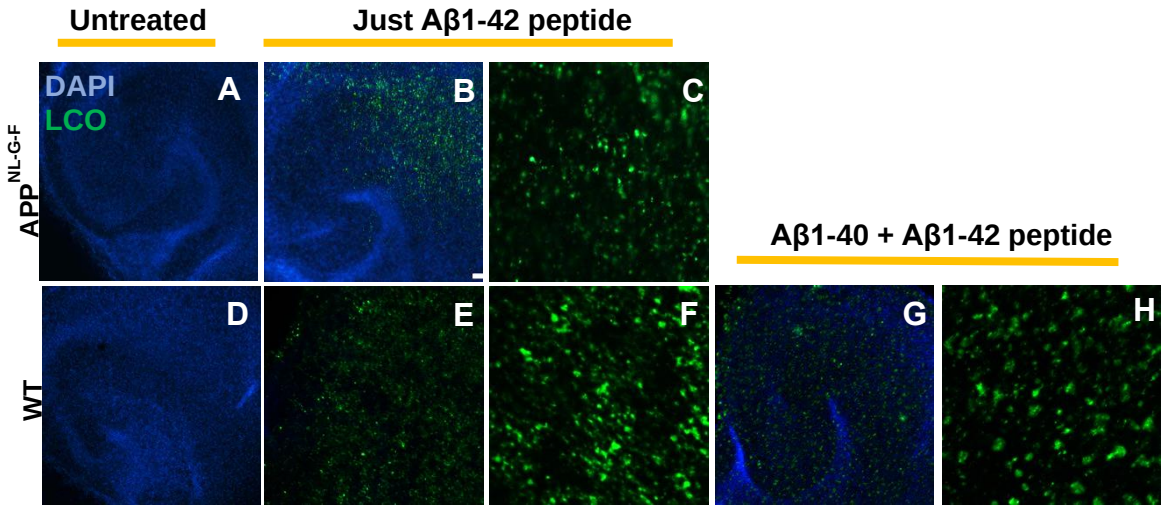

Figure 11. Supplementation of solely synthetic Aβ peptide in feeding media results in small Aβ aggregates. Representative fluorescence microscopy images of OHSCs from P5-7 (A-C) *App*$^{NL-G-F}$ and (D-H) WT pups. OHSCs were: (A and D) untreated; or treated with 1.5 µm synthetic

(B, C, E and F) just Aβ1-42; or (G and H) both Aβ1-42 and Aβ1-40 peptide continuously supplemented in the media three times a week for 9 weeks. LCO double staining for Aβ and DAPI co-staining for cell nuclei was performed. LCO (qFTAA and hFTAA) double staining for Aβ and DAPI co-staining for cell nuclei was performed. Images are taken at either 4X (A, B, D, E and G) or 20X magnification (C, F and H). Abbreviations: LCO, luminescent conjugated oligothiophene; OHSCs, organotypic hippocampal slice culture; WT, wild-type.

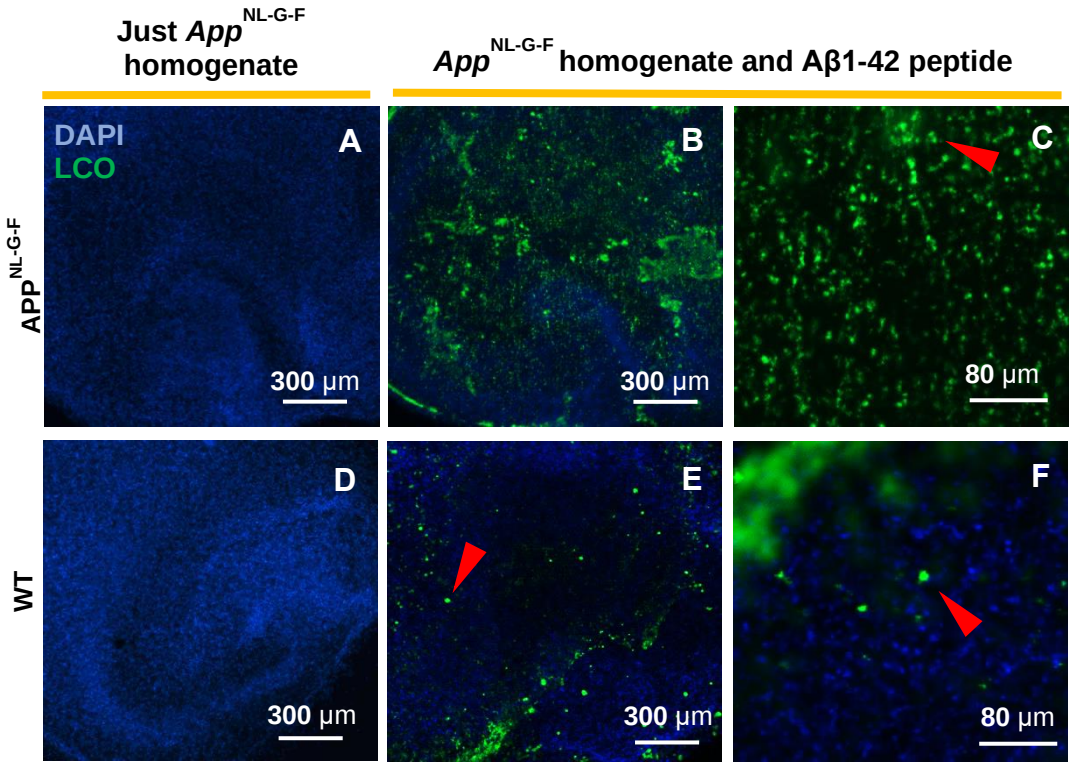

Figure 12. Application of brain homogenate from aged *App*$^{NL-G-F}$ mice plus supplementation of synthetic Aβ peptide in the feeding media results in aggregation of small Aβ deposits on the surface of the slice. Representative fluorescence microscopy images of OHSCs from P5-7 (A-C) APP^{NL-G-F} and (D-H) WT pups, which were either: (A and D) treated once with brain homogenate from aged *App*$^{NL-G-F}$ mice at 10 DIV; or (B, C, E and F) additionally supplemented with 1.5 µm synthetic Aβ peptide supplemented in the media three times a week for 9 weeks. LCO (qFTAA and hFTAA) double staining for Aβ and DAPI co-staining for cell nuclei was performed. Images are taken at either 4X (A, B, D and E) or 20X magnification (C and F). Red arrows highlight areas of aggregation. Abbreviations: LCO, luminescent conjugated oligothiophene; OHSCs, organotypic hippocampal slice culture; WT, wild-type; DIV, days *in vitro*.

In both *App*$^{NL-G-F}$ (Fig. 12A) and WT (Fig. 12D) OHSCs, treatment with just brain homogenate was not sufficient to seed any form of plaque pathology. OHSCs from *App*$^{NL-G-F}$ (Fig. 12B and C) and WT (Fig. 12E and F) treated with both brain homogenate and synthetic Aβ1-42 peptide had a layer of LCO signal on the

surface of the slice, which may be the homogenate and synthetic peptide interacting in some way and superficially aggregating. Again, these results were inconsistent between different cultures.

Interestingly, when we then tried to more closely replicate the work by (Novotny et al., 2016) by using brain homogenate from aged TASTPM animals (harbouring the Swedish mutation in *App* and the M146V mutation in *PS1*, and have plaques richer in Aβ1-40 compared with APP^{NL-G-F} animals (Howlett et al., 2004)) plus addition of Aβ1-42 (Fig. 13B and C) or Aβ1-40 (Fig. 13D and E) in the media, it was observed that unlike in their paper, here there was negligible LCO signal within the cell body layer of OHSCs. Again, the superficial layer of amyloid was visible on the surface of the slice, which is not seen in OHSCs treated with just synthetic peptide but no homogenate (Fig. 11). Overall, this highlights how the combination of synthetic peptide or type of homogenate applied to OHSCs determines aggregation regardless of genetic background, and closer examination of precisely which mechanisms determine this is required. Additionally, further research is required to see if these aggregates are formed over time via interaction with cellular mechanisms within the slice, as opposed to just pooling on the surface.

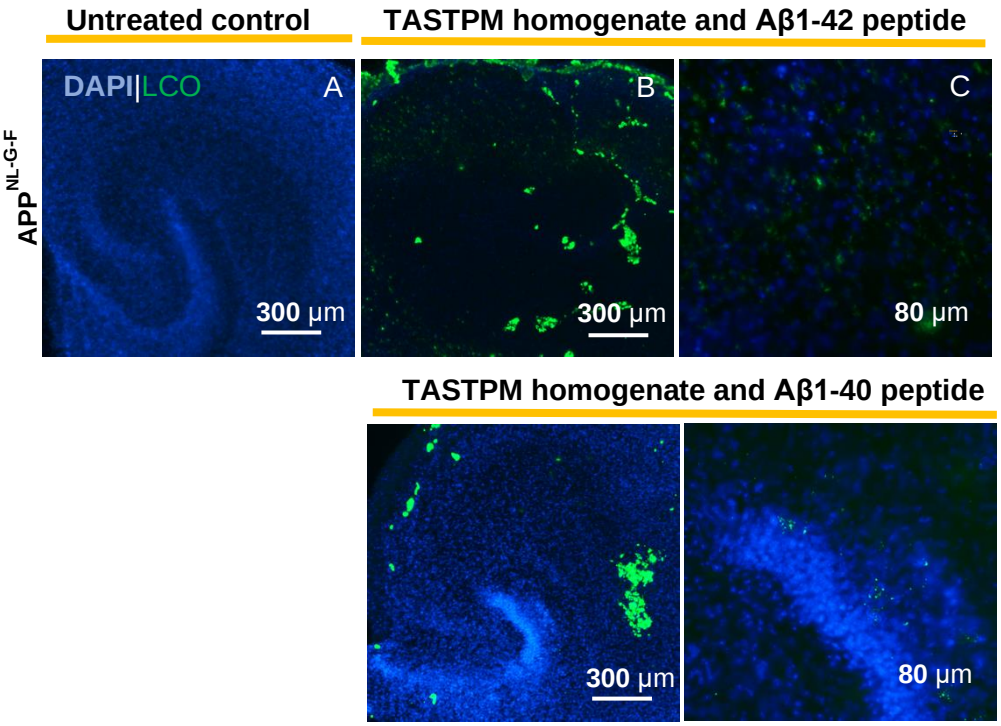

Figure 13. Brain homogenate from aged TASTPM mice plus supplementatıon of synthetic Aβ peptide does not induce Aβ deposition. Representative fluorescence microscopy images of OHSCs from P5-7 *App*$^{NL-G-F}$ pups, which were (A) left untreated, or treated once with brain homogenate from aged TASTPM mice once at 10 DIV plus 1.5 μm synthetic (B and C) Aβ1-42 or (D and E) Aβ1-40 peptide continuously supplemented in the media three times a week for 9 weeks. Images are taken at either 4X (A, B, D) or 20X magnification (C and E). Abbreviations: LCO, luminescent conjugated oligothiophene; OHSCs, organotypic hippocampal slice culture; DIV, days *in vitro*.

3.4 Chapter summary

This chapter explored the potential to model amyloid deposition in OHSCs, based on a previous study showing that plaques can be induced in OHSCs from *App* transgenic mice after seeding once with brain homogenate from aged *App* transgenic mice while supplementing the media continuously with synthetic Aβ (Novotny et al., 2016). Therefore, here I tested a protocol involving seeding OHSCs once with brain homogenate from older plaque-bearing animals, in combination with continuous supplementation of synthetic Aβ in the media. This approach was tested on a range of brain homogenates and on OHSCs from both *App*$^{NL-G-F}$ and WT backgrounds. Despite some visible amyloid aggregation after application of exogenous Aβ, the results were inconsistent and there was no robust plaque pathology in OHSCs even after 9 weeks in culture. Additionally, it is likely that the amyloid aggregation observed was due to exogenous Aβ pooling on the surface of the slice, but due to inconsistency in results and time constraints, this was not explored further. Therefore, it was concluded here that these methods are not sufficient to promote cellular-induced plaque deposition in OHSCs.

Chapter 4: Modelling amyloid deposition in *App* KI models

4.1 Introduction

Amyloid plaques are a hallmark pathology of AD, whereby continuous plaque growth exerts neurotoxic effects on surrounding neurons, axons and dendritic processes, eventually leading to cell death via phosphorylation of tau and formation of NFTs. However, precisely what plaques are composed of, how individual plaques grow, and how amyloid deposition spreads across brain regions over time, remains unclear.

Traditionally, human post-mortem studies have categorised amyloid plaques into 'dense-core' and 'diffuse' morphologies, based on CR or Th positivity (Howie and Brewer, 2009). It has been suggested that diffuse plaques are an earlier and possibly neuroprotective form, by recruiting soluble Aβ to localise the damage, whereas cored plaques are formed at later stages of disease and trigger cognitive deficits (Dickson and Vickers, 2001). However, the mechanisms around this remain uncertain, and further complexity lies in that the aggregation properties of Aβ are likely far more varied; for example, sAD and fAD patients display differences in Aβ structure within plaques (Cohen et al., 2015; Rasmussen et al., 2017). These conformational polymorphisms thus pose a huge challenge to the detection of plaques for diagnostics, and for the development of therapeutics targeting Aβ aggregates. Therefore, it is important to identify and understand plaque heterogeneity in AD, to be able to tailor the most effective therapeutics.

Plaque growth and spread is a complicated event, and may involve selective processing of APP into its metabolites, followed by recruitment of different peptides over time. Indeed, our previous work involving metabolic labelling in $App^{NL\text{-}G\text{-}F}$ mice showed that Aβ1-38 secretion and deposition occurs after Aβ1-42 deposition, as evidenced by an Aβ1-42-rich core and more Aβ1-38 in the periphery of plaques (Enzlein et al., 2020; Michno et al., 2021), suggesting that individual plaques evolve over time. Previous work in our lab showed that plaque

deposition varies between *App* KI models and over time; for example, older *App*$^{NL\text{-}G\text{-}F}$ mice have a larger number of smaller-sized plaques compared to their younger counterparts; and *App*$^{NL\text{-}F}$/*Trem2*^{R47H} mice exhibit a higher density of plaques in the hippocampus than APP$^{NL\text{-}F}$ mice, driven by a larger number of smaller sized plaques. Overall, this highlights how plaque formation, growth and spread are complex events, and are mediated by genetic mutation. Therefore, understanding these processes in *App* KI models would certainly drive understanding of plaque dynamics in human fAD.

The characterisation of amyloid has been aided by LCOs, a group of β-pleated sheet-specific fluorescent dyes. LCOs have been used to detect plaque heterogeneity in samples from both humans (Cohen et al., 2015; Liu et al., 2016; Rasmussen et al., 2017) and animals (Heilbronner et al., 2013; Michno et al., 2021). When bound to amyloid, LCOs emit a unique fluorescence spectrum that reflects the 3D structure of protein aggregates (Aslund et al., 2009), thereby allowing for detection of different plaque conformations. qFTAA binds predominantly to more putatively mature structures (such as the core of the plaque) and has a more left-shifted spectral signature (with an emission maximum at 500 nm), whereas hFTAA binds to more diffuse, putatively immature structures and has a more right-shifted spectral signature (with an emission maximum at 580 nm). Thus, double-staining plaques followed by hyperspectral imaging (where the spectrum for each pixel in the image is determined) can yield important information about plaque conformation and maturity.

Therefore, in this chapter I aimed to assess conformational amyloid plaque polymorphism across genotypes in *App* KI mice, in early vs. late plaque pathology. The hypothesis is that upon plaque maturation, plaques undergo conformational changes that are particularly prominent at the cored centre. Biochemically, this amyloid maturation and resulting structural amyloid polymorphism includes changes in the content and density of amyloid cross-beta sheet motifs (Almstedt et al., 2009). As cortical and hippocampal brain regions show selective vulnerability to plaque pathology, I also aimed to examine potential differences between the two regions in these mice. To do this, I combined LCO fluorescent amyloid staining with hyperspectral imaging, to examine potential differences in plaque structure.

4.2 Finding 1 – Plaque core structures continuously mature over time

First, I aimed to assess the conformational heterogeneity of plaque cores in young vs. old *App* KI mice. This was achieved by examining the 500/580 nm emission ratio of LCOs, recorded at the centre of plaques in the cortex and hippocampus of *App*$^{NL\text{-}G\text{-}F}$ mice at 4 and 18 months old, and APP$^{NL\text{-}F}$ mice at 9 and 18 months old (Fig. 14). These ages were chosen as they represent early and late stages of amyloid pathology in these models (*App*$^{NL\text{-}G\text{-}F}$ mice develop plaques at around 2 months old; *App*$^{NL\text{-}F}$ at 9 months old).

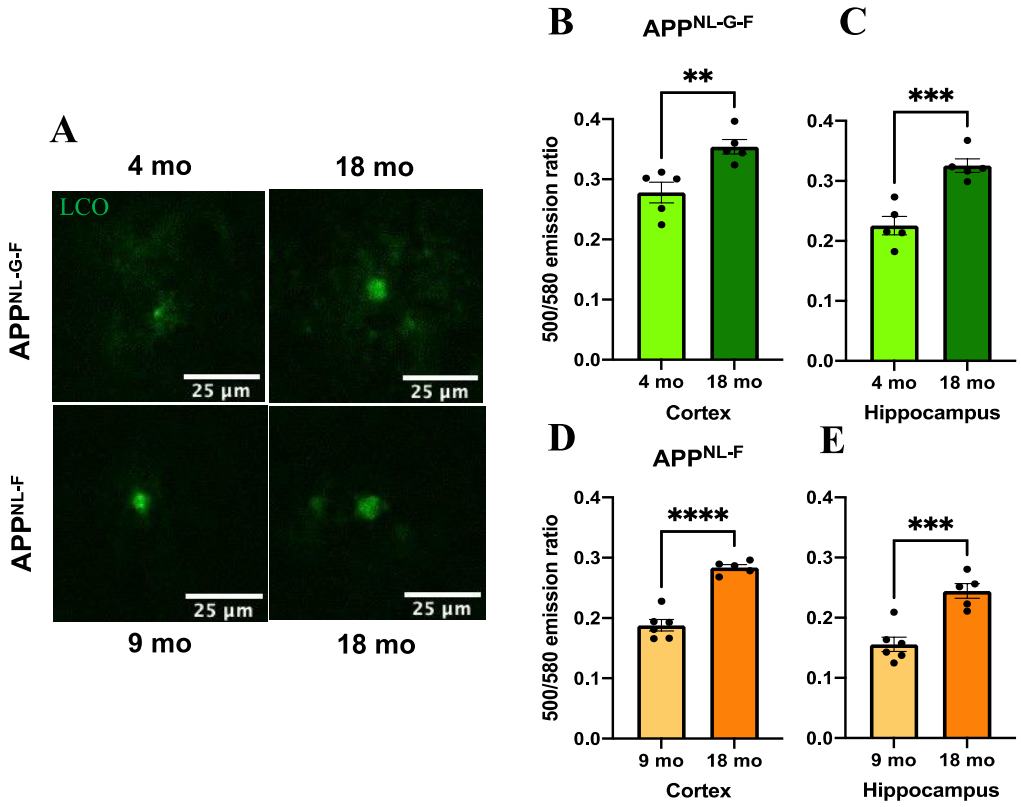

Figure 14. Age-associated increase in plaque maturity in *App* KI mice.

(A) Representative confocal images of LCO double staining (qFTAA and hFTAA) of cortical plaques in young and old *App*$^{NL\text{-}G\text{-}F}$ and *App*$^{NL\text{-}F}$ mice, taken at 20X magnification. Quantification with an unpaired t-test revealed a statistically significant age-associated increase in the 500/580 nm emission ratio of plaques in the (B) cortex and (C) hippocampus of *App*$^{NL\text{-}G\text{-}F}$ mice; and the (D) cortex and (E) hippocampus of APP$^{NL\text{-}F}$ mice. Number of animals: N=4-5 per group. **P<0.01; ***P<0.001; ****P<0.0001.

Abbreviations: LCO, luminescent conjugated oligothiophene; mo, months old.

Visually, 4 month-old *App*$^{NL-G-F}$ mice had less compact plaques than their 18 month-old counterparts (Fig. 14A); and likewise, 9 month-old *App*$^{NL-F}$ mice, who only have a few plaques across the whole brain section at this age, displayed fewer plaques than those at 18 months old (Fig. 14A). Statistical analysis showed that in *App*$^{NL-G-F}$ mice, the emission ratio of plaques at 18 months was significantly increased compared to at 4 months, in both the cortex (Fig. 14B; $P<0.01$) and the hippocampus (Fig. 14C; $P<0.001$). Likewise, in *App*$^{NL-F}$ mice, the emission ratio of plaques at 18 months was significantly increased compared to at 9 months, in both the cortex (Fig. 14D; $P<0.0001$) and the hippocampus (Fig. 14E; $P<0.001$).

Firstly, this approach demonstrates that plaque maturity is measurable using the 500/580 nm emission ratio of LCOs. Secondly, these results indicate that plaque maturation is a continuous event across multiple brain regions, at least up to the age of 18 months. Additionally, the lack of extreme variability in plaque emission ratio within each mouse indicates that individual plaques grow over time, as opposed to consistent seeding of new plaques which then plateau in growth.

App^{NL-F} mice at 9 months only have one or two plaques in the cortex or hippocampus at this age, so an advantage is that every plaque was captured in this analysis. However, it should be noted that due to the experimental setup and time constraints, the smallest 'seeds' of plaques were not examined. Thus, very newly growing plaques may have been overlooked in this analysis. In the future it would be interesting to examine the emission ratio of very small plaques in older mice, to see if these also have a very mature structure, or if they represent young/early plaques and thus have a lower emission ratio.

4.3 Finding 2 – Plaque structural maturity is dependent on mutations in *App* and *Trem2*

Knowing that plaque structure (and therefore maturity) can indeed be assessed using LCOs, next, I aimed to examine potential differences in plaque conformation between *App* KI models. The addition of the Arctic mutation in *App*$^{NL-G-F}$ predisposes Aβ to oligomerise and aggregate more compared to *App*$^{NL-F}$. Therefore, we hypothesised that plaques in *App*$^{NL-G-F}$ would display a more cored and mature structure. Additionally, previous research has shown that the

Trem2^{R47H} mutation causes an impairment in the ability of microglia to promote formation of compact plaques (Cheng-Hathaway et al., 2018). Therefore, it was hypothesised that plaques in *App*$^{NL-F}$/*Trem2*^{R47H} mice may show interesting conformational differences, compared to *App*$^{NL-F}$.

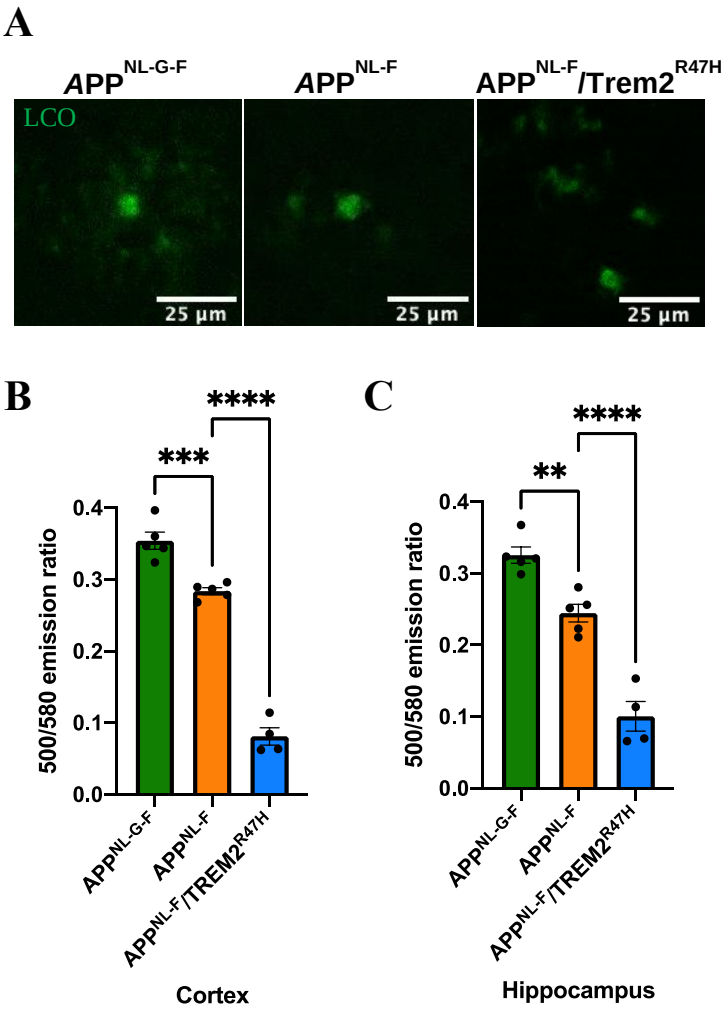

Figure 15. Genotype-associated alterations in plaque maturity in *App* KI mice.

(A) Representative hyperspectral images of LCO double staining (qFTAA and hFTAA) of cortical plaques in 18 month-old *App*$^{NL-G-F}$, *App*$^{NL-F}$ and *App*$^{NL-F}$/*Trem2*^{R47H} mice, taken at 20X magnification. Quantification with one-way ANOVA followed by Holm-Šídák's multiple comparisons test revealed statistically significant genotype-associated alterations in the 500/580 nm emission ratio of plaques in the (B) cortex and (C) hippocampus of *App*$^{NL-G-F}$, *App*$^{NL-F}$ and *App*$^{NL-F}$/Trem2^{R47H} mice. Number of animals: N=4-5 per group. **P<0.01; ***P<0.001; ****P<0.0001.

Abbreviations: LCO, luminescent conjugated oligothiophene.

Therefore, to assess the effect of genotype on plaque conformation, I performed qFTAA and hFTAA LCO double-staining followed by hyperspectral confocal imaging of amyloid plaques in the cortex and hippocampus of 18 month-old *App* KI mice. The staining showed that plaques in *App*$^{NL-G-F}$ had a dense core and a halo of staining around the periphery; whereas *App*$^{NL-F}$ mice had smaller plaques composed of mainly a core (Fig. 15A). Pathology in *App*$^{NL-F}$/*Trem2*^{R47H} mice, on the other hand, consisted of clusters of smaller plaques (Fig. 15A). A one-way ANOVA revealed a main effect of genotype between *App*$^{NL-G-F}$ and *App*$^{NL-F}$, and again between *App*$^{NL-F}$ and *App*$^{NL-F}$/*Trem2*^{R47H} mice. Post-hoc analysis with Holm-Šídák's multiple comparisons test demonstrated significance between *App*$^{NL-G-F}$ and *App*$^{NL-F}$ in the cortex (Fig. 15B; $P<0.001$) and hippocampus (Fig. 15C; $P<0.001$). *App*$^{NL-F}$ mice, in turn, displayed an increased plaque emission ratio compared to *App*$^{NL-F}$/*Trem2*^{R47H} mice, in both the cortex (Fig. 15B; $P<0.0001$) and hippocampus (Fig. 15C; $P<0.0001$). Overall, as predicted, this suggests that the addition of the Arctic mutation in *App*$^{NL-G-F}$ mice results in plaques with a more mature dense core structure compared to *App*$^{NL-F}$. Additionally, compared to *App*$^{NL-F}$, the presence of the *Trem2*^{R47H} mutation decreases the average plaque emission ratio across brain regions, inferring a loss-of-function of microglia and strongly implicating their role in determining plaque structure/promoting plaque maturation.

4.4 Finding 3 - Plaques mature over time, where cortical plaques are more structurally mature than hippocampal plaques

Amyloid pathology precipitates in distinct brain regions followed by a defined spread throughout the brain (Thal et al., 2015). Similar to human pathology, plaque formation in the KI mice studied here is initiated in cortical areas followed by spreading to subcortical and neocortical areas (Saito et al., 2014). Therefore, another way of considering the comparisons above (Fig. 15) is to compare the maturation of plaques in the cortex vs. hippocampus.

After visualisation of plaques with fluorescent amyloid imaging (Fig. 16A), quantification of plaque emission ratios was performed followed by statistical comparisons. The results showed that the plaque emission ratio was significantly

higher in older animals as compared to younger animals within the respective genotype, suggesting continuous plaque maturation with age (Fig. 16B,C).

Moreover, when comparing brain regions within each genotype and age group, the results show that cortical plaques had a higher 500/580 nm ratio compared with hippocampal deposits in 9- (P<0.05) and 18 (P<0.01) month-old *App*$^{NL-F}$ (Fig. 16B) as well as for 4 month-old *App*$^{NL-G-F}$ (Fig. 16C; P<0.05) mice.

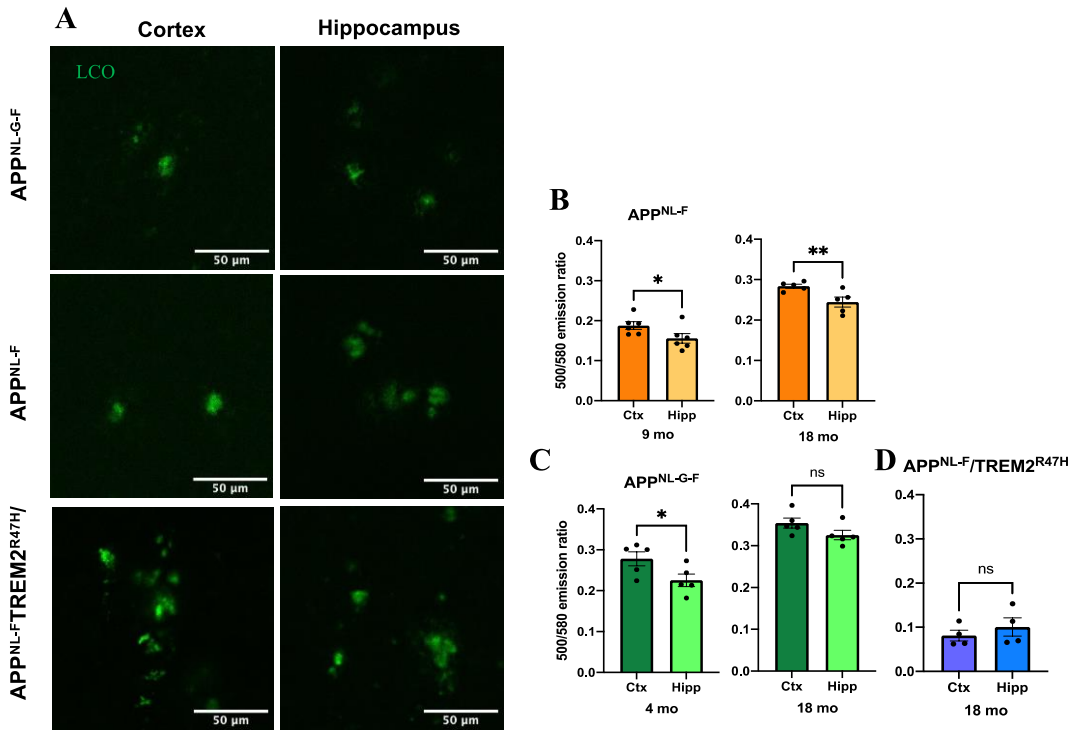

Figure 16. Regional alterations in plaque maturity in *App* KI mice.

(A) Representative hyperspectral images of LCO double staining (qFTAA and hFTAA) of cortical and hippocampal plaques in 18 month-old *App*$^{NL-G-F}$, *App*$^{NL-F}$ and *App*$^{NL-F}$/*Trem2*^{R47H} mice, taken at 20X magnification. (B) Quantification with a t-test revealed a significant increase in the 500/580 nm emission ratio of plaques in the cortex compared to the hippocampus of *App*$^{NL-F}$ mice, at both 9 and 18 months old. (C) This effect was only seen in 4 month old *App*$^{NL-G-F}$ mice: there were no significant differences between regions in both 18 month-old *App*$^{NL-G-F}$ and (D) 18 month-old *App*$^{NL-F}$/*Trem2*^{R47H} mice. Number of animals: N=4-5 per group. *P<0.05; **P<0.01; ns, non-significant.

Abbreviations: LCO, luminescent conjugated oligothiophenes; mo, months old; Ctx, cortex; Hipp, hippocampus.

Interestingly, both *App*$^{NL-G-F}$ and *App*$^{NL-F}$/*Trem2*^{R47H} mice at 18 months (Fig. 16C and 16D, respectively) did not display significant differences in the plaque emission ratio between the two brain regions.

A potential explanation for these results could be that in *App*$^{NL-G-F}$ mice, Aβ is structurally changed to more rapidly deposit, so by 18 months old, hippocampal plaques have experienced a 'ceiling effect', whereby plaques have reached the maximum maturity that they will reach in both regions. Plaques in *App*$^{NL-F}$/*Trem2*^{R47H} mice, on the other hand, may have undergone a 'floor effect', where they never start to mature and are thus similar across both regions. It is important to note that due to time constraints not every plaque per animal was analysed, so smaller newly growing plaques may have been overlooked. In future studies, it would be interesting to sub-divide the plaques into smaller and larger ones for comparison.

In terms of *App*$^{NL-F}$/*Trem2*^{R47H} mice, previous research has shown that the *Trem2*^{R47H} mutation causes dysfunction of microglia in compacting plaques (Cheng-Hathaway et al., 2018). Indeed, previous work by our lab showed that compared with 18 month-old *App*$^{NL-F}$, 18 month-old *App*$^{NL-F}$/*Trem2*^{R47H} show a greater plaque area coverage in the hippocampus, which is reflected by a greater density of small plaques, rather than larger ones (Wood et al., 2022). Overall, this indicates that microglia have a role in shaping plaque morphology, and that there is an impairment in this function in these mice. Hence it would be of interest for future studies to expand these experiments covering younger timepoints of *App*$^{NL-F}$/*Trem2*^{R47H} mice for comparison.

4.5 Chapter summary

This chapter explored the plaque conformation of *App* KI mice in early and late plaque pathology, and in the cortex and hippocampus, to understand how genetic background, brain region and age affects the nature of amyloid deposition.

Both *App*$^{NL-G-F}$ and *App*$^{NL-F}$ demonstrated an age-associated increase in plaque structural maturity, indicating that the majority of plaques grow and mature over

time. When examining plaques across different brain regions, it was established that both young and old *App*$^{NL-F}$, and young *App*$^{NL-G-F}$, have more mature plaques in the cortex compared with the hippocampus. However, aged *App*$^{NL-G-F}$ mice did not display regional alterations in plaque maturity. A potential explanation for this could be that because the additional Arctic mutation in *App*$^{NL-G-F}$ mice causes rapid aggregation and deposition of Aβ, by 18 months old, these mice are at a much later stage of pathology compared to *App*$^{NL-F}$. Therefore, by this age, hippocampal plaques have experienced a growth ceiling effect, despite being initially deposited after cortical plaques. *App*$^{NL-F}$ mice, on the other hand, are a more physiological model of human AD in that they have rising soluble Aβ that subsequently leads to gradual plaque deposition (Saito et al., 2014). Therefore, these 18 month-old mice may only be at mid-stage amyloid pathology, whereby excess soluble Aβ is still being recruited to plaques and causing further growth.

Finally, it was found that genetic background determines the morphology of plaques. *App*$^{NL-G-F}$ mice, harbouring three fAD mutations, including the Arctic which increases the propensity of Aβ to oligomerise and aggregate, had plaques with the most mature and cored structure. *App*$^{NL--F}$ mice, in turn, had more cored plaques compared to their counterparts with a *Trem2*^{R47H} mutation. Overall, this further supports previous human studies that plaque type is dependent on dementia subtype (Rasmussen et al., 2017), and also implicates the role of TREM2 in determining plaque structure and promoting plaque maturation.

Overall, these data provide interesting implications about how both fAD mutations and Trem2 interactions shape plaque structure and maturity. This could provide a basis for understanding not only the biochemical processes underlying plaque deposition dynamics, but also how to individualise anti-amyloid therapies depending on disease type.

Chapter 5: Chemical imaging of plaque formation dynamics with iSILK

5.1 Introduction

Aβ plaque formation represents the earliest key pathological hallmark of AD, and has been identified as a critical earliest pathogenic driver of AD pathogenesis. However, amyloid peptide accumulation, aggregation and deposition are highly dynamic processes that are hard to capture in an *in vivo* model, or even more so in patients. A major challenge of studying Aβ accumulation is the lack of robust imaging technologies that provide the necessary spatial resolution, sensitivity and specificity. The gap in our understanding of subcellular amyloidogenic protein aggregation dynamics in AD relates to the lack of effective imaging tools with high chemical, spatial and temporal precision.

Previous studies often utilise antibody-based assessment of proteins, including Aβ and tau, for example combined with biochemical purification and MS analysis (Alcalay et al., 2016; Hark et al., 2021). Whilst no doubt useful as a foundation for understanding the steady state of Aβ, these studies do not examine dynamic Aβ. These challenges are overcome by the development of *in vivo* SIL, also referred to as metabolic labelling followed by MS, which has been demonstrated as a powerful tool to measure protein turnover in both cells (SILAC) (Ong et al., 2002), mice (SILAM) and humans (SILK) (Bateman et al., 2006b). Particularly, in the context of AD pathology, pioneering SIL work has been reported in both mice (Hark et al., 2021; Savas et al., 2016) and humans (Bateman et al., 2006b), where protein turnover is measured in brain extracts or CSF *ex vivo*.

Consequently, while, these SIL-MS tools are highly useful, they are performed *ex vivo* and thus provide only limited spatial information about isotope incorporation or cellular behaviour. This can be overcome using IMS, whereby the spatial intensity of distribution profiles of molecular species in tissue can be analysed (McDonnell and Heeren, 2007). A particular advantage of IMS is that previous knowledge of the target species is not required, and this method is not dependent

on antibody specificity. The application of IMS to study AD plaque pathology has previously been pioneered by our group, including applications to transgenic *App* mice (Carlred et al., 2016; Kaya et al., 2017b; Michno et al., 2019c; Michno et al., 2019d; Michno et al., 2019e) and *post-mortem* human brain (Michno et al., 2019a).

5.2 Finding 1 – iSILK allows for analysis of amyloid plaque formation over time in *App*$^{NL-G-F}$ mice

Over the course of this thesis, I was involved in the first experiments where we made use of this expertise and developed a dynamic chemical imaging paradigm based on *in vivo* SIL and IMS. Here we established a SIL method in which *App*$^{NL-G-F}$ mice were fed a diet enriched with ^{15}N stable isotopes, which are then incorporated into the proteome allowing for analysis of the time course and of App production, Aβ secretion and Aβ plaque deposition (Michno et al., 2021). The principles of iSILK are outlined in Fig. 17.

Subsequent MALDI-IMS allows for visualisation of Aβ aggregation dynamics within single plaques across both the cortex and hippocampus. First, the composition of plaques as well as the degree of label incorporation was evaluated. Using a full stop PULSE labelling scheme (Scheme 1, Fig. 18A-E), it was determined that the main peptide depositing was Aβ1-42, along with Aβ1-38 to a lesser degree. All Aβ species were found to contain ^{15}N atoms. This confirmed that starting labelling at week 7 is sufficient to allow metabolic incorporation into App and Aβ, prior to plaque pathology onset that is estimated to be at week 8-10 for these mice.

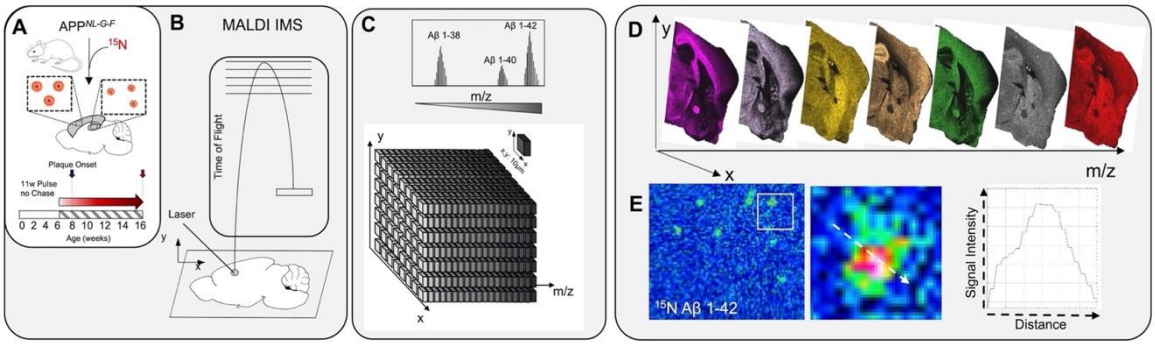

Figure 17. Principle of iSILK. (A) Mice are metabolically labelled with ^{15}N protein diet leading to incorporation into Aβ plaques. Stable isotope incorporation into plaques can be delineated with imaging mass spectrometry. (B) MALDI-IMS employs a laser analyte desorption and ionisation and allows for detection of intact Aβ peptides (C) at 10 µm resolution. (D) Single ion images can be generated for different peptides in parallel, including and Aβ peptide outlining spatial peptide localization across different brain regions and within single Aβ plaques. (E) This further includes delineation of different Aβ isotopologues at the single plaque level. Here, pronounced localisation of ^{15}N labelled Aβ1-42 (E) to the core of the plaques (rainbow Int.). Figure adapted from (Michno et al., 2021).
Abbreviations: MALDI-IMS, matrix-assisted laser desorption/ionisation imaging mass spectrometry.

Second, differences in isotope incorporation across intra-plaque structures, i.e. the core and periphery, were investigated. For the first labelling scheme, it was found that the degree of ^{15}N content in Aβ1-42 was less in the core than in the periphery. More labelled Aβ1-42 was found to deposit homogenously across the entire plaque (Fig. 18A-E). Given that according to the labelling scheme, less labelled App and Aβ are secreted earlier than the later secreted proteins that contain consequently more label, this suggests that the core of these plaques was the earliest structure formed within the plaque.

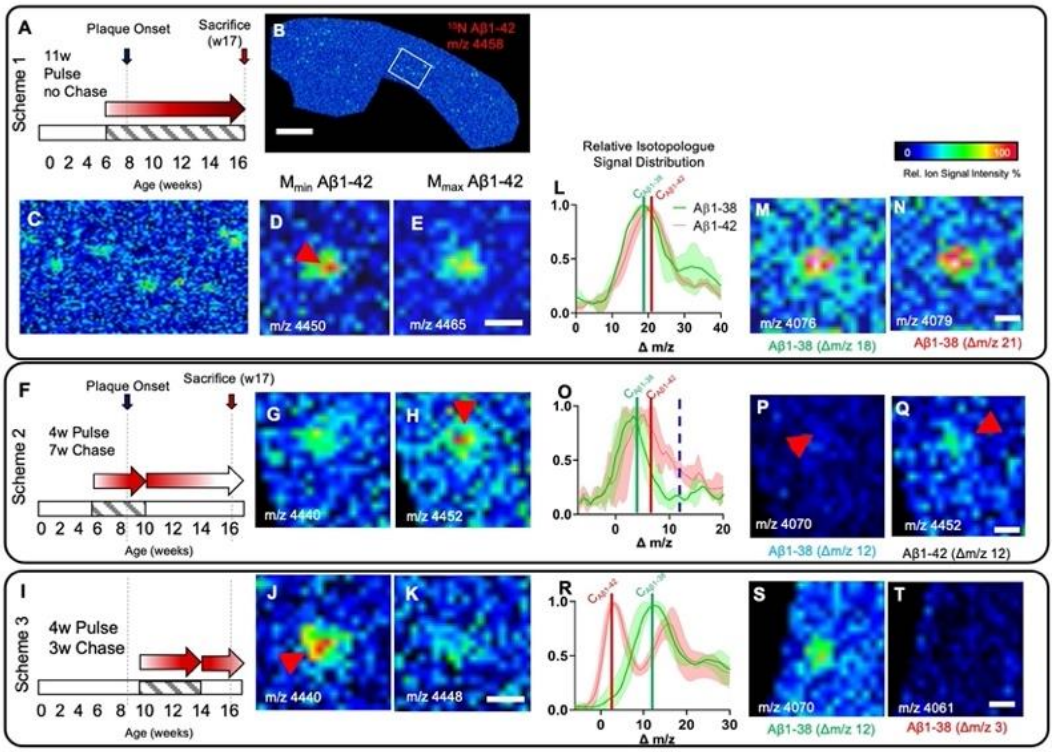

Figure 18. iSILK from *App*$^{NL-G-F}$ KI mice. (A, F, I) PULSE/CHASE schemes to analyse protein expression before and during plaque pathology onset. (B, C) MALDI-IMS allows delineation of different Aβ1-42 isotopologues across single plaques in different brain regions at 10 µm resolution. (D, E) IMS single ion images show that the initially deposited Aβ42 (D, H, J), localize to the core structure, while Aβ1-42 deposited later is homogenously distributed (E, G, K). Moreover, iSILK allows us to delineate the timeline of deposition for multiple Aβ peptides. Here, Aβ1-38 was found to be deposit after Aβ1-42, as shown by different levels of ^{15}N encoded in the respective isotopic envelopes (L, O, R). Using appropriate PULSE/CHASE labelling scheme 2 and 3, allows us to resolve differential label incorporation as illustrated in the single ion images (P, Q; S,T).

We further validated these observations by modifying and devising two additional labelling schemes (Fig. 18F, I). Both additional experiments further confirmed that the plaques in this *App* mouse model form first as small compact core and grow upon homogenous deposition of later secreted Aβ (Fig. 18F-K).

Third, label incorporation across different brain regions was compared to evaluate where in the brain plaque deposition precipitates first. Similar to the intra plaque region comparison, we statistically evaluated the average degree of label incorporation in cortical and hippocampal plaques. The results showed that cortical plaques contained more earlier-formed Aβ, which suggests that the cortex is the primary site of pathology onset.

Finally, we evaluated the sequence upon which the different Aβ species deposit. By comparing relative isotope incorporation in Aβ1-42 and 1-38, we observed that Aβ1-42 is the earlier formed species as confirmed across the three independent labelling schemes (Fig. 18L-T). Moreover, we could delineate that Aβ1-38 is secreted independently and at a later time than Aβ1-42. This rejects the hypothesis that Aβ1-38 is a product of on-plaque Aβ1-42 processing (Szaruga et al., 2017). This also proves that Aβ1-38 is secreted at a later time and is not derived from the same early Aβ1-42/App through instant Aβ1-42 processing, where delayed deposition can be explained through e.g. transmembrane interactions as suggested earlier. This is important as this further shows that later Aβ1-38 secretion occurs as a result of early Aβ1-42 mediated effects, such as gamma secretase modulation (De Strooper et al., 2012).

In summary, these experiments highlight the potential of using iSILK to follow Aβ plaque formation in an AD mouse model, with great temporal and chemical precision.

5.3 Finding 2 – In *App*$^{NL-F}$ KI mice, amyloid plaques precipitate first in the cortex as small, cored deposits consisting of Aβ1-42

While these initial experiments were key for establishing the technique and its feasibility, there are limitations with respect to the Arctic mutation in APP^{NL-G-F} mice, whereby the chemical properties of Aβ are altered, leading to increased aggregation propensity. This results in rapid plaque onset and pronounced formation of cored deposits. Therefore, by building on the previous findings from *App*$^{NL-G-F}$ mice, in these experiments I aimed to follow Aβ aggregation in evolving and progressing plaque pathology in *App*$^{NL-F}$ mice, which represent a more physiological model of amyloid aggregation, and are more comparable to human pathology.

For this, 6 month-old *App*$^{NL-F}$ mice were labelled for four months with ^{15}N and culled at either immediately at 10 months old, or after a 6-month CHASE at 18 months old, to obtain two groups with both early and established plaque pathology.

First, we evaluated the isotope content in 10 month-old animals that did not undergo any CHASE period following ^{15}N PULSE. Here, we observed solely sparse Aβ plaque deposition in the cortex, with the plaques containing solely Aβ1-42. Importantly, it was observed that all Aβ1-42 peptides detected showed ^{15}N incorporation (data not shown), thereby ensuring that the onset of PULSE scheme at 6 months old was sufficient to introduce the ^{15}N label into APP prior to pathology onset.

Secondly, to address the question on intra-plaque heterogeneity (core vs. periphery), the relative ^{15}N content of these plaque structures was evaluated. Here, plaques in 10 month-old *App*$^{NL-F}$ mice (PULSE age 6-10 months, no CHASE) displayed lower ^{15}N content for Aβ1-42 in the core compared with the periphery (Fig. 19A, $P<0.01$). This suggests that earlier secreted, less ^{15}N

containing Aβ1-42 is deposited at the core, while later secreted Aβ1-42 deposits at the periphery, which is consequently formed later. In 18 month-old animals (PULSE age 6-10 months, 6-month CHASE), the pattern is reversed due to the significant deposition of unlabelled Aβ1-42 during the CHASE period (Fig. 19B-D, $P<0.05$).

Both experiments suggest that indeed that these plaques deposit as small compact plaque cores that grow upon homogenous deposition across the entire plaque area.

Third, differential label incorporation across cortical and hippocampal plaques was evaluated, to identify the initial sites of plaque formation, similar as for the *App*$^{NL-G-F}$ mice. While at 10 months no plaques were detected in the hippocampus, in 18 month-old mice the average degree of label incorporation in cortical plaques was higher as compared to hippocampal plaques (Fig.19E). Keeping in mind the design of the labelling scheme used, these data indicate that cortical plaques contain more earlier-formed Aβ, which in turn suggests that the cortex is the primary site of pathology onset.

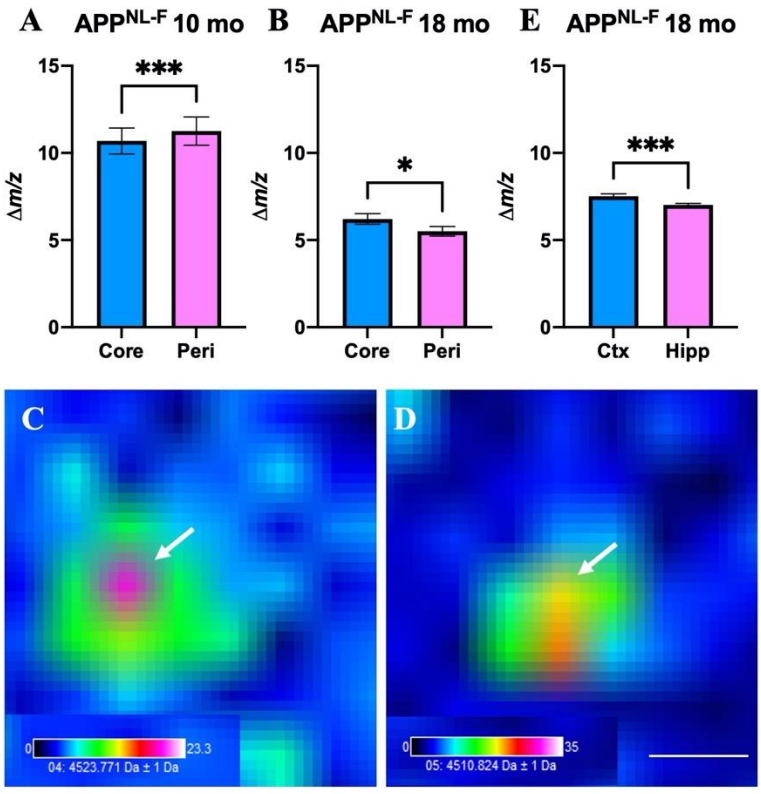

Figure 19. iSILK results from 18 month-old *App*$^{NL-F}$ mice.

(A,B) Spatial stable isotope labelled Aβ1-42 deposition patterns associated with intra plaque heterogeneity to determine plaque formation dynamics. Quantification of ^{15}N incorporation was performed by determining the centroid of the curve fitted to the isotopologue envelope for Aβ1-42. (A) At 10 months, core structures contained less labelled, hence earlier secreted Aβ1-42. At 18 months after a CHASE period, core structures contained more labelled Aβ1-42 compared to peripheral deposited Aβ1-42. IMS single ion images show that the initially deposited Aβ1-42, localise to the core structure (arrow, m/z 4523, C), while Aβ1-42 deposited later is distributed more to the periphery (m/z 4512, D). iSILK allows us to delineate the timeline of deposition across different brain areas as shown by different levels of ^{15}N encoded in the respective isotopic envelopes (E). Here cortical plaques contained more ^{15}N label than hippocampal plaques. Number of animals: N=3 per group. Number of plaques 10 months: N=5/animal; 18 months: N=5-10/region/animal. Scalebar E,F: 20 μm.

Abbreviations: IMS, imaging mass spectrometry; iSILK, imaging mass spectrometry combined with stable isotope labelling kinetics; mo, months old; Peri, periphery; Ctx, cortex; Hipp, hippocampus.

5.4 Finding 3 – Plaques mature with age, as revealed by correlative iSILK/LCO imaging

The previous LCO imaging experiments determined that an average increase in plaque maturation is observed with age across brain regions in both genotypes. This strongly suggests that plaque mature with age, and that this is reflected in the LCO signatures, though conclusions are drawn at the group level. To ultimately validate that plaque maturation (as observed by increased LCO emission ratios with age) is a continuous process for each plaque, I set out to correlate iSILK isotope signals with corresponding LCO signatures at the single plaque level. This is important as a correlation of Aβ peptide labelling results with LCO plaque aggregation state will thus reveal the degree of newly synthesised Aβ over time for individual Aβ plaques across brain regions.

To achieve this, consecutive sections were taken from *App*$^{NL-F}$ mice at 18 months old (PULSE 6-10 months old, CHASE 10-18 months old), where one section was used for MALDI-IMS and the other for LCO amyloid staining and hyperspectral imaging. In this way, individual plaques (partially on each section) were assessed, and MALDI-IMS data subsequently correlated with LCO data, in both the cortex and hippocampus.

In terms of the MALDI-IMS data, the results showed that in 18 month-old APP^{NL-F} mice, cortical plaques (Fig. 20A) have a higher level of ^{15}N incorporation, whereas plaques in the hippocampus have a lower level of incorporation (Fig. 20B), as reflected by a higher fourth isotopic peak (black arrows indicate, Fig. 20A and B). In line with this, LCO hyperspectral analysis of the same plaque on a consecutive section revealed that cortical plaques have a higher 500/580 nm LCO emission ratio compared with hippocampal plaques, which is indicative of a more mature plaque structure.

A Pearson r correlation of these two findings in three individual 18 month-old mice showed that across all mice, cortical plaques have higher ^{15}N incorporation (indicated by the $4^{th}/3^{rd}$ isotopologue peak ratio) and higher LCO emission ratio values compared to hippocampal plaques (Fig. 20G, mouse 2, $R=0.8350$, $P<0.01$, $N=9$; Fig. 20H, mouse 3, $R=0.8936$, $P<0.01$, $N=7$; Fig. 20I, mouse 4, $R=0.6386$, $P<0.05$, $N=10$). Further, there was a positive correlation between plaque age (^{15}N content) and maturation (LCO emission profiles) (Fig. 20G-I). This validates that more structurally mature plaques are older than those less structurally mature. Overall, this confirms that plaques maturation occurs continuously over time until the age of the here studied mice (18 months old), representing fully developed amyloid pathology. The interesting question arising from these results is what other cellular processes modulate plaque maturation.

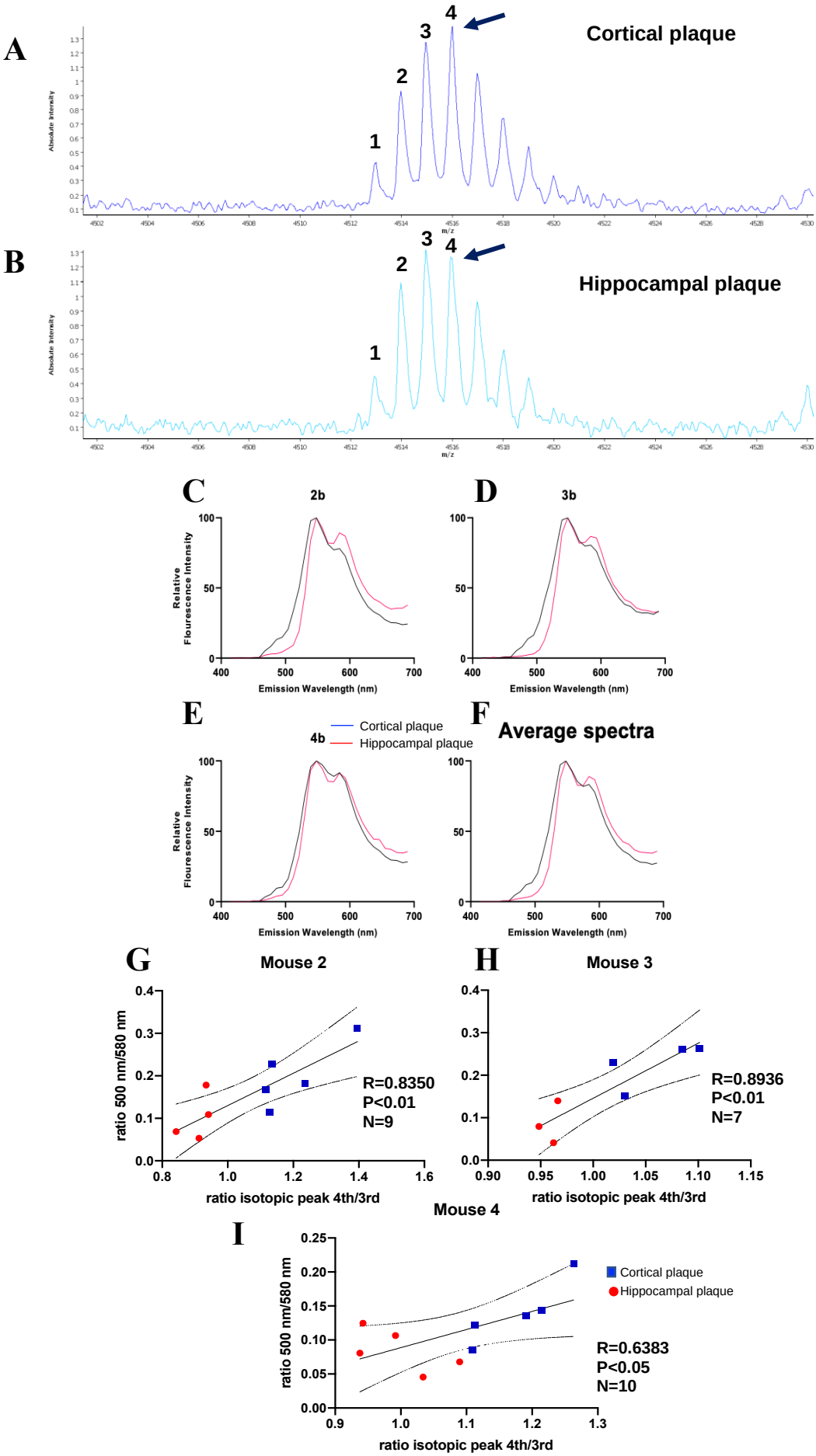
A
Cortical plaque
1
2
3
4
Absolute Intensity
m/z
B
Hippocampal plaque
1
2
3
4
Absolute Intensity
m/z
C
2b
Relative Flourescence Intensity
Emission Wavelength (nm)
D
3b
Emission Wavelength (nm)
E
4b
Cortical plaque
Hippocampal plaque
Relative Flourescence Intensity
Emission Wavelength (nm)
F
Average spectra
Emission Wavelength (nm)
G
Mouse 2
ratio 500 nm/580 nm
ratio isotopic peak 4th/3rd
R=0.8350
P<0.01
N=9
H
Mouse 3
ratio isotopic peak 4th/3rd
R=0.8936
P<0.01
N=7
I
Mouse 4
ratio 500 nm/580 nm
ratio isotopic peak 4th/3rd
Cortical plaque
Hippocampal plaque
R=0.6383
P<0.05
N=10

Figure 20. iSILK/LCO correlations in 18 month-old *App*$^{NL-F}$ mice.

Representative MALDI-IMS mass spectrum of Aβ1-42 for a single (A) cortical- and (B) hippocampal plaque in stable isotope labelled mice (PULSE 6-10 months old, CHASE 10-18 months old). Elevation of the fourth isotopologue peak most prominently illustrates ^{15}N incorporation (black arrows, A,B), whereby the absolute intensity is higher in the cortical plaque than the hippocampal plaques. (C-F) LCO hyperspectral emission profiles from the same cortical and hippocampal plaques used for IMS (C, mouse 2; D, mouse 3; E, mouse 4; F, average spectra of all three mice). Cortical plaques have a more mature structure than hippocampal plaques, as shown by higher emission intensities at around 500 nm due to higher qFTAA binding. (G-I) Two-tailed Pearson r correlation of IMS values with LCO emission values for the same cortical and hippocampal plaques (G, mouse 2; H, mouse 3; I, mouse 4). Here a higher IMS $4^{th}/3^{rd}$ isotopic peak ratio positively correlates with the LCO 500/580 nm emission ratio. XY pairs (N number), significance and r values are indicated accordingly. Number of animals: N=3 per group. Number of plaques: N=3-5/region; N=7-10/animal.

Abbreviations: IMS, imaging mass spectrometry; SILK, stable isotope labelling kinetics; LCO, luminescent conjugated oligothiophenes.

5.5 Chapter summary

In this chapter, I utilised a novel chemical imaging paradigm involving *in vivo* SIL of *App* KI mice to determine early and progressing Aβ peptide accumulation, aggregation and deposition dynamics with great temporal and chemical precision.

Here, it was found that iSILK allows for analysis of amyloid plaque formation over time in *App*$^{NL-G-F}$ mice, where all Aβ species were found to contain 15N atoms, indicating that initiation of labelling at week 7 is early enough to capture initial plaque deposition in these mice. Furthermore, the timeline of plaque deposition was established by comparing the relative isotope incorporation of Aβ peptides: first, plaques are deposited as an initial core formed entirely of Aβ1-42, followed by further deposition of Aβ1-42 along with Aβ1-38 to a lesser degree; second, that plaque cores form first, followed by the periphery; and third, that cortical plaques form prior to hippocampal plaques. Additionally, Aβ1-38 secretion was established as secondary to and independent of Aβ1-42, suggesting that it is a product of on-plaque Aβ1-42 processing.

These experiments were repeated in *App*$^{NL-F}$ mice, a more physiological model of human AD. Again, at 10 months, all Aβ peptides contained ^{15}N atoms, confirming that undergoing PULSE labelling at 6 months old was sufficient. Much like *App*$^{NL-G-F}$ animals, *App*$^{NL-F}$ mice also deposit plaques as a core formed of Aβ1-42 followed by further deposition of Aβ1-42 into the periphery, and in the cortex prior to the hippocampus.

Furthermore, correlative iSILK/LCO imaging analysis in 18 month-old *App*$^{NL-F}$ mice revealed a positive correlation between plaque age (^{15}N content) and LCO emission profiles (maturation). This confirms firstly: that both methods of measuring plaque age are valid, and secondly: that cortical plaques are older and thus formed prior to hippocampal plaques, in line with the iSILK data from *App*$^{NL-G-F}$ mice (Michno et al., 2021). Furthermore, this is consistent with the LCO results established in Chapter 4, providing further validation that in these mice, plaque deposition is dynamic and continuous over at least the first 18 months of life.

Overall, these findings highlight how SIL in combination with MALDI-IMS is an effective tool to study Aβ deposition dynamics in *App* KI mouse models. The results showed that Aβ deposition is temporally dynamic, with certain brain regions consistently more vulnerable to earlier deposition, and production of different Aβ species occurring at varying stages of pathology.

Chapter 6: The association between plaque conformation and microgliosis in *App* KI mice

6.1 Introduction

It is well-documented that in AD, gliosis occurs in line with accumulating Aβ pathology (Itagaki et al., 1989), and AD mouse models have provided insight into the potential roles of microglia around plaques. Initially, microglia are thought to be neuroprotective by removing synaptic damage in and around plaques (Condello et al., 2015). Murine microglia have been shown to cluster round plaques and promote them to become denser and more compact, by compartmentalising them to restrict the formation of protofibrillar Aβ, thereby reducing neuritic dystrophy (Bolmont et al., 2008; Condello et al., 2015; Meyer-Luehmann et al., 2008).

App KI mice have been reported to display unaltered microglial dynamics in the early stages of plaque pathology. In *App*$^{NL-G-F}$ mice, microglial activation has been shown to occur from about 5 months of age (Sacher et al., 2019), followed by altered expression of genes related to microglia modulation functions at 6 months of age (Castillo et al., 2017). Previous work in our lab showed that hippocampal microglial density and activation were unchanged compared to WTs at 3.5 months of age (Benitez, 2021). However, by 9 months old, when *App*$^{NL-G-F}$ mice have a heavy plaque load, they display increased numbers of Iba1+ microglia and increased microglial *Trem2* expression (Benitez et al., 2021; Saito et al., 2014). By 24 months old, *App*$^{NL-G-F}$ mice have large plaques and reactive gliosis throughout the brain (including the cortex and hippocampus) (Sakakibara et al., 2019). *App*$^{NL-F}$ mice, who start developing plaques at around 9 months old, have also been shown to have unchanged microglial density and activation at 10 months old compared to WT mice (Benitez, 2021). This suggests that it is late, rather than early Aβ accumulation which has a more significant effect on microglial behaviour. However, at what point and for what reason this occurs is unclear. Therefore, it would be useful to compare alterations in microglial density

and activation in early vs. late plaque pathology, to see if there is indeed a 'switch' in microglia behaviour over time.

Numerous studies have reported that Trem2-deficient mouse models show decreased microglial activation, resulting in a reduction of plaque-associated microglia and altered plaque morphology (Jay et al., 2015; Wang et al., 2015; Yuan et al., 2016). Indeed, recently our lab demonstrated that gene expression of microglial phagocytic markers was dependent on *Trem2* genotype (Wood et al., 2022). This same study showed that *App*$^{NL-F}$/*Trem2*^{R47H} mice exhibit a higher density of plaques in the hippocampus than *App*$^{NL-F}$ mice, driven by a larger number of smaller sized plaques (Wood et al., 2022). Overall this suggests that a perturbed microglial response in *App*$^{NL-F}$/*Trem2*^{R47H} mice may be affecting plaque clearance. Therefore, microglia may have an essential role for the clearance of smaller plaques, whilst not having much of an effect on larger plaques. Alternatively, the barrier formation function of microglia (Condello et al., 2015) may be lost in these mice, resulting in increased breaking off of smaller plaques from bigger plaques. Therefore, it would be useful in this context to further explore the effects that the *Trem2*^{R47H} mutation has on microglial activation and plaque morphology.

The present chapter will therefore explore microglial activation and distribution changes across two brain regions (cortex vs. hippocampus) in *App*$^{NL-G-F}$, *App*$^{NL-F}$ and *App*$^{NL-F}$/*Trem2*^{R47H} mice, and also compare these dynamics in early vs. late plaque pathology.

To do this, plaque-associated microglial distribution and activation (as determined by Iba1+ microglia counts and CD68 intensity, respectively) were quantified in these three mouse models. Alterations in the cortex vs. hippocampus were also examined, to see if microglial distribution or level of activation around plaques is influenced by brain region or plaque age (cortical plaques are older as they form there prior to the hippocampus, as established in the previous chapter). Additionally, in *App*$^{NL-G-F}$ and *App*$^{NL-F}$ mice, microglial dynamics in 18 month-old mice were compared to a time point that reflected early plaque pathology (4 and 9 months old, respectively), to assess if more mature plaques attract greater quantities of activated microglia. Previous work by our lab

demonstrated that in *App*$^{NL-F}$ mice, total hippocampal microglial distribution changes occur at around 24 months of age (Benitez et al., 2021); however, it is unclear whether there are plaque-associated alterations, or changes in the cortex. Furthermore, as *App*$^{NL-F}$/*Trem2*^{R47H} mice exhibit alterations in microglial response, in addition to reduced levels of *Trem2* (Wood et al., 2022), examining this model will add interesting insight into how addition of the *Trem2*^{R47H} mutation affects microglia dynamics.

6.2 Microglial activation and distribution changes across brain regions with age in *App* KI mice

Here, I compared the distribution of microglia around individual plaques by comparing the distribution of Iba1+ cells in concentric circles increasing by 20 μm radius out from the plaque edge. Microglia within the 0 – 10 μm circles were classed as 'on-plaque', those in the 10 – 30 μm circles were 'peri-plaque', and those in the 30 – 50 μm circles were 'away-from-plaque'. When a microglial cell is overlapping the border of on-plaque vs. per-plaque, or peri-plaque vs. away-from-plaque, it is counted on the innermost side.

6.2.1 Finding 1 – Alterations in microglial clustering across genotype

Firstly, I aimed to compare the distribution of microglia across the three genotypess at the same age, to determine if genetic background (and therefore level of plaque pathology) contributes to alterations in microgliosis, without age as a confounding factor. Therefore, microglia positive for both Iba1 and DAPI were counted in concentric circles around the plaques of 18 month-old *App*$^{NL-G-F}$, *App*$^{NL-F}$ and *App*$^{NL-F}$/*Trem2*^{R47H} mice, and compared with age-matched WT mice. Figure 21 outlines the method of counting, whereby the macro draws concentric circles increasing in 10 μm distance around each plaque, here illustrated with an Iba1/DAPI co-stained section from a 9 month-old *App*$^{NL-F}$ mice (Fig. 21A). As can be seen, the macro has correctly identified plaques, as confirmed by LCO staining (Fig. 21B). For WT mice, the macro draws a pseudo-plaque (Fig. 21C). Only microglia positive for both Iba1 and DAPI were counted. As individual microglia often overlap with two concentric circles, counts were pooled into 'on-plaque', 'peri-plaque' and 'away-from-plaque' areas, as described above. For

normalisation, microglial density was calculated as per mm^2 rather than exact counts, due to varying radius sizes of the rings measured depending on the size of the plaque.

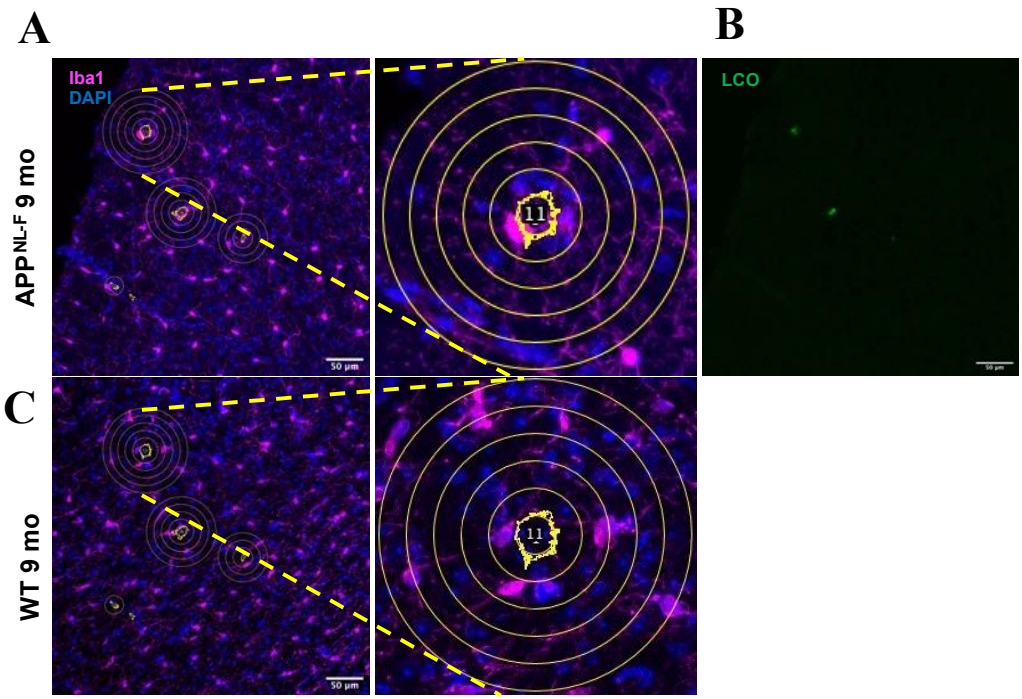

Figure 21. Counting method for microglia around plaques. (A) The macro identifies plaques within an image obtained by fluorescence confocal microscopy, and draws concentric circles increasing in 10 μm distance around each plaque. (B) LCO amyloid imaging in the same section as for (A) confirms the correct localisation of plaques. Only microglia positive for both Iba1 (pink) and DAPI (blue) are counted. As individual microglia often overlap with two concentric circles, counts are pooled into 'on-plaque' (circles 0 – 10 μm), 'peri-plaque' (circles 10 – 30 μm) and 'away-from-plaque' (circles 30 – 50 μm) areas. When a microglial cell is overlapping the border of on-plaque vs. per-plaque, or peri-plaque vs. away-from-plaque, it is counted on the innermost side. (C) For WT mice, who do not bear plaques, pseudo-plaques are drawn by the macro, and microglia are counted as for *App* KI mice.
Abbreviations: WT, wild-type; mo, months old.

In 18 month-old *App* KI mice, who exhibit widespread amyloid pathology, antibody staining for Iba1 (for microglia) followed by LCO staining for plaques and DAPI staining for nuclei was performed. Visualisation after confocal imaging revealed that as expected, microglia cluster around plaques, with their density clearly increased in plaque-associated regions (Fig. 22). In particular, microglia around plaques in App^{NL-F} (Fig. 22A) and App^{NL-G-F} (Fig. 22B) mice demonstrate increased clustering compared with $App^{NL-F}/Trem2^{R47H}$ (Fig. 22C).

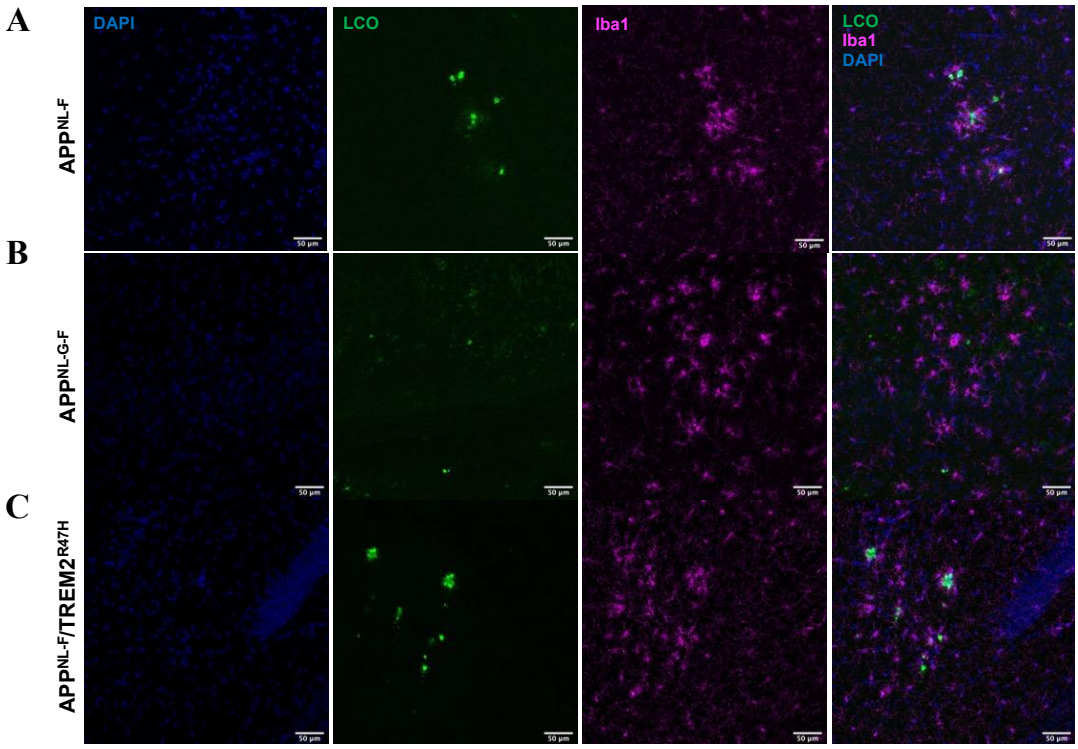

Figure 22. Clustering of microglia around plaques in 18 month-old *App* KI mice.
Representative confocal images of Iba1, LCO double staining (qFTAA and hFTAA) and DAPI of hippocampal plaques in 18 month-old (A) *App*$^{NL-G-F}$, (B) *App*$^{NL-G-F}$ and (C) *App*$^{NL-F}$/*Trem2*^{R47H} mice. All images are captured at 20X magnification.
Abbreviations: LCO, luminescent conjugated oligothiophenes.

Quantification with a two-way ANOVA revealed a main effect of genotype on the plaque for *App*$^{NL-F}$ vs. *App*$^{NL-F}$/*Trem2*^{R47H} mice. Post-hoc comparisons using Holm-Šídák's test confirmed that on the plaque, APP^{NL-F} mice had significantly more microglia compared to *App*$^{NL-F}$/*Trem2*^{R47H} (Fig. 23A, P<0.01 cortex; Fig. 23B P<0.05 hippocampus). This trend was also seen in the peri-plaque and away-from-plaque regions, although this was not statistically significant. Interestingly, the difference in microglial density around plaques was not statistically significant between *App*$^{NL-G-F}$ and *App*$^{NL-F}$ mice, demonstrating that microglia from both genotypes have effective microglial clustering mechanisms around plaques. All three *App* KI groups exhibited significantly increased microglial density on the plaque compared to WT mice in both the cortex and hippocampus (red dotted line represents WT; Fig. 23A and B), although this effect evened out the further away from the plaque.

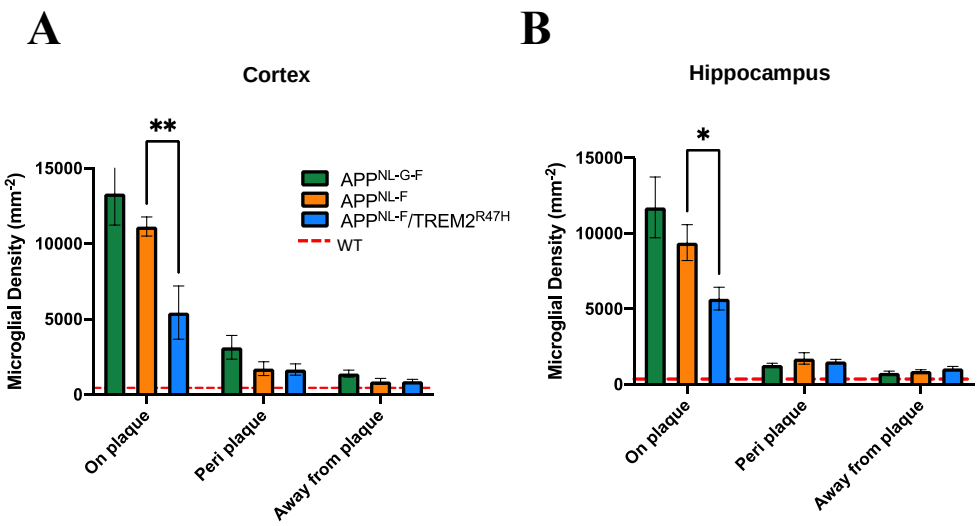

Figure 23. Genotype-associated alterations in microglial clustering in *App* KI mice.
Quantification with a two-way ANOVA followed by Holm-Šídák's multiple comparisons test revealed statistically significant genotype-associated alterations in microglial density around plaques in the (A) cortex and (B) hippocampus of *App*$^{NL-G-F}$, *App*$^{NL-F}$ and *App*$^{NL-F}$/*Trem2*^{R47H} mice. Numbers of microglia are expressed as per mm^2 rather than exact counts due to varying radius sizes of rings measured depending on the size of the plaque. Number of animals: N=4-5 per group. Number of plaques: N=15-20/region/animal. *P<0.05; **P<0.01.
Abbreviations: WT, wild-type.

Interestingly, when comparing *App*$^{NL-G-F}$ and *App*$^{NL-F}$/*Trem2*^{R47H}, the decreased microglial density around plaques in the latter suggests that the *Trem2*^{R47H} mutation impairs the ability of microglia to cluster around plaques. This is in line with previous research showing that *Trem2*^{R47H} mice display reduced quantities of dense-core plaques (Cheng-Hathaway et al., 2018), suggesting an impairment in the ability of microglia to compact plaques. Additionally, Trem2-deficient mouse models show decreased microglial activation, resulting in a reduction of plaque-associated microglia and altered plaque morphology (Jay et al., 2015; Wang et al., 2015; Yuan et al., 2016). Also, as microglia counts were largely not significantly changed between the three genotypes or compared to WT in the peri-plaque and away-from-plaque regions, this suggests that in 18 month-old mice, microglial alterations are related to plaque-response mechanisms.

6.2.2 Finding 2 – Microglial clustering around plaques and across brain regions

After establishing genotype-associated alterations in microglial density, next, I aimed to explore changes in clustering with increasing distance from the plaque, and also if these alterations are consistent between brain regions. Therefore, here I assessed cortical vs. hippocampal microglial density at 20-µm increments around plaques in *App*$^{NL-F}$ (9 and 18 months old), *App*$^{NL-F}$/*Trem2*^{R47H} (18 months old) and *App*$^{NL-G-F}$ (4 and 18 months old) mice.

Visually, it is difficult to detect differences between the two regions after Iba1 IHC for microglia and LCO/DAPI co-staining for plaques and nuclei, respectively (data not shown). Quantification with a two-way ANOVA revealed a main effect of plaque distance for all genotypes and age groups assessed (Fig. 24A-E). Post-hoc comparisons using Holm-Šídák's test confirmed that on-plaque microglial density was significantly increased compared to peri-plaque and away-from-plaque areas, in both the cortex and hippocampus (Fig. 24A-E). The only exception was in 9 month-old *App*$^{NL-F}$ mice, where there were no differences between on-plaque and peri-plaque microglial counts in the cortex (Fig. 24C).

Across all age groups and genotypes, there was no main effect of brain region (cortex vs. hippocampus), apart from in 4 month-old *App*$^{NL-G-F}$ mice (Fig. 24A); although after post hoc analysis, this was not statistically significant.

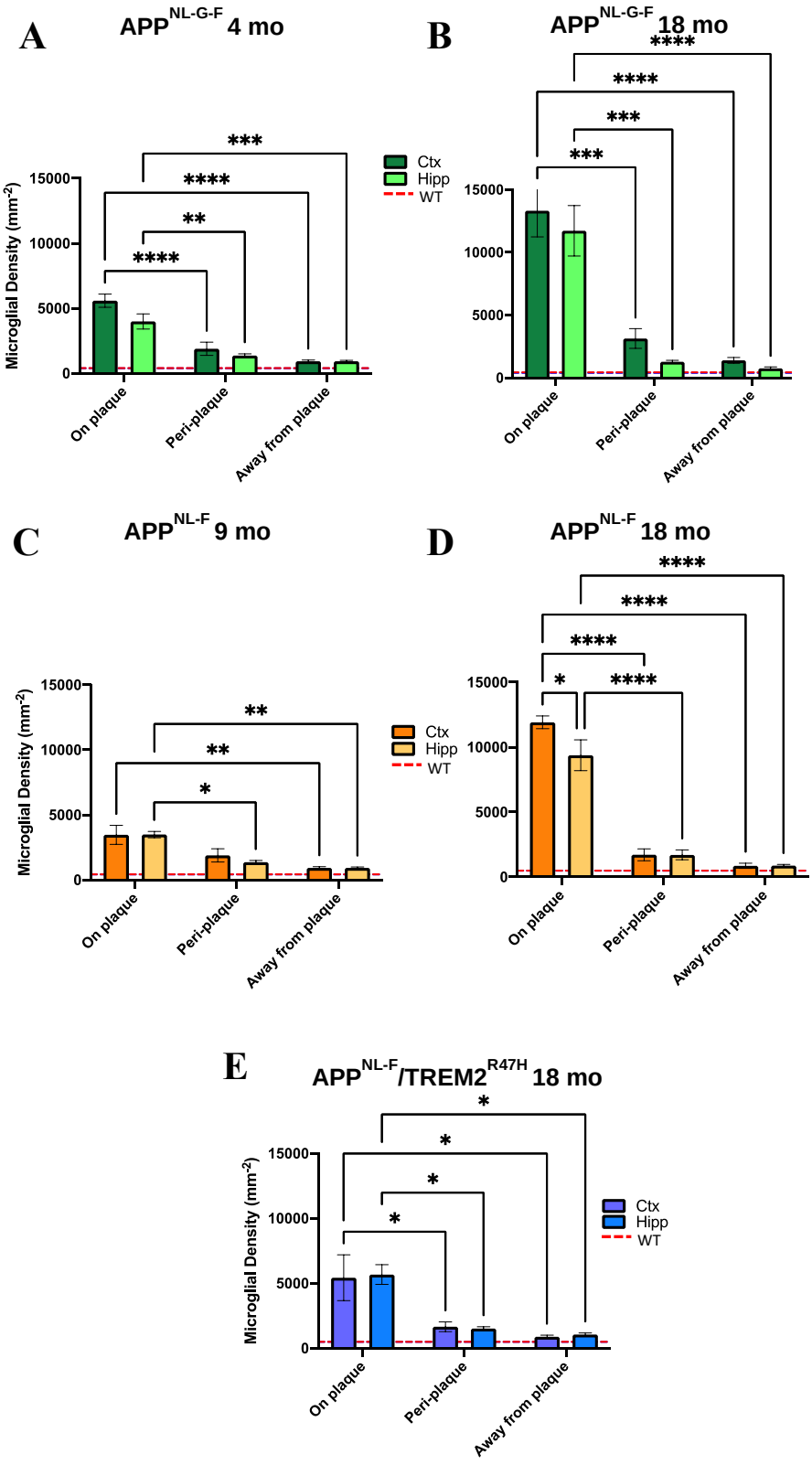

Figure 24. Plaque-associated microglial clustering in *App* KI mice.

Quantification with a two-way ANOVA followed by Holm-Šídák's multiple comparisons test revealed statistically significant plaque-associated alterations in microglial density in *App*$^{NL-G-F}$ mice at (A) 4 and (B) 18 months old; APP^{NL-F} at (C) 9 and (D) 18 months old; and (E) 18 month-old *App*$^{NL-F}$/*Trem2*^{R47H} mice. Numbers of microglia are expressed as per mm^2 rather than exact

counts due to varying radius sizes of rings measured depending on the size of the plaque. Number of animals: N=4-5 per group. Number of plaques: N=15-20/region/animal. *P<0.05; **P<0.01; ***P<0.001; ****P<0.0001.
Abbreviations: Ctx, cortex; Hipp, hippocampus; WT, wild-type; mo, months old.

6.2.3 Finding 3 – Age-associated changes in microglial clustering

Both *App*$^{NL-F}$ and *App*$^{NL-G-F}$ models exhibit a progressive rise in amyloidosis, with *App*$^{NL-F}$ mice starting to develop plaques at around 9 months, and *App*$^{NL-G-F}$ at 2 months. Hence, the former is an excellent model for studying early pathological changes, whereas the latter is good for examining advanced, post-plaque alterations in the brain. Therefore, I aimed to examine age-associated changes in microglia around plaques, using the same counting method as above. Due to lack of tissue, I was unable to assess *App*$^{NL-F}$/*Trem2*^{R47H} mice at a younger age, and therefore this group is not included in this analysis.

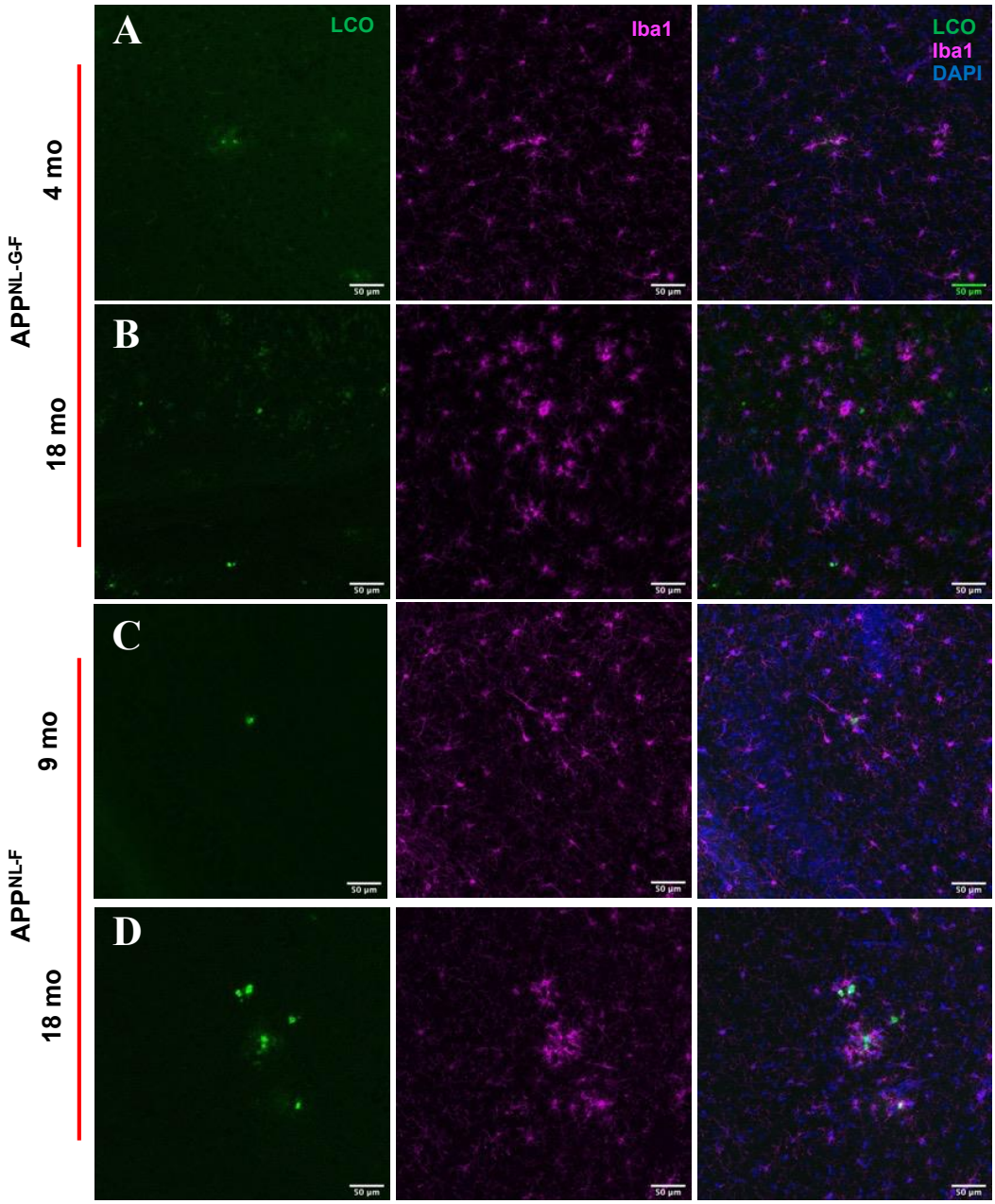

Figure 25. Alterations in microglial clustering around plaques in young vs. old *App* KI mice. Representative confocal images of Iba1, LCO (qFTAA and hFTAA) and DAPI co-staining of hippocampal plaques in *App*$^{NL-G-F}$ mice at (A) 4 and (B) 18 months old; and *App*$^{NL-F}$ at (C) 9 and (D) 18 months old. All images are captured at 20X magnification. Number of animals: N=4-5 per group. Number of plaques: N=15-20/region/animal.
Abbreviations: mo, months old.

The confocal imaging results showed that younger *App* KI mice have fewer plaques than their older counterparts, and fewer microglia clustered around those

plaques (Fig. 25). The difference is particularly noticeable in *App*$^{NL-F}$ mice, where microglia are more consistently spaced throughout the section in 9 month-old mice (Fig. 25C) compared with 18 month olds (Fig. 25D). This effect is also seen when comparing young (Fig. 25A) vs. old APP^{NL-G-F} (Fig. 25B).

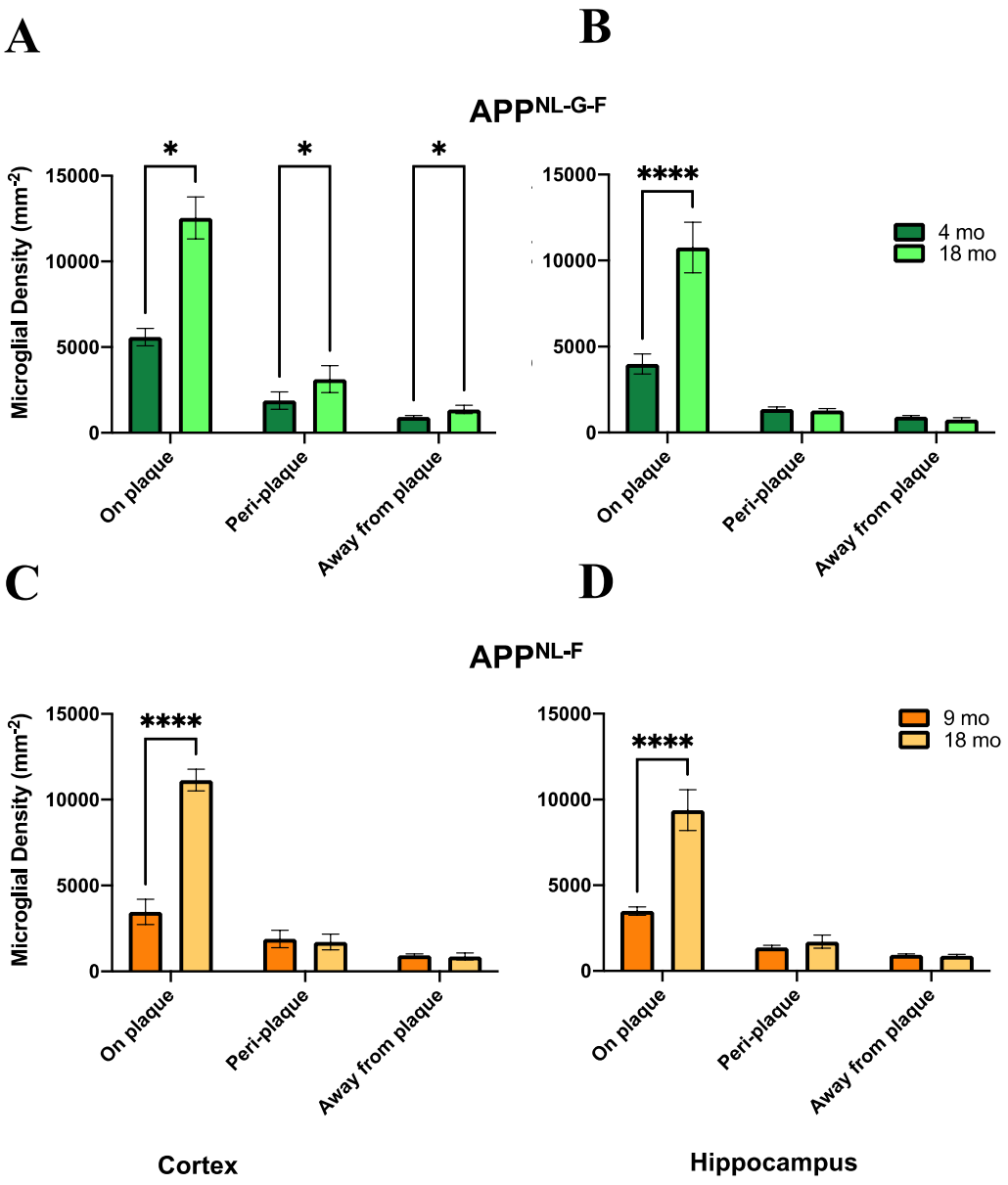

Figure 26. Age-associated alterations in microglial clustering in *App* KI mice.

Quantification with a two-way ANOVA followed by Holm-Šídák's multiple comparisons test revealed statistically significant age-associated alterations in microglial density directly around plaques in the (A) cortex and (B) hippocampus of *App*$^{NL-G-F}$ mice; and the (C) cortex and (D) hippocampus of *App*$^{NL-F}$ mice. Numbers of microglia are expressed as per mm^2 rather than exact counts due to varying radius sizes of rings measured depending on the size of the plaque. Number of animals: N=4-5 per group. Number of plaques: N=15-20/region/animal. *P<0.05; ****P<0.0001.

Abbreviations: mo, months old.

Quantification with a two-way ANOVA followed by Holm-Šídák's multiple comparisons test showed that for both *App* KI models and for both the cortex and hippocampus, older mice have significantly increased microglial counts around the plaque (Fig. 26). The peri-plaque and away-from-plaque regions were not significantly altered between ages; however, except for in the cortex of *App*$^{NL-G-F}$ (Fig. 26A). Overall this suggests that recruitment of microglia occurs following plaque formation, implicating microgliosis as a secondary event to amyloid deposition.

6.3 Microglial activation

After establishing alterations in microglial distribution around plaques in *App* KI mice, next, I aimed to understand the activation status of these microglia by staining sections with CD68, a well-established marker of microglial phagocytic activity (Hopperton et al., 2018). For drawing of circles, the same macro was used as for microglial counting. An additional macro calculated CD68 signal only within Iba1 signal, to be certain that microglia-specific activity was being measured. Microglial CD68 immunoreactivity was measured in 10-μm concentric circles around plaques until a 50-μm radius was reached around the plaques. This radius was chosen as it is the furthest to reliably measure from a plaque at this age without other plaques impinging on the measurement.

6.3.1 Finding 1 – Microglial activation around plaques is dependent on genetic background

Firstly, I aimed to compare microglial activation across the three genotypes at the same age, to determine if genetic background contributes to alterations in microgliosis, without age as a confounding factor. Therefore, microglial CD68 immunoreactivity was measured in 10-μm concentric circles around plaques in 18 month-old *App*$^{NL-G-F}$, *App*$^{NL-F}$ and *App*$^{NL-F}$/*Trem2*^{R47H} mice, and compared with age-matched WT mice.

Visualisation of CD68 immunoreactivity with confocal microscopy showed that APP^{NL-G-F} mice had the greatest level of activation not only directly around

plaques, but also in the periphery (Fig. 27A). *App*$^{NL-F}$ mice demonstrated CD68 immunoreactivity more tightly clustered around the plaque (Fig. 27B). *App*$^{NL-F}$/*Trem2*^{R47H} mice, on the other hand, had the lowest levels of activation around plaques (Fig. 27C). Quantification with a two-way ANOVA revealed a significant plaque distance x genotype interaction in the cortex ($P<0.01$) and hippocampus ($P<0.001$), with post-hoc tests revealing that at almost every 10-μm increment from the plaque, *App*$^{NL-G-F}$ mice had significantly increased microglial activation compared to APP^{NL-F} in both brain regions (Fig. 27D cortex; Fig. 27E hippocampus). In *App*$^{NL-F}$ mice, on the other hand, this effect was only seen compared with *App*$^{NL-F}$/*Trem2*^{R47H} near the plaque, in both brain regions (Fig. 27D and E). Additionally, compared to WT, *App*$^{NL-G-F}$ mice had significantly increased CD68 immunoreactivity at all distances measured from the plaque, whereas in *App*$^{NL-F}$ and *App*$^{NL-F}$/*Trem2*^{R47H}, this effect was only seen nearest the plaque (up to circle 20 μm; Fig. 27D and E). This was consistent across both brain regions (Fig. 27D and E).

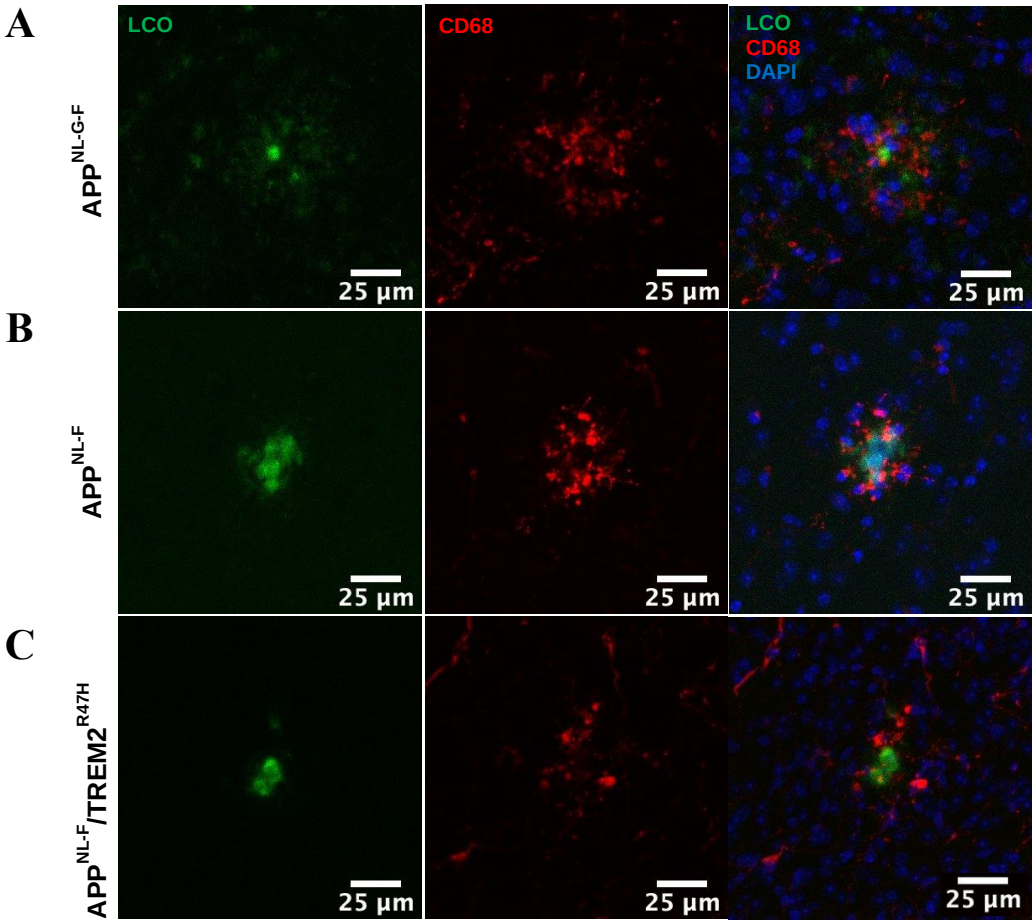
A
B
C
LCO
CD68
LCO
CD68
DAPI
25 µm
APP^NL-G-F
APP^NL-F
APP^NL-F/TREM2^R47H

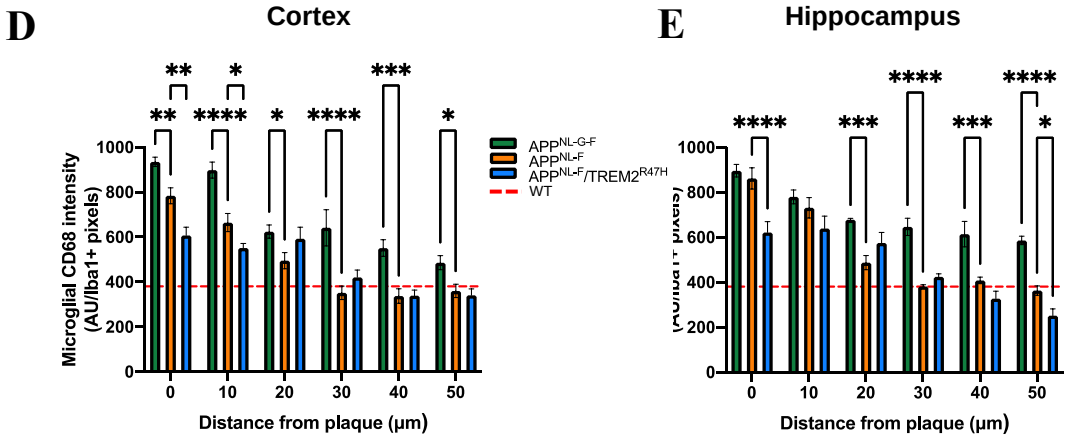
D
Cortex
E
Hippocampus
Microglial CD68 intensity (AU/Iba1+ pixels)
Distance from plaque (µm)
APP^NL-G-F
APP^NL-F
APP^NL-F/TREM2^R47H
WT

Figure 27. Genotype-associated alterations in microglial activation around plaques in 18 month-old *App* KI mice. Representative confocal images of CD68, LCOs (qFTAA and hFTAA) and DAPI co-staining of cortical plaques in (A) *App*$^{NL-G-F}$, (B) *App*$^{NL-F}$ and (C) *App*$^{NL-F}$/*Trem2*^{R47H} mice at 18 months old. All images are captured at 20X magnification. Quantification of microglial CD68 intensity in the (D) cortex and (E) hippocampus of 18 month-old *App* KI mice, and all compared to age-matched WT mice (red dotted line). Columns indicate mean ± SEM. Number of animals: N=4-5 per group. Number of plaques: N=15-20/region/animal. Interactions within plaque distances from a two-way ANOVA followed by Holm-Šídák's multiple comparisons test indicated by: *P<0.05; **P<0.01; ***P<0.001; ****P<0.0001.
Abbreviations: WT, wild-type; LCOs, luminescent conjugated oligothiophenes.

Interestingly, CD68 protein expression in *App*$^{NL-G-F}$ mice remained significantly higher than *App*$^{NL-F}$ and *App*$^{NL-F}$/TREM2^{R47H} even at 40 μm away from the plaque (in both cortex and hippocampus), and at 50 μm in the hippocampus. This is in contrast to the microglial density data, where I found no difference in microglial counts between genotypes in the peri-plaque and away-from-plaque regions. This suggests that at 18 months old, despite plaque-associated microglial distribution being the same as the other two genotypes, each microglia is expressing more CD68. Additionally, microglia are activated not only on the plaque, but also in the periphery, suggesting that microglia-associated toxic Aβ species in these mice are not only confined to nearest the plaque, but also in the surrounding areas.

6.3.2 Finding 2 – Microglial activation around plaques is not altered between the cortex and hippocampus in both early- and late-stage pathology in *App* KI mice

Next, I aimed to assess differences in microglial activation between the cortex and hippocampus, at both early and late-stage pathology in *App* KI mice. Even though *App*$^{NL-G-F}$ and *App*$^{NL-F}$ mice show increased microglial density on the plaque in the cortex compared to the hippocampus, this was not replicated in activation levels. At all distances from the plaque, there were no differences in CD68 intensity between the cortex and hippocampus in both 4 and 18 month-old *App*$^{NL-G-F}$ (Fig. 28A), and 9 and 18 month-old *App*$^{NL-F}$ (Fig. 28B).

For *App*$^{NL-F}$/*Trem2*^{R47H}, the only tissue available was from 18 month-old animals, therefore it was not possible to compare pathology to an earlier timepoint. However, consistent with the other two genotypes, *App*$^{NL-F}$/*Trem2*^{R47H} mice also did not display regional differences in microglial activation at 18 months old (Fig. 28C). Overall, these results indicate that despite alterations in plaque-associated microglial clustering between cortical and hippocampal regions, this is not associated with changes in microglial activation.

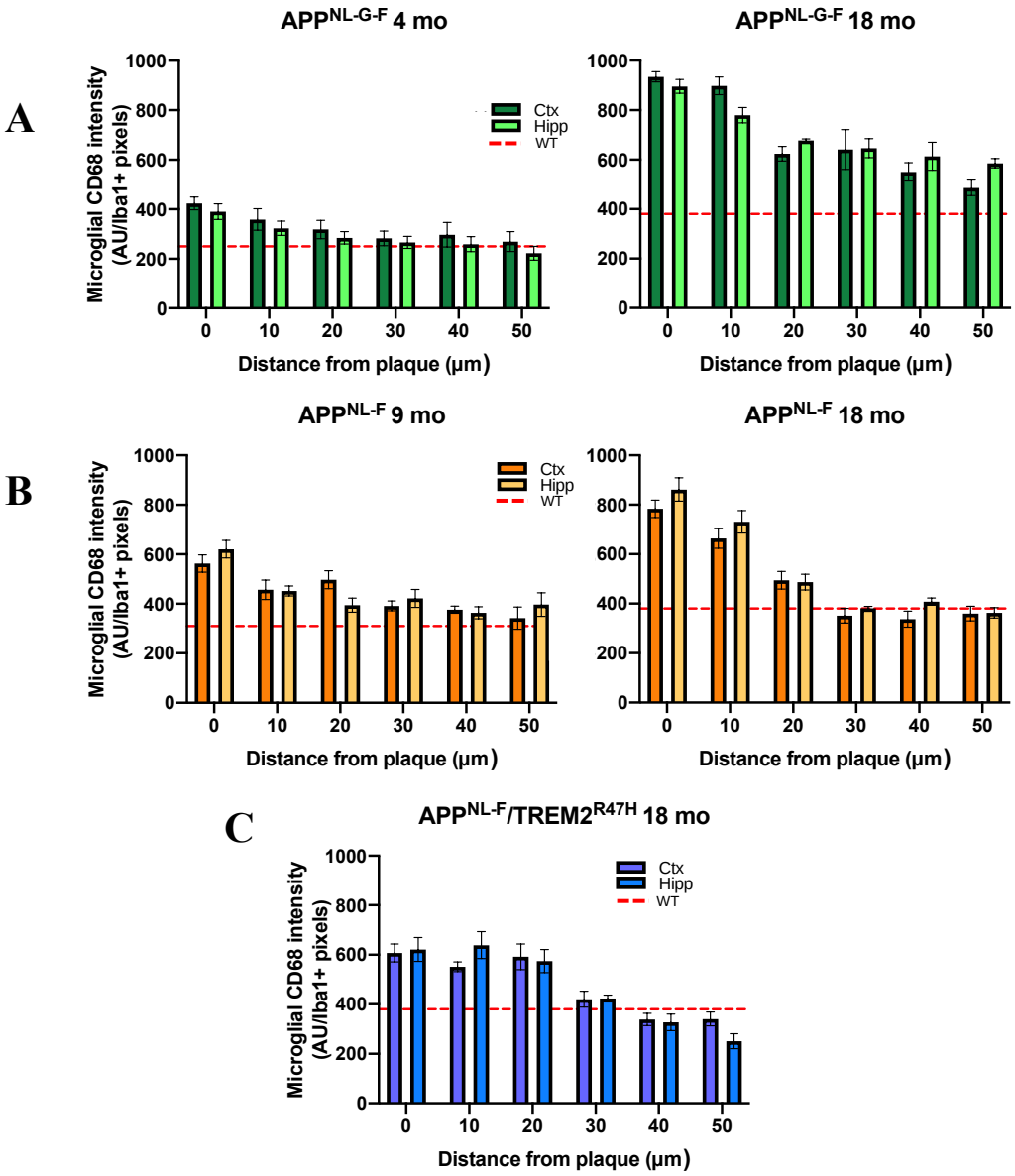

Figure 28. Cortical vs. hippocampal microglial activation around plaques in *App* KI mice. Microglial CD68 intensity around plaques in the cortex and hippocampus of (A) *App*$^{NL-G-F}$ (B) *App*$^{NL-F}$ and (C) *App*$^{NL-F}$/*Trem2*^{R47H} mice, and all compared to age-matched WT mice (red dotted

line). Columns indicate mean ± SEM. Number of animals: N=4-5 per group. Number of plaques: N=15-20/region/animal.
Abbreviations: Ctx, cortex; Hipp, hippocampus; WT, wild-type.

6.3.3 Finding 3 – Age-associated increase in microgliosis in *App* KI mice

With the knowledge that microglial activation differs between *App* KI models, next, I sought to understand how early vs. late plaque pathology affects microgliosis.

First, in $App^{NL\text{-}G\text{-}F}$ mice, who develop fast and aggressive amyloid pathology from around 2 months old (Benitez et al., 2021; Saito et al., 2014), microglial activation around plaques was compared between 4 and 18 month-old mice, to understand potential alterations at different stages of plaque pathology.

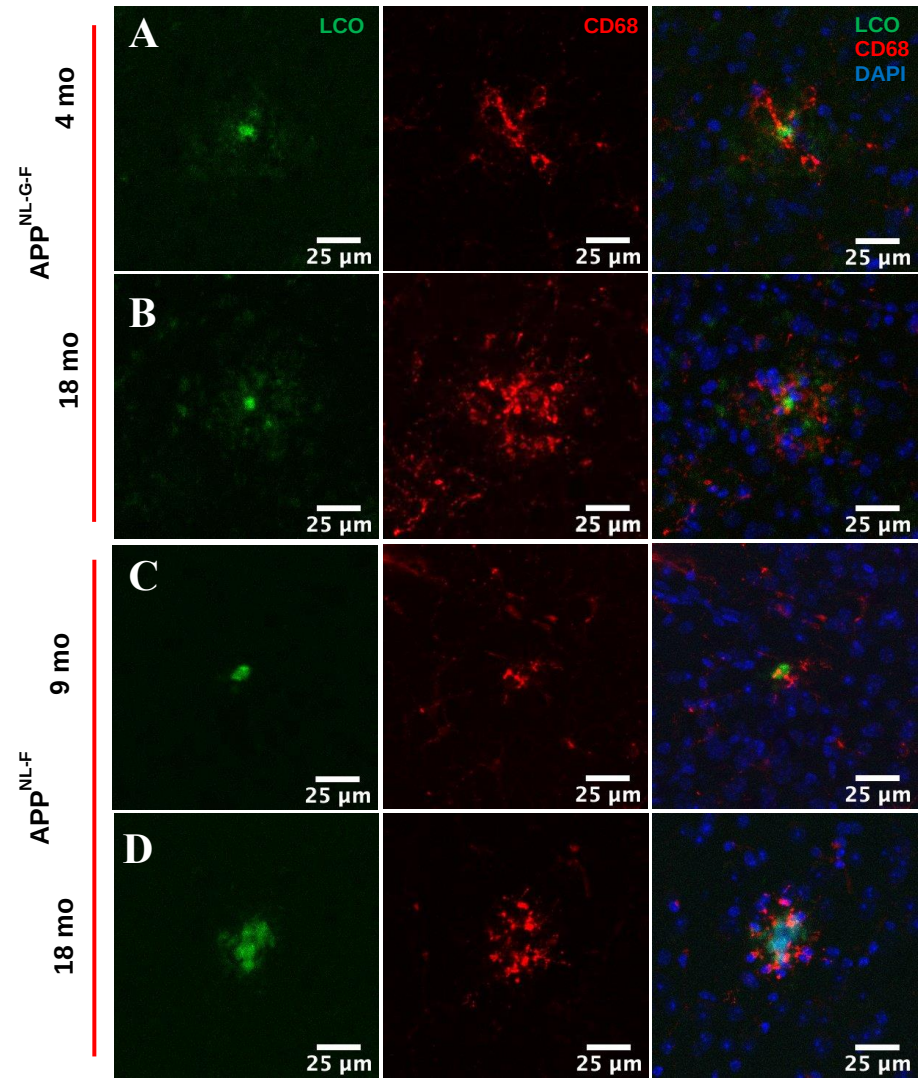
A
LCO
CD68
LCO
CD68
DAPI
25 µm
B
C
D
4 mo
18 mo
9 mo
18 mo
APP^NL-G-F
APP^NL-F

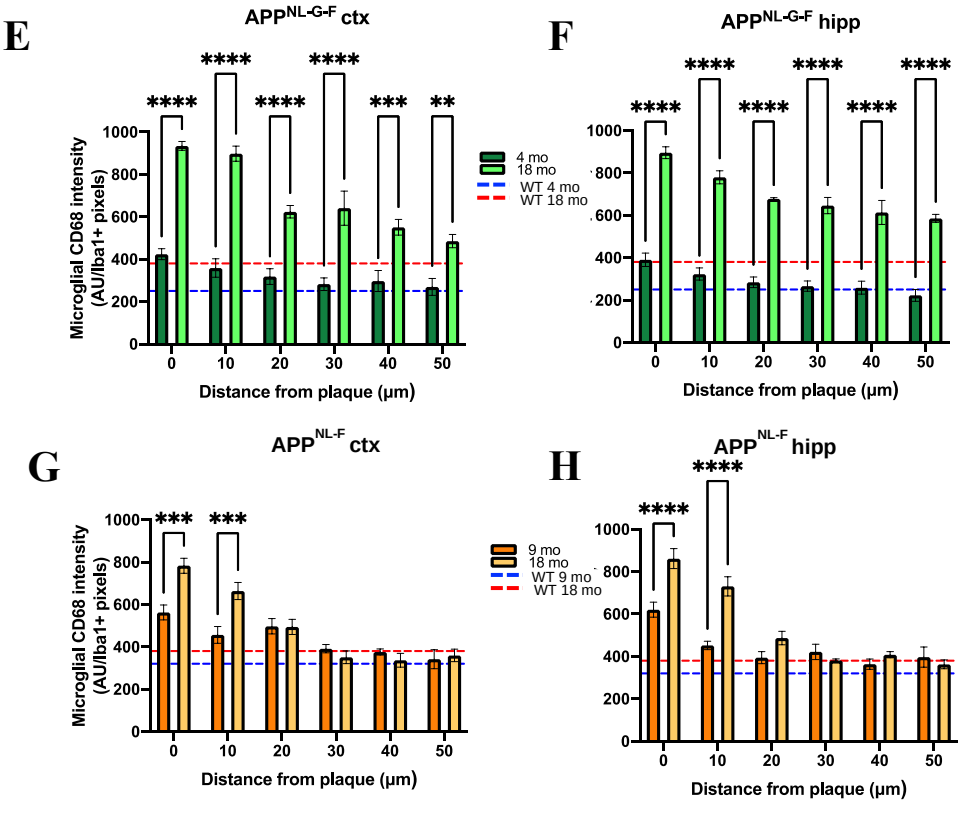
E
APP^NL-G-F ctx
F
APP^NL-G-F hipp
G
APP^NL-F ctx
H
APP^NL-F hipp
Microglial CD68 intensity (AU/Iba1+ pixels)
Distance from plaque (µm)
4 mo
18 mo
WT 4 mo
WT 18 mo
9 mo
18 mo
WT 9 mo
WT 18 mo

Figure 29. Age-associated changes in microglial activation around plaques in *App* KI mice. Representative confocal images of CD68, LCO (qFTAA and hFTAA) and DAPI co-staining of cortical plaques in *App*$^{NL-G-F}$ mice at (A) 4 and (B) 18 months old; and APP^{NL-F} mice at (C) 9 and (D) 18 months old. All images are captured at 20X magnification. Quantification of age-associated alterations in microglial CD68 intensity in the (E) cortex and (F) hippocampus of APP^{NL-G-F} mice; and the (G) cortex and (H) hippocampus of *App*$^{NL-F}$ mice. Columns indicate mean ± SEM. Number of animals: N=4-5 per group. Number of plaques: N=15-20/region/animal. Interactions within plaque distances from a two-way ANOVA followed by Holm-Šídák's multiple comparisons test indicated by: **P<0.01; ***P<0.001; ****P<0.0001.
Abbreviations: Ctx, cortex; Hipp, hippocampus; WT, wild-type; LCOs, luminescent conjugated oligothiophenes.

Observation of CD68 staining showed a clear increase in CD68 immunoreactivity not only directly around the plaque, but also in the periphery in older animals (Fig. 29B) compared with their younger counterparts (Fig. 29A). Statistical analysis with a two-way ANOVA revealed a significant plaque distance x genotype interaction only in the cortex (P<0.001). Subsequent Holm-Šídák's multiple comparisons test showed that in cortex, older *App*$^{NL-G-F}$ mice displayed significantly increased levels of CD68 intensity at every 10-μm increment from the plaque, compared with their younger counterparts (P<0.0001; P<0.001; P<0.01). Additionally, 18 month-old *App*$^{NL-F}$ and *App*$^{NL-G-F}$ animals had upregulated on-plaque microgliosis compared with age-matched WT mice in both the cortex and hippocampus; however, this effect was also only seen in young *App*$^{NL-F}$ and not *App*$^{NL-G-F}$ mice (Fig. 29E-H).

These data combined thus suggest that plaque-associated microglial activation is a late, rather than early pathological response.

6.3.4 Finding 4 – Plaque-associated microgliosis is dependent on Trem2genotype and stage of pathology

Earlier in this chapter, it was established that, in *App*$^{NL-F}$ and *App*$^{NL-G-F}$ mice, individual plaque structures mature over time, and that this corresponds with increased microglial clustering and activation around plaques. *App*$^{NL-F}$/*Trem2*^{R47H}

mice, on the other hand, display altered plaque morphology and an impairment in microglial clustering, likely due to the *TREM2*^{R47H} mutation causing a loss-of-function effect in the ability of microglia to form a protective barrier around plaques and/or compact them properly.

With this knowledge, next, I aimed to examine the LCO profile of each individual plaque within *App* KI mice, i.e. its maturation state, and correlate this with CD68 intensity in the 'on-plaque' (0 – 10 µm), 'peri-plaque' (10 – 30 µm) and 'away-from-plaque' (30 – 50 µm) regions. The aim of this analysis was to determine:
1. Do more mature plaques (with a higher 500/580 nm emission ratio) show increased CD68 immunoreactivity?;
If so:
2. Is this effect is only directly around the plaque, or also in the vicinity?;
3. Is this different among genotypes?;
4. Does this change with age?; and
4. Is this different in the cortex vs. hippocampus?

Thus, this will give interesting insight into the behaviour of microglia around individual plaques. If more mature/cored plaques have more microglial activation directly around them, this confirms microgliosis as a secondary event, i.e. amyloid aggregation and deposition draws in a microglial response. However, if it is in fact younger/less mature plaques with more activated microglia, this suggests that microglial activation precedes plaque maturation, and implicates their role in plaque formation.

Spearman's r correlation analysis showed that in 4 month-old *App*$^{NL-G-F}$ mice, who are at early stages of plaque pathology, there is a strong positive correlation between increased plaque emission ratio and microglial CD68 intensity directly on the plaque, which is seen in both the cortical (Fig. 30A, R=0.57, P<0.0003) and hippocampal (Fig. 30B, R=0.53, P<0.0006) regions. This effect was lost the further away from the plaque, with no correlation observed in both brain regions (Fig. 30A and B). In 18 month-old *App*$^{NL-G-F}$ mice, who have widespread amyloid pathology and more structurally mature plaques compared to *App*$^{NL-F}$ and *App*$^{NL-F}$/*Trem2*^{R47H}, again there is a significantly positive correlation. This effect was most prominent on the plaque in both cortical (Fig. 30C, R=0.71, P<0.0001) and

hippocampal regions (Fig. 30D, R=0.64, P<0.0001), but was also seen in the peri-plaque area for both brain regions (cortex: Fig. 30C, R=0.52, P<0.0027; hippocampus: Fig. 30D, R=0.64, P<0.0003). This effect was lost in the 'away-from-plaque' area, where no correlation was observed. This suggests that even at 30 – 50 μm away from the plaque, microglia may be responding to toxic species being diffused out from the plaque, which would be an interesting avenue to further explore.

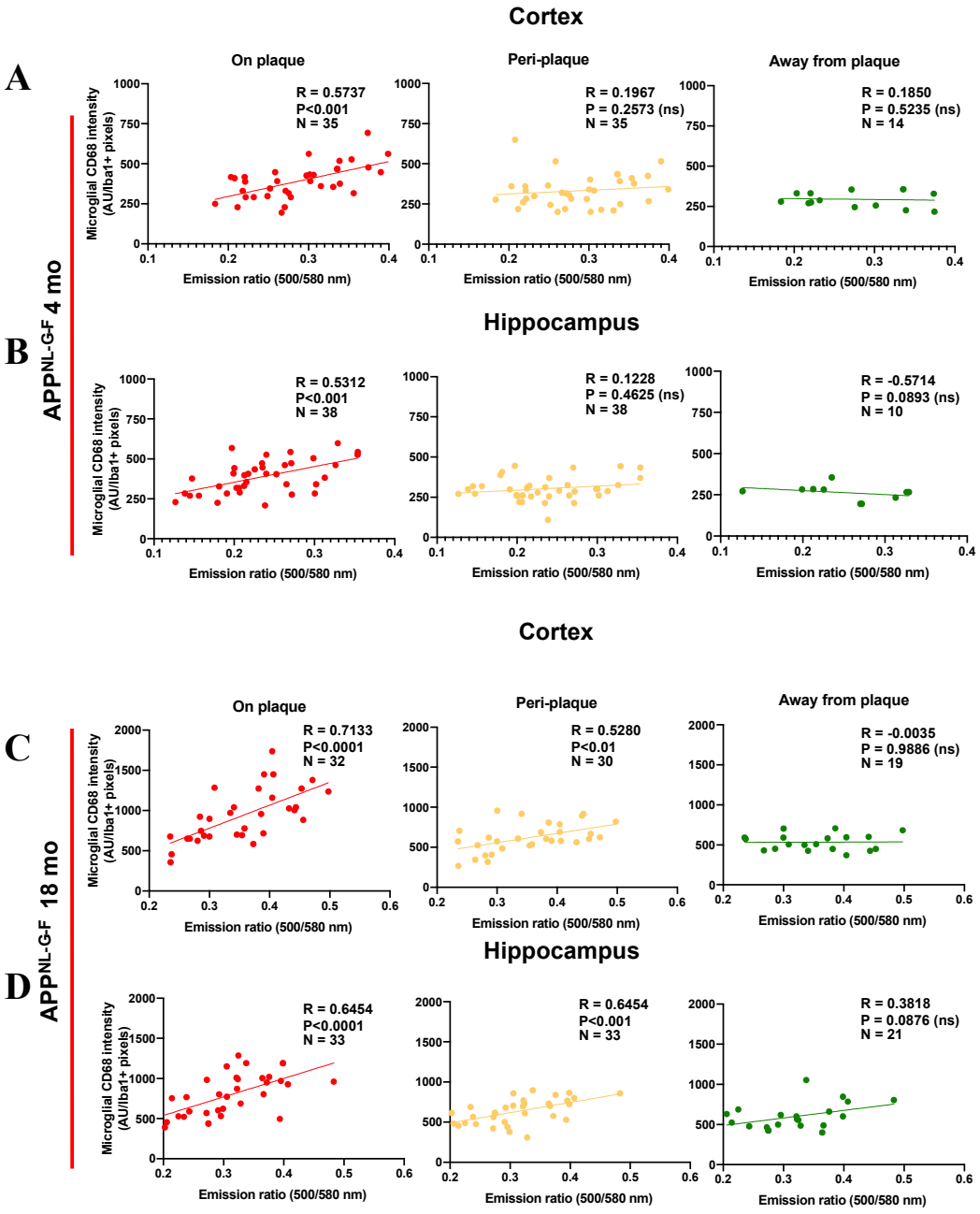

Figure 30. Spearman's r correlation analysis of plaque maturity and microglial activation in *App*$^{NL-G-F}$ mice. Correlations of plaque emission ratio (500/580 nm) against microglial CD68 intensity in on-plaque (0 – 10 μm), peri-plaque (10 – 30 μm) and away-from-plaque (30 – 50 μm) areas; in the (A) cortex and (B) hippocampus of 4 month-old; and (C) cortex and (D) hippocampus of 18 month-old APP^{NL-G-F} mice. Linear regression lines are presented. XY pairs (N number), significance and r values are indicated accordingly. Red dots, on-plaque; yellow dots: peri-plaque; green dots: away-from-plaque.
Abbreviations: ns, non-significant; mo, months old.

When examining *App*$^{NL-F}$ mice, similar effects were observed. In 9 month-old *App*$^{NL-F}$ mice, on the plaque, there was a positive correlation with increased plaque emission ratio and microglial activation (cortex: Fig. 31A, $R=0.65$, $P<0.05$ cortex; hippocampus: Fig. 31B, $R=0.78$, $P<0.01$); however, this effect was lost in the peri-plaque and away-from-plaque regions. 18 month-old mice, on the other hand, showed a positive correlation for both the on-plaque ($R=0.73$, $P<0.0001$ for both cortex and hippocampus) and peri-plaque (cortex: Fig. 31C, $R=0.46$, $P<0.001$; hippocampus: Fig. 31B, $R=0.37$, $P<0.05$) areas, consistent with *App*$^{NL-G-F}$ mice of the same age.

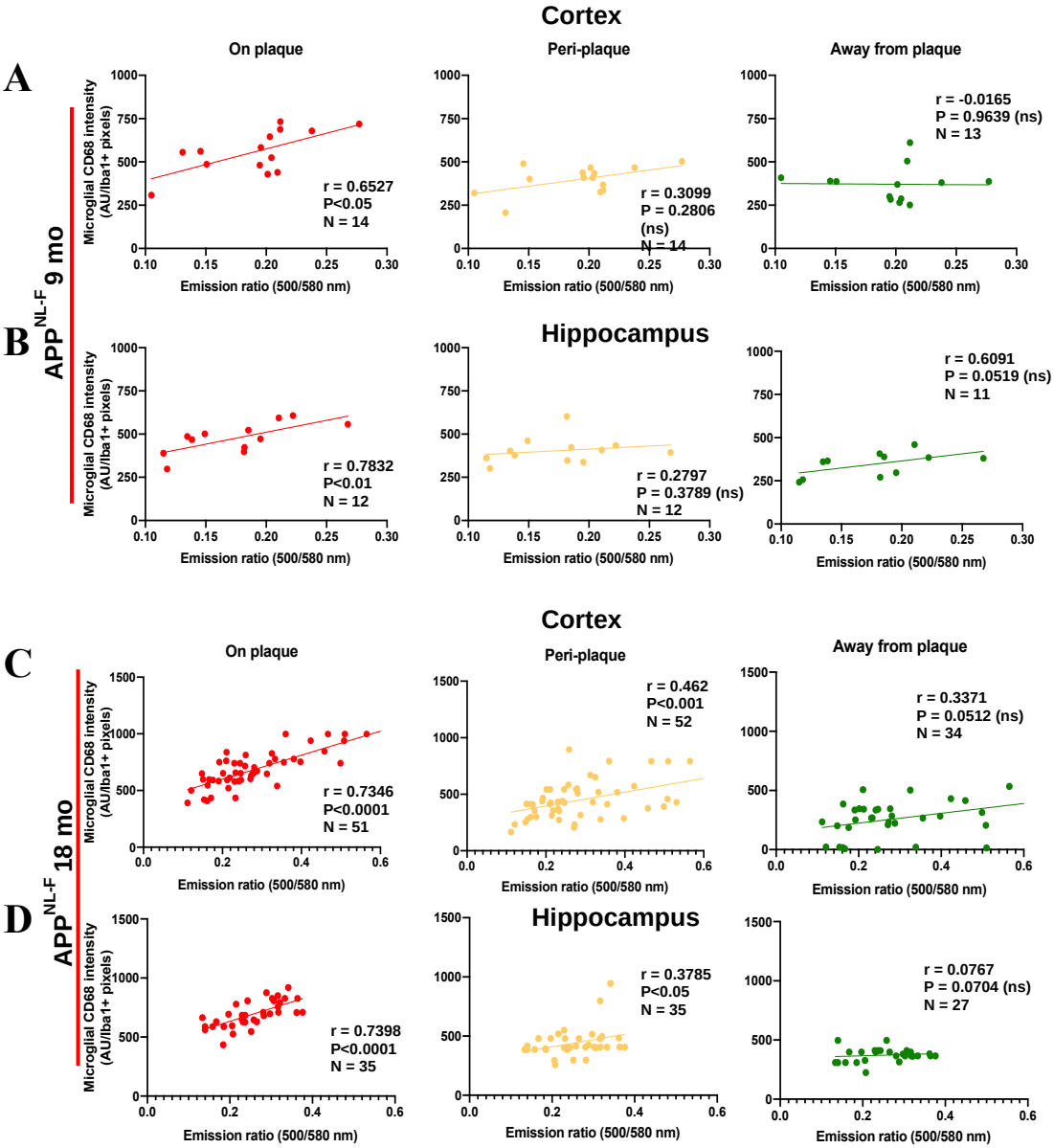

Figure 31. Spearman's r correlation analysis of plaque maturity and microglial activation in *App*$^{NL-F}$ mice. Correlations of plaque emission ratio (500/580 nm) against microglial CD68 intensity in on-plaque (0 – 10 μm), peri-plaque (10 – 30 μm) and away-from-plaque (30 – 50 μm) areas; in the (A) cortex and (B) hippocampus of 9 month-old; and (C) cortex and (D) hippocampus of 18 month-old *App*$^{NL-G-F}$ mice. Linear regression lines are presented. XY pairs (N number), significance and r values are indicated accordingly. Red dots, on-plaque; yellow dots: peri-plaque; green dots: away-from-plaque.

Abbreviations: ns, non-significant; mo, months old.

Interestingly, the pronounced plaque maturity-associated increase in CD68 was totally lost in *App*$^{NL-F}$/*Trem2*^{R47H} mice, where no correlation was observed between plaque morphology and microglial activation, in any of the concentric circles radiating from the plaque. This effect was consistent in both the cortex (Fig. 32A) and hippocampus (Fig. 32B).

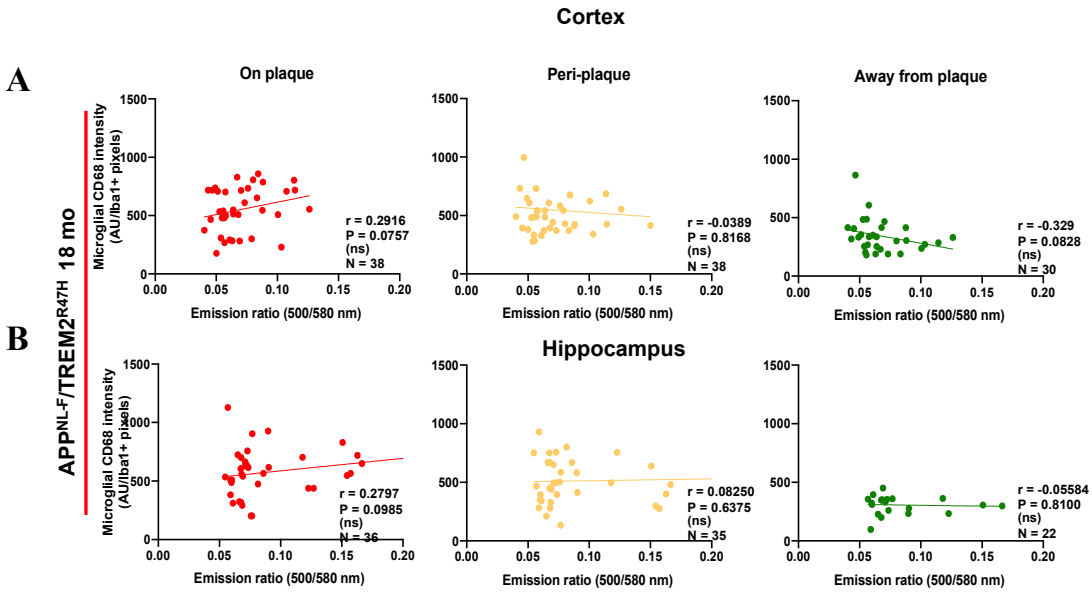

Figure 32. Spearman's r correlation analysis of plaque maturity and microglial activation in 18 month-old *App*$^{NL-F}$/*Trem2*^{R47H} mice. Correlations of plaque emission ratio (500/580 nm) against microglial CD68 intensity in on-plaque (0 – 10 μm), peri-plaque (10 – 30 μm) and away-from-plaque (30 – 50 μm) areas; in the (A) cortex and (B) hippocampus of 18 month-old *App*$^{NL-F}$/*Trem2*^{R47H} mice. Linear regression lines are presented. XY pairs (N number), significance and r values are indicated accordingly. Red dots, on-plaque; yellow dots: peri-plaque; green dots: away-from-plaque.

Abbreviations: ns, non-significant; mo, months old.

Overall this data is showing that in *App*$^{NL-G-F}$ and *App*$^{NL-F}$ mice, increasing plaque maturity correlates with more microglial activation. In early plaque pathology, this only occurs directly around the plaque, whereas in later plaque pathology, microgliosis spreads to the peri-plaque regions too. Additionally, this mechanism is likely mediated by Trem2, because microglia in *App*$^{NL-F}$/*Trem2*^{R47H} mice are dysfunctional in becoming appropriately activated around mature plaques.

Next, I aimed for a more detailed comparison of plaque conformation/microglial activity correlations on the plaque, to understand genotype- and age-associated alterations in *App*$^{NL-G-F}$ and *App*$^{NL-F}$ mice. As no correlations were observed in *App*$^{NL-F}$/*Trem2*^{R47H} mice, they were excluded from this analysis. Therefore, the correlation data specifically for the on-plaque area (0 – 10 μm) was pooled across all ages and genotypes (Fig. 33A). Here, it is clear that 18 month-old *App*$^{NL-G-F}$ mice exhibit the highest levels of microgliosis in relation to plaque pathology.

Additionally, the difference in CD68-LCO correlation between old and young mice is most pronounced in *App*$^{NL-G-F}$, suggesting that microgliosis starts off at low levels, and increases with age and accumulating amyloid pathology (Fig. 33A).

Intriguingly, plaques in *App*$^{NL-G-F}$ mice at 4 months old display lower CD68 intensity values than plaque in *App*$^{NL-F}$ mice at 9 months old, despite *App*$^{NL-G-F}$ having more cored plaques. This could either be an age effect (as *App*$^{NL-F}$ mice are 5 months older in this comparison), or is indicative of the fact that amyloid deposition and aggregation occur first, followed by microgliosis at later stages of pathology. Positive correlations were statistically significant for both all groups measured (Fig. 33B).

Overall, these results show that *App*$^{NL-F}$ experience a more gradual increase in plaque-associated microgliosis compared to *App*$^{NL-G-F}$ mice, in line with previous findings (Benitez et al., 2021; Saito et al., 2014).

A

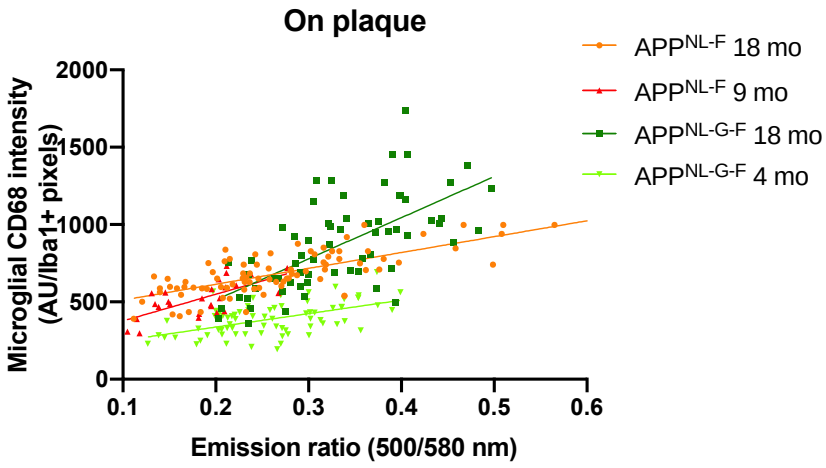

B

	APP^{NL-F} 18 mo	APP^{NL-F} 9 mo	APP^{NL-G-F} 18 mo	APP^{NL-G-F} 4 mo
Spearman r	0.6999	0.7087	0.6972	0.4881
P	<0.0001	<0.0001	<0.0001	<0.0001
XY pairs	87	26	65	73

C

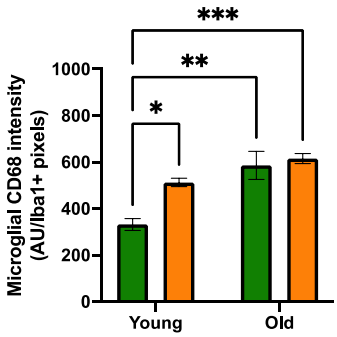

Figure 33. Alterations in plaque-associated microgliosis between genotypes and across ages in *App* KI mice. (A) Correlations of plaque emission ratio (500/580 nm) against microglial CD68 intensity in the on-plaque (0 – 10 μm) area. Simple linear regression lines are presented. (B) Corresponding XY pairs, significance and r values. (C) Plaques with a 500/580 nm emission ratio 0.25 or over were excluded, and their corresponding CD68 intensity values in the on-plaque area are presented. Columns indicate mean ± SEM. Number of animals: N=4-5 per group. Number of plaques: N=15-20/region/animal. Interactions from a two-way ANOVA followed by Holm-Šídák's multiple comparisons test indicated by: *P<0.05; **P<0.01; ***P<0.001. Abbreviations: ns, non-significant; mo, months old.

With the understanding that plaque maturity indeed correlates with increasing microglial activation, next, I aimed to more closely examine differences in CD68 immunoreactivity around less structurally mature plaques, to see whether age or genotype drive early activation, or if it is the other way around.

To do this, I focused solely on plaques with an LCO emission ratio below 0.25. The results showed that even when selectively looking at less cored plaques, there were alterations in microglial activation around, them depending on age or genotype, between young and old *App*$^{NL\text{-}G\text{-}F}$ and *App*$^{NL\text{-}F}$ mice (Fig. 33C). Interestingly, young APP$^{NL\text{-}F}$ had significantly increased CD68 levels compared with young *App*$^{NL\text{-}G\text{-}F}$ even when the analysis was confined to less cored plaques only (Fig. 33C), consistent with the previous correlation across all plaques (Fig. 33A). This again suggests that it is not only plaque pathology that encourages microglial activation, but also the age of the animal. Additionally, APP$^{NL\text{-}F}$ mice have higher levels of soluble Aβ than *App*$^{NL\text{-}G\text{-}F}$, so there certainly may be microglial responses to other forms of Aβ in *App*$^{NL\text{-}G\text{-}F}$ mice that were out of the scope of the present study. Overall, this data shows that in older animals, particularly *App*$^{NL\text{-}G\text{-}F}$, plaques of the same structural maturity display more activated microglia directly around them than their younger counterparts. Therefore, it is important not to discount age as a contributing factor to microglial behaviour.

6.4 Chapter summary

In this chapter, I examined the relationship between early and late plaque morphology and microgliosis in *App*$^{NL\text{-}G\text{-}F}$ and *App*$^{NL\text{-}F}$ mice, and whether these phenotypes are altered in the presence of the *Trem2*^{R47H} mutation. As established in the previous chapter, in late-stage pathology, *App*$^{NL\text{-}G\text{-}F}$ mice (who experience increased Aβ oligomerisation) exhibit plaques with the most mature structure compared to *App*$^{NL\text{-}F}$; and in turn, plaque morphology was altered as a result of the R47H variant of *TREM2*, with *App*$^{NL\text{-}F}$/*Trem2*^{R47H} mice exhibiting structurally less mature plaques compared to age-matched *App*$^{NL\text{-}F}$ mice. In order to understand if these plaque changes are driven by alterations in microglial

behaviour, microglial distribution and activation around plaques were also examined.

In general, microglial activation and distribution around plaques were fairly consistent with each other. Both young and old *App*$^{NL-G-F}$ mice displayed the greatest levels of microglial clustering around plaques, and 18 month-olds had widespread microglial activation not just confined to directly around the plaque, unlike in 18 month-old APP^{NL-F} mice. A potential mechanism for this could be that in aged *App*$^{NL-G-F}$ mice, the sheer density of plaques results in soluble Aβ or other toxic substances diffusing from plaques may have a contribution from many nearby plaques, resulting in a more widespread microglial response. In *App*$^{NL-F}$ mice, on the other hand, plaques are physically smaller with less of a surrounding halo of Aβ (as evidenced by LCO staining); therefore, it is more likely that only microglia directly around the plaque are in their activated state. The low levels of clustering and activation of microglia around plaques in *App*$^{-F}$/*Trem2*^{R47H} mice further confirm how Trem2 is a key factor in mediating plaque/microglia interactions.

Interestingly, there were very few differences in plaque-associated microgliosis between the cortex and hippocampus in any of the groups, despite differences in plaque structural maturity as mentioned in Chapter 5. It could be that at the ages measured, it is too early or late to catch dynamic regional alterations, or in fact that there are no regional alterations at all.

The correlation analysis provides an interesting link between plaque conformation and microglial response. The positive correlations for plaque maturity/on-plaque microglial activation for both *App*$^{NL-F}$ and *App*$^{NL-G-F}$ mice indicate that there is continuous promotion of plaque growth and peptide folding, with microglial activation as a secondary response.

It is interesting that upon addition of the *Trem2*^{R47H} mutation, these effects are completely abolished, highlighting how microglial behaviour around plaques is Trem2-dependent. This is supported by a previous study, which found that Trem2 has a significant role in the early containment of plaque diffusion by microglia, in addition to its influence on the structure, composition and toxicity of Aβ deposits

(Wang et al., 2016). A potential consequence of long-term impaired Trem2 functioning, as is the case in *App*$^{NL-F}$/*Trem2*^{R47H} mice, is increased toxic Aβ species in the brain (Wang et al., 2015), leading to further and uncontrolled seeding of plaques. These data give insight into TREM2-mediated mechanisms in the early stages of AD development, and provide a basis to further understand the pathological risks in individuals with a *TREM2* mutation.

Chapter 7: Discussion

AD is the most common form of dementia and is currently a worldwide crisis, with 152 million individuals predicted to be affected by 2050 (Livingston et al., 2017). The impact of AD on the individual is significant; sufferers experience reduced quality of life as a result of cognitive decline and behavioural impairments. Although the amyloid cascade hypothesis has been established for decades, it is only recently that we have developed our understanding of the impact of pathological factors other than amyloid plaques, NFTs and synaptic dysfunction. The role of glial cells in AD pathogenesis has been widely researched over the past few years, with GWAS highlighting variants of several microglial genes, notably *TREM2*, as conferring an increased risk of developing AD (Guerreiro et al., 2013b; Jonsson et al., 2013). Furthermore, the original school of thought that microglia adopt either a classic pro- or anti-inflammatory state has been challenged in recent years, with multiple studies showing that they exist as heterogenous populations across different brain regions, with a multitude of functions. In terms of amyloid plaques, the significance of Aβ deposition in AD has long been recognised, but past technology lacked the chemical specificity and sensitivity to examine the specific dynamics of how plaques grow over time, what they are composed of, and their effects on the surrounding cellular environment.

Therefore, in this project I aimed to assess, in detail, Aβ dynamics and the interaction with surrounding microglia. I examined two *App* KI models, $App^{NL\text{-}F}$ and $App^{NL\text{-}G\text{-}F}$, and initially tried to model amyloid deposition in OHSCs derived from postnatal pups, based on a previous publication (Novotny et al., 2016). I then characterised plaque conformation in young and adult $App^{NL\text{-}F}$ and $App^{NL\text{-}F}$ mice using amyloid beta-sheet-sensitive dyes (LCOs), which have increased amyloid binding specificity and selectivity, compared to traditional amyloid stains, along with aggregation-induced fluorescence and differential emission properties. In this context, two LCOs (qFTAA and hFTAA) in combination are useful for the delineation of both mature cored and immature diffuse aggregates. Subsequent hyperspectral confocal microscopy can provide detailed information into the specific structural conformation within and across single plaques. I additionally examined $App^{NL\text{-}F}$ mice harbouring a $Trem2^{R47H}$ mutation to assess the impact of

loss-of-function of microglia on plaque maturity and conformation. Unlike traditional transgenic models, knock in models, including *App*$^{NL-F}$/*Trem2*^{R47H} mice, do not have overexpression of *App* or *Trem2* nor other associated problems occurring with use of the transgenic technology. Instead, rising soluble Aβ leads to a gradual increase in plaque burden from 9 to 24 months of age (Benitez et al., 2021), resulting in more subtle gene expression changes. This is more representative of human sAD, where plaque development starts in middle age and over the course of many decades, combines with other factors to result in clinical outcomes.

In addition to the novel mouse models, in this work, I took advantage of recent advances in chemical imaging techniques, specifically a newly developed imaging paradigm termed 'iSILK', whereby stable isotope labelling combined with MALDI mass spectrometry imaging is employed to follow plaque development over time with high chemical specificity (Hanrieder et al., 2015; Hanrieder et al., 2013; Michno et al., 2019b; Michno et al., 2021). The aim here was to apply these novel techniques *in vivo* to *APP* KI mice and correlate plaque growth and amyloid deposition dynamics with measures of plaque maturation (LCO) at the single plaque level across plaques and brain regions in different ages and genotypes. Finally, I assessed microglial distribution and activation levels in young and old *App* KI mice, to further understand the temporal relation of these immune cells in mediating plaque formation and maturation.

7.1 OHSCs derived from postnatal *App* KI pups do not develop amyloid plaques representative of the *in vivo* phenotype

OHSCs are a three-dimensional cell culture system so have advantages over primary cell culture, as cell types and connections are maintained. The initial aim for OHSCs was to develop an *in vitro* model of amyloid plaque deposition that successfully recaptured representative pathology compared to *in vivo* in these mice. This would allow for a more easily manipulated system to assess early plaque formation and deposition, and also reduce the number of animals required.

Optimisation studies revealed that without extra manipulation, even after 16 weeks in culture, there was no evidence of Aβ deposits in OHSCs from *App*$^{NL-G-}$

^{F} mice (these mice develop plaques *in vivo* at 2 months old or younger). Various research groups also have unsuccessfully attempted this approach using OHSCs from mice overexpressing App (Harwell and Coleman, 2016; Hellwig et al., 2015a; Johansson et al., 2006; Novotny et al., 2016). This failure may be due to microglia behaving differently *in vitro*; the slicing process appears to trigger an inflammatory response and chronically-activated microglia and astrocytes (Gerlach et al., 2016), which may ingest Aβ and prevent it from depositing (Hellwig et al., 2015a). Additionally, as Aβ is released from the slice into the surrounding media, the process of replenishing the media several times a week may wash out excess soluble Aβ, limiting the opportunity for it to build up and aggregate in the slice. Therefore, in these experiments, replenishing media was limited to once a week with a 50% media change, which still allows for adequate delivery of nutrients (Harwell and Coleman, 2016). However, even with this adapted feeding protocol, Aβ deposition was not seen after 16 weeks in culture.

To overcome the issue of OHSCs not naturally developing Aβ deposits, here we seeded slices with synthetic Aβ1-40 or Aβ1-42 and brain homogenate from aged plaque-bearing animals, based on a previously published protocol (Novotny et al., 2016). The concept of seeding, whereby misfolded proteins serve as a template to induce misfolding and aggregation of more proteins, is a common phenomenon in neurodegenerative disease (Jucker and Walker, 2013), and has been demonstrated for Aβ both in animal models (Kane et al., 2000; Meyer-Luehmann et al., 2006; Morales et al., 2015) and humans (Jaunmuktane et al., 2015; Jaunmuktane et al., 2018). Additionally, different conformations of Aβ are present in the AD brain (Rasmussen et al., 2017), and distinct structures may affect the speed of disease progression (Cohen et al., 2015), indicating that different species vary in levels of toxicity. Therefore, we hypothesised that the type of synthetic peptide or brain homogenate added would affect the level of Aβ deposition in OHSCs.

Here it was demonstrated that the specific combination of synthetic Aβ1-40 or Aβ1-42 in the media, and whether the brain homogenate contained mainly Aβ1-42 (APP^{NL-G-F}) (Saito et al., 2014) or both Aβ1-40 and Aβ1-42 (TASTPM) (Cummings et al., 2015), determined Aβ aggregation outcome in OHSCs. However, the results were inconsistent between cultures, and fluorescent

amyloid imaging showed that much of the LCO was pooled on the surface of the section, indicating that seeded and exogenous Aβ were interacting and aggregating without being taken up by the cells within the OHSC.

Additionally, the genetic background of OHSCs did not appear to influence deposition, indicating that OHSC-derived Aβ is not required for initial seeding. However, Novotny et al. (2016) observed that OHSC-generated Aβ appears to co-deposit with the induced Aβ deposits, suggesting that there is a cellular mechanism within the slice contributing to deposition. However, closer examination of exactly how much of the deposits contain OHSC-derived Aβ is required, and this can be performed with metabolic labelling of OHSCs (see Future Directions).

While OHSCs may not be a good model to study natural plaque deposition, they are certainly useful to assess other AD-related mechanisms. An interesting recent study made use of collagen hydrogels to apply human Aβ peptides into OHSCs from transgenic AD mice, and assessed the spreading capability over the entire section. They found that of all the peptides studied, Aβ1-42 had the most potent spreading activity, which subsequently activated glial cells and was mostly taken up by microglia (Moelgg et al., 2021). Therefore, OHSCs can be successfully used to study certain Aβ dynamics and the effect on the surrounding environment, and can provide a good basis for further study using other AD models.

It should be noted that OHSCs as a model system have certain limitations. Whilst they have an advantage over primary cell culture systems in that cellular networks and multiple cell types are maintained, it is important to remember that OHSCs are derived from early postnatal mouse donors. Therefore, in the context of studying ageing and neurodegenerative diseases, OHSC-derived cells may not have developed a mature phenotype and therefore do not have the same molecular architecture as the adult mouse brain. It is uncertain at what point an OHSC represents a mature adult environment, even after long-term culture. This may partially explain why here, amyloid plaque formation did not naturally occur in OHSCs; for example, if adult neurons and microglia are required to propagate and seed Aβ.

7.2 Plaque maturation in *App* KI mice is influenced by *App* genotype and Trem2

The phenotypic variability of AD pathology, including plaque pathology, is currently not well understood. This heterogeneity is likely to involve many factors, including time of disease onset, inflammatory response, localisation and spread of brain pathology, and existence of comorbid conditions. Previous studies have shown that AD heterogeneity may be mediated by variability in the molecular architecture of Aβ aggregates in the brain (Rasmussen et al., 2017).

Therefore, here I investigated whether structural polymorphism of Aβ plaques is altered depending on *App* genotype, brain region or disease stage, and also when inflammatory systems are perturbed. I examined two *App* KI models: App^{NL-G-F} and App^{NL-F}, and also App^{NL-G-F} mice harbouring a $Trem2^{R47H}$ mutation. I first determined that in App^{NL-G-F} and App^{NL-F} mice, the structural maturity of the centre of plaques was increased in older mice compared to younger mice. This indicates that plaques continuously mature over time via age-related conformational rearrangement of Aβ, in line with previous findings (Nystrom et al., 2013). These results additionally build on previous data from a multiphoton *in vivo* imaging study, in which tracking of new plaque growth in young *App/Ps1* mice over 6 months revealed that both newly formed and existing plaques grew radially at a rate of 0.3 µm per week (Hefendehl et al., 2011). It would be interesting in the future to employ *in vivo* imaging techniques in *Appp* KI models, as *App/PS1* transgenic mice may have plaques unrepresentative of the human phenotype.

In this chapter, I also found that in young and old App^{NL-F} mice, but only young App^{NL-G-F} mice, cortical plaques were more cored and mature than hippocampal plaques, and therefore are likely to have deposited earlier. The Arctic mutation in App^{NL-G-F} mice causes rapid and aggressive deposition of Aβ (Nilsberth et al., 2001), so by 18 months old, hippocampal plaques may have experienced a growth ceiling effect, despite being initially deposited after cortical plaques. This can be explained by the fact that App^{NL-F} mice have slower Aβ deposition and much more soluble Aβ compared to App^{NL-G-F} (Saito et al., 2014); thus, by 18 months old, these mice may only be at mid-stage amyloid pathology, whereby

excess soluble Aβ is still being recruited to plaques causing further growth. The findings in young *App*$^{NL\text{-}G\text{-}F}$ mice are supported by a previous study by our group, which employed stable isotope labelling combined with MALDI-IMS to show that in these animals, plaques deposit in the cortex prior to the hippocampus (Michno et al., 2021).

Importantly, I also found that genetic background influences plaque structure: *App*$^{NL\text{-}G\text{-}F}$ mice, harbouring three fAD mutations, including the arctic *APP* mutation E693G, had plaques with a significantly more dense-core and mature structure compared to *App*$^{NL\text{-}F}$. This is likely due to the increased hydrophobicity of $A\beta_{arc}$ and aggregation propensity respectively, which is consistent with previous data in transgenic *App*^{ArcSwe} mice (Lord et al., 2011).

In turn, in these experiments, loss-of-function of Trem2 caused by a *Trem2*^{R47H} mutation dramatically decreased the structural maturity of plaques compared to *App*$^{NL\text{-}F}$ mice without the mutation. Furthermore, *App*$^{NL\text{-}F}$/*Trem2*^{R47H} mice showed no regional differences in plaque conformation. Therefore, here plaques may have undergone a 'floor effect', where they never began to mature and are thus similar across both regions. This is backed up by a notable previous study, where it was established that the *Trem2*^{R47H} variant leads to a reduction of compact ThS-positive plaques without altering 6E10-positive plaque burden (Cheng-Hathaway et al., 2018). Additionally, previous work by our lab showed that *App*$^{NL\text{-}F}$/*Trem2*^{R47H} mice have a greater density of smaller plaques covering a larger area than *App*$^{NL\text{-}F}$ mice (Wood et al., 2022). This overall suggests that loss-of-function of Trem2 causes an impairment in the ability of microglia to organise and compact plaques. In the future, it would be interesting to expand these experiments to young *App*$^{NL\text{-}F}$/*Trem2*^{R47H} mice, to understand whether this loss-of-function also occurs in earlier plaque pathology.

In addition to the insights into drivers of Aβ behaviour, this approach also demonstrates that combined qFTAA and hFTAA amyloid staining together with hyperspectral microscopy is a straightforward and effective tool to delineate heterogenous plaque structures and plaque maturation levels *in situ*. Indeed, this approach to probe amyloid polymorphism has previously been used for the study

of both mouse and human AD tissue (Michno et al., 2019a; Nystrom et al., 2017; Nystrom et al., 2013; Rasmussen et al., 2017).

It should be noted that due to the experimental setup and time constraints, the smallest seeds of plaques were not examined. Therefore, very newly growing plaques may have been overlooked in this analysis. In the future it would be of use to sub-divide plaques into size categories and to assess over a wider range of ages, to truly determine if plaque growth is continuous.

In conclusion, these plaque data support previous studies about how both fAD mutation and Trem2 interactions shape plaque structure and maturity, and further highlights the strong interaction between microglia and plaques. This provides a strong basis for understanding the biochemical processes underlying plaque deposition dynamics, but also how to individualise anti-amyloid therapies depending on disease type.

7.3 iSILK can be applied to *App* KI mice to study temporal and spatial Aβ peptide deposition

The experiments presented above show that LCO imaging allows for delineation of plaque maturation over time. However, these results are limited to plaque structure and do not reveal how these plaques form and what Aβ species are associated with plaque formation, plaque growth and maturation, respectively. It is particularly difficult to elucidate the earliest events of plaque formation, as highlighted by the *App*$^{NL\text{-}G\text{-}F}$ results, where plaques between different regions showed similar levels of maturation.

In general, early Aβ deposition is not well understood, mainly due to difficulty in studying the earliest pathogenic events in AD as cognitive symptoms appear many years after disease onset (Bateman et al., 2012). It has been previously reported that a wide variety of Aβ species are present and differentially distributed in both human AD and transgenic mouse brain (Carlred et al., 2016; Philipson et al., 2009; Portelius et al., 2010; Tekirian, 2001)**.** Furthermore, LCO and mass spectrometry studies have aimed to elucidate the connection between Aβ peptide

content, structural plaque polymorphism and type of cerebral amyloid pathology (Michno et al., 2019a) as well as different subtypes of AD (Rasmussen et al., 2017). Together, these results suggest that the Aβ signature is associated with plaque conformation phenotype (Michno et al., 2019a).

Both early deposition as well as continuous plaque growth at later stages has not been thoroughly studied due to lack of biochemical techniques that provide the necessary temporal and chemical precision. As mentioned above, this is further complicated by the fact that in humans, plaques are structurally diverse (Maxwell et al., 2021; Roher et al., 2017), which has been suggested to depend on underlying Aβ peptide composition. Furthermore, different mutations associated with Aβ pathology (e.g. *App* and *PS1*) result in different Aβ signatures, and previous findings show that plaques across different fAD groups constitute distinct clouds of polymorphism (Rasmussen et al., 2017), suggesting genotype associated differences in deposition mechanisms. Therefore, our aim here was to examine the combined effects of two or three *App* mutations on the spatial distribution of Aβ peptides and the timeline of early Aβ deposition.

To elucidate the sequence of Aβ plaque formation, we took advantage of a new imaging paradigm, iSILK, involving a comprehensive PULSE/CHASE metabolic labelling scheme followed by MALDI-IMS of isotope enriched Aβ in single plaques. These analyses revealed that in *App*$^{NL-G-F}$ mice, Aβ1-42 is deposited first and localises to the core of plaques, creating a seed that induces aggregation and deposition of shorter forms of Aβ such as Aβ1-38 (Michno et al., 2021). This is consistent with previous work indicating that Aβ1-40 and C-terminally truncated species such as Aβ1-38 are associated with plaque maturation (Michno et al., 2019c). Indeed, here, Aβ1-38 was found in a certain proportion of plaques and was totally labelled, implicating it as a secondary event. A recent study involving MALDI-based 3D-reconstruction of plaques demonstrated that in old *App*$^{NL-G-F}$ mice, plaques consist of a Aβ1-42 core surrounded by Aβ1-38 in most but not at all plaques (Enzlein et al., 2020). An interesting future experiment would be to replicate these experiments in *App*$^{NL-F}$/*Trem2*^{R47H} mice, to understand if Trem2 impairment influences the secretion or deposition of particular Aβ species; for example, if they are unable to phagocytose soluble Aβ1-38 in the surrounding area.

Additionally, we observed that the earliest deposition of plaques occurs in the cortex prior to the hippocampus. Human imaging studies have also demonstrated increased early susceptibility to Aβ in cortical brain regions (Buckner et al., 2005), and in the entorhinal cortex compared with the hippocampus (Huijbers et al., 2014). This may be due to different neuronal circuits within the brain displaying selective vulnerability to amyloidosis. Therefore, further examination of plaque load and type in these two regions would be of interest.

We then aimed to further examine the timeline of plaque deposition in 10 and 18 month-old *App*$^{NL-F}$ mice, who have a slower rate of amyloid deposition. For individual plaques, SILK/MALDI-IMS was performed to obtain ^{15}N incorporation rates. The results show that plaques *App*$^{NL-F}$ mice form the same way as in *App*$^{NL-G-F}$ animals, i.e. through formation of a small core formation consisting of Aβ1-42, and homogenous growth upon further deposition of Aβ1-42.

We then performed correlative LCO imaging on consecutive sections to obtain LCO emission values for the same plaques and eventually link plaque age (iSILK) to plaque maturation (LCO) for individual plaques across different brain regions and animals. Here, the results show that cortical plaques have higher ^{15}N incorporation and higher LCO emission ratio values compared to hippocampal plaques. Further, there was a positive correlation between plaque age (^{15}N content) and LCO emission profiles (maturation).

These results are important as this confirms firstly: that both methods of measuring plaque age are valid, and secondly: that cortical plaques are older and thus formed prior to hippocampal plaques, in line with the iSILK data from *App*$^{NL-G-F}$ mice (Michno et al., 2021).

Importantly, this is consistent with the LCO results established in Chapter 4, providing further validation that in these mice, plaque deposition is dynamic and continuous over at least the first 18 months of life.

It should be noted that not all plaques are able to be assessed in this setup, because the centre of a plaque has to be on two adjacent tissue sections (one for MALDI-IMS and one for LCO staining) in order for the correlation to be accurate. Therefore, further optimisation of this protocol is required to streamline the process in the future, and to allow for faster assessment of more plaques, including small compact plaques, if present.

Overall, these findings highlight how stable isotope labelling in combination with MALDI-IMS is an effective tool to study Aβ deposition dynamics in *App* KI mouse models. The results showed that Aβ deposition is temporally dynamic, with certain brain regions consistently more vulnerable to earlier deposition, and production of different Aβ species occurring at varying stages of pathology. Further analysis of how these early plaques grow and accumulate additional peptide and lipid species will provide useful therapeutic information on which species can be targeted and when.

With the ever-increasing spatial resolution of MALDI-IMS, the applications of this technique are vast, and will potentially even allow for analysis of tau pathology. These novel methods are already being applied to patients, whereby AD hospice patients take an infusion or bolus of heavy isotopes (Bateman 2006). It is hoped that heavy isotope incorporation into the proteome will yield information about amyloid pathogenicity or other proteinopathic mechanism that can be delineated with MALDI imaging of *post-mortem* brain tissue. Furthermore, the iSILK approach holds significant clinical relevance. For example, the enhanced spatial resolution of MALDI-IMS makes it a valuable tool for mapping the distribution of lipids and peptides for biomarker discovery and disease diagnosis (Ucal et al., 2017). Additionally, assessment of dynamic protein turnover from SILK studies can provide immediate *in vivo* evidence of target engagement in clinical trials, thereby enhancing therapeutic discovery (Paterson et al., 2019).

However, it should be noted that such experiments have their limitations, primarily with respect of spatial resolution and sensitivity to capture the earlies seeds of aggregated Aβ. To date, it remains unclear how Aβ exerts its neurotoxic effects and how this relates to plaque formation and plaque polymorphism.

Potentially soluble forms of Aβ drive neuron death and synaptic dysfunction (Deshpande et al., 2006) and exert their effects independently of plaques (Bloom, 2014). Because soluble Aβ can propagate and spread through brain regions (Walker et al., 2016), it is important to detect these species before excessive damage to the neural network occurs.

7.4 Alterations in plaque-associated microgliosis are dependent on *APP* mutation and TREM2

The effects upon which Aβ exerts its pathogenic potential remain unclear. Here, the interaction of both soluble and aggregated Aβ with surrounding neural cells, including both nerve cells and glial cells, have been suggested to be critical in driving disease progression. Specifically, microglia have been extensively studied in the context of AD, and numerous roles have been reported. There is evidence that they are instrumental to the formation of plaques (Spangenberg et al., 2019); or actively phagocytose Aβ (Yu and Ye, 2015); or act as a barrier to compartmentalise Aβ-related toxicity (Clayton et al., 2021; Condello et al., 2015); or phagocytose plaque-associated synapses to limit the spread of damage (Edwards, 2019). The functions are believed to be dependent on Trem2 functioning (Keren-Shaul et al., 2017), and are altered in the face of the *Trem2*^{R47H} mutation (Cheng-Hathaway et al., 2018; Zhong et al., 2018).

Previous studies have demonstrated that *App*$^{NL\text{-}G\text{-}F}$ mice exhibit pronounced microgliosis (Sacher et al., 2019) and gene expression alterations (Castillo et al., 2017) by 5 months old, and changes in the microglial proteome by 6 months old (Keren-Shaul et al., 2017; Sebastian Monasor et al., 2020). Additionally, a recent publication by our lab reported that compared to WT controls, *App*$^{NL\text{-}G\text{-}F}$ mice exhibit increased microglial density and *TREM2* expression per microglial cell at 9 months old (Benitez et al., 2021), and that 18 month-old *App*$^{NL\text{-}F}$ display upregulated microglial density compared to WT around even the smallest-sized plaques (Wood et al., 2022).

Building on these previous findings, here I found clear genotype-associated alterations in microgliosis directly around plaques, in age-matched mice (all 18 months old). We observed significantly increased microglial clustering and

activation in *App*$^{NL-G-F}$ compared to *App*$^{NL-F}$ mice; and again, in *App*$^{NL-F}$ compared to *App*$^{NL-F}$/*Trem2*^{R47H} mice; and in all three models compared to age-matched WT controls.

7.4.1 Alterations in microglial activation around plaques in App^{NL-G-F} and App^{NL-F} mice

A first, major finding of these experiments was that only on-plaque microglial activation and not solely microglial density was increased in 18 month-old *App*$^{NL-G-F}$ mice compared to *App*$^{NL-F}$ mice. This suggests that both models have effective microglial clustering mechanisms around plaques; however, each microglia in *App*$^{NL-G-F}$ mice is expressing more CD68, a lyosomal marker indicative of phagocytic activity (Walker and Lue, 2015). This may be a response to the length of exposure to Aβ, as by 18 months old, *App*$^{NL-G-F}$ have experienced an extra 7 months of plaque deposition compared to *App*$^{NL-F}$ mice, given the increased aggregation propensity due to the arctic mutation. It may be that at late-stage pathology, plaque-associated microglia in *App*$^{NL-G-F}$ mice have transitioned from protective to detrimental, whereby they become overactivated (Muzio et al., 2021). This is in contrast to early-stage pathology, where here it was observed that young *App*$^{NL-F}$ mice had increased on-plaque microgliosis compared to young *App*$^{NL-G-F}$ mice (further discussed below). Therefore, it would be of use to further characterise at what point this switch in microglial behaviour occurs, and potential transcriptional changes involved.

A second main finding in the present work was that both *App*$^{NL-G-F}$ and *App*$^{NL-F}$ mice demonstrate an age-associated increase in microglial activation and clustering directly around plaques. This effect was most prominent on-plaque but evened out in the peri-plaque and away-from-plaque regions between old and young mice. This shows that microgliosis increases in line with accumulating Aβ deposition primarily in plaque-associated areas, rather than across the whole brain region. A potential explanation for this could be that over time, both soluble and insoluble Aβ species and composition are changing (Michno et al., 2019a), resulting in a dynamic temporal microglial response. In line with this, a human *post-mortem* study showed that AD brains exhibit a change in the ratio of ramified

to reactive microglia populations over time, rather than a change in overall microglial density (Franco-Bocanegra et al., 2021).

Interestingly, here we observed that young *App*$^{NL-F}$ mice (9 months old) have increased on-plaque microgliosis compared to young *App*$^{NL-G-F}$ mice (4 months old), despite the latter being a more aggressive model of amyloidosis and showing higher aggregation propensity. This effect was consistent even when solely focusing on plaques with an LCO emission ratio of under 0.25 (i.e. less structurally mature plaques), suggesting that higher microgliosis observed for *App*$^{NL-F}$ mice compared to *App*$^{NL-G-F}$ mice is not related to plaque maturity.

This shows is that at least in early amyloid pathology, the age of the mouse is a significant factor in contributing to plaque-associated microgliosis. The underlying mechanisms of this would be interesting to explore further; however, a potential explanation is that the equilibrium of Aβ is different between the two genotypes particularly at the younger ages. Indeed, *App*$^{NL-F}$ display significantly increased levels of Aβ1-42 and a higher Aβ1-42/Aβ1-40 ratio compared to age-matched WT and even App23 mice (Saito et al., 2014), showing that even 7 months before plaque deposition, there is a strong upregulation of pathogenic forms of Aβ. Additionally, *App*$^{NL-F}$ mice display synaptic alterations such as loss of presynaptic synaptophysin and postsynaptic PSD95 (Saito et al., 2014), which may be induced by soluble oligomeric Aβ (Dore et al., 2021; Liu et al., 2010a). Therefore, microglia in 9 month-old *App*$^{NL-F}$ mice may also be responding to other toxic forms of Aβ around plaques.

Furthermore, independent of genotype, the general ageing process heightens the inflammatory status of the brain (Currais, 2015; Norden and Godbout, 2013; Raj et al., 2017). Despite *App*$^{NL-G-F}$ mice only being 2 months old and *App*$^{NL-F}$ 9 months old, this 7-month age-gap may have resulted in important physiological and pathophysiological changes between the two, which warrants further investigation. Other age-associated pathologies such as synaptic alterations (Mostany et al., 2013) and astrocyte-microglial interactions may also play a role. For example, during ageing, impairments in astrocyte-mediated pathways promotes increased cytotoxicity of microglia (Trivino and von Bernhardi, 2021). Therefore, the increased microgliosis in young *App*$^{NL-F}$ vs. *App*$^{NL-G-F}$ mice

observed here may be mediated by other cellular mechanisms and pathogenic factors, in addition to aggregated Aβ. In the wider context of human AD, environmental factors such as stress, infection and diet have also been shown to promote microglial activation (Madore et al., 2020; Sugama et al., 2019), and should be considered.

Tying the above results together, in the present study it was established that for both young and old *App*$^{NL-F}$ and *App*$^{NL-G-F}$ mice, a higher LCO spectral ratio (and therefore both plaque age and Aβ structural maturity) was positively correlated with increased microglial activation directly around individual plaques, in both the cortex and hippocampus. Together with the fact that plaque age and maturity (iSILK and LCO) correlate, this establishes that plaque deposition precedes microglial activation, given the positive correlation of plaque maturity and microgliosis.

In addition, old but not young *App*$^{NL-G-F}$ and *App*$^{NL-F}$ mice also had positive correlations in the peri-plaque area in both brain regions, suggesting that plaque growth and spread over time causes activation of a wider radius of microglia. This may be due to the plaque simply increasing in size, or the presence of other forms of Aβ or toxic substances in the peri-plaque area that are triggering an immune response. Additionally, these results support the idea of a feed-forward loop; i.e. amyloid deposition initiates a microglial response, which further promotes continuous plaque growth.

It would hence be very interesting to further investigate how microglia are contributing to amyloidosis. For example, to elucidate whether they are clearing excess Aβ (Bolmont et al., 2008; Liu et al., 2010b), or phagocytosing Aβ and then releasing it to contribute to the spread of new plaques (Baik et al., 2016), and also to understand the potential involvement in non-Aβ mechanisms such as tau propagation (Clayton et al., 2021).

Here, a potential alternative role of microglia could be that Aβ-induced synaptotoxicity triggers phagocytosis of damaged synapses rather than Aβ, limiting the spread of damage (Edwards, 2019). Indeed, pharmacological depletion of microglia does not change plaque load once plaques are already

established (Benitez et al., 2021; Spangenberg et al., 2016), suggesting that plaque growth can occur independently of microglia. However, it is possible that the actual Aβ composition and morphology of plaques in these mice may have been altered, as was the case in the present study when microglia were impaired. Furthermore, several studies have suggested that microglia are initiators of plaque formation (Huang et al., 2021a; Spangenberg et al., 2019); therefore, further analysis is required to establish at what point in pathology this initiation occurs, or if in fact both mechanisms are true, i.e. there are sub-populations of activated microglia that precede and follow plaque formation.

A third major finding was that young and old *App* KI models largely do not display regional alterations in plaque-associated microgliosis, despite differences in plaque structural maturity as mentioned in Chapter 5. The one exception was in 18 month-old *App*$^{NL-F}$ mice, who had increased on-plaque microglial clustering in the cortex compared to the hippocampus. Therefore, despite increased plaque maturity in the cortex in young *App* KI mice, perhaps inflammation has reached a ceiling effect by 18 months old, whereby amyloid burden has caused maximal microgliosis across brain regions. The discrepancy observed in older *App*$^{NL-F}$ mice may be reflective of their phenotype, where Aβ accumulates at a much slower rate compared to *App*$^{NL-G-F}$ mice (Saito et al., 2014), therefore at 18 months old these mice may be at mid rather than late-stage pathology, overall leading to a shift in the dynamic of microglial behaviour.

Overall, these results show that microglia do not initiate, but are critical for plaque maturation and compaction. If microglia were the initiators, then we would expect to see higher or the same level of activation in younger animals. In line with this, previous studies have shown that microglial alterations occur following plaque formation in AD mice (Benitez et al., 2021; Jung et al., 2015; Rodriguez et al., 2013). It would be interesting to assess an older age (e.g. 30 months), to see if this effect remains consistent over time, or if there comes a point when microglia become dysfunctional and fail to carry out their roles. These results provide insight into mechanisms in early AD, and highlight the significant microglial response to plaques in *App* KI models of AD. It appears that microglial activity in response to early changes could in fact be protective, and implicating these immune cells as important therapeutic targets for future research.

7.4.2 The Trem2 mutation affects the ability of microglia to compact plaques

Upregulation of Trem2 in line with plaque deposition is well-documented in studies of both mouse models (Benitez et al., 2021; Matarin et al., 2015) and *post-mortem* human tissue (Gratuze et al., 2018). Additionally, microglial behaviour around plaques is Trem2-dependent and altered in the presence of the *Trem2*^{R47H} risk factor mutation (Korvatska et al., 2015; Wood et al., 2022).

The results here demonstrated that compared to age-matched *App*$^{NL-F}$ mice, 18 month-old APP^{NL-F}/TREM2^{R47H} mice exhibit significant impairments in microglial clustering and activation around plaques. As established from the LCO spectral data, this corresponds to a dramatic decrease in plaque structural maturity. What this tells us is that Trem2 plays an important role in shaping plaques, in line with previous findings that mice with the *Trem2*^{R47H} mutation display reduced quantities of plaque-associated microglia and altered plaque morphology (Cheng-Hathaway et al., 2018; Jay et al., 2015; Wang et al., 2015; Yuan et al., 2016).

There are two potential mechanisms underlying these observations; either, microglia are not appropriately accumulating around plaques to limit growth, or Trem2 is affecting the phagocytic activity of microglia, thus also contributing to changes in plaque structure. A two-photon study demonstrated that microglial deposition of previously phagocytosed Aβ material was essential for formation of dense-core plaques (Baik et al., 2016). Additionally, lysosomes within microglia have an acidic environment, which promotes the formation of dense protease-resistant Aβ fibrils (Fu et al., 2012). Therefore, it could be concluded that Aβ fibrils are routed to lysosomes and subsequently become compacted into dense-core material that is indigestible, and must be released via exocytosis, further contributing to plaque compaction.

It has been shown previously that microglia form a barrier around plaques, preventing toxic Aβ species from damaging neurites (Cheng-Hathaway et al.,

2018), which would suggest that the impaired clustering observed here would lead to increased neuritic dystrophy. While this was not measured here, Cheng-Hathaway and colleagues (2018) showed that *Trem2*^{R47H} mice have an increase in dystrophic neurites in relation to plaque size, suggesting that larger plaques are more affected by Trem2 impairment and reduced clustering of microglia. These data implicate Trem2 in clearance of dystrophic neurites, which would be interesting to investigate in a future study.

It is important to highlight that other mechanisms may also be affected by Trem2 impairment. A previous unpublished study by our lab demonstrated a clear reduction in the area occupied by astrocytes in the vicinity of plaques in *App*$^{NL-F}$/*Trem2*^{R47H} mice compared to *App*$^{NL-F}$ mice, implicating an impairment in the normal response of astrocytes to Aβ aggregates (Vitanova, 2021). Overall, this highlights an interesting interaction between Trem2, astrocytes and microglia, in line with a previous study demonstrating that microglial activation initiates astrogliosis (Liddelow et al., 2017). Future studies could focus on the precise mechanisms underlying Trem2-mediated alterations in astrocyte associations with plaques.

Additionally, Trem2 is involved in signalling with many downstream factors. One notable recent study highlighted crucial roles of the TAM receptor kinases Axl and Mer in microglial recognition, response and phagocytosis of Aβ plaques (Huang et al., 2021b). They also found that the TAM system is required for microglial phagocytosis of Aβ and formation of dense-core plaques (Huang et al., 2021b). One key implication from this study was that dense-core Aβ plaques do not form spontaneously, but are constructed from Aβ material by phagocytic microglia, mediated by TAM receptors, which suggests that microglia initiate dense-core plaque formation.

In contrast to this, in the present study, the LCO imaging data revealed that *App*$^{NL-F}$/*Trem2*^{R47H} mice had plaques of a significantly decreased structural maturity compared to *App*$^{NL-F}$ animals. Previous work in our lab showed that there are little alterations in plaque load but a greater number of smaller plaques in *App*$^{NL-F}$/*Trem2*^{R47H} mice compared to *App*$^{NL-F}$ mice (Wood et al., 2022). This could suggest that the activation of microglia expressing WT Trem2 may be involved in

the removal of very small plaques. However, when these plaques grow past a certain size (e.g. 100 μm^2) they are no longer effective in their removal. An alternative explanation could be that the *Trem2*^{R47H} mutation results in constant seeding of plaques either *de novo* (Friedrich et al., 2010) or by small plaques breaking off from the larger plaques. However, it seems that these extra plaques are not destined to grow into larger plaques.

Overall this shows that plaque formation occurs first, followed by microgliosis. The conflicting data in the aforementioned study once again implicates the possibility of subpopulations of microglia with different roles, which would be interesting to further explore.

An important question arising from this work is how the results observed here relate to human sAD patients carrying the *Trem2*^{R47H} variant. Excitingly, here we have used direct and quantitative methods to show that in these mouse models, loss-of-function of Trem2 causes an impairment in microglial response to plaque pathology, resulting in altered plaque composition. This strengthens previous reports that microglia play a pivotal role in plaque compaction and maturation, and suggests that targeting TREM2 may alleviate disease progression. Additionally, *TREM2*^{R47H} is implicated in numerous other neurodegenerative diseases such as FTD, ALS and PD (Borroni et al., 2014; Cady et al., 2014; Guerreiro and Hardy, 2013; Rayaprolu et al., 2013); therefore, these results provide a basis for understanding therapeutic targets in other disease areas.

Limitations of *App* KI models

App KI mice avoid many issues associated with transgenic models, especially overexpression and inappropriate expression of App driven by non-endogenous promoters. *App*$^{NL-G-F}$ mice have been widely used in recent years to quickly examine amyloid aggregation and deposition; however, this model does have several limitations. In AD, plaque deposition occurs up to decades before cognitive symptoms first emerge. Subsequently, neuroinflammation, development of tau tangles, and synaptic loss and activity alterations leads to noticeable clinical symptoms. The presence of the *App* Arctic mutation in *App*$^{NL-}$

$^{G-F}$ mice, which predisposes Aβ to aggregate, causes such rapid plaque deposition that it does not replicate the gradual build-up of pathological events in line with rising soluble Aβ as is the case in humans. Additionally, the structural change of Aβ may mean that the plaques formed are only specific to individuals with the fAD Arctic mutation, rather than those with sAD. Our previous research into *App*$^{NL-G-F}$ plaques showed that they initially form a plaque core composed entirely of Aβ1-42, followed by further recruitment and deposition of Aβ1-42, and finally secretion and deposition of Aβ1-38 (Michno et al., 2021). On the other hand, in human sAD, maturation of diffuse into cored plaques is associated with increased Aβ1-40 (Michno et al., 2019a), whereas both *App*$^{NL-F}$ and *App*$^{NL-G-F}$ mice have almost no Aβ1-40 (Saito et al., 2014). Therefore, it is important to bear in mind firstly, there are key differences between mice and humans, and secondly, that the dynamics of plaque maturation and spread may involve different processes depending on AD subtype, which further supports the need for individualised anti-amyloid therapies.

One way to overcome some of these issues is to study *App*$^{NL-F}$ mice, a less aggressive model of amyloidosis. In these mice, rising Aβ leads to a gradual rise in plaque load from 9 to 24 months of age (Benitez et al., 2021), resulting in more subtle gene expression changes compared to *App*$^{NL-G-F}$ mice or other transgenic models. However, a disadvantage is that these mice are less time-efficient and costlier to study.

With regard to the *App*$^{NL-F}$/*Trem2*^{R47H} mice used in this study, *Trem2*^{R47H} KI mice have previously been shown to have decreased *Trem2* expression that was not found in human *post-mortem* tissue from individuals with the *TREM2*^{R47H} mutation. Therefore, it is unclear whether this effect is mouse-specific, and requires further study. However, these previous studies assessed very young mice or iPSCs, therefore the results are potentially not comparable to aged humans. Thus, this decreased expression may be age-related, and highlights how *TREM2*-related alterations occur even in early development.

It should be noted that unlike human AD, none of these mouse models naturally develop tau tangles as a result of progressive amyloidosis. However, they

nonetheless serve as good models for understanding early amyloid-associated mechanisms in AD.

7.6 Conclusions

In this project I examined Aβ dynamics and the interaction with surrounding microglia in *App* KI mice. Additionally, I utilised a newly developed paradigm involving stable isotope labelling combined with MALDI-IMS, to elucidate the timeline of Aβ deposition in these mice with high chemical sensitivity and specificity. Overall, the results of this study highlight important differences in amyloid plaque composition and microglial response depending on fAD genetic mutation, and also implicate the role of TREM2 in facilitating plaque maturation. Both Aβ composition within plaques and plaque-associated microgliosis are altered in the presence of the *App* Arctic or *Trem2*^{R47H} mutations; thus, this work provides a basis for further development of therapeutic targets for individuals with these variants. It is clear that AD is in fact a multifactorial disease involving many cell types and interactions. With the continuous development of new and more physiologically relevant mouse models, it would be of use to further explore the interaction between microglia and plaques, in addition to other known drivers of AD such as synapses, tau and astrocytes.

7.7 Future directions

In light of the results presented here, there are many future research directions that could be taken. It is important to re-highlight the key differences between mice and humans; therefore, a natural next step would be to expand into human studies to further validate the results demonstrated here. SILK as a method has already been used to measure tau, APOE and Aβ turnover in the human CNS (Paterson et al., 2019). An innovative and intriguing next step, which is already in the pipeline, is to obtain human brain tissue (during routine surgery) from stable-isotope infused patients. This tissue can subsequently be subjected to MALDI-IMS, providing a novel way of measuring spatial protein dynamics in humans. However, the applicability of SILK in both humans and mice is still

limited by the high cost of labelled amino acids, the availability of MS facilities and the time and effort involved, and should be considered.

As highlighted in this thesis, there is large heterogeneity between human and mouse microglia. Therefore, a useful next experiment would be to further establish the precise role of murine microglia around plaques, such as clearing excess Aβ, or phagocytosing Aβ and then releasing it to contribute to plaque growth, perhaps using electron microscopy or super high-resolution microscopy to see whether Aβ is colocalised within microglial processes. It would then be interesting to validate these results with a comparative human microglia study, for example using microglia-like iPSCs derived from human donors. At this stage, the incorporation of novel technologies such as spatial transcriptomics would be of use, to assess gene expression changes in plaque-associated or non plaque-associated microglia and astrocytes in both murine and human microglia. This would provide important human/mouse comparative information about the localisation of transcriptomic changes in response to Aβ.

Regarding Aβ plaques, here it was shown that AD genotype has a strong influence on resulting plaque conformation. Further work is needed to improve the understanding of Aβ plaque pathology in AD, such as a broader analytical approach to incorporate other classes of biomolecules, such as the proteome, lipids or glycans to truly understand the local environment around Aβ plaques. In this context, IMS or electron microscopy-based approaches provide a powerful and accurate way to study these interactions at the single-plaque level. Furthermore, as the iSILK paradigm presented here proved to be an effective way to measure Aβ behaviour with high chemical specificity and sensitivity, this technique could be used to assess dynamic changes in other AD-associated pathologies, such as tau, alpha-synuclein, or synaptic alterations. Indeed, the PULSE/CHASE method has previously been applied to *App* KI mice to assess other AD-related pathologies, which revealed that upon initial Aβ accumulation, protein turnover in presynaptic terminals is selectively impaired (Hark et al., 2021). This highlights the vulnerability of the presynaptic terminal in early AD, which would be interesting to further explore.

A particular limitation of the present studies was that mice harbouring fAD mutations were examined, which genetically speaking are only relevant to a small population of AD sufferers. Genetic risk factors for late-onset AD, such as APOE4 and TREM2, are much more prevalent in the general population and thus are a better reflection of sporadic AD. Creating a rodent model of sporadic AD is no doubt a highly complex task; however, it would be interesting in the future to expand the technologies used here into ApoE knock-out mice, for example, to assess alterations in certain biomolecules (such as lipids) at the single plaque level. It should be noted that ApoE knock-out mice have already been developed; however, murine and human forms of ApoE are only 70% homologus (Tai et al., 2011).

In terms of *TREM2,* this relatively newly discovered risk factor for Alzheimer's requires much further investigation. In the present study, only Aβ/Trem2 protein interactions were examined; however, TREM2 has previously been shown to be interact with dystrophic neurites, tau and TAM receptors. For example, a recent paper showed that murine Trem2 may be protective at all stages of AD pathogenesis (Lee et al., 2021). With the development of new *App* and human tau KI mouse models, it would be interesting to explore the potential relationship between Trem2 and Aβ in the presence of tau.

The long-term implications of the results of this thesis are significant. Firstly, the methodologies used here pave the way for future SILK and MALDI-IMS based experiments, be that in neurodegenerative disorders or others, such as oncology. Notably, SILK can be applied *in vivo* to humans, meaning that human and mouse studies can be run in parallel to examine AD-related protein synthesis and turnover from all angles. Additionally, PULSE/CHASE experiments are a powerful and flexible tool to examine the timeline of amyloid pathology. Importantly, these results also contribute to the understanding of microglia/plaque interactions in AD. In a clinical context, the importance of studying Aβ has been highlighted over the last few decades, with so many anti-amyloid antibodies failing clinical trials, likely because they are introduced too late into disease progression. Furthermore, the role of Aβ has been confirmed by the recent success of Biogen/Eisai's anti-amyloid antibody lecanumab, highlighting the importance of further

understanding amyloid. Overall, the use of pre-clinical mouse models in SILK, MALDI-IMS and wider cellular analysis provides a powerful and straight-forward way to investigate AD pathology, providing the opportunity to reveal early disease targets before onset of cognitive symptoms.

Contribution statement

For organotypic hippocampal slice culture experiments, K.S. performed all culturing, staining, imaging and analysis. For iSILK experiments, K.S. fed mice, processed tissue and contributed to experiment design, performed image construction and analysis for *App*$^{NL-F}$ and for the *App*$^{NL-G-F}$ together with W.M. and J.G. For LCO plaque and microglia experiments, K.S. performed all immunohistochemistry, confocal imaging and analysis.

References

. OFF CAMPUS ENDNOTE SETTINGS.

Abels, E.R., Nieland, L., Hickman, S., Broekman, M.L.D., El Khoury, J., and Maas, S.L.N. (2021). Comparative Analysis Identifies Similarities between the Human and Murine Microglial Sensomes. Int J Mol Sci *22*.

Aebersold, R., and Mann, M. (2003). Mass spectrometry-based proteomics. Nature *422*, 198-207.

Ajami, B., Samusik, N., Wieghofer, P., Ho, P.P., Crotti, A., Bjornson, Z., Prinz, M., Fantl, W.J., Nolan, G.P., and Steinman, L. (2018). Single-cell mass cytometry reveals distinct populations of brain myeloid cells in mouse neuroinflammation and neurodegeneration models. Nat Neurosci *21*, 541-551.

Alcalay, R.N., Levy, O.A., Wolf, P., Oliva, P., Zhang, X.K., Waters, C.H., Fahn, S., Kang, U., Liong, C., Ford, B*., et al.* (2016). SCARB2 variants and glucocerebrosidase activity in Parkinson's disease. NPJ Parkinsons Dis *2*, 16004.

Alevra, M., Mandad, S., Ischebeck, T., Urlaub, H., Rizzoli, S.O., and Fornasiero, E.F. (2019). A mass spectrometry workflow for measuring protein turnover rates in vivo. Nat Protoc *14*, 3333-3365.

Allen, B., Ingram, E., Takao, M., Smith, M.J., Jakes, R., Virdee, K., Yoshida, H., Holzer, M., Craxton, M., Emson, P.C*., et al.* (2002). Abundant tau filaments and nonapoptotic neurodegeneration in transgenic mice expressing human P301S tau protein. J Neurosci *22*, 9340-9351.

Almstedt, K., Nystrom, S., Nilsson, K.P., and Hammarstrom, P. (2009). Amyloid fibrils of human prion protein are spun and woven from morphologically disordered aggregates. Prion *3*, 224-235.

Alonso, A.C., Li, B., Grundke-Iqbal, I., and Iqbal, K. (2008). Mechanism of tau-induced neurodegeneration in Alzheimer disease and related tauopathies. Curr Alzheimer Res *5*, 375-384.

Alzheimer, A. (1907). About a peculiar disease of the cerebral cortex. (Translation by L. Jarvik and H. Greenson in 1987). Alzheimer Dis Assoc Disord *1*, 3-8.

Andorfer, C., Kress, Y., Espinoza, M., de Silva, R., Tucker, K.L., Barde, Y.A., Duff, K., and Davies, P. (2003). Hyperphosphorylation and aggregation of tau in mice expressing normal human tau isoforms. J Neurochem *86*, 582-590.

Andrew, R.J., Fisher, K., Heesom, K.J., Kellett, K.A.B., and Hooper, N.M. (2019). Quantitative interaction proteomics reveals differences in the interactomes of amyloid precursor protein isoforms. J Neurochem *149*, 399-412.

Aslund, A., Sigurdson, C.J., Klingstedt, T., Grathwohl, S., Bolmont, T., Dickstein, D.L., Glimsdal, E., Prokop, S., Lindgren, M., Konradsson, P*., et al.* (2009). Novel pentameric thiophene derivatives for in vitro and in vivo optical imaging of a plethora of protein aggregates in cerebral amyloidoses. Acs Chem Biol *4*, 673-684.

Atagi, Y., Liu, C.C., Painter, M.M., Chen, X.F., Verbeeck, C., Zheng, H., Li, X., Rademakers, R., Kang, S.S., Xu, H*., et al.* (2015). Apolipoprotein E Is a Ligand for Triggering Receptor Expressed on Myeloid Cells 2 (TREM2). The Journal of biological chemistry *290*, 26043-26050.

Baik, S.H., Kang, S., Son, S.M., and Mook-Jung, I. (2016). Microglia contributes to plaque growth by cell death due to uptake of amyloid beta in the brain of Alzheimer's disease mouse model. Glia *64*, 2274-2290.

Ballard, C., Mobley, W., Hardy, J., Williams, G., and Corbett, A. (2016). Dementia in Down's syndrome. Lancet Neurol *15*, 622-636.
Barnard, N.D., Bush, A.I., Ceccarelli, A., Cooper, J., de Jager, C.A., Erickson, K.I., Fraser, G., Kesler, S., Levin, S.M., Lucey, B.*, et al.* (2014). Dietary and lifestyle guidelines for the prevention of Alzheimer's disease. Neurobiol Aging *35 Suppl 2*, S74-78.
Barnes, D.E., and Yaffe, K. (2011). The projected effect of risk factor reduction on Alzheimer's disease prevalence. Lancet Neurol *10*, 819-828.
Bateman, R.J., Munsell, L.Y., Morris, J.C., Swarm, R., Yarasheski, K.E., and Holtzman, D.M. (2006a). Human amyloid-beta synthesis and clearance rates as measured in cerebrospinal fluid in vivo. Nature Medicine *12*, 856-861.
Bateman, R.J., Munsell, L.Y., Morris, J.C., Swarm, R., Yarasheski, K.E., and Holtzman, D.M. (2006b). Human amyloid-beta synthesis and clearance rates as measured in cerebrospinal fluid in vivo. Nat Med *12*, 856-861.
Bateman, R.J., Xiong, C., Benzinger, T.L., Fagan, A.M., Goate, A., Fox, N.C., Marcus, D.S., Cairns, N.J., Xie, X., Blazey, T.M.*, et al.* (2012). Clinical and biomarker changes in dominantly inherited Alzheimer's disease. N Engl J Med *367*, 795-804.
Beach, T.G., Walker, R., and McGeer, E.G. (1989). Patterns of gliosis in Alzheimer's disease and aging cerebrum. Glia *2*, 420-436.
Benitez, B.A., Cooper, B., Pastor, P., Jin, S.C., Lorenzo, E., Cervantes, S., and Cruchaga, C. (2013). TREM2 is associated with the risk of Alzheimer's disease in Spanish population. Neurobiol Aging *34*, 1711 e1715-1717.
Benitez, D. (2021). Assessment of microglia influence in synaptic transmission and early amiloid-B plaque deposition in knock-in mouse models for Alzheimer's disese. In Neuroscience, Physiology and Pharmacology (UCL).
Benitez, D.P., Jiang, S., Wood, J., Wang, R., Hall, C.M., Peerboom, C., Wong, N., Stringer, K.M., Vitanova, K.S., Smith, V.C.*, et al.* (2021). Knock-in models related to Alzheimer's disease: synaptic transmission, plaques and the role of microglia. Mol Neurodegener *16*, 47.
Berezovska, O., Lleo, A., Herl, L.D., Frosch, M.P., Stern, E.A., Bacskai, B.J., and Hyman, B.T. (2005). Familial Alzheimer's disease presenilin 1 mutations cause alterations in the conformation of presenilin and interactions with amyloid precursor protein. J Neurosci *25*, 3009-3017.
Bialas, A.R., and Stevens, B. (2013). TGF-beta signaling regulates neuronal C1q expression and developmental synaptic refinement. Nat Neurosci *16*, 1773-1782.
Biogen, E. (2022). LECANEMAB CONFIRMATORY PHASE 3 CLARITY AD STUDY MET PRIMARY ENDPOINT, SHOWING HIGHLY STATISTICALLY SIGNIFICANT REDUCTION OF CLINICAL DECLINE IN LARGE GLOBAL CLINICAL STUDY OF 1,795 PARTICIPANTS WITH EARLY ALZHEIMER'S DISEASE.
Bitan, G., Kirkitadze, M.D., Lomakin, A., Vollers, S.S., Benedek, G.B., and Teplow, D.B. (2003). Amyloid beta -protein (Abeta) assembly: Abeta 40 and Abeta 42 oligomerize through distinct pathways. Proc Natl Acad Sci U S A *100*, 330-335.
Blennow, K., de Leon, M.J., and Zetterberg, H. (2006). Alzheimer's disease. Lancet *368*, 387-403.
Blennow, K., Mattsson, N., Scholl, M., Hansson, O., and Zetterberg, H. (2015). Amyloid biomarkers in Alzheimer's disease. Trends Pharmacol Sci *36*, 297-309.
Blennow, K., and Wallin, A. (1992). Clinical heterogeneity of probable Alzheimer's disease. J Geriatr Psychiatry Neurol *5*, 106-113.
Bloom, G.S. (2014). Amyloid-beta and tau: the trigger and bullet in Alzheimer disease pathogenesis. JAMA Neurol *71*, 505-508.

Bolmont, T., Haiss, F., Eicke, D., Radde, R., Mathis, C.A., Klunk, W.E., Kohsaka, S., Jucker, M., and Calhoun, M.E. (2008). Dynamics of the microglial/amyloid interaction indicate a role in plaque maintenance. J Neurosci *28*, 4283-4292.
Borroni, B., Ferrari, F., Galimberti, D., Nacmias, B., Barone, C., Bagnoli, S., Fenoglio, C., Piaceri, I., Archetti, S., Bonvicini, C.*, et al.* (2014). Heterozygous TREM2 mutations in frontotemporal dementia. Neurobiol Aging *35*, 934 e937-910.
Braak, H., Alafuzoff, I., Arzberger, T., Kretzschmar, H., and Del Tredici, K. (2006). Staging of Alzheimer disease-associated neurofibrillary pathology using paraffin sections and immunocytochemistry. Acta neuropathologica *112*, 389-404.
Braak, H., and Braak, E. (1991). Neuropathological stageing of Alzheimer-related changes. Acta neuropathologica *82*, 239-259.
Braak, H., and Braak, E. (1997). Frequency of stages of Alzheimer-related lesions in different age categories. Neurobiol Aging *18*, 351-357.
Brownjohn, P.W., Smith, J., Solanki, R., Lohmann, E., Houlden, H., Hardy, J., Dietmann, S., and Livesey, F.J. (2018). Functional Studies of Missense TREM2 Mutations in Human Stem Cell-Derived Microglia. Stem Cell Reports *10*, 1294-1307.
Buchberger, A.R., DeLaney, K., Johnson, J., and Li, L. (2018). Mass Spectrometry Imaging: A Review of Emerging Advancements and Future Insights. Anal Chem *90*, 240-265.
Buckner, R.L., Snyder, A.Z., Shannon, B.J., LaRossa, G., Sachs, R., Fotenos, A.F., Sheline, Y.I., Klunk, W.E., Mathis, C.A., Morris, J.C.*, et al.* (2005). Molecular, structural, and functional characterization of Alzheimer's disease: evidence for a relationship between default activity, amyloid, and memory. J Neurosci *25*, 7709-7717.
Butovsky, O., Jedrychowski, M.P., Moore, C.S., Cialic, R., Lanser, A.J., Gabriely, G., Koeglsperger, T., Dake, B., Wu, P.M., Doykan, C.E.*, et al.* (2014). Identification of a unique TGF-beta-dependent molecular and functional signature in microglia. Nat Neurosci *17*, 131-143.
Cady, J., Koval, E.D., Benitez, B.A., Zaidman, C., Jockel-Balsarotti, J., Allred, P., Baloh, R.H., Ravits, J., Simpson, E., Appel, S.H.*, et al.* (2014). TREM2 variant p.R47H as a risk factor for sporadic amyotrophic lateral sclerosis. JAMA Neurol *71*, 449-453.
Campion, D., Dumanchin, C., Hannequin, D., Dubois, B., Belliard, S., Puel, M., Thomas-Anterion, C., Michon, A., Martin, C., Charbonnier, F.*, et al.* (1999). Early-onset autosomal dominant Alzheimer disease: prevalence, genetic heterogeneity, and mutation spectrum. American journal of human genetics *65*, 664-670.
Cannon, J.P., O'Driscoll, M., and Litman, G.W. (2012). Specific lipid recognition is a general feature of CD300 and TREM molecules. Immunogenetics *64*, 39-47.
Carlred, L., Michno, W., Kaya, I., Sjovall, P., Syvanen, S., and Hanrieder, J. (2016). Probing amyloid-beta pathology in transgenic Alzheimer's disease (tgArcSwe) mice using MALDI imaging mass spectrometry. J Neurochem *138*, 469-478.
Carulla, N., Zhou, M., Arimon, M., Gairi, M., Giralt, E., Robinson, C.V., and Dobson, C.M. (2009). Experimental characterization of disordered and ordered aggregates populated during the process of amyloid fibril formation. Proc Natl Acad Sci U S A *106*, 7828-7833.
Castillo, E., Leon, J., Mazzei, G., Abolhassani, N., Haruyama, N., Saito, T., Saido, T., Hokama, M., Iwaki, T., Ohara, T.*, et al.* (2017). Comparative profiling of cortical gene expression in Alzheimer's disease patients and mouse models demonstrates a link between amyloidosis and neuroinflammation. Sci Rep *7*, 17762.
Chartier-Harlin, M.C., Crawford, F., Houlden, H., Warren, A., Hughes, D., Fidani, L., Goate, A., Rossor, M., Roques, P., Hardy, J.*, et al.* (1991). Early-onset Alzheimer's

disease caused by mutations at codon 717 of the beta-amyloid precursor protein gene. Nature *353*, 844-846.
Cheng-Hathaway, P.J., Reed-Geaghan, E.G., Jay, T.R., Casali, B.T., Bemiller, S.M., Puntambekar, S.S., von Saucken, V.E., Williams, R.Y., Karlo, J.C., Moutinho, M.*, et al.* (2018). The Trem2 R47H variant confers loss-of-function-like phenotypes in Alzheimer's disease. Mol Neurodegener *13*, 29.
Chughtai, K., and Heeren, R.M. (2010). Mass spectrometric imaging for biomedical tissue analysis. Chem Rev *110*, 3237-3277.
Clayton, K., Delpech, J.C., Herron, S., Iwahara, N., Ericsson, M., Saito, T., Saido, T.C., Ikezu, S., and Ikezu, T. (2021). Plaque associated microglia hyper-secrete extracellular vesicles and accelerate tau propagation in a humanized APP mouse model. Mol Neurodegener *16*, 18.
Cleary, J.P., Walsh, D.M., Hofmeister, J.J., Shankar, G.M., Kuskowski, M.A., Selkoe, D.J., and Ashe, K.H. (2005). Natural oligomers of the amyloid-beta protein specifically disrupt cognitive function. Nat Neurosci *8*, 79-84.
Cohen, M.L., Kim, C., Haldiman, T., ElHag, M., Mehndiratta, P., Pichet, T., Lissemore, F., Shea, M., Cohen, Y., Chen, W.*, et al.* (2015). Rapidly progressive Alzheimer's disease features distinct structures of amyloid-beta. Brain : a journal of neurology *138*, 1009-1022.
Condello, C., Yuan, P., Schain, A., and Grutzendler, J. (2015). Microglia constitute a barrier that prevents neurotoxic protofibrillar Abeta42 hotspots around plaques. Nat Commun *6*, 6176.
Corder, E.H., Saunders, A.M., Strittmatter, W.J., Schmechel, D.E., Gaskell, P.C., Small, G.W., Roses, A.D., Haines, J.L., and Pericak-Vance, M.A. (1993). Gene dose of apolipoprotein E type 4 allele and the risk of Alzheimer's disease in late onset families. Science *261*, 921-923.
Correani, V., Di Francesco, L., Mignogna, G., Fabrizi, C., Leone, S., Giorgi, A., Passeri, A., Casata, R., Fumagalli, L., Maras, B.*, et al.* (2017). Plasma Membrane Protein Profiling in Beta-Amyloid-Treated Microglia Cell Line. Proteomics *17*.
Croft, C.L., Cruz, P.E., Ryu, D.H., Ceballos-Diaz, C., Strang, K.H., Woody, B.M., Lin, W.L., Deture, M., Rodriguez-Lebron, E., Dickson, D.W.*, et al.* (2019). rAAV-based brain slice culture models of Alzheimer's and Parkinson's disease inclusion pathologies. J Exp Med *216*, 539-555.
Croft, C.L., Wade, M.A., Kurbatskaya, K., Mastrandreas, P., Hughes, M.M., Phillips, E.C., Pooler, A.M., Perkinton, M.S., Hanger, D.P., and Noble, W. (2017). Membrane association and release of wild-type and pathological tau from organotypic brain slice cultures. Cell Death Dis *8*, e2671.
Cullen, N., Janelidze, S., Palmqvist, S., Stomrud, E., Mattsson-Carlgren, N., and Hansson, O. (2021). Association of CSF Abeta38 Levels With Risk of Alzheimer Disease-Related Decline. Neurology.
Cummings, D.M., Liu, W., Portelius, E., Bayram, S., Yasvoina, M., Ho, S.H., Smits, H., Ali, S.S., Steinberg, R., Pegasiou, C.M.*, et al.* (2015). First effects of rising amyloid-beta in transgenic mouse brain: synaptic transmission and gene expression. Brain : a journal of neurology *138*, 1992-2004.
Currais, A. (2015). Ageing and inflammation - A central role for mitochondria in brain health and disease. Ageing Res Rev *21*, 30-42.
Daborg, J., Andreasson, U., Pekna, M., Lautner, R., Hanse, E., Minthon, L., Blennow, K., Hansson, O., and Zetterberg, H. (2012). Cerebrospinal fluid levels of complement proteins C3, C4 and CR1 in Alzheimer's disease. J Neural Transm (Vienna) *119*, 789-797.

Davies, D.C., Wilmott, A.C., and Mann, D.M. (1988). Senile plaques are concentrated in the subicular region of the hippocampal formation in Alzheimer's disease. Neurosci Lett *94*, 228-233.
De Felice, F.G., Wu, D., Lambert, M.P., Fernandez, S.J., Velasco, P.T., Lacor, P.N., Bigio, E.H., Jerecic, J., Acton, P.J., Shughrue, P.J.*, et al.* (2008). Alzheimer's disease-type neuronal tau hyperphosphorylation induced by A beta oligomers. Neurobiol Aging *29*, 1334-1347.
De Strooper, B., Iwatsubo, T., and Wolfe, M.S. (2012). Presenilins and gamma-secretase: structure, function, and role in Alzheimer Disease. Cold Spring Harbor perspectives in medicine *2*, a006304.
DeKosky, S.T., and Scheff, S.W. (1990). Synapse loss in frontal cortex biopsies in Alzheimer's disease: correlation with cognitive severity. Ann Neurol *27*, 457-464.
Deshpande, A., Mina, E., Glabe, C., and Busciglio, J. (2006). Different conformations of amyloid beta induce neurotoxicity by distinct mechanisms in human cortical neurons. J Neurosci *26*, 6011-6018.
Dickson, T.C., and Vickers, J.C. (2001). The morphological phenotype of beta-amyloid plaques and associated neuritic changes in Alzheimer's disease. Neuroscience *105*, 99-107.
Dominguez, D., Tournoy, J., Hartmann, D., Huth, T., Cryns, K., Deforce, S., Serneels, L., Camacho, I.E., Marjaux, E., Craessaerts, K.*, et al.* (2005). Phenotypic and biochemical analyses of BACE1- and BACE2-deficient mice. The Journal of biological chemistry *280*, 30797-30806.
Dore, K., Carrico, Z., Alfonso, S., Marino, M., Koymans, K., Kessels, H.W., and Malinow, R. (2021). PSD-95 protects synapses from beta-amyloid. Cell Rep *35*, 109194.
Duff, K., Noble, W., Gaynor, K., and Matsuoka, Y. (2002). Organotypic slice cultures from transgenic mice as disease model systems. J Mol Neurosci *19*, 317-320.
Dunkelberger, J.R., and Song, W.C. (2010). Complement and its role in innate and adaptive immune responses. Cell Res *20*, 34-50.
Edwards, F.A. (2019). A Unifying Hypothesis for Alzheimer's Disease: From Plaques to Neurodegeneration. Trends Neurosci *42*, 310-322.
Eikelenboom, P., and Stam, F.C. (1982). Immunoglobulins and complement factors in senile plaques. An immunoperoxidase study. Acta neuropathologica *57*, 239-242.
Enzlein, T., Cordes, J., Munteanu, B., Michno, W., Serneels, L., De Strooper, B., Hanrieder, J., Wolf, I., Chavez-Gutierrez, L., and Hopf, C. (2020). Computational Analysis of Alzheimer Amyloid Plaque Composition in 2D- and Elastically Reconstructed 3D-MALDI MS Images. Anal Chem *92*, 14484-14493.
Esch, F.S., Keim, P.S., Beattie, E.C., Blacher, R.W., Culwell, A.R., Oltersdorf, T., McClure, D., and Ward, P.J. (1990). Cleavage of amyloid beta peptide during constitutive processing of its precursor. Science *248*, 1122-1124.
Fagan, A.M., Watson, M., Parsadanian, M., Bales, K.R., Paul, S.M., and Holtzman, D.M. (2002). Human and murine ApoE markedly alters A beta metabolism before and after plaque formation in a mouse model of Alzheimer's disease. Neurobiol Dis *9*, 305-318.
Fenn, J.B., Mann, M., Meng, C.K., Wong, S.F., and Whitehouse, C.M. (1989). Electrospray ionization for mass spectrometry of large biomolecules. Science *246*, 64-71.
Finelli, D., Rollinson, S., Harris, J., Jones, M., Richardson, A., Gerhard, A., Snowden, J., Mann, D., and Pickering-Brown, S. (2015). TREM2 analysis and increased risk of Alzheimer's disease. Neurobiol Aging *36*, 546 e549-513.

Franco-Bocanegra, D.K., Gourari, Y., McAuley, C., Chatelet, D.S., Johnston, D.A., Nicoll, J.A.R., and Boche, D. (2021). Microglial morphology in Alzheimer's disease and after Aβ immunotherapy. Sci Rep-Uk *11*, 15955.
Frank, S., Burbach, G.J., Bonin, M., Walter, M., Streit, W., Bechmann, I., and Deller, T. (2008). TREM2 is upregulated in amyloid plaque-associated microglia in aged APP23 transgenic mice. Glia *56*, 1438-1447.
Friedman, B.A., Srinivasan, K., Ayalon, G., Meilandt, W.J., Lin, H., Huntley, M.A., Cao, Y., Lee, S.H., Haddick, P.C.G., Ngu, H.*, et al.* (2018). Diverse Brain Myeloid Expression Profiles Reveal Distinct Microglial Activation States and Aspects of Alzheimer's Disease Not Evident in Mouse Models. Cell Rep *22*, 832-847.
Friedrich, R.P., Tepper, K., Ronicke, R., Soom, M., Westermann, M., Reymann, K., Kaether, C., and Fandrich, M. (2010). Mechanism of amyloid plaque formation suggests an intracellular basis of Abeta pathogenicity. Proc Natl Acad Sci U S A *107*, 1942-1947.
Fu, H., Liu, B., Frost, J.L., Hong, S., Jin, M., Ostaszewski, B., Shankar, G.M., Costantino, I.M., Carroll, M.C., Mayadas, T.N.*, et al.* (2012). Complement component C3 and complement receptor type 3 contribute to the phagocytosis and clearance of fibrillar Abeta by microglia. Glia *60*, 993-1003.
Gajera, C.R., Fernandez, R., Montine, K.S., Fox, E.J., Mrdjen, D., Postupna, N.O., Keene, C.D., Bendall, S.C., and Montine, T.J. (2021). Mass-tag barcoding for multiplexed analysis of human synaptosomes and other anuclear events. Cytometry A *99*, 939-945.
Gajera, C.R., Fernandez, R., Postupna, N., Montine, K.S., Fox, E.J., Tebaykin, D., Angelo, M., Bendall, S.C., Keene, C.D., and Montine, T.J. (2019). Mass synaptometry: High-dimensional multi parametric assay for single synapses. J Neurosci Methods *312*, 73-83.
Garcia-Osta, A., and Alberini, C.M. (2009). Amyloid beta mediates memory formation. Learning & memory (Cold Spring Harbor, NY *16*, 267-272.
Garcia-Reitboeck, P., Phillips, A., Piers, T.M., Villegas-Llerena, C., Butler, M., Mallach, A., Rodrigues, C., Arber, C.E., Heslegrave, A., Zetterberg, H.*, et al.* (2018). Human Induced Pluripotent Stem Cell-Derived Microglia-Like Cells Harboring TREM2 Missense Mutations Show Specific Deficits in Phagocytosis. Cell Rep *24*, 2300-2311.
Gautier, E.L., Shay, T., Miller, J., Greter, M., Jakubzick, C., Ivanov, S., Helft, J., Chow, A., Elpek, K.G., Gordonov, S.*, et al.* (2012). Gene-expression profiles and transcriptional regulatory pathways that underlie the identity and diversity of mouse tissue macrophages. Nat Immunol *13*, 1118-1128.
Gerlach, J., Donkels, C., Munzner, G., and Haas, C.A. (2016). Persistent Gliosis Interferes with Neurogenesis in Organotypic Hippocampal Slice Cultures. Front Cell Neurosci *10*, 131.
Ginhoux, F., Greter, M., Leboeuf, M., Nandi, S., See, P., Gokhan, S., Mehler, M.F., Conway, S.J., Ng, L.G., Stanley, E.R.*, et al.* (2010). Fate mapping analysis reveals that adult microglia derive from primitive macrophages. Science *330*, 841-845.
Gkanatsiou, E., Portelius, E., Toomey, C.E., Blennow, K., Zetterberg, H., Lashley, T., and Brinkmalm, G. (2019). A distinct brain beta amyloid signature in cerebral amyloid angiopathy compared to Alzheimer's disease. Neurosci Lett *701*, 125-131.
Goate, A., Chartier-Harlin, M.C., Mullan, M., Brown, J., Crawford, F., Fidani, L., Giuffra, L., Haynes, A., Irving, N., James, L.*, et al.* (1991). Segregation of a missense mutation in the amyloid precursor protein gene with familial Alzheimer's disease. Nature *349*, 704-706.

Goedert, M., Spillantini, M.G., Jakes, R., Rutherford, D., and Crowther, R.A. (1989). Multiple isoforms of human microtubule-associated protein tau: sequences and localization in neurofibrillary tangles of Alzheimer's disease. Neuron *3*, 519-526.
Gratuze, M., Leyns, C.E.G., and Holtzman, D.M. (2018). New insights into the role of TREM2 in Alzheimer's disease. Mol Neurodegener *13*, 66.
Gremer, L., Scholzel, D., Schenk, C., Reinartz, E., Labahn, J., Ravelli, R.B.G., Tusche, M., Lopez-Iglesias, C., Hoyer, W., Heise, H.*, et al.* (2017). Fibril structure of amyloid-beta(1-42) by cryo-electron microscopy. Science *358*, 116-119.
Guerreiro, R., and Bras, J. (2015). The age factor in Alzheimer's disease. Genome Med *7*, 106.
Guerreiro, R., and Hardy, J. (2013). TREM2 and neurodegenerative disease. N Engl J Med *369*, 1569-1570.
Guerreiro, R., Wojtas, A., Bras, J., Carrasquillo, M., Rogaeva, E., Majounie, E., Cruchaga, C., Sassi, C., Kauwe, J.S., Younkin, S.*, et al.* (2013a). TREM2 variants in Alzheimer's disease. N Engl J Med *368*, 117-127.
Guerreiro, R., Wojtas, A., Bras, J., Carrasquillo, M., Rogaeva, E., Majounie, E., Cruchaga, C., Sassi, C., Kauwe, J.S.K., Younkin, S.*, et al.* (2013b). TREM2 variants in Alzheimer's disease. N Engl J Med *368*, 117-127.
Guerreiro, R.J., Lohmann, E., Bras, J.M., Gibbs, J.R., Rohrer, J.D., Gurunlian, N., Dursun, B., Bilgic, B., Hanagasi, H., Gurvit, H.*, et al.* (2013c). Using exome sequencing to reveal mutations in TREM2 presenting as a frontotemporal dementia-like syndrome without bone involvement. JAMA Neurol *70*, 78-84.
Hall, A.M., and Roberson, E.D. (2012). Mouse models of Alzheimer's disease. Brain Res Bull *88*, 3-12.
Hammarstrom, P., Simon, R., Nystrom, S., Konradsson, P., Aslund, A., and Nilsson, K.P. (2010). A fluorescent pentameric thiophene derivative detects in vitro-formed prefibrillar protein aggregates. Biochemistry *49*, 6838-6845.
Hanrieder, J., Malmberg, P., and Ewing, A.G. (2015). Spatial neuroproteomics using imaging mass spectrometry. Biochim Biophys Acta *1854*, 718-731.
Hanrieder, J., Phan, N.T., Kurczy, M.E., and Ewing, A.G. (2013). Imaging mass spectrometry in neuroscience. ACS Chem Neurosci *4*, 666-679.
Hardy, J., and Selkoe, D.J. (2002). The amyloid hypothesis of Alzheimer's disease: progress and problems on the road to therapeutics. Science *297*, 353-356.
Hardy, J.A., and Higgins, G.A. (1992). Alzheimer's disease: the amyloid cascade hypothesis. Science *256*, 184-185.
Hark, T.J., Rao, N.R., Castillon, C., Basta, T., Smukowski, S., Bao, H., Upadhyay, A., Bomba-Warczak, E., Nomura, T., O'Toole, E.T.*, et al.* (2021). Pulse-Chase Proteomics of the App Knockin Mouse Models of Alzheimer's Disease Reveals that Synaptic Dysfunction Originates in Presynaptic Terminals. Cell Syst *12*, 141-158 e149.
Harper, J.D., and Lansbury, P.T., Jr. (1997). Models of amyloid seeding in Alzheimer's disease and scrapie: mechanistic truths and physiological consequences of the time-dependent solubility of amyloid proteins. Annu Rev Biochem *66*, 385-407.
Harwell, C.S., and Coleman, M.P. (2016). Synaptophysin depletion and intraneuronal Abeta in organotypic hippocampal slice cultures from huAPP transgenic mice. Mol Neurodegener *11*, 44.
Hashimoto, T., Serrano-Pozo, A., Hori, Y., Adams, K.W., Takeda, S., Banerji, A.O., Mitani, A., Joyner, D., Thyssen, D.H., Bacskai, B.J.*, et al.* (2012). Apolipoprotein E, especially apolipoprotein E4, increases the oligomerization of amyloid β peptide. J Neurosci *32*, 15181-15192.

Hefendehl, J.K., Wegenast-Braun, B.M., Liebig, C., Eicke, D., Milford, D., Calhoun, M.E., Kohsaka, S., Eichner, M., and Jucker, M. (2011). Long-term in vivo imaging of beta-amyloid plaque appearance and growth in a mouse model of cerebral beta-amyloidosis. J Neurosci *31*, 624-629.
Heilbronner, G., Eisele, Y.S., Langer, F., Kaeser, S.A., Novotny, R., Nagarathinam, A., Aslund, A., Hammarstrom, P., Nilsson, K.P., and Jucker, M. (2013). Seeded strain-like transmission of beta-amyloid morphotypes in APP transgenic mice. EMBO Rep *14*, 1017-1022.
Hellwig, S., Masuch, A., Nestel, S., Katzmarski, N., Meyer-Luehmann, M., and Biber, K. (2015a). Forebrain microglia from wild-type but not adult 5xFAD mice prevent amyloid-beta plaque formation in organotypic hippocampal slice cultures. Sci Rep *5*, 14624.
Hellwig, S., Masuch, A., Nestel, S., Katzmarski, N., Meyer-Luehmann, M., and Biber, K. (2015b). Forebrain microglia from wild-type but not adult 5xFAD mice prevent amyloid-beta plaque formation in organotypic hippocampal slice cultures. Sci Rep *5*, 14624.
Heneka, M.T., Carson, M.J., El Khoury, J., Landreth, G.E., Brosseron, F., Feinstein, D.L., Jacobs, A.H., Wyss-Coray, T., Vitorica, J., Ransohoff, R.M.*, et al.* (2015). Neuroinflammation in Alzheimer's disease. Lancet Neurol *14*, 388-405.
Herms, J., Anliker, B., Heber, S., Ring, S., Fuhrmann, M., Kretzschmar, H., Sisodia, S., and Muller, U. (2004). Cortical dysplasia resembling human type 2 lissencephaly in mice lacking all three APP family members. The EMBO journal *23*, 4106-4115.
Hickman, S.E., Kingery, N.D., Ohsumi, T.K., Borowsky, M.L., Wang, L.C., Means, T.K., and El Khoury, J. (2013). The microglial sensome revealed by direct RNA sequencing. Nat Neurosci *16*, 1896-1905.
Hochstrasser, T., Hohsfield, L.A., Sperner-Unterweger, B., and Humpel, C. (2013). beta-Amyloid induced effects on cholinergic, serotonergic, and dopaminergic neurons is differentially counteracted by anti-inflammatory drugs. J Neurosci Res *91*, 83-94.
Holtman, I.R., Raj, D.D., Miller, J.A., Schaafsma, W., Yin, Z., Brouwer, N., Wes, P.D., Moller, T., Orre, M., Kamphuis, W.*, et al.* (2015). Induction of a common microglia gene expression signature by aging and neurodegenerative conditions: a co-expression meta-analysis. Acta Neuropathol Commun *3*, 31.
Hong, S., Beja-Glasser, V.F., Nfonoyim, B.M., Frouin, A., Li, S., Ramakrishnan, S., Merry, K.M., Shi, Q., Rosenthal, A., Barres, B.A.*, et al.* (2016). Complement and microglia mediate early synapse loss in Alzheimer mouse models. Science *352*, 712-716.
Honig, L.S., Vellas, B., Woodward, M., Boada, M., Bullock, R., Borrie, M., Hager, K., Andreasen, N., Scarpini, E., Liu-Seifert, H.*, et al.* (2018). Trial of Solanezumab for Mild Dementia Due to Alzheimer's Disease. N Engl J Med *378*, 321-330.
Hopperton, K.E., Mohammad, D., Trepanier, M.O., Giuliano, V., and Bazinet, R.P. (2018). Markers of microglia in post-mortem brain samples from patients with Alzheimer's disease: a systematic review. Mol Psychiatry *23*, 177-198.
Howie, A.J., and Brewer, D.B. (2009). Optical properties of amyloid stained by Congo red: history and mechanisms. Micron *40*, 285-301.
Howlett, D.R., Richardson, J.C., Austin, A., Parsons, A.A., Bate, S.T., Davies, D.C., and Gonzalez, M.I. (2004). Cognitive correlates of Abeta deposition in male and female mice bearing amyloid precursor protein and presenilin-1 mutant transgenes. Brain Res *1017*, 130-136.

Huang, Y., Happonen, K.E., Burrola, P.G., O'Connor, C., Hah, N., Huang, L., Nimmerjahn, A., and Lemke, G. (2021a). Microglia use TAM receptors to detect and engulf amyloid beta plaques. Nat Immunol *22*, 586-594.
Huang, Y., Happonen, K.E., Burrola, P.G., O'Connor, C., Hah, N., Huang, L., Nimmerjahn, A., and Lemke, G. (2021b). Microglia use TAM receptors to detect and engulf amyloid β plaques. Nat Immunol *22*, 586-594.
Huang, Y.A., Zhou, B., Wernig, M., and Sudhof, T.C. (2017). ApoE2, ApoE3, and ApoE4 Differentially Stimulate APP Transcription and Abeta Secretion. Cell *168*, 427-441 e421.
Hudry, E., Dashkoff, J., Roe, A.D., Takeda, S., Koffie, R.M., Hashimoto, T., Scheel, M., Spires-Jones, T., Arbel-Ornath, M., Betensky, R.*, et al.* (2013). Gene transfer of human Apoe isoforms results in differential modulation of amyloid deposition and neurotoxicity in mouse brain. Sci Transl Med *5*, 212ra161.
Huijbers, W., Mormino, E.C., Wigman, S.E., Ward, A.M., Vannini, P., McLaren, D.G., Becker, J.A., Schultz, A.P., Hedden, T., Johnson, K.A.*, et al.* (2014). Amyloid deposition is linked to aberrant entorhinal activity among cognitively normal older adults. J Neurosci *34*, 5200-5210.
Humpel, C. (2015a). Organotypic brain slice cultures: A review. Neuroscience *305*, 86-98.
Humpel, C. (2015b). Organotypic vibrosections from whole brain adult Alzheimer mice (overexpressing amyloid-precursor-protein with the Swedish-Dutch-Iowa mutations) as a model to study clearance of beta-amyloid plaques. Front Aging Neurosci *7*, 47.
Ingelsson, M., Fukumoto, H., Newell, K.L., Growdon, J.H., Hedley-Whyte, E.T., Frosch, M.P., Albert, M.S., Hyman, B.T., and Irizarry, M.C. (2004). Early Abeta accumulation and progressive synaptic loss, gliosis, and tangle formation in AD brain. Neurology *62*, 925-931.
Israel, M.A., Yuan, S.H., Bardy, C., Reyna, S.M., Mu, Y., Herrera, C., Hefferan, M.P., Van Gorp, S., Nazor, K.L., Boscolo, F.S.*, et al.* (2012). Probing sporadic and familial Alzheimer's disease using induced pluripotent stem cells. Nature *482*, 216-220.
Itagaki, S., McGeer, P.L., Akiyama, H., Zhu, S., and Selkoe, D. (1989). Relationship of microglia and astrocytes to amyloid deposits of Alzheimer disease. J Neuroimmunol *24*, 173-182.
Ittner, A., and Ittner, L.M. (2018). Dendritic Tau in Alzheimer's Disease. Neuron *99*, 13-27.
Ittner, L.M., Ke, Y.D., Delerue, F., Bi, M., Gladbach, A., van Eersel, J., Wolfing, H., Chieng, B.C., Christie, M.J., Napier, I.A.*, et al.* (2010). Dendritic function of tau mediates amyloid-beta toxicity in Alzheimer's disease mouse models. Cell *142*, 387-397.
Iwatsubo, T., Mann, D.M., Odaka, A., Suzuki, N., and Ihara, Y. (1995). Amyloid beta protein (A beta) deposition: A beta 42(43) precedes A beta 40 in Down syndrome. Ann Neurol *37*, 294-299.
Jack, C.R., Jr., Knopman, D.S., Jagust, W.J., Petersen, R.C., Weiner, M.W., Aisen, P.S., Shaw, L.M., Vemuri, P., Wiste, H.J., Weigand, S.D.*, et al.* (2013). Tracking pathophysiological processes in Alzheimer's disease: an updated hypothetical model of dynamic biomarkers. Lancet Neurol *12*, 207-216.
Jankowsky, J.L., Fadale, D.J., Anderson, J., Xu, G.M., Gonzales, V., Jenkins, N.A., Copeland, N.G., Lee, M.K., Younkin, L.H., Wagner, S.L.*, et al.* (2004). Mutant presenilins specifically elevate the levels of the 42 residue beta-amyloid peptide in vivo: evidence for augmentation of a 42-specific gamma secretase. Hum Mol Genet *13*, 159-170.

Jarrett, J.T., Berger, E.P., and Lansbury, P.T., Jr. (1993). The carboxy terminus of the beta amyloid protein is critical for the seeding of amyloid formation: implications for the pathogenesis of Alzheimer's disease. Biochemistry *32*, 4693-4697.
Jaunmuktane, Z., Mead, S., Ellis, M., Wadsworth, J.D., Nicoll, A.J., Kenny, J., Launchbury, F., Linehan, J., Richard-Loendt, A., Walker, A.S.*, et al.* (2015). Evidence for human transmission of amyloid-beta pathology and cerebral amyloid angiopathy. Nature *525*, 247-250.
Jaunmuktane, Z., Quaegebeur, A., Taipa, R., Viana-Baptista, M., Barbosa, R., Koriath, C., Sciot, R., Mead, S., and Brandner, S. (2018). Evidence of amyloid-beta cerebral amyloid angiopathy transmission through neurosurgery. Acta neuropathologica *135*, 671-679.
Jay, T.R., Hirsch, A.M., Broihier, M.L., Miller, C.M., Neilson, L.E., Ransohoff, R.M., Lamb, B.T., and Landreth, G.E. (2017). Disease Progression-Dependent Effects of TREM2 Deficiency in a Mouse Model of Alzheimer's Disease. J Neurosci *37*, 637-647.
Jay, T.R., Miller, C.M., Cheng, P.J., Graham, L.C., Bemiller, S., Broihier, M.L., Xu, G., Margevicius, D., Karlo, J.C., Sousa, G.L.*, et al.* (2015). TREM2 deficiency eliminates TREM2+ inflammatory macrophages and ameliorates pathology in Alzheimer's disease mouse models. J Exp Med *212*, 287-295.
Jiang, T., Yu, J.T., Zhu, X.C., Tan, M.S., Gu, L.Z., Zhang, Y.D., and Tan, L. (2014). Triggering receptor expressed on myeloid cells 2 knockdown exacerbates aging-related neuroinflammation and cognitive deficiency in senescence-accelerated mouse prone 8 mice. Neurobiol Aging *35*, 1243-1251.
Jin, S.C., Benitez, B.A., Karch, C.M., Cooper, B., Skorupa, T., Carrell, D., Norton, J.B., Hsu, S., Harari, O., Cai, Y.*, et al.* (2014). Coding variants in TREM2 increase risk for Alzheimer's disease. Hum Mol Genet *23*, 5838-5846.
Johansson, S., Radesater, A.C., Cowburn, R.F., Thyberg, J., and Luthman, J. (2006). Modelling of amyloid beta-peptide induced lesions using roller-drum incubation of hippocampal slice cultures from neonatal rats. Exp Brain Res *168*, 11-24.
Johnson, E.C.B., Dammer, E.B., Duong, D.M., Ping, L., Zhou, M., Yin, L., Higginbotham, L.A., Guajardo, A., White, B., Troncoso, J.C.*, et al.* (2020). Large-scale proteomic analysis of Alzheimer's disease brain and cerebrospinal fluid reveals early changes in energy metabolism associated with microglia and astrocyte activation. Nat Med.
Johnston, J.A., Liu, W.W., Todd, S.A., Coulson, D.T., Murphy, S., Irvine, G.B., and Passmore, A.P. (2005). Expression and activity of beta-site amyloid precursor protein cleaving enzyme in Alzheimer's disease. Biochem Soc Trans *33*, 1096-1100.
Jonsson, T., Stefansson, H., Steinberg, S., Jonsdottir, I., Jonsson, P.V., Snaedal, J., Bjornsson, S., Huttenlocher, J., Levey, A.I., Lah, J.J.*, et al.* (2013). Variant of TREM2 associated with the risk of Alzheimer's disease. N Engl J Med *368*, 107-116.
Jost, B.C., and Grossberg, G.T. (1995). The natural history of Alzheimer's disease: a brain bank study. J Am Geriatr Soc *43*, 1248-1255.
Jucker, M., and Walker, L.C. (2013). Self-propagation of pathogenic protein aggregates in neurodegenerative diseases. Nature *501*, 45-51.
Jung, C.K., Keppler, K., Steinbach, S., Blazquez-Llorca, L., and Herms, J. (2015). Fibrillar amyloid plaque formation precedes microglial activation. PLoS One *10*, e0119768.
Kakuda, N., Funamoto, S., Yagishita, S., Takami, M., Osawa, S., Dohmae, N., and Ihara, Y. (2006). Equimolar production of amyloid beta-protein and amyloid precursor protein intracellular domain from beta-carboxyl-terminal fragment by gamma-secretase. The Journal of biological chemistry *281*, 14776-14786.
Kakuda, N., Miyasaka, T., Iwasaki, N., Nirasawa, T., Wada-Kakuda, S., Takahashi-Fujigasaki, J., Murayama, S., Ihara, Y., and Ikegawa, M. (2017). Distinct deposition of

amyloid-beta species in brains with Alzheimer's disease pathology visualized with MALDI imaging mass spectrometry. Acta Neuropathol Commun *5*, 73.
Kane, M.D., Lipinski, W.J., Callahan, M.J., Bian, F., Durham, R.A., Schwarz, R.D., Roher, A.E., and Walker, L.C. (2000). Evidence for seeding of beta -amyloid by intracerebral infusion of Alzheimer brain extracts in beta -amyloid precursor protein-transgenic mice. J Neurosci *20*, 3606-3611.
Karas, M., and Hillenkamp, F. (1988). Laser desorption ionization of proteins with molecular masses exceeding 10,000 daltons. Anal Chem *60*, 2299-2301.
Karch, C.M., and Goate, A.M. (2015). Alzheimer's disease risk genes and mechanisms of disease pathogenesis. Biol Psychiatry *77*, 43-51.
Katz, L.C., and Shatz, C.J. (1996). Synaptic activity and the construction of cortical circuits. Science *274*, 1133-1138.
Kaya, I., Brinet, D., Michno, W., Baskurt, M., Zetterberg, H., Blenow, K., and Hanrieder, J. (2017a). Novel Trimodal MALDI Imaging Mass Spectrometry (IMS3) at 10 mum Reveals Spatial Lipid and Peptide Correlates Implicated in Abeta Plaque Pathology in Alzheimer's Disease. ACS Chem Neurosci *8*, 2778-2790.
Kaya, I., Brinet, D., Michno, W., Syvanen, S., Sehlin, D., Zetterberg, H., Blennow, K., and Hanrieder, J. (2017b). Delineating Amyloid Plaque Associated Neuronal Sphingolipids in Transgenic Alzheimer's Disease Mice (tgArcSwe) Using MALDI Imaging Mass Spectrometry. ACS Chem Neurosci *8*, 347-355.
Kaya, I., Zetterberg, H., Blennow, K., and Hanrieder, J. (2018). Shedding Light on the Molecular Pathology of Amyloid Plaques in Transgenic Alzheimer's Disease Mice Using Multimodal MALDI Imaging Mass Spectrometry. ACS Chem Neurosci *9*, 1802-1817.
Keren-Shaul, H., Spinrad, A., Weiner, A., Matcovitch-Natan, O., Dvir-Szternfeld, R., Ulland, T.K., David, E., Baruch, K., Lara-Astaiso, D., Toth, B.*, et al.* (2017). A Unique Microglia Type Associated with Restricting Development of Alzheimer's Disease. Cell *169*, 1276-1290 e1217.
Kettenmann, H., Hanisch, U.K., Noda, M., and Verkhratsky, A. (2011). Physiology of microglia. Physiol Rev *91*, 461-553.
Killin, L.O., Starr, J.M., Shiue, I.J., and Russ, T.C. (2016). Environmental risk factors for dementia: a systematic review. BMC Geriatr *16*, 175.
Klingstedt, T., Aslund, A., Simon, R.A., Johansson, L.B., Mason, J.J., Nystrom, S., Hammarstrom, P., and Nilsson, K.P. (2011). Synthesis of a library of oligothiophenes and their utilization as fluorescent ligands for spectral assignment of protein aggregates. Org Biomol Chem *9*, 8356-8370.
Koffie, R.M., Hashimoto, T., Tai, H.C., Kay, K.R., Serrano-Pozo, A., Joyner, D., Hou, S., Kopeikina, K.J., Frosch, M.P., Lee, V.M.*, et al.* (2012). Apolipoprotein E4 effects in Alzheimer's disease are mediated by synaptotoxic oligomeric amyloid-beta. Brain : a journal of neurology *135*, 2155-2168.
Korvatska, O., Leverenz, J.B., Jayadev, S., McMillan, P., Kurtz, I., Guo, X., Rumbaugh, M., Matsushita, M., Girirajan, S., Dorschner, M.O.*, et al.* (2015). R47H Variant of TREM2 Associated With Alzheimer Disease in a Large Late-Onset Family: Clinical, Genetic, and Neuropathological Study. JAMA Neurol *72*, 920-927.
Kurz, A., and Perneczky, R. (2011). Amyloid clearance as a treatment target against Alzheimer's disease. J Alzheimers Dis *24 Suppl 2*, 61-73.
Lacor, P.N., Buniel, M.C., Furlow, P.W., Clemente, A.S., Velasco, P.T., Wood, M., Viola, K.L., and Klein, W.L. (2007). Abeta oligomer-induced aberrations in synapse composition, shape, and density provide a molecular basis for loss of connectivity in Alzheimer's disease. J Neurosci *27*, 796-807.

Lambert, M.P., Barlow, A.K., Chromy, B.A., Edwards, C., Freed, R., Liosatos, M., Morgan, T.E., Rozovsky, I., Trommer, B., Viola, K.L*., et al.* (1998). Diffusible, nonfibrillar ligands derived from Abeta1-42 are potent central nervous system neurotoxins. Proc Natl Acad Sci U S A *95*, 6448-6453.
Lanier, L.L., Corliss, B.C., Wu, J., Leong, C., and Phillips, J.H. (1998). Immunoreceptor DAP12 bearing a tyrosine-based activation motif is involved in activating NK cells. Nature *391*, 703-707.
Latif-Hernandez, A., Sabanov, V., Ahmed, T., Craessaerts, K., Saito, T., Saido, T., and Balschun, D. (2020). The two faces of synaptic failure in App(NL-G-F) knock-in mice. Alzheimers Res Ther *12*, 100.
Lee, J., Retamal, C., Cuitino, L., Caruano-Yzermans, A., Shin, J.E., van Kerkhof, P., Marzolo, M.P., and Bu, G. (2008). Adaptor protein sorting nexin 17 regulates amyloid precursor protein trafficking and processing in the early endosomes. The Journal of biological chemistry *283*, 11501-11508.
Lee, K.M., Hawi, Z.H., Parkington, H.C., Parish, C.L., Kumar, P.V., Polo, J.M., Bellgrove, M.A., and Tong, J. (2020). The application of human pluripotent stem cells to model the neuronal and glial components of neurodevelopmental disorders. Mol Psychiatry *25*, 368-378.
Lee, S.H., Meilandt, W.J., Xie, L., Gandham, V.D., Ngu, H., Barck, K.H., Rezzonico, M.G., Imperio, J., Lalehzadeh, G., Huntley, M.A*., et al.* (2021). Trem2 restrains the enhancement of tau accumulation and neurodegeneration by beta-amyloid pathology. Neuron *109*, 1283-1301 e1286.
Lehmann, S., Dumurgier, J., Ayrignac, X., Marelli, C., Alcolea, D., Ormaechea, J.F., Thouvenot, E., Delaby, C., Hirtz, C., Vialaret, J*., et al.* (2020). Cerebrospinal fluid A beta 1-40 peptides increase in Alzheimer's disease and are highly correlated with phospho-tau in control individuals. Alzheimers Res Ther *12*, 123.
Lemere, C.A., Blusztajn, J.K., Yamaguchi, H., Wisniewski, T., Saido, T.C., and Selkoe, D.J. (1996). Sequence of deposition of heterogeneous amyloid beta-peptides and APO E in Down syndrome: implications for initial events in amyloid plaque formation. Neurobiol Dis *3*, 16-32.
Leroy, K., Ando, K., Laporte, V., Dedecker, R., Suain, V., Authelet, M., Heraud, C., Pierrot, N., Yilmaz, Z., Octave, J.N*., et al.* (2012). Lack of tau proteins rescues neuronal cell death and decreases amyloidogenic processing of APP in APP/PS1 mice. The American journal of pathology *181*, 1928-1940.
Lesne, S.E., Sherman, M.A., Grant, M., Kuskowski, M., Schneider, J.A., Bennett, D.A., and Ashe, K.H. (2013). Brain amyloid-beta oligomers in ageing and Alzheimer's disease. Brain : a journal of neurology *136*, 1383-1398.
Li, Q., and Barres, B.A. (2018). Microglia and macrophages in brain homeostasis and disease. Nat Rev Immunol *18*, 225-242.
Li, Q., Cheng, Z., Zhou, L., Darmanis, S., Neff, N.F., Okamoto, J., Gulati, G., Bennett, M.L., Sun, L.O., Clarke, L.E*., et al.* (2019). Developmental Heterogeneity of Microglia and Brain Myeloid Cells Revealed by Deep Single-Cell RNA Sequencing. Neuron *101*, 207-223 e210.
Li, Y., Schindler, S.E., Bollinger, J.G., Ovod, V., Mawuenyega, K.G., Weiner, M.W., Shaw, L.M., Masters, C.L., Fowler, C.J., Trojanowski, J.Q*., et al.* (2022). Validation of Plasma Amyloid-beta 42/40 for Detecting Alzheimer Disease Amyloid Plaques. Neurology *98*, e688-e699.

Liddelow, S.A., Guttenplan, K.A., Clarke, L.E., Bennett, F.C., Bohlen, C.J., Schirmer, L., Bennett, M.L., Munch, A.E., Chung, W.S., Peterson, T.C.*, et al.* (2017). Neurotoxic reactive astrocytes are induced by activated microglia. Nature *541*, 481-487.
Liu, J., Chang, L., Roselli, F., Almeida, O.F., Gao, X., Wang, X., Yew, D.T., and Wu, Y. (2010a). Amyloid-beta induces caspase-dependent loss of PSD-95 and synaptophysin through NMDA receptors. J Alzheimers Dis *22*, 541-556.
Liu, J., Costantino, I., Venugopalan, N., Fischetti, R.F., Hyman, B.T., Frosch, M.P., Gomez-Isla, T., and Makowski, L. (2016). Amyloid structure exhibits polymorphism on multiple length scales in human brain tissue. Sci Rep *6*, 33079.
Liu, Z., Condello, C., Schain, A., Harb, R., and Grutzendler, J. (2010b). CX3CR1 in microglia regulates brain amyloid deposition through selective protofibrillar amyloid-beta phagocytosis. J Neurosci *30*, 17091-17101.
Livingston, G., Sommerlad, A., Orgeta, V., Costafreda, S.G., Huntley, J., Ames, D., Ballard, C., Banerjee, S., Burns, A., Cohen-Mansfield, J.*, et al.* (2017). Dementia prevention, intervention, and care. Lancet *390*, 2673-2734.
Lord, A., Philipson, O., Klingstedt, T., Westermark, G., Hammarstrom, P., Nilsson, K.P., and Nilsson, L.N. (2011). Observations in APP bitransgenic mice suggest that diffuse and compact plaques form via independent processes in Alzheimer's disease. The American journal of pathology *178*, 2286-2298.
Lu, J.X., Qiang, W., Yau, W.M., Schwieters, C.D., Meredith, S.C., and Tycko, R. (2013). Molecular structure of beta-amyloid fibrils in Alzheimer's disease brain tissue. Cell *154*, 1257-1268.
Lucey, B.P., Hicks, T.J., McLeland, J.S., Toedebusch, C.D., Boyd, J., Elbert, D.L., Patterson, B.W., Baty, J., Morris, J.C., Ovod, V.*, et al.* (2018). Effect of sleep on overnight cerebrospinal fluid amyloid beta kinetics. Ann Neurol *83*, 197-204.
Ma, J., Jiang, T., Tan, L., and Yu, J.T. (2015). TYROBP in Alzheimer's disease. Mol Neurobiol *51*, 820-826.
Madore, C., Yin, Z., Leibowitz, J., and Butovsky, O. (2020). Microglia, Lifestyle Stress, and Neurodegeneration. Immunity *52*, 222-240.
Magnusson, K., Simon, R., Sjolander, D., Sigurdson, C.J., Hammarstrom, P., and Nilsson, K.P. (2014). Multimodal fluorescence microscopy of prion strain specific PrP deposits stained by thiophene-based amyloid ligands. Prion *8*, 319-329.
Mahley, R.W., and Rall, S.C., Jr. (2000). Apolipoprotein E: far more than a lipid transport protein. Annual review of genomics and human genetics *1*, 507-537.
Mann, D.M., Yates, P.O., Marcyniuk, B., and Ravindra, C.R. (1986). The topography of plaques and tangles in Down's syndrome patients of different ages. Neuropathol Appl Neurobiol *12*, 447-457.
Marksteiner, J., and Humpel, C. (2008). Beta-amyloid expression, release and extracellular deposition in aged rat brain slices. Mol Psychiatry *13*, 939-952.
Masuda, A., Kobayashi, Y., Kogo, N., Saito, T., Saido, T.C., and Itohara, S. (2016). Cognitive deficits in single App knock-in mouse models. Neurobiol Learn Mem *135*, 73-82.
Matarin, M., Salih, D.A., Yasvoina, M., Cummings, D.M., Guelfi, S., Liu, W., Nahaboo Solim, M.A., Moens, T.G., Paublete, R.M., Ali, S.S.*, et al.* (2015). A genome-wide gene-expression analysis and database in transgenic mice during development of amyloid or tau pathology. Cell Rep *10*, 633-644.
Matej, R., Tesar, A., and Rusina, R. (2019). Alzheimer's disease and other neurodegenerative dementias in comorbidity: A clinical and neuropathological overview. Clin Biochem *73*, 26-31.

Mathys, H., Davila-Velderrain, J., Peng, Z., Gao, F., Mohammadi, S., Young, J.Z., Menon, M., He, L., Abdurrob, F., Jiang, X.*, et al.* (2019). Single-cell transcriptomic analysis of Alzheimer's disease. Nature *570*, 332-337.
Mawuenyega, K.G., Sigurdson, W., Ovod, V., Munsell, L., Kasten, T., Morris, J.C., Yarasheski, K.E., and Bateman, R.J. (2010). Decreased clearance of CNS beta-amyloid in Alzheimer's disease. Science *330*, 1774.
Maxwell, A.M., Yuan, P., Rivera, B.M., Schaaf, W., Mladinov, M., Prasher, V.P., Robinson, A.C., DeGrado, W.F., and Condello, C. (2021). Emergence of distinct and heterogeneous strains of amyloid beta with advanced Alzheimer's disease pathology in Down syndrome. Acta Neuropathol Commun *9*, 201.
Mazaheri, F., Snaidero, N., Kleinberger, G., Madore, C., Daria, A., Werner, G., Krasemann, S., Capell, A., Trumbach, D., Wurst, W.*, et al.* (2017). TREM2 deficiency impairs chemotaxis and microglial responses to neuronal injury. EMBO Rep *18*, 1186-1198.
McClatchy, D.B., Dong, M.Q., Wu, C.C., Venable, J.D., and Yates, J.R., 3rd (2007). 15N metabolic labeling of mammalian tissue with slow protein turnover. J Proteome Res *6*, 2005-2010.
McClatchy, D.B., and Yates, J.R., 3rd (2008). Stable Isotope Labeling of Mammals (SILAM). CSH Protoc *2008*, pdb prot4940.
McClatchy, D.B., and Yates, J.R., 3rd (2014). Stable isotope labeling in mammals (SILAM). Methods Mol Biol *1156*, 133-146.
McDonnell, L.A., and Heeren, R.M. (2007). Imaging mass spectrometry. Mass Spectrom Rev *26*, 606-643.
McGowan, E., Eriksen, J., and Hutton, M. (2006). A decade of modeling Alzheimer's disease in transgenic mice. Trends Genet *22*, 281-289.
Medawar, E., Benway, T.A., Liu, W., Hanan, T.A., Haslehurst, P., James, O.T., Yap, K., Muessig, L., Moroni, F., Nahaboo Solim, M.A.*, et al.* (2019). Effects of rising amyloidbeta levels on hippocampal synaptic transmission, microglial response and cognition in APPSwe/PSEN1M146V transgenic mice. EBioMedicine *39*, 422-435.
Mehla, J., Lacoursiere, S.G., Lapointe, V., McNaughton, B.L., Sutherland, R.J., McDonald, R.J., and Mohajerani, M.H. (2019). Age-dependent behavioral and biochemical characterization of single APP knock-in mouse (APP(NL-G-F/NL-G-F)) model of Alzheimer's disease. Neurobiol Aging *75*, 25-37.
Mehta, D., Jackson, R., Paul, G., Shi, J., and Sabbagh, M. (2017). Why do trials for Alzheimer's disease drugs keep failing? A discontinued drug perspective for 2010-2015. Expert Opin Investig Drugs *26*, 735-739.
Meyer-Luehmann, M., Coomaraswamy, J., Bolmont, T., Kaeser, S., Schaefer, C., Kilger, E., Neuenschwander, A., Abramowski, D., Frey, P., Jaton, A.L.*, et al.* (2006). Exogenous induction of cerebral beta-amyloidogenesis is governed by agent and host. Science *313*, 1781-1784.
Meyer-Luehmann, M., Spires-Jones, T.L., Prada, C., Garcia-Alloza, M., de Calignon, A., Rozkalne, A., Koenigsknecht-Talboo, J., Holtzman, D.M., Bacskai, B.J., and Hyman, B.T. (2008). Rapid appearance and local toxicity of amyloid-beta plaques in a mouse model of Alzheimer's disease. Nature *451*, 720-724.
Michno, W., Kaya, I., Nystrom, S., Guerard, L., Nilsson, K.P.R., Hammarstrom, P., Blennow, K., Zetterberg, H., and Hanrieder, J. (2018). Multimodal Chemical Imaging of Amyloid Plaque Polymorphism Reveals Abeta Aggregation Dependent Anionic Lipid Accumulations and Metabolism. Anal Chem *90*, 8130-8138.

Michno, W., Nystrom, S., Wehrli, P., Lashley, T., Brinkmalm, G., Guerard, L., Syvanen, S., Sehlin, D., Kaya, I., Brinet, D.*, et al.* (2019a). Pyroglutamation of amyloid-betax-42 (Abetax-42) followed by Abeta1-40 deposition underlies plaque polymorphism in progressing Alzheimer's disease pathology. The Journal of biological chemistry *294*, 6719-6732.
Michno, W., Stringer, K., Escrig, S., Enzlein, T., Passarelli, M., Hopf, C., Blennow, K., Zetterberg, H., Meiborn, A., edwards, F.*, et al.* (2019b). Imaging spatial Aβ plaque aggregation dynamics in evolving AD pathology using iSILK. Unpublished.
Michno, W., Stringer, K.M., Enzlein, T., Passarelli, M.K., Escrig, S., Vitanova, K., Wood, J., Blennow, K., Zetterberg, H., Meibom, A.*, et al.* (2021). Following spatial Abeta aggregation dynamics in evolving Alzheimer's disease pathology by imaging stable isotope labeling kinetics. Sci Adv *7*, eabg4855.
Michno, W., Wehrli, P., Meier, S., Sehlin, D., Syvanen, S., Zetterberg, H., Blennow, K., and Hanrieder, J. (2019c). Chemical Imaging of Evolving Amyloid Plaque Pathology and Associated Abeta Peptide Aggregation in a Transgenic Mouse Model of Alzheimer's Disease. J Neurochem.
Michno, W., Wehrli, P.M., Blennow, K., Zetterberg, H., and Hanrieder, J. (2019d). Molecular imaging mass spectrometry for probing protein dynamics in neurodegenerative disease pathology. J Neurochem *151*, 488-506.
Michno, W., Wehrli, P.M., Zetterberg, H., Blennow, K., and Hanrieder, J. (2019e). GM1 locates to mature amyloid structures implicating a prominent role for glycolipid-protein interactions in Alzheimer pathology. Biochim Biophys Acta Proteins Proteom *1867*, 458-467.
Minett, T., Classey, J., Matthews, F.E., Fahrenhold, M., Taga, M., Brayne, C., Ince, P.G., Nicoll, J.A., Boche, D., and Mrc, C. (2016). Microglial immunophenotype in dementia with Alzheimer's pathology. J Neuroinflammation *13*, 135.
Miura, D., Fujimura, Y., Yamato, M., Hyodo, F., Utsumi, H., Tachibana, H., and Wariishi, H. (2010). Ultrahighly sensitive in situ metabolomic imaging for visualizing spatiotemporal metabolic behaviors. Anal Chem *82*, 9789-9796.
Moelgg, K., Jummun, F., and Humpel, C. (2021). Spreading of Beta-Amyloid in Organotypic Mouse Brain Slices and Microglial Elimination and Effects on Cholinergic Neurons. Biomolecules *11*.
Morales, R., Bravo-Alegria, J., Duran-Aniotz, C., and Soto, C. (2015). Titration of biologically active amyloid-beta seeds in a transgenic mouse model of Alzheimer's disease. Sci Rep *5*, 9349.
Mostany, R., Anstey, J.E., Crump, K.L., Maco, B., Knott, G., and Portera-Cailliau, C. (2013). Altered synaptic dynamics during normal brain aging. J Neurosci *33*, 4094-4104.
Mu, Y., and Gage, F.H. (2011). Adult hippocampal neurogenesis and its role in Alzheimer's disease. Mol Neurodegener *6*, 85.
Mucke, L., Masliah, E., Yu, G.Q., Mallory, M., Rockenstein, E.M., Tatsuno, G., Hu, K., Kholodenko, D., Johnson-Wood, K., and McConlogue, L. (2000). High-level neuronal expression of abeta 1-42 in wild-type human amyloid protein precursor transgenic mice: synaptotoxicity without plaque formation. J Neurosci *20*, 4050-4058.
Mullan, M., Crawford, F., Axelman, K., Houlden, H., Lilius, L., Winblad, B., and Lannfelt, L. (1992). A pathogenic mutation for probable Alzheimer's disease in the APP gene at the N-terminus of beta-amyloid. Nat Genet *1*, 345-347.
Muller, U.C., Deller, T., and Korte, M. (2017). Not just amyloid: physiological functions of the amyloid precursor protein family. Nat Rev Neurosci *18*, 281-298.

Muratore, C.R., Rice, H.C., Srikanth, P., Callahan, D.G., Shin, T., Benjamin, L.N., Walsh, D.M., Selkoe, D.J., and Young-Pearse, T.L. (2014). The familial Alzheimer's disease APPV717I mutation alters APP processing and Tau expression in iPSC-derived neurons. Hum Mol Genet *23*, 3523-3536.
Murrell, J., Farlow, M., Ghetti, B., and Benson, M.D. (1991). A mutation in the amyloid precursor protein associated with hereditary Alzheimer's disease. Science *254*, 97-99.
Muzio, L., Viotti, A., and Martino, G. (2021). Microglia in Neuroinflammation and Neurodegeneration: From Understanding to Therapy. Front Neurosci *15*, 742065.
Nelson, P.T., Alafuzoff, I., Bigio, E.H., Bouras, C., Braak, H., Cairns, N.J., Castellani, R.J., Crain, B.J., Davies, P., Del Tredici, K.*, et al.* (2012). Correlation of Alzheimer disease neuropathologic changes with cognitive status: a review of the literature. J Neuropathol Exp Neurol *71*, 362-381.
Nikolaev, A., McLaughlin, T., O'Leary, D.D., and Tessier-Lavigne, M. (2009). APP binds DR6 to trigger axon pruning and neuron death via distinct caspases. Nature *457*, 981-989.
Nilsberth, C., Westlind-Danielsson, A., Eckman, C.B., Condron, M.M., Axelman, K., Forsell, C., Stenh, C., Luthman, J., Teplow, D.B., Younkin, S.G.*, et al.* (2001). The 'Arctic' APP mutation (E693G) causes Alzheimer's disease by enhanced Abeta protofibril formation. Nat Neurosci *4*, 887-893.
Norden, D.M., and Godbout, J.P. (2013). Review: microglia of the aged brain: primed to be activated and resistant to regulation. Neuropathol Appl Neurobiol *39*, 19-34.
Novotny, R., Langer, F., Mahler, J., Skodras, A., Vlachos, A., Wegenast-Braun, B.M., Kaeser, S.A., Neher, J.J., Eisele, Y.S., Pietrowski, M.J.*, et al.* (2016). Conversion of Synthetic Abeta to In Vivo Active Seeds and Amyloid Plaque Formation in a Hippocampal Slice Culture Model. J Neurosci *36*, 5084-5093.
Nystrom, S., Back, M., Nilsson, K.P.R., and Hammarstrom, P. (2017). Imaging Amyloid Tissues Stained with Luminescent Conjugated Oligothiophenes by Hyperspectral Confocal Microscopy and Fluorescence Lifetime Imaging. J Vis Exp.
Nystrom, S., Psonka-Antonczyk, K.M., Ellingsen, P.G., Johansson, L.B., Reitan, N., Handrick, S., Prokop, S., Heppner, F.L., Wegenast-Braun, B.M., Jucker, M.*, et al.* (2013). Evidence for age-dependent in vivo conformational rearrangement within Abeta amyloid deposits. Acs Chem Biol *8*, 1128-1133.
Oakley, H., Cole, S.L., Logan, S., Maus, E., Shao, P., Craft, J., Guillozet-Bongaarts, A., Ohno, M., Disterhoft, J., Van Eldik, L.*, et al.* (2006). Intraneuronal beta-amyloid aggregates, neurodegeneration, and neuron loss in transgenic mice with five familial Alzheimer's disease mutations: potential factors in amyloid plaque formation. J Neurosci *26*, 10129-10140.
Ochalek, A., Mihalik, B., Avci, H.X., Chandrasekaran, A., Teglasi, A., Bock, I., Giudice, M.L., Tancos, Z., Molnar, K., Laszlo, L.*, et al.* (2017). Neurons derived from sporadic Alzheimer's disease iPSCs reveal elevated TAU hyperphosphorylation, increased amyloid levels, and GSK3B activation. Alzheimers Res Ther *9*, 90.
Oda, Y., Huang, K., Cross, F.R., Cowburn, D., and Chait, B.T. (1999). Accurate quantitation of protein expression and site-specific phosphorylation. Proc Natl Acad Sci U S A *96*, 6591-6596.
Oddo, S., Caccamo, A., Kitazawa, M., Tseng, B.P., and LaFerla, F.M. (2003a). Amyloid deposition precedes tangle formation in a triple transgenic model of Alzheimer's disease. Neurobiol Aging *24*, 1063-1070.
Oddo, S., Caccamo, A., Shepherd, J.D., Murphy, M.P., Golde, T.E., Kayed, R., Metherate, R., Mattson, M.P., Akbari, Y., and LaFerla, F.M. (2003b). Triple-transgenic model of

Alzheimer's disease with plaques and tangles: intracellular Abeta and synaptic dysfunction. Neuron *39*, 409-421.
Ohno, M., Cole, S.L., Yasvoina, M., Zhao, J., Citron, M., Berry, R., Disterhoft, J.F., and Vassar, R. (2007). BACE1 gene deletion prevents neuron loss and memory deficits in 5XFAD APP/PS1 transgenic mice. Neurobiol Dis *26*, 134-145.
Ohno, M., Sametsky, E.A., Younkin, L.H., Oakley, H., Younkin, S.G., Citron, M., Vassar, R., and Disterhoft, J.F. (2004). BACE1 deficiency rescues memory deficits and cholinergic dysfunction in a mouse model of Alzheimer's disease. Neuron *41*, 27-33.
Oksanen, M., Petersen, A.J., Naumenko, N., Puttonen, K., Lehtonen, S., Gubert Olive, M., Shakirzyanova, A., Leskela, S., Sarajarvi, T., Viitanen, M*., et al.* (2017). PSEN1 Mutant iPSC-Derived Model Reveals Severe Astrocyte Pathology in Alzheimer's Disease. Stem Cell Reports *9*, 1885-1897.
Ong, S.E., Blagoev, B., Kratchmarova, I., Kristensen, D.B., Steen, H., Pandey, A., and Mann, M. (2002). Stable isotope labeling by amino acids in cell culture, SILAC, as a simple and accurate approach to expression proteomics. Molecular & cellular proteomics : MCP *1*, 376-386.
Paloneva, J., Manninen, T., Christman, G., Hovanes, K., Mandelin, J., Adolfsson, R., Bianchin, M., Bird, T., Miranda, R., Salmaggi, A*., et al.* (2002). Mutations in two genes encoding different subunits of a receptor signaling complex result in an identical disease phenotype. American journal of human genetics *71*, 656-662.
Paolicelli, R.C., Bolasco, G., Pagani, F., Maggi, L., Scianni, M., Panzanelli, P., Giustetto, M., Ferreira, T.A., Guiducci, E., Dumas, L*., et al.* (2011). Synaptic pruning by microglia is necessary for normal brain development. Science *333*, 1456-1458.
Park, J., Wetzel, I., Marriott, I., Dreau, D., D'Avanzo, C., Kim, D.Y., Tanzi, R.E., and Cho, H. (2018). A 3D human triculture system modeling neurodegeneration and neuroinflammation in Alzheimer's disease. Nat Neurosci *21*, 941-951.
Paterson, R.W., Gabelle, A., Lucey, B.P., Barthelemy, N.R., Leckey, C.A., Hirtz, C., Lehmann, S., Sato, C., Patterson, B.W., West, T*., et al.* (2019). SILK studies - capturing the turnover of proteins linked to neurodegenerative diseases. Nat Rev Neurol *15*, 419-427.
Paterson, R.W., Slattery, C.F., Poole, T., Nicholas, J.M., Magdalinou, N.K., Toombs, J., Chapman, M.D., Lunn, M.P., Heslegrave, A.J., Foiani, M.S*., et al.* (2018). Cerebrospinal fluid in the differential diagnosis of Alzheimer's disease: clinical utility of an extended panel of biomarkers in a specialist cognitive clinic. Alzheimers Res Ther *10*, 32.
Patterson, B.W., Elbert, D.L., Mawuenyega, K.G., Kasten, T., Ovod, V., Ma, S., Xiong, C., Chott, R., Yarasheski, K., Sigurdson, W*., et al.* (2015). Age and amyloid effects on human central nervous system amyloid-beta kinetics. Ann Neurol *78*, 439-453.
Pauls, E., Bayod, S., Mateo, L., Alcalde, V., Juan-Blanco, T., Saido, T.C., Saito, T., Berrenguer-Llergo, A., Attolini, C.S.-O., Gay, M*., et al.* (2021). Identification and drug-induced reversion of molecular signatures of Alzheimer's disease onset and progression in App^{NL-G-F}, App^{NL-F} and 3xTg-AD mouse models. bioRxiv, 2021.2003.2017.435753.
Perez-Nievas, B.G., Stein, T.D., Tai, H.C., Dols-Icardo, O., Scotton, T.C., Barroeta-Espar, I., Fernandez-Carballo, L., de Munain, E.L., Perez, J., Marquie, M*., et al.* (2013). Dissecting phenotypic traits linked to human resilience to Alzheimer's pathology. Brain : a journal of neurology *136*, 2510-2526.
Philipson, O., Hammarstrom, P., Nilsson, K.P., Portelius, E., Olofsson, T., Ingelsson, M., Hyman, B.T., Blennow, K., Lannfelt, L., Kalimo, H*., et al.* (2009). A highly insoluble state

of Abeta similar to that of Alzheimer's disease brain is found in Arctic APP transgenic mice. Neurobiol Aging *30*, 1393-1405.
Phongpreecha, T., Gajera, C.R., Liu, C.C., Vijayaragavan, K., Chang, A.L., Becker, M., Fallahzadeh, R., Fernandez, R., Postupna, N., Sherfield, E.*, et al.* (2021). Single-synapse analyses of Alzheimer's disease implicate pathologic tau, DJ1, CD47, and ApoE. Sci Adv *7*, eabk0473.
Piccio, L., Buonsanti, C., Mariani, M., Cella, M., Gilfillan, S., Cross, A.H., Colonna, M., and Panina-Bordignon, P. (2007). Blockade of TREM-2 exacerbates experimental autoimmune encephalomyelitis. Eur J Immunol *37*, 1290-1301.
Porsteinsson, A.P., Isaacson, R.S., Knox, S., Sabbagh, M.N., and Rubino, I. (2021). Diagnosis of Early Alzheimer's Disease: Clinical Practice in 2021. J Prev Alzheimers Dis *8*, 371-386.
Portelius, E., Bogdanovic, N., Gustavsson, M.K., Volkmann, I., Brinkmalm, G., Zetterberg, H., Winblad, B., and Blennow, K. (2010). Mass spectrometric characterization of brain amyloid beta isoform signatures in familial and sporadic Alzheimer's disease. Acta neuropathologica *120*, 185-193.
Portelius, E., Tran, A.J., Andreasson, U., Persson, R., Brinkmalm, G., Zetterberg, H., Blennow, K., and Westman-Brinkmalm, A. (2007). Characterization of amyloid beta peptides in cerebrospinal fluid by an automated immunoprecipitation procedure followed by mass spectrometry. J Proteome Res *6*, 4433-4439.
Portelius, E., Westman-Brinkmalm, A., Zetterberg, H., and Blennow, K. (2006). Determination of beta-amyloid peptide signatures in cerebrospinal fluid using immunoprecipitation-mass spectrometry. J Proteome Res *5*, 1010-1016.
Potter, R., Patterson, B.W., Elbert, D.L., Ovod, V., Kasten, T., Sigurdson, W., Mawuenyega, K., Blazey, T., Goate, A., Chott, R.*, et al.* (2013). Increased in vivo amyloid-beta42 production, exchange, and loss in presenilin mutation carriers. Sci Transl Med *5*, 189ra177.
Qiang, W., Yau, W.M., Lu, J.X., Collinge, J., and Tycko, R. (2017). Structural variation in amyloid-beta fibrils from Alzheimer's disease clinical subtypes. Nature *541*, 217-221.
Radde, R., Bolmont, T., Kaeser, S.A., Coomaraswamy, J., Lindau, D., Stoltze, L., Calhoun, M.E., Jaggi, F., Wolburg, H., Gengler, S.*, et al.* (2006). Abeta42-driven cerebral amyloidosis in transgenic mice reveals early and robust pathology. EMBO Rep *7*, 940-946.
Raj, D., Yin, Z., Breur, M., Doorduin, J., Holtman, I.R., Olah, M., Mantingh-Otter, I.J., Van Dam, D., De Deyn, P.P., den Dunnen, W.*, et al.* (2017). Increased White Matter Inflammation in Aging- and Alzheimer's Disease Brain. Front Mol Neurosci *10*, 206.
Rapoport, M., Dawson, H.N., Binder, L.I., Vitek, M.P., and Ferreira, A. (2002). Tau is essential to beta -amyloid-induced neurotoxicity. Proc Natl Acad Sci U S A *99*, 6364-6369.
Rasmussen, J., Mahler, J., Beschorner, N., Kaeser, S.A., Hasler, L.M., Baumann, F., Nystrom, S., Portelius, E., Blennow, K., Lashley, T.*, et al.* (2017). Amyloid polymorphisms constitute distinct clouds of conformational variants in different etiological subtypes of Alzheimer's disease. Proc Natl Acad Sci U S A *114*, 13018-13023.
Rayaprolu, S., Mullen, B., Baker, M., Lynch, T., Finger, E., Seeley, W.W., Hatanpaa, K.J., Lomen-Hoerth, C., Kertesz, A., Bigio, E.H.*, et al.* (2013). TREM2 in neurodegeneration: evidence for association of the p.R47H variant with frontotemporal dementia and Parkinson's disease. Mol Neurodegener *8*, 19.
Reich, M., Paris, I., Ebeling, M., Dahm, N., Schweitzer, C., Reinhardt, D., Schmucki, R., Prasad, M., Kochl, F., Leist, M.*, et al.* (2020). Alzheimer's Risk Gene TREM2 Determines

Functional Properties of New Type of Human iPSC-Derived Microglia. Front Immunol *11*, 617860.
Rice, H.C., Marcassa, G., Chrysidou, I., Horre, K., Young-Pearse, T.L., Muller, U.C., Saito, T., Saido, T.C., Vassar, R., de Wit, J.*, et al.* (2020). Contribution of GABAergic interneurons to amyloid-beta plaque pathology in an APP knock-in mouse model. Mol Neurodegener *15*, 3.
Roberson, E.D., Scearce-Levie, K., Palop, J.J., Yan, F., Cheng, I.H., Wu, T., Gerstein, H., Yu, G.Q., and Mucke, L. (2007). Reducing endogenous tau ameliorates amyloid beta-induced deficits in an Alzheimer's disease mouse model. Science *316*, 750-754.
Roch, J.M., Masliah, E., Roch-Levecq, A.C., Sundsmo, M.P., Otero, D.A., Veinbergs, I., and Saitoh, T. (1994). Increase of synaptic density and memory retention by a peptide representing the trophic domain of the amyloid beta/A4 protein precursor. Proc Natl Acad Sci U S A *91*, 7450-7454.
Rodrigue, K.M., Kennedy, K.M., and Park, D.C. (2009). Beta-amyloid deposition and the aging brain. Neuropsychol Rev *19*, 436-450.
Rodriguez, G.A., Tai, L.M., LaDu, M.J., and Rebeck, G.W. (2014). Human APOE4 increases microglia reactivity at Abeta plaques in a mouse model of Abeta deposition. J Neuroinflammation *11*, 111.
Rodriguez, J.J., Noristani, H.N., Hilditch, T., Olabarria, M., Yeh, C.Y., Witton, J., and Verkhratsky, A. (2013). Increased densities of resting and activated microglia in the dentate gyrus follow senile plaque formation in the CA1 subfield of the hippocampus in the triple transgenic model of Alzheimer's disease. Neurosci Lett *552*, 129-134.
Rogers, J., Luber-Narod, J., Styren, S.D., and Civin, W.H. (1988). Expression of immune system-associated antigens by cells of the human central nervous system: relationship to the pathology of Alzheimer's disease. Neurobiol Aging *9*, 339-349.
Roher, A.E., Kokjohn, T.A., Clarke, S.G., Sierks, M.R., Maarouf, C.L., Serrano, G.E., Sabbagh, M.S., and Beach, T.G. (2017). APP/Abeta structural diversity and Alzheimer's disease pathogenesis. Neurochem Int *110*, 1-13.
Rowan, M.J., Klyubin, I., Cullen, W.K., and Anwyl, R. (2003). Synaptic plasticity in animal models of early Alzheimer's disease. Philos Trans R Soc Lond B Biol Sci *358*, 821-828.
Ruiz, A., Dols-Icardo, O., Bullido, M.J., Pastor, P., Rodriguez-Rodriguez, E., Lopez de Munain, A., de Pancorbo, M.M., Perez-Tur, J., Alvarez, V., Antonell, A.*, et al.* (2014). Assessing the role of the TREM2 p.R47H variant as a risk factor for Alzheimer's disease and frontotemporal dementia. Neurobiol Aging *35*, 444 e441-444.
Sacher, C., Blume, T., Beyer, L., Peters, F., Eckenweber, F., Sgobio, C., Deussing, M., Albert, N.L., Unterrainer, M., Lindner, S.*, et al.* (2019). Longitudinal PET Monitoring of Amyloidosis and Microglial Activation in a Second-Generation Amyloid-beta Mouse Model. J Nucl Med *60*, 1787-1793.
Safaiyan, S., Besson-Girard, S., Kaya, T., Cantuti-Castelvetri, L., Liu, L., Ji, H., Schifferer, M., Gouna, G., Usifo, F., Kannaiyan, N.*, et al.* (2021). White matter aging drives microglial diversity. Neuron *109*, 1100-1117 e1110.
Saido, T., and Leissring, M.A. (2012). Proteolytic degradation of amyloid beta-protein. Cold Spring Harbor perspectives in medicine *2*, a006379.
Saito, T., Matsuba, Y., Mihira, N., Takano, J., Nilsson, P., Itohara, S., Iwata, N., and Saido, T.C. (2014). Single App knock-in mouse models of Alzheimer's disease. Nat Neurosci *17*, 661-663.
Sakakibara, Y., Sekiya, M., Saito, T., Saido, T.C., and Iijima, K.M. (2018). Cognitive and emotional alterations in App knock-in mouse models of Abeta amyloidosis. BMC Neurosci *19*, 46.

Sakakibara, Y., Sekiya, M., Saito, T., Saido, T.C., and Iijima, K.M. (2019). Amyloid-beta plaque formation and reactive gliosis are required for induction of cognitive deficits in App knock-in mouse models of Alzheimer's disease. BMC Neurosci *20*, 13.
Salih, D.A., Bayram, S., Guelfi, S., Reynolds, R.H., Shoai, M., Ryten, M., Brenton, J.W., Zhang, D., Matarin, M., Botia, J.A*., et al.* (2019). Genetic variability in response to amyloid beta deposition influences Alzheimer's disease risk. Brain Commun *1*, fcz022.
Salloway, S., Sperling, R., Fox, N.C., Blennow, K., Klunk, W., Raskind, M., Sabbagh, M., Honig, L.S., Porsteinsson, A.P., Ferris, S*., et al.* (2014). Two phase 3 trials of bapineuzumab in mild-to-moderate Alzheimer's disease. N Engl J Med *370*, 322-333.
Sanan, D.A., Weisgraber, K.H., Russell, S.J., Mahley, R.W., Huang, D., Saunders, A., Schmechel, D., Wisniewski, T., Frangione, B., Roses, A.D*., et al.* (1994). Apolipoprotein E associates with beta amyloid peptide of Alzheimer's disease to form novel monofibrils. Isoform apoE4 associates more efficiently than apoE3. J Clin Invest *94*, 860-869.
Sato, C., Barthelemy, N.R., Mawuenyega, K.G., Patterson, B.W., Gordon, B.A., Jockel-Balsarotti, J., Sullivan, M., Crisp, M.J., Kasten, T., Kirmess, K.M*., et al.* (2018). Tau Kinetics in Neurons and the Human Central Nervous System. Neuron *97*, 1284-1298 e1287.
Savas, J.N., Park, S.K., and Yates, J.R., 3rd (2016). Proteomic Analysis of Protein Turnover by Metabolic Whole Rodent Pulse-Chase Isotopic Labeling and Shotgun Mass Spectrometry Analysis. Methods Mol Biol *1410*, 293-304.
Sawada, M., Sawada, H., and Nagatsu, T. (2008). Effects of aging on neuroprotective and neurotoxic properties of microglia in neurodegenerative diseases. Neurodegener Dis *5*, 254-256.
Sayed, F.A., Kodama, L., Udeochu, J.C., Fan, L., Carling, G.K., Le, D., Li, Q., Zhou, L., Mathys, H., Wang, M*., et al.* (2020). AD-linked R47H-TREM2 mutation induces disease-enhancing proinflammatory microglial states in mice and humans. bioRxiv, 2020.2007.2024.218719.
Schedin-Weiss, S., Nilsson, P., Sandebring-Matton, A., Axenhus, M., Sekiguchi, M., Saito, T., Winblad, B., Saido, T., and Tjernberg, L.O. (2020). Proteomics Time-Course Study of App Knock-In Mice Reveals Novel Presymptomatic Abeta42-Induced Pathways to Alzheimer's Disease Pathology. J Alzheimers Dis *75*, 321-335.
Scheff, S.W., and Price, D.A. (2006). Alzheimer's disease-related alterations in synaptic density: neocortex and hippocampus. J Alzheimers Dis *9*, 101-115.
Scheuner, D., Eckman, C., Jensen, M., Song, X., Citron, M., Suzuki, N., Bird, T.D., Hardy, J., Hutton, M., Kukull, W*., et al.* (1996). Secreted amyloid beta-protein similar to that in the senile plaques of Alzheimer's disease is increased in vivo by the presenilin 1 and 2 and APP mutations linked to familial Alzheimer's disease. Nat Med *2*, 864-870.
Schmechel, D.E., Saunders, A.M., Strittmatter, W.J., Crain, B.J., Hulette, C.M., Joo, S.H., Pericak-Vance, M.A., Goldgaber, D., and Roses, A.D. (1993). Increased amyloid beta-peptide deposition in cerebral cortex as a consequence of apolipoprotein E genotype in late-onset Alzheimer disease. Proc Natl Acad Sci U S A *90*, 9649-9653.
Scholl, M., Lockhart, S.N., Schonhaut, D.R., O'Neil, J.P., Janabi, M., Ossenkoppele, R., Baker, S.L., Vogel, J.W., Faria, J., Schwimmer, H.D*., et al.* (2016). PET Imaging of Tau Deposition in the Aging Human Brain. Neuron *89*, 971-982.
Schuff, N., Woerner, N., Boreta, L., Kornfield, T., Shaw, L.M., Trojanowski, J.Q., Thompson, P.M., Jack, C.R., Jr., Weiner, M.W., and Alzheimer's Disease Neuroimaging, I. (2009). MRI of hippocampal volume loss in early Alzheimer's disease in relation to ApoE genotype and biomarkers. Brain : a journal of neurology *132*, 1067-1077.

Sebastian Monasor, L., Muller, S.A., Colombo, A.V., Tanrioever, G., Konig, J., Roth, S., Liesz, A., Berghofer, A., Piechotta, A., Prestel, M.*, et al.* (2020). Fibrillar Abeta triggers microglial proteome alterations and dysfunction in Alzheimer mouse models. Elife *9*.
Serrano-Pozo, A., Frosch, M.P., Masliah, E., and Hyman, B.T. (2011). Neuropathological alterations in Alzheimer disease. Cold Spring Harbor perspectives in medicine *1*, a006189.
Shah, D., Latif-Hernandez, A., De Strooper, B., Saito, T., Saido, T., Verhoye, M., D'Hooge, R., and Van der Linden, A. (2018). Spatial reversal learning defect coincides with hypersynchronous telencephalic BOLD functional connectivity in APP(NL-F/NL-F) knock-in mice. Sci Rep *8*, 6264.
Shankar, G.M., Li, S., Mehta, T.H., Garcia-Munoz, A., Shepardson, N.E., Smith, I., Brett, F.M., Farrell, M.A., Rowan, M.J., Lemere, C.A.*, et al.* (2008). Amyloid-beta protein dimers isolated directly from Alzheimer's brains impair synaptic plasticity and memory. Nat Med *14*, 837-842.
Shoji, M., Matsubara, E., Kanai, M., Watanabe, M., Nakamura, T., Tomidokoro, Y., Shizuka, M., Wakabayashi, K., Igeta, Y., Ikeda, Y.*, et al.* (1998). Combination assay of CSF tau, A beta 1-40 and A beta 1-42(43) as a biochemical marker of Alzheimer's disease. J Neurol Sci *158*, 134-140.
Sierra, A., Encinas, J.M., Deudero, J.J., Chancey, J.H., Enikolopov, G., Overstreet-Wadiche, L.S., Tsirka, S.E., and Maletic-Savatic, M. (2010). Microglia shape adult hippocampal neurogenesis through apoptosis-coupled phagocytosis. Cell Stem Cell *7*, 483-495.
Sims, R., van der Lee, S.J., Naj, A.C., Bellenguez, C., Badarinarayan, N., Jakobsdottir, J., Kunkle, B.W., Boland, A., Raybould, R., Bis, J.C.*, et al.* (2017). Rare coding variants in PLCG2, ABI3, and TREM2 implicate microglial-mediated innate immunity in Alzheimer's disease. Nat Genet *49*, 1373-1384.
Song, W., Hooli, B., Mullin, K., Jin, S.C., Cella, M., Ulland, T.K., Wang, Y., Tanzi, R.E., and Colonna, M. (2017). Alzheimer's disease-associated TREM2 variants exhibit either decreased or increased ligand-dependent activation. Alzheimers Dement *13*, 381-387.
Song, W.M., Joshita, S., Zhou, Y., Ulland, T.K., Gilfillan, S., and Colonna, M. (2018). Humanized TREM2 mice reveal microglia-intrinsic and -extrinsic effects of R47H polymorphism. J Exp Med *215*, 745-760.
Spangenberg, E., Severson, P.L., Hohsfield, L.A., Crapser, J., Zhang, J., Burton, E.A., Zhang, Y., Spevak, W., Lin, J., Phan, N.Y.*, et al.* (2019). Sustained microglial depletion with CSF1R inhibitor impairs parenchymal plaque development in an Alzheimer's disease model. Nat Commun *10*, 3758.
Spangenberg, E.E., Lee, R.J., Najafi, A.R., Rice, R.A., Elmore, M.R., Blurton-Jones, M., West, B.L., and Green, K.N. (2016). Eliminating microglia in Alzheimer's mice prevents neuronal loss without modulating amyloid-beta pathology. Brain : a journal of neurology *139*, 1265-1281.
Spires-Jones, T.L., and Hyman, B.T. (2014). The intersection of amyloid beta and tau at synapses in Alzheimer's disease. Neuron *82*, 756-771.
Staal, J.A., Alexander, S.R., Liu, Y., Dickson, T.D., and Vickers, J.C. (2011). Characterization of cortical neuronal and glial alterations during culture of organotypic whole brain slices from neonatal and mature mice. PLoS One *6*, e22040.
Stevens, B., Allen, N.J., Vazquez, L.E., Howell, G.R., Christopherson, K.S., Nouri, N., Micheva, K.D., Mehalow, A.K., Huberman, A.D., Stafford, B.*, et al.* (2007). The classical complement cascade mediates CNS synapse elimination. Cell *131*, 1164-1178.

Stewart, C.R., Stuart, L.M., Wilkinson, K., van Gils, J.M., Deng, J., Halle, A., Rayner, K.J., Boyer, L., Zhong, R., Frazier, W.A*., et al.* (2010). CD36 ligands promote sterile inflammation through assembly of a Toll-like receptor 4 and 6 heterodimer. Nat Immunol *11*, 155-161.
Stoppini, L., Buchs, P.A., and Muller, D. (1991). A simple method for organotypic cultures of nervous tissue. J Neurosci Methods *37*, 173-182.
Strozyk, D., Blennow, K., White, L.R., and Launer, L.J. (2003). CSF Abeta 42 levels correlate with amyloid-neuropathology in a population-based autopsy study. Neurology *60*, 652-656.
Sturchio, A., Dwivedi, A.K., Young, C.B., Malm, T., Marsili, L., Sharma, J.S., Mahajan, A., Hill, E.J., Andaloussi, S.E., Poston, K.L*., et al.* (2021). High cerebrospinal amyloid-beta 42 is associated with normal cognition in individuals with brain amyloidosis. EClinicalMedicine *38*, 100988.
Sturchler-Pierrat, C., Abramowski, D., Duke, M., Wiederhold, K.H., Mistl, C., Rothacher, S., Ledermann, B., Burki, K., Frey, P., Paganetti, P.A*., et al.* (1997). Two amyloid precursor protein transgenic mouse models with Alzheimer disease-like pathology. Proc Natl Acad Sci U S A *94*, 13287-13292.
Su, T., Paradiso, B., Long, Y.S., Liao, W.P., and Simonato, M. (2011). Evaluation of cell damage in organotypic hippocampal slice culture from adult mouse: a potential model system to study neuroprotection. Brain Res *1385*, 68-76.
Suarez-Calvet, M., Araque Caballero, M.A., Kleinberger, G., Bateman, R.J., Fagan, A.M., Morris, J.C., Levin, J., Danek, A., Ewers, M., Haass, C*., et al.* (2016). Early changes in CSF sTREM2 in dominantly inherited Alzheimer's disease occur after amyloid deposition and neuronal injury. Sci Transl Med *8*, 369ra178.
Sugama, S., Takenouchi, T., Hashimoto, M., Ohata, H., Takenaka, Y., and Kakinuma, Y. (2019). Stress-induced microglial activation occurs through beta-adrenergic receptor: noradrenaline as a key neurotransmitter in microglial activation. J Neuroinflammation *16*, 266.
Suppiah, S., Didier, M.A., and Vinjamuri, S. (2019). The Who, When, Why, and How of PET Amyloid Imaging in Management of Alzheimer's Disease-Review of Literature and Interesting Images. Diagnostics (Basel) *9*.
Szaruga, M., Munteanu, B., Lismont, S., Veugelen, S., Horre, K., Mercken, M., Saido, T.C., Ryan, N.S., De Vos, T., Savvides, S.N*., et al.* (2017). Alzheimer's-Causing Mutations Shift Abeta Length by Destabilizing gamma-Secretase-Abetan Interactions. Cell *170*, 443-456 e414.
Takahashi, K., Prinz, M., Stagi, M., Chechneva, O., and Neumann, H. (2007). TREM2-transduced myeloid precursors mediate nervous tissue debris clearance and facilitate recovery in an animal model of multiple sclerosis. PLoS Med *4*, e124.
Takami, M., Nagashima, Y., Sano, Y., Ishihara, S., Morishima-Kawashima, M., Funamoto, S., and Ihara, Y. (2009). gamma-Secretase: successive tripeptide and tetrapeptide release from the transmembrane domain of beta-carboxyl terminal fragment. J Neurosci *29*, 13042-13052.
Tekirian, T.L. (2001). Commentary: Abeta N- Terminal Isoforms: Critical contributors in the course of AD pathophysiology. J Alzheimers Dis *3*, 241-248.
Terry, R.D., Masliah, E., Salmon, D.P., Butters, N., DeTeresa, R., Hill, R., Hansen, L.A., and Katzman, R. (1991). Physical basis of cognitive alterations in Alzheimer's disease: synapse loss is the major correlate of cognitive impairment. Ann Neurol *30*, 572-580.

Thal, D.R., Rub, U., Orantes, M., and Braak, H. (2002). Phases of A beta-deposition in the human brain and its relevance for the development of AD. Neurology *58*, 1791-1800.
Thal, D.R., Walter, J., Saido, T.C., and Fandrich, M. (2015). Neuropathology and biochemistry of Abeta and its aggregates in Alzheimer's disease. Acta neuropathologica *129*, 167-182.
Townsend, M., Shankar, G.M., Mehta, T., Walsh, D.M., and Selkoe, D.J. (2006). Effects of secreted oligomers of amyloid beta-protein on hippocampal synaptic plasticity: a potent role for trimers. J Physiol *572*, 477-492.
Trivino, J.J., and von Bernhardi, R. (2021). The effect of aged microglia on synaptic impairment and its relevance in neurodegenerative diseases. Neurochem Int *144*, 104982.
Tycko, R. (2015). Amyloid polymorphism: structural basis and neurobiological relevance. Neuron *86*, 632-645.
Ucal, Y., Durer, Z.A., Atak, H., Kadioglu, E., Sahin, B., Coskun, A., Baykal, A.T., and Ozpinar, A. (2017). Clinical applications of MALDI imaging technologies in cancer and neurodegenerative diseases. Biochim Biophys Acta Proteins Proteom *1865*, 795-816.
Vassar, R., Kovacs, D.M., Yan, R., and Wong, P.C. (2009). The beta-secretase enzyme BACE in health and Alzheimer's disease: regulation, cell biology, function, and therapeutic potential. J Neurosci *29*, 12787-12794.
Venegas, C., Kumar, S., Franklin, B.S., Dierkes, T., Brinkschulte, R., Tejera, D., Vieira-Saecker, A., Schwartz, S., Santarelli, F., Kummer, M.P.*, et al.* (2017). Microglia-derived ASC specks cross-seed amyloid-beta in Alzheimer's disease. Nature *552*, 355-361.
Verghese, P.B., Castellano, J.M., and Holtzman, D.M. (2011). Apolipoprotein E in Alzheimer's disease and other neurological disorders. Lancet Neurol *10*, 241-252.
Viola, K.L., and Klein, W.L. (2015). Amyloid beta oligomers in Alzheimer's disease pathogenesis, treatment, and diagnosis. Acta neuropathologica *129*, 183-206.
Vitanova, K. (2021). Assessment of the effects of plaques and glia on synaptic transmission in App knock-in models of Alzheimer’s disease. PhD Thesis.
Walker, D.G., and Lue, L.F. (2015). Immune phenotypes of microglia in human neurodegenerative disease: challenges to detecting microglial polarization in human brains. Alzheimers Res Ther *7*, 56.
Walker, L.C., Schelle, J., and Jucker, M. (2016). The Prion-Like Properties of Amyloid-beta Assemblies: Implications for Alzheimer's Disease. Cold Spring Harbor perspectives in medicine *6*.
Wang, P., Yang, G., Mosier, D.R., Chang, P., Zaidi, T., Gong, Y.D., Zhao, N.M., Dominguez, B., Lee, K.F., Gan, W.B.*, et al.* (2005). Defective neuromuscular synapses in mice lacking amyloid precursor protein (APP) and APP-Like protein 2. J Neurosci *25*, 1219-1225.
Wang, Y., Cella, M., Mallinson, K., Ulrich, J.D., Young, K.L., Robinette, M.L., Gilfillan, S., Krishnan, G.M., Sudhakar, S., Zinselmeyer, B.H.*, et al.* (2015). TREM2 lipid sensing sustains the microglial response in an Alzheimer's disease model. Cell *160*, 1061-1071.
Wang, Y., Ulland, T.K., Ulrich, J.D., Song, W., Tzaferis, J.A., Hole, J.T., Yuan, P., Mahan, T.E., Shi, Y., Gilfillan, S.*, et al.* (2016). TREM2-mediated early microglial response limits diffusion and toxicity of amyloid plaques. J Exp Med *213*, 667-675.
Wang, Z., Jackson, R.J., Hong, W., Taylor, W.M., Corbett, G.T., Moreno, A., Liu, W., Li, S., Frosch, M.P., Slutsky, I.*, et al.* (2017). Human Brain-Derived Abeta Oligomers Bind to Synapses and Disrupt Synaptic Activity in a Manner That Requires APP. J Neurosci *37*, 11947-11966.

Whyte, L.S., Hemsley, K.M., Lau, A.A., Hassiotis, S., Saito, T., Saido, T.C., Hopwood, J.J., and Sargeant, T.J. (2018). Reduction in open field activity in the absence of memory deficits in the App(NL-G-F) knock-in mouse model of Alzheimer's disease. Behav Brain Res *336*, 177-181.
Wildsmith, K.R., Basak, J.M., Patterson, B.W., Pyatkivskyy, Y., Kim, J., Yarasheski, K.E., Wang, J.X., Mawuenyega, K.G., Jiang, H., Parsadanian, M.*, et al.* (2012). In vivo human apolipoprotein E isoform fractional turnover rates in the CNS. PLoS One *7*, e38013.
Wiltfang, J., Esselmann, H., Bibl, M., Hull, M., Hampel, H., Kessler, H., Frolich, L., Schroder, J., Peters, O., Jessen, F.*, et al.* (2007). Amyloid beta peptide ratio 42/40 but not A beta 42 correlates with phospho-Tau in patients with low- and high-CSF A beta 40 load. J Neurochem *101*, 1053-1059.
Wood, J., Wong, E., Joghee, R., Balbaa, A., Vitanova, K.S., Vanshoiack, A., Phelan, S.-L.J., Desai, S., Tripathi, T., Hanrieder, J.*, et al.* (2022). Upregulation of Trem2 expression occurs exclusively on microglial contact with plaques. bioRxiv; under resubmission to Cell Reports, https://doi.org/10.1101/2022.1101.1126.477873.
Xia, D., Lianoglou, S., Sandmann, T., Calvert, M., Suh, J.H., Thomsen, E., Dugas, J., Pizzo, M.E., DeVos, S.L., Earr, T.K.*, et al.* (2021). Fibrillar Aβ causes profound microglial metabolic perturbations in a novel APP knock-in mouse model. bioRxiv, 2021.2001.2019.426731.
Xiang, X., Piers, T.M., Wefers, B., Zhu, K., Mallach, A., Brunner, B., Kleinberger, G., Song, W., Colonna, M., Herms, J.*, et al.* (2018). The Trem2 R47H Alzheimer's risk variant impairs splicing and reduces Trem2 mRNA and protein in mice but not in humans. Mol Neurodegener *13*, 49.
Xu, K., Malouf, A.T., Messing, A., and Silver, J. (1999). Glial fibrillary acidic protein is necessary for mature astrocytes to react to beta-amyloid. Glia *25*, 390-403.
Yang, J., and Caprioli, R.M. (2011). Matrix sublimation/recrystallization for imaging proteins by mass spectrometry at high spatial resolution. Anal Chem *83*, 5728-5734.
Yang, L.B., Lindholm, K., Yan, R., Citron, M., Xia, W., Yang, X.L., Beach, T., Sue, L., Wong, P., Price, D.*, et al.* (2003). Elevated beta-secretase expression and enzymatic activity detected in sporadic Alzheimer disease. Nat Med *9*, 3-4.
Yeh, F.L., Wang, Y., Tom, I., Gonzalez, L.C., and Sheng, M. (2016). TREM2 Binds to Apolipoproteins, Including APOE and CLU/APOJ, and Thereby Facilitates Uptake of Amyloid-Beta by Microglia. Neuron *91*, 328-340.
Yu, Y., and Ye, R.D. (2015). Microglial Abeta receptors in Alzheimer's disease. Cell Mol Neurobiol *35*, 71-83.
Yuan, P., Condello, C., Keene, C.D., Wang, Y., Bird, T.D., Paul, S.M., Luo, W., Colonna, M., Baddeley, D., and Grutzendler, J. (2016). TREM2 Haplodeficiency in Mice and Humans Impairs the Microglia Barrier Function Leading to Decreased Amyloid Compaction and Severe Axonal Dystrophy. Neuron *90*, 724-739.
Zhong, L., Wang, Z., Wang, D., Wang, Z., Martens, Y.A., Wu, L., Xu, Y., Wang, K., Li, J., Huang, R.*, et al.* (2018). Amyloid-beta modulates microglial responses by binding to the triggering receptor expressed on myeloid cells 2 (TREM2). Mol Neurodegener *13*, 15.